Faculty of Aerospace Engineering

Structuring airspace into lateral zones for conflict prevention

A.J.G.T. Scholtes

January 31, 2018

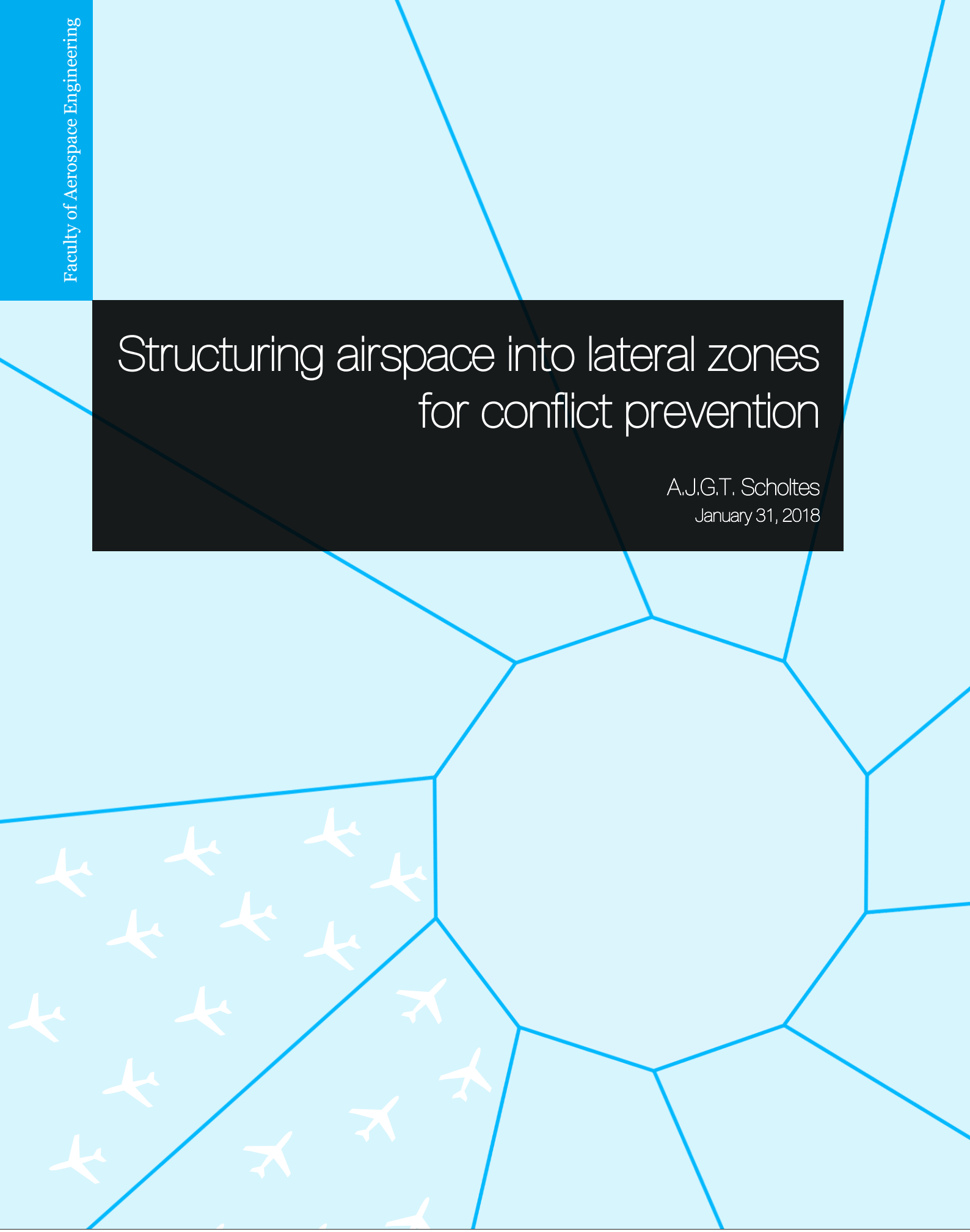

TU Delft Delft University of Technology

Challenge the future

Structuring airspace into lateral zones for conflict prevention

by

A.J.G.T. Scholtes

to obtain the degree of Master of Science
at the Delft University of Technology,
to be defended publicly on Wednesday January 31, 2018 at 9:30.

Student number:	4139011	
Project duration:	March 6, 2017 – January 31, 2018	
Thesis committee:	Prof. dr. ir. J. M. Hoekstra	TU Delft, supervisor
	Dr. ir. J. Ellerbroek	TU Delft, supervisor
	Dr. A. Sharpanskykh	TU Delft
	Ing. F. Bussink	NLR

An electronic version of this thesis is available at `http://repository.tudelft.nl/`.

TU Delft Delft University of Technology

Preface

This report concludes the work done on my MSc Thesis entitled “Structuring airspace into lateral zones for conflict prevention". Performing this research was challenging, but also very satisfactory. I would like to thank my thesis supervisors for their guidance and support. Jacco and Joost, your expertise and enthusiasm were really important for making this research a success.

This report also marks the end of my student years in Delft. I can look back at an amazing six and a half years, in which I learned a lot, but more importantly, in which I had a lot of fun. Therefore, I would like to thank everyone that helped creating all the great memories along the way. Bestuursgenoten, commissiegenoten, studiegenoten, huisgenoten, afstudeerkamergenoten, reisgenoten: bedankt, ik had geen moment willen missen.

I would also like to thank my parents and sisters. You have taught me to be eager, to follow my dreams, and you have always supported my decisions. Thanks to you I was able to say yes to every adventure that crossed my path. Finally, I want to thank my boyfriend Luka. Thank you for always being there for me, and for all the effort that went into reading my paper. I am looking forward to our adventure in Australia together.

Anouk Scholtes
Delft, January 2018

Contents

List of Figures viii

List of Tables xii

List of Abbreviations xiv

List of Symbols xv

Report Outline 1

I Scientific paper 2

II Appendices 19

A Zone radius experiment 21
A.1 Single-layer Point Merge System . . . 21
A.1.1 Safety . . . 21
A.1.2 Efficiency . . . 25
A.1.3 Stability . . . 25
A.2 Multi-layer Point Merge Systems . . . 26
A.2.1 Safety . . . 26
A.2.2 Efficiency . . . 30
A.2.3 Stability . . . 30

B Absorption capability of the Point Merge Systems 32
B.1 Scenario generation . . . 32
B.2 Results . . . 34

C Details conflicts and intrusions measured in the main experiment 36
C.1 Conflicts . . . 36
C.1.1 Box plots categorized by traffic mix . . . 36
C.1.2 Box plots categorized by aircraft type . . . 37
C.1.3 Conflict locations categorized by traffic mix . . . 40
C.1.4 Summarizing tables . . . 45
C.2 Intrusions . . . 46
C.2.1 Box plots categorized by traffic mix . . . 46
C.2.2 Box plots categorized by aircraft type . . . 47
C.2.3 Intrusion locations categorized by intrusion severity . . . 50
C.2.4 Intrusion locations categorized by traffic mix . . . 55
C.2.5 Summarizing tables . . . 60

D Significance tables 61
D.1 Number of conflicts . . . 61
D.2 Number of intrusions . . . 62
D.3 Intrusion severity . . . 63
D.4 Intrusion Prevention Rate . . . 64
D.5 Number of sequencing errors . . . 65
D.6 Average delays . . . 66
D.7 Extra distance flown . . . 67
D.8 Domino Effect Parameter . . . 68

E Source code BlueSky plug-in 70

III Preliminary report (already graded) 76

1 Introduction 78

2 Network organization 80
2.1 Centralized network . . . 81
2.2 Decentralized network . . . 81
2.3 Distributed network . . . 81
2.4 Network organization in the context of ATM . . . 81

3 Metropolis: urban airspace design 83
3.1 Traffic scenarios. . . . 84
3.1.1 Population size. . . . 84
3.1.2 Traffic volumes. . . . 84
3.1.3 Simulation area . . . 85
3.2 Concepts . . . 86
3.2.1 Common elements. . . . 86
3.2.2 Full mix . . . 87
3.2.3 Layers . . . 87
3.2.4 Zones . . . 88
3.2.5 Tubes . . . 90
3.3 Results . . . 91
3.3.1 Traffic volume and density . . . 91
3.3.2 Complexity. . . . 91
3.3.3 Safety . . . 93
3.3.4 Route efficiency . . . 95
3.3.5 Stability . . . 96
3.3.6 Capacity . . . 97
3.4 Conclusions. . . . 97
3.5 Lessons learned . . . 98
3.5.1 Setting up an experiment . . . 98
3.5.2 Zone specific results . . . 98

4 Influence of traffic structure on airspace capacity 99
4.1 Global conflict rate . . . 99
4.2 Spreading effect . . . 100
4.3 Reduction of relative velocity effect . . . 101
4.4 Conflict rate in terms of airspace design parameters . . . 102
4.5 Onion research proposal . . . 103

5 Conflict detection & resolution algorithms 104
5.1 State estimation and projection . . . 105
5.2 Conflict detection . . . 106
5.3 Conflict resolution . . . 106
5.4 Modified voltage potential algorithm . . . 107
5.5 Modifications for small vehicles. . . . 108

6 Merging 110
6.1 Theory of point merge technique . . . 111
6.2 Different configurations of the Point Merge method . . . 112

7 Sequencing 113
7.1 Arrival Manager tool . . . 113
7.2 Combining sequencing tools with point merge . . . 114

8 Experiment proposal **116**
8.1 Scenario selection. . . . 116
8.2 Selecting independent variables . . . 117
8.2.1 Experiment phase I . . . 118
8.2.2 Experiment phase II . . . 119
8.2.3 Experiment phase III. . . . 119
8.3 Dependent variables . . . 120
8.3.1 Safety . . . 120
8.3.2 Efficiency . . . 120
8.3.3 Stability . . . 121
8.3.4 Structural complexity . . . 122
8.4 Vehicle types . . . 123
8.4.1 PAVs . . . 123
8.4.2 UAVs . . . 123
8.4.3 Scalability of the zone concept . . . 124
8.5 Conflict detection & resolution . . . 125
8.6 Traffic separation in the inner circle. . . . 126
8.6.1 Arriving traffic . . . 126
8.6.2 Departing traffic . . . 128
8.7 Simulation area . . . 128
8.8 Project planning . . . 129

Bibliography **131**

List of Figures

A.1 Effect of traffic flow on number of conflicts for different zone radii with single-layer Point Merge Systems. . . . 22
A.2 Effect of traffic flow on number of intrusions for different zone radii with single-layer Point Merge Systems. . . . 22
A.3 Effect of traffic flow on maximum intrusion severity in the scenario for different zone radii with single-layer Point Merge Systems. . . . 23
A.4 Effect of traffic flow on the intrusion severity for different zone radii with single-layer Point Merge Systems. . . . 23
A.5 Effect of traffic flow on the Intrusion Prevention Rate for different zone radii with single-layer Point Merge Systems. . . . 24
A.6 Effect of traffic flow on the total number of sequencing problems per scenario for different zone radii with single-layer Point Merge Systems. . . . 24
A.7 Effect of traffic flow on the average delay w.r.t. earliest possible arrival time for different zone radii with single-layer Point Merge Systems. . . . 25
A.8 Effect of traffic flow on the extra distance flown w.r.t. a direct flight for different zone radii with single-layer Point Merge Systems. . . . 25
A.9 Effect of traffic flow on the Domino Effect Parameter for different zone radii with single-layer Point Merge Systems. . . . 26
A.10 Effect of traffic flow on number of conflicts for different zone radii with multi-layer Point Merge Systems. . . . 26
A.11 Effect of traffic flow on number of intrusions for different zone radii with multi-layer Point Merge Systems. . . . 27
A.12 Effect of traffic flow on maximum intrusion severity in the scenario for different zone radii with multi-layer Point Merge Systems. . . . 27
A.13 Effect of traffic flow on the intrusion severity for different zone radii with multi-layer Point Merge Systems. . . . 28
A.14 Effect of traffic flow on the Intrusion Prevention Rate for different zone radii with multi-layer Point Merge Systems. . . . 28
A.15 Effect of traffic flow on the total number of sequencing problems per scenario for different zone radii with multi-layer Point Merge Systems. . . . 29
A.16 Effect of traffic flow on the average delay w.r.t. the earliest possible arrival time for different zone radii with multi-layer Point Merge Systems. . . . 30
A.17 Effect of traffic flow on the extra distance flown w.r.t. a direct flight for different zone radii with multi-layer Point Merge Systems. . . . 30
A.18 Effect of traffic flow on the Domino Effect Parameter for different zone radii with multi-layer Point Merge Systems. . . . 31

B.1 PAL-V trails in the inner circle after flying the full sequencing leg of the Point Merge System. . . . 33
B.2 PAL-V trails in the inner circle after a direct-to instruction upon entry of the sequencing leg of the Point Merge System. . . . 33
B.3 The Point Merge Systems in the concept with 6 zones are designed to be similar in size to the ones in the concept with 10 zones. . . . 34
B.4 Absorption capability of the sequencing leg of the Point Merge System (PMS) per aircraft type. . . . 34
B.5 The earliest safe arrival slot, indicated with a blue star, can be determined by combining the logged arrival time with the absorption capability, the arrival time of the preceding aircraft, and the time separation requirement. . . . 35

C.1 Number of conflicts measured for low traffic flow, sorted by traffic mix for different airspace concepts. . . . 36

C.2 Number of conflicts measured for medium traffic flow, sorted by traffic mix for different airspace concepts. . . . 37
C.3 Number of conflicts measured for high traffic flow, sorted by traffic mix for different airspace concepts. . . . 37
C.4 Number of conflicts measured for low traffic flow, sorted by aircraft type for different airspace concepts. . . . 38
C.5 Number of conflicts measured for medium traffic flow, sorted by aircraft type for different airspace concepts. . . . 38
C.6 Number of conflicts measured for high traffic flow, sorted by aircraft type for different airspace concepts. . . . 39
C.7 Conflict locations at low traffic flow for the unstructured airspace concept, categorized by traffic mix. . . . 40
C.8 Conflict locations at low traffic flow for the airspace concept with 6 zones, categorized by traffic mix. . . . 40
C.9 Conflict locations at low traffic flow for the airspace concept with 10 zones, categorized by traffic mix. . . . 41
C.10 Conflict locations at medium traffic flow for the unstructured airspace concept, categorized by traffic mix. . . . 41
C.11 Conflict locations at medium traffic flow for the airspace concept with 6 zones, categorized by traffic mix. . . . 42
C.12 Conflict locations at medium traffic flow for the airspace concept with 10 zones, categorized by traffic mix. . . . 42
C.13 Conflict locations at high traffic flow for the unstructured airspace concept, categorized by traffic mix. . . . 43
C.14 Conflict locations at high traffic flow for the airspace concept with 6 zones, categorized by traffic mix. . . . 43
C.15 Conflict locations at high traffic flow for the airspace concept with 10 zones, categorized by traffic mix. . . . 44
C.16 Number of intrusions measured for low traffic flow, sorted by traffic mix for different airspace concepts. . . . 46
C.17 Number of intrusions measured for medium traffic flow, sorted by traffic mix for different airspace concepts. . . . 47
C.18 Number of intrusions measured for high traffic flow, sorted by traffic mix for different airspace concepts. . . . 47
C.19 Number of intrusions measured for low traffic flow, sorted by aircraft type for different airspace concepts. . . . 48
C.20 Number of intrusions measured for medium traffic flow, sorted by aircraft type for different airspace concepts. . . . 48
C.21 Number of intrusions measured for high traffic flow, sorted by aircraft type for different airspace concepts. . . . 49
C.22 Intrusion locations at low traffic flow for the unstructured airspace concept, categorized by intrusion severity. . . . 50
C.23 Intrusion locations at low traffic flow for the airspace concept with 6 zones, categorized by intrusion severity. . . . 50
C.24 Intrusion locations at low traffic flow for the airspace concept with 10 zones, categorized by intrusion severity. . . . 51
C.25 Intrusion locations at medium traffic flow for the unstructured airspace concept, categorized by intrusion severity. . . . 51
C.26 Intrusion locations at medium traffic flow for the airspace concept with 6 zones, categorized by intrusion severity. . . . 52
C.27 Intrusion locations at medium traffic flow for the airspace concept with 10 zones, categorized by intrusion severity. . . . 52
C.28 Intrusion locations at high traffic flow for the unstructured airspace concept, categorized by intrusion severity. . . . 53
C.29 Intrusion locations at high traffic flow for the airspace concept with 6 zones, categorized by intrusion severity. . . . 53

C.30 Intrusion locations at high traffic flow for the airspace concept with 10 zones, categorized by intrusion severity. . . . 54
C.31 Intrusion locations at low traffic flow for the unstructured airspace concept, categorized by traffic mix. . . . 55
C.32 Intrusion locations at low traffic flow for the airspace concept with 6 zones, categorized by traffic mix. . . . 55
C.33 Intrusion locations at low traffic flow for the airspace concept with 10 zones, categorized by traffic mix. . . . 56
C.34 Intrusion locations at medium traffic flow for the unstructured airspace concept, categorized by traffic mix. . . . 56
C.35 Intrusion locations at medium traffic flow for the airspace concept with 6 zones, categorized by traffic mix. . . . 57
C.36 Intrusion locations at medium traffic flow for the airspace concept with 10 zones, categorized by traffic mix. . . . 57
C.37 Intrusion locations at high traffic flow for the unstructured airspace concept, categorized by traffic mix. . . . 58
C.38 Intrusion locations at high traffic flow for the airspace concept with 6 zones, categorized by traffic mix. . . . 58
C.39 Intrusion locations at high traffic flow for the airspace concept with 10 zones, categorized by traffic mix. . . . 59

2.1 Different network structures: a) centralized b) decentralized c) distributed [4] . . . 80

3.1 Work plan of the Metropolis project [25] . . . 83
3.2 The experiment area is a pie slice of the entire city, with a background area around it [26] . . . 85
3.3 Final simulation area geometry: trapezoidal experiment area surrounded by a squared background area [26] . . . 86
3.4 Four Metropolis concepts: number of constraints is incrementally increased [49] . . . 86
3.5 Layer concept for PAVs and UAVs [23] . . . 88
3.6 Top view on grid-like topology for UAVs [23] . . . 88
3.7 Side view of zone concept [23] . . . 89
3.8 Zone topology with distributor/collector areas and rings [23] . . . 89
3.9 Major flow areas in the zone concept enables safe merging of the flows [23] . . . 89
3.10 Side view of traffic exchange area [23] . . . 90
3.11 Example topology for the tube concept, illustrating the difference between the layers [23] . . . 90
3.12 Number of simulated flights per run for four different traffic volumes [25] . . . 91
3.13 Traffic density in simulation area (left) and experiment area (right) [25] . . . 92
3.14 Complexity function and proximity-convergence graph for different periods of the day [25] . . . 93
3.15 Average complexity value for different traffic densities [25] . . . 94
3.16 Means and 95% confidence intervals of the number of conflicts per flight [49] . . . 94
3.17 Means and 95% confidence intervals of the number of intrusions per flight [25] . . . 95
3.18 Means and 95% confidence intervals of the intrusion severity [25] . . . 95
3.19 Means and 95% confidence intervals of the IPR [49] . . . 96
3.20 Means and 95% confidence intervals of the work done [25] . . . 96
3.21 Venn diagram visualizing the DEP [49] . . . 96
3.22 Means and 95% confidence intervals of DEP [49] . . . 97
3.23 Variation of safety with traffic demand [25] . . . 97

4.1 Research to increase airspace capacity can be subdivided into different categories . . . 99
4.2 Relationship between the number of aircraft in the airspace and the global ('ground') and local ('air') conflict rate [22] . . . 100
4.3 Relative velocity of two aircraft flying with the same ground speed [20] . . . 101
4.4 The probability density function of the absolute difference between two uniform distributions becomes triangular [20] . . . 102

5.1 Conflict Detection & Resolution process [33] . . . 105
5.2 Different state propogation methods: nominal, worst case, probabilistic [33] . . . 105

5.3 Three steps of the Modified Voltage Potential algorithm [36] . . . 107
5.4 Computation of the MVP displacement vector [36] . . . 108

6.1 The merging of arrival flows can be represented as a black box [11] . . . 110
6.2 Different merging and spacing techniques[19] . . . 111
6.3 Example geometry of a Point Merge System [11] . . . 111
6.4 Means and standard diviation of the flight level inside the TMA [27] . . . 112
6.5 Different PMS configurations [11] . . . 112

7.1 Pre-sequencing is needed to meet downstream capacity constraints [11] . . . 113
7.2 Different modules of the AMAN tool [55] . . . 114
7.3 Flown trajectories with AMAN (left) and AMAN+ASAS (right) [5] . . . 115
7.4 Throughput with AMAN (left) and AMAN+ASAS (right) [5] . . . 115

8.1 Different departure/arrival areas that were considered . . . 117
8.2 Selected concept configuration . . . 118
8.3 Intrusion path through the protected zone (gray area) of an aircraft [49] . . . 121
8.4 Venn diagram visualizing the DEP [49] . . . 121
8.5 Converging and diverging aircraft [24] . . . 122
8.6 Similar average complexity can be a result of different complexity functions [24] . . . 123
8.7 Computation of the MVP displacement vector [36] . . . 126
8.8 Example geometry of a Point Merge System [11] . . . 127
8.9 Arriving traffic flows from the zones will be merged by using multiple Point Merge Systems . . . 127
8.10 Departing traffic leaves the inner circle perpendicular to the radius . . . 128
8.11 The circular shapes of the zones are designed to be polygonal shapes . . . 128
8.12 Proposed work breakdown structure . . . 129
8.13 Gantt chart with work packages and milestones . . . 130

List of Tables

A.1 Experiment matrix: Zone radius selection 21

B.1 Altitude restrictions for the sequencing legs of the Point Merge Systems per aircraft type 32
B.2 Experiment matrix: Point Merge System absorption 32

C.1 Total number of conflicts for low traffic flow 45
C.2 Total number of conflicts for medium traffic flow 45
C.3 Total number of conflicts for high traffic flow 46
C.4 Total number of intrusions for low traffic flow 60
C.5 Total number of intrusions for medium traffic flow 60
C.6 Total number of intrusions for high traffic flow 60

D.1 Mauchly's test of sphericity for the number of conflicts 61
D.2 Tests of within-subjects effects for the number of conflicts 61
D.3 Pairwise comparison effect of the number of zones on the number of conflicts 62
D.4 Pairwise comparison effect of the traffic flow on the number of conflicts 62
D.5 Mauchly's test of sphericity for the number of intrusions 62
D.6 Tests of within-subjects effects for the number of intrusions 62
D.7 Pairwise comparison effect of the number of zones on the number of intrusions 63
D.8 Pairwise comparison effect of the traffic flow on the number of intrusions 63
D.9 Mauchly's test of sphericity for the intrusions severity 63
D.10 Tests of within-subjects effects for the intrusions severity 63
D.11 Pairwise comparison effect of the number of zones on the intrusions severity 64
D.12 Pairwise comparison effect of the traffic flow on the intrusions severity 64
D.13 Mauchly's test of sphericity for the Intrusion Prevention Rate 64
D.14 Tests of within-subjects effects for the Intrusion Prevention Rate 64
D.15 Pairwise comparison effect of the number of zones on the Intrusion Prevention Rate 65
D.16 Pairwise comparison effect of the traffic flow on the Intrusion Prevention Rate 65
D.17 Mauchly's test of sphericity for the number of sequencing issues 65
D.18 Tests of within-subjects effects for the number of sequencing issues 65
D.19 Pairwise comparison effect of the number of zones on the number of sequencing issues 66
D.20 Pairwise comparison effect of the traffic flow on the number of sequencing issues 66
D.21 Mauchly's test of sphericity for the average arrival delay with respect to a direct-to at the entrance of the Point Merge System 66
D.22 Tests of within-subjects effects for the average arrival delay with respect to a direct-to at the entrance of the Point Merge System 66
D.23 Pairwise comparison effect of the number of zones on the average arrival delay with respect to a direct-to at the entrance of the Point Merge System 67
D.24 Pairwise comparison effect of the traffic flow on the average arrival delay with respect to a direct-to at the entrance of the Point Merge System 67
D.25 Mauchly's test of sphericity for the extra distance flown with respect to a direct flight 67
D.26 Tests of within-subjects effects for the extra distance flown with respect to a direct flight 67
D.27 Pairwise comparison effect of the number of zones on the extra distance flown with respect to a direct flight 68
D.28 Pairwise comparison effect of the traffic flow on the extra distance flown with respect to a direct flight 68
D.29 Mauchly's test of sphericity for the Domino Effect Parameter 68
D.30 Tests of within-subjects effects for the Domino Effect Parameter 68
D.31 Pairwise comparison effect of the number of zones on the Domino Effect Parameter 69

D.32 Pairwise comparison effect of the traffic flow on the Domino Effect Parameter 69

8.1 Variables to be computed in experiment phase I 118
8.2 Experiment matrix of phase II 119
8.3 Performance specifications PAL-V Europe [42] 124
8.4 Performance specifications Terrafugia TF-X [52] [24] 124
8.5 Performance specifications AW609 [35] 124
8.6 Performance specifications MD4-3000 [24] 125
8.7 Proposed project milestones 129

List of Abbreviations

AAH	Active Advisory Horizon
ADS-B	Automatic Dependent Surveillance-Broadcast
AMAN	Arrival Manager
AOCC	Airline Operation Control Center
ARSIM	AMAN Research Simulator
ATC	Air Traffic Control
ATCo	Air Traffic Control Officer
ATM	Air Traffic Management
BADA	Base of Aircraft Data
CD	Conflict Detection
CD&R	Collision Detection & Resolution
CP	Conflict Prevention
CPA	Closest Point of Approach
CR	Conflict Resolution
DEP	Domino Effect Parameter
EH	Eligibility Horizon
ETA	Expected Time of Arrival
E-TMA	Extended Terminal Area
ETO	Expected Time Over
FH	Freeze Horizon
IAF	Initial Approach Fix
IPR	Intrusion Prevention Rate
IPZ	Intruder Protected Zone
KPA	Key Performance Area
LAS	Last Assigned Slot
LIV	Landing Interval
LNAV	Lateral Navigation
LOS	Loss of Separation
NASA	National Aeronautics and Space Administration
NLR	Nederlands Lucht- en Ruimtevaartcentrum
MSA	Minimum Safe Altitude
MTOW	Maximum Take-Off Weight
MVP	Modified Voltage Potential
NDB	Non-Directional Beacon
PAV	Personal Aerial Vehicle
PMS	Point Merge System
RNAV	Area Navigation
STA	Scheduled Time of Arrival
SYSCO	System Supported Coordination
TCAS	Traffic alert and Collision Avoidance System
TFM	Traffic Flow Management
TMA	Terminal Area
UAV	Unmanned Aerial Vehicle

List of Symbols

α	Heading span [°]
A	Airspace area [m^2]
C	Convergence [−]
CR	Conflict rate [−]
d	Distance between aircraft [m]
d_{ij}	Relative distance between aircraft i and j [m]
$\text{int}_{\text{severity}}$	Intrusion severity [−]
L	Number of layers [−]
N	Number of aircraft in a sector [−]
P	Proximity [−]
p_{ij}	Normalized relative distance between aircraft i and j [m]
p_{layer}	Probability of two aircraft having a conflict in one layer [−]
p_2	Probability of two aircraft having a conflict when flying a direct route through an airspace [−]
R	Minimum separation distance [m]
r_{ij}	Level of variation of the relative distance between aircraft i and j [m/s]
R_{inner}	Radius of the inner circle [m]
R_{zones}	Radius of the zones [m]
s	Displacement vector [m]
T	Thrust vector [N]
T_{FL}	Average time aircraft spends in the airspace [s]
T_{tot}	Total observation time [s]
t_C	Time at which the closest point of approach is predicted [s]
$\overline{V}$	Average ground speed [m/s]
v_{rel}	Relative velocity [m/s]
W	Work done [Nm]
x_{rel}	Relative distance [m]

Report Outline

This thesis report is divided into three parts:

I. **Scientific paper:** Contains all relevant information and results about the conducted research.

II. **Appendices:** Contains additional details and plots.

III. **Preliminary report:** Contains the literature review and experiment proposal of the research.

The last part is already evaluated and graded, and is only attached for completeness of this document.

Part I
Scientific paper

Can structuring airspace into lateral zones act as conflict prevention mechanism?

A.J.G.T. Scholtes (MSc Student)
Supervisors: Prof. dr. ir. J.M. Hoekstra, dr. ir. J. Ellerbroek
Section Control & Simulation, Department Control and Operations, Faculty of Aerospace Engineering, Delft University of Technology, Delft, Netherlands

***Abstract*— In an effort to accommodate the increasing air traffic demand, research is conducted to increase future airspace capacity. In addition to the growing demand, new forms of air transport are entering the market. Although a distributed control strategy seems unavoidable to cope with the introduction of Unmanned Aerial Vehicles and Personal Air Vehicles, research on how this distributed control should be organized has not yet reached consensus. Prior research has demonstrated that structuring airspace into layers results in a lower conflict rate compared to an unstructured airspace. The principles of aircraft dispersion and relative velocity reduction in the layers have a positive effect on airspace capacity, and these principles are further explored in this research. In a large-scale simulation experiment with a mix of different Personal Air Vehicles, the value of defining lateral zones in a departure/arrival area was investigated. By comparing the zones concept with an unstructured airspace concept, it was found that structuring the airspace can act as a conflict prevention mechanism. The added value of the zones becomes more apparent at higher traffic densities. Different zone configurations were evaluated and compared. Simulation results show that a configuration with a higher number of zones results in the lowest overall number of conflicts, at the cost of a slight efficiency loss.**

***Index Terms*—urban airspace, structure, lateral zones, airborne separation assurance, self-separation, conflict prevention, Modified Voltage Potential (MVP), Personal Air Vehicle (PAV)**

I. Introduction

CONVENTIONAL air traffic has traditionally been guided and separated by centralized control [1]. As a result, the current breakdown of the airspace is mainly based on controller workload limitations [2], [3]. In the meantime, air traffic demand is still increasing, and the current architecture is reaching the limits of its ability to accommodate this increasing demand [4].

Much research in the field of air traffic control is dedicated to finding the airspace organization that best suits future needs. Some research focuses on upgrading the current centralized control by restructuring sectors or by changing the sectors more dynamically based on demand [2]. An alternative path concentrates on the use of a distributed control to achieve the needed capacity increase. A distributed control strategy seems to be inevitable to remove controller workload limitations in the future, but research on how this distributed control should be organized has not yet reached consensus. Free flight research predicts that higher traffic densities can be achieved when the traffic flow constraints are reduced [5], [6]. Other projects predict that structuring of airspace is key in increasing the airspace capacity [7], [8]. This illustrates that the research community has not yet found the optimal level of structuring to maximize capacity.

In addition to the growing demand of conventional air traffic, new forms of air transport such as drones and Personal Air Vehicles (PAVs) are entering the market. The current airspace structure is not able to support these new types of airspace usage [9], and in the future the number of vehicles in the airspace will definitely exceed the capacity of the current structure. Although the first flying cars are now for sale [10], it is still unclear how the airspace and air traffic control need to be re-organized to facilitate them.

Little research has been done in the field of urban airspace design. Prior research by TU Delft has shown that in urban areas, distributed control with a limited structure of layers can result in a safer and more efficient use of the airspace than an unstructured airspace [11]. It was demonstrated that the conflict rate can be reduced by spreading the traffic over altitude layers and by sorting the traffic by heading [12].

However, when considering traffic scenarios that have primarily horizontal demand patterns, for example in an en-route funnel generated by multiple weather cells or special use airspace blocks, the layers concept is no longer adequate. Around a departure/arrival area the layers concept is also not suitable. In these scenarios, all aircraft are trying to leave or reach the same location on the ground. Spreading aircraft into altitude layers based on their heading is no longer an option, since aircraft from all different directions intend to reach the same altitude. In this research it will be investigated whether in these areas it is best to provide a different structure, or to switch to an unstructured airspace. It is chosen to investigate the lateral zone concept in a departure/arrival area, since the benefit of a horizontal structure is expected to be highest here.

The objective of this research is to investigate the value of defining lateral zones in a departure/arrival area, by running and comparing fast-time simulations of high density traffic in a structured and unstructured airspace. This objective is linked to the following research question: How does a structured airspace with lateral zones compare to an unstructured airspace in terms of safety, efficiency and stability in high density traffic scenarios in a departure/arrival area? It is expected that the aircraft dispersion and relative velocity reduction in the structured concept will result in a reduced conflict rate. By separating aircraft into diverging and converging lateral zones, it is hypothesized that fewer conflicts will arise. The benefit

of the zone structure is expected to be highest in scenarios with high traffic densities, when aircraft have less maneuvering space. It is expected that the improvement in safety comes at the cost of a slight decrease in efficiency.

Section II introduces the different airspace concepts investigated and compared in this research. In Section III, the experiment design is outlined. The resulting performance is presented in Section IV. In Section V the results are discussed, and finally Section VI concludes the research.

II. Concepts

In this section, the different airspace concepts compared in this research are described in more detail. Section II-A and II-B describe the unstructured and structured airspace concepts respectively.

A. Unstructured airspace concept

The unstructured airspace concept is based on the assumption that higher traffic densities can be achieved when the traffic flow constraints are reduced as much as possible [5], [6], [13]. Aircraft in this concept fly a direct route from origin to final approach, and no restrictions are set on the flight path. To enable a fair comparison between the unstructured and structured concepts, the merging of arrival and departure streams has to be equal. In the subsequent sections, the chosen Collision Detection and Resolution (CD&R) method, and the merging of arriving and departing traffic is described.

1) CD&R: In a free flight study performed by the Netherlands Aerospace Center (NLR) and National Aeronautics and Space Administration (NASA), several different conflict resolution algorithms were tested. The resolution method that was developed by Eby [14] proved to be most effective for decentralized control, also in high traffic density scenarios [6]. The algorithm of Eby makes use of nominal state propagation assumption, and considers the horizontal and vertical dimensions.

An analogy for the method that forms the basis of Eby's algorithm is the voltage potential. This method compares aircraft and their destinations to electrically charged particles. As a result, repulsive forces between the aircraft exist, and by summing all the repulsive forces of the traffic, a vector can be determined that ensures separation with other aircraft is maintained. Eby's method was slightly adapted by Hoekstra et al. to provide a more pragmatic approach to solving conflicts [15]. Additionally, rules of implicit coordination were added to Eby's method. The resulting method is known as the Modified Voltage Potential (MVP). The MVP method was selected for this research, since its success in a decentralized airspace is well established.

The geometry of a conflict situation should be evaluated more thoroughly to understand how the resolution vector is computed. Figure 1 shows two aircraft, A and B; the relative velocity of aircraft B with respect to aircraft A is pointing through the Intruder Protected Zone (IPZ) of A. The Closest Point of Approach (CPA) of A and B is point C, and the goal is to move point C outside of the IPZ. Point O is the closest distance out of the IPZ, however the straight line from B to O still crosses the IPZ of A. Therefore, line CO needs to be multiplied with a slight factor, computed by [15]:

$$\frac{|CO|}{|CO'|} = \left|\cos\left(\arcsin\left(\frac{R}{AB}\right) - \arcsin\left(\frac{AC}{AB}\right)\right)\right| \quad (1)$$

The resolution vector (V_{MVP}) is perpendicular to the relative velocity. MVP makes use of implicit coordination, and the other aircraft is automatically resolving in the opposite direction.

The separation requirements are computed to ensure minimum 1 second spacing between two vehicles with respect to the fastest flying vehicle in the airspace. Within the look-ahead time, two vehicles of the fastest type should still be able to solve a head-on conflict. Incorporating a 10% safety margin and rounding up to the nearest multiple of 50 results in a 350 m horizontal separation requirement in this experiment. The vertical separation requirement is determined to be 50 m. Trial runs demonstrated that a look-ahead time of 60 s that was adopted in the Metropolis project [16], was also adequate for this experiment.

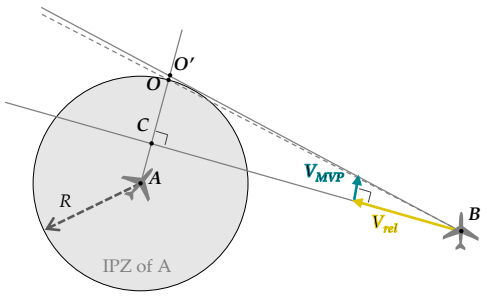

Fig. 1. Computation of the MVP displacement vector (adapted from [17]).

2) Merging of arrival traffic: In a departure/arrival area, the merging and sequencing of the arriving traffic is a big challenge. Since it is not part of the research objective to develop and evaluate a new merging concept, the Point Merge method was chosen. This method fully relies on existing technology and it has been proven to be safe and efficient [18]. The so called Point Merge System makes use of merge points and pre-defined sequencing legs that can be used to stretch or shorten the aircraft path [18]. The sequencing legs are designed to always have the same distance away from the merge point. An example geometry of a Point Merge System with two entry points and sequencing legs is shown in Figure 2. The entire sequencing leg is programmed in the Flight Management System (FMS) and therefore no controller intervention is required to perform path stretching. Spacing is monitored by giving aircraft a "direct-to merge point" instruction at the appropriate time [19]. This instruction can be given at any location in the sequencing leg, resulting in a shorter path to the merge point.

Using a single-layer Point Merge System for multiple aircraft types resulted in merging problems, since the differences

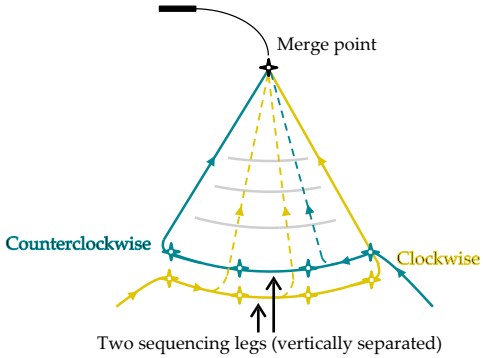

Fig. 2. Example geometry of a Point Merge System (adapted from [19]).

in speed and maneuverability were too high. In a preliminary experiment, it was found that a system of multi-layer Point Merge Systems was effective in merging the arrival streams of different aircraft types. In literature, a framework of multi-layer Point Merge Systems is also mentioned to show promising results in the development of an autonomous system for arrival aircraft in the terminal area [20], [21]. For each aircraft type, one clockwise and one counterclockwise sequencing leg was designed based on the outcome of the preliminary experiment. Table I summarizes the chosen altitudes for the Point Merge Systems used in this research.

TABLE I
ALTITUDE RESTRICTIONS FOR THE SEQUENCING LEGS OF THE POINT MERGE SYSTEMS

Aircraft type	Clockwise leg	Counterclockwise leg
Heavy	FL70	FL60
Medium	FL50	FL40
Light	FL30	FL20

3) Departing traffic: The departing aircraft leave the inner circle of the concept as illustrated in Figure 3. Aircraft fly towards the edge of the inner circle and from there they fly a circular path. As soon as possible, they leave the inner circle at the location that suits their flight plan best. For this study, finding the optimal method to separate departing and arriving aircraft inside the inner circle is considered out of scope. However, a possible solution could be to direct departing aircraft to the outer edge of the circle, and let them perform a spiral climb to the point where they want to leave the circle. Arriving aircraft fly a continuous descent from their sequencing leg. By assuring that departing aircraft fly immediately to the edge of the inner circle and do not climb higher than the lowest sequencing leg in their spiral climb, departing and arriving aircraft are separated inside the circle.

B. Laterally structured airspace concept

The structured airspace concept consists of lateral zones that are used to separate arriving and departing aircraft close to the center of the departure/arrival area. The hypothesis is that by moving the conflicts between arriving and departing

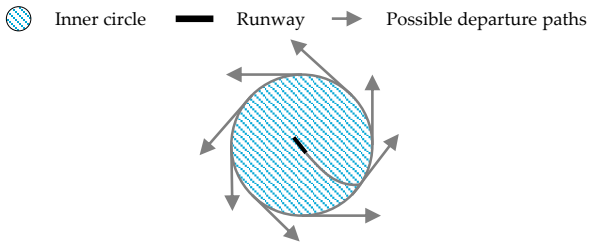

Fig. 3. Departing traffic leaves the inner circle perpendicular to the radius.

traffic away from the center, the maneuvering space increases, therefore reducing the overall number of conflicts in the scenario.

During the design phase of the zone structure, multiple concepts were evaluated. Starting with an area with 8 zones, it was found that the traffic in the opposing zones would result in potential head-on conflicts as illustrated in Figure 4. To ensure that traffic in opposing zones does not have opposing travel directions, the following relationship should hold:

$$N = 4k + 2 \quad \text{for} \quad \{k \in \mathbb{Z} \mid k > 0\} \tag{2}$$

Here, N is the number of zones. For example, if $k = 1$, this results in a configuration with 6 zones.

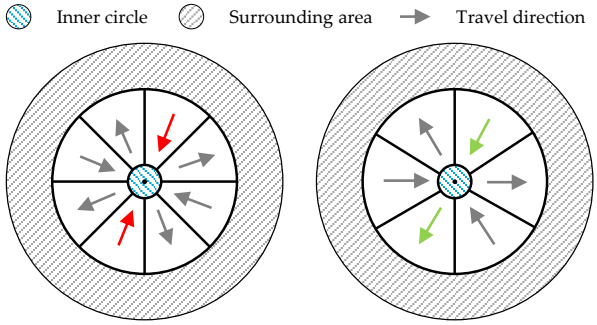

Fig. 4. A structure with 8 zones results in potential head-on conflicts, directly affecting safety.

The inner circle in Figure 4 facilitates the merging of arriving and departing traffic as explained in the previous section. In each arrival zone, a Point Merge System is designed at the inner radius. Departing traffic should be able to leave the inner circle similar to the departing traffic in the unstructured concept. Therefore, some refinements to the zone structure are required. From Figure 3 it can be seen that departing aircraft use counterclockwise circling to leave the inner circle. To facilitate the departure, the zones are slightly skewed counterclockwise as shown in Figure 5. Departing aircraft can only leave through a diverging zone once the zone structure is active, and therefore some of the possible paths in Figure 3 are no longer allowed.

The proposed zone structure is enforced both strategically and tactically, as will be discussed in the next sections.

1) Strategic: In the flight planning phase, the zone structure can already be taken into account to prevent drastic maneuvers

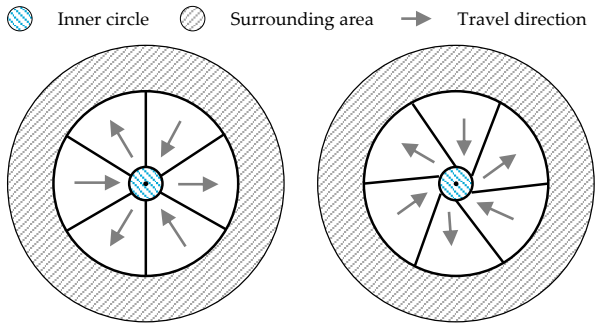

Fig. 5. To facilitate efficient departure and arrival, the zones are slightly skewed.

near the edges of the zones. Therefore, an additional waypoint is added in the planning phase, enforcing the structure pre-flight. Arriving aircraft could be directed to the arrival zone closest to their origin. However, as illustrated in Figure 6, this results in potential head-on conflicts directly outside the zone structure.

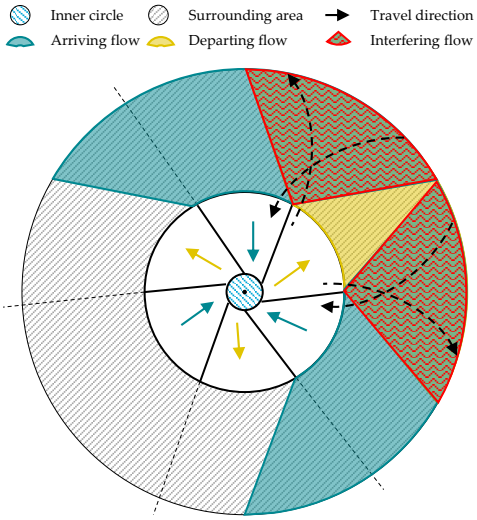

Fig. 6. Directing arriving aircraft to the arrival zone closest to their origin results in potential head-on conflicts in the red regions.

This problem is solved by directing arriving aircraft to the first arrival zone that they can reach clockwise. In this way, the location of the additional waypoint is corresponding with the skewed structure of the zones. Departing aircraft are assigned to a departure zone based on their destination. In case the destination is in line with an arrival zone, the aircraft is assigned to the departure zone clockwise of this arrival zone. Similarly, arriving aircraft that are not directly in line with an arrival zone are directed to the zone clockwise to the departure zone. Figure 7 illustrates this by showing the angles from which aircraft are directed to the designated zone.

Arriving aircraft that entered the surrounding area in line of a departure zone can be assigned a waypoint directly at the edge of the arrival zone clockwise to it to ensure the least degradation of efficiency given the zone structure. However,

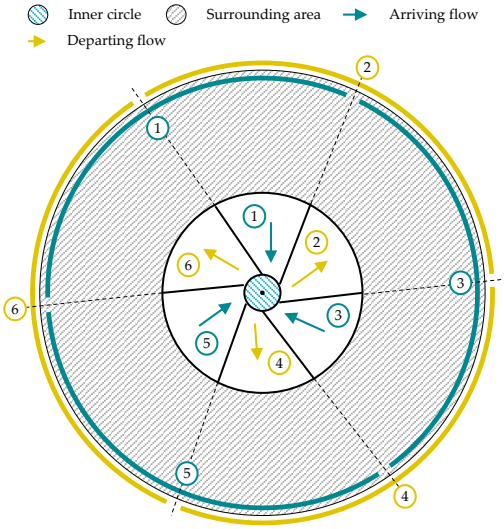

Fig. 7. Based on the origin of arriving aircraft, and the destination of departing aircraft, aircraft are assigned and directed to the designated zone.

this results in an accumulation of arrival streams at the edge of the zone, directly increasing the conflict likelihood. To solve this issue, arrival streams are spread uniformly over the zone. The arc at the edge of the surrounding area stretches double the angle of the associated arrival zone. The waypoint on the zone edge is directly proportional to the location of entrance at the edge of the surrounding area, as illustrated in Figure 8.

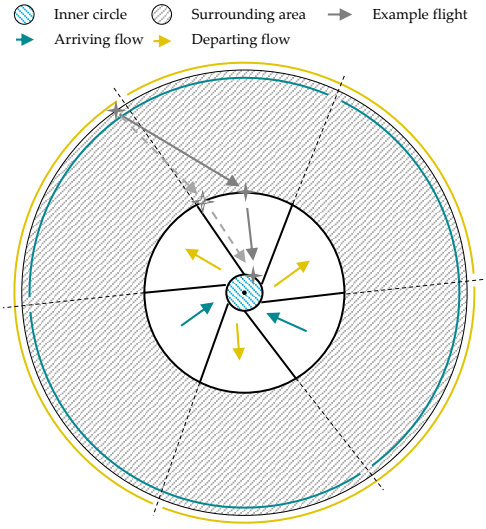

Fig. 8. Instead of adding a waypoint that results in the shortest flight path (dashed gray flight path), arriving aircraft are spread uniformly over the entire zone.

2) Tactical: Due to conflict resolution, aircraft can start to deviate from their original flight plan. Therefore, tactical control should be in place to ensure aircraft do not enter the wrong zone. The two mechanisms in place will be discussed in this section.

First, aircraft that have already entered a zone can be pushed outside the zone through conflict resolution. A line intersection

method is used to predict edge surpassing, in order to steer an aircraft away from the edge before it leaves its zone. The line intersection can be approached as a two-dimensional vector problem, and by using cross products intersection can be evaluated [22]. As illustrated in Figure 9, the current aircraft position is known to be ac_1. By means of a nominal state propagation method, the position in the future can be determined to be ac_2. The corners of the zone edge are fixed ($edge_1$ and $edge_2$). The latitudes and longitudes of the ac and $edge$ positions are converted to a Cartesian coordinate system with the center of the zone concept used as $(0, 0)$. The flight path can be described as a line segment that runs from ac_1 to $ac_1 + r$, where r is equal to $ac_2 - ac_1$. Similarly, the zone edge can be described as a line segment that runs from $edge_1$ to $edge_1 + s$, where s is equal to $edge_2 - edge_1$.

The two line segments intersect if we can find a t and u where:

$$\overrightarrow{ac}_1 + t \cdot \overrightarrow{r} = \overrightarrow{edge}_1 + u \cdot \overrightarrow{s} \tag{3}$$

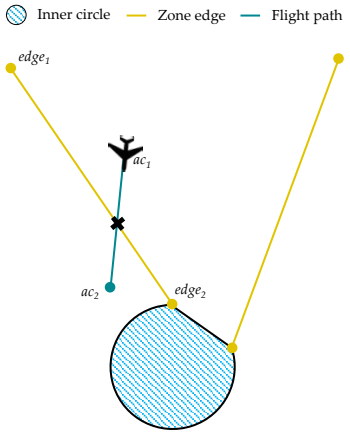

Fig. 9. A line intersection method is used to predict if an aircraft is about to cross a zone edge.

By taking the cross product of both sides of Equation 3 with s, and by using the fact that $s \times s = 0$, the problem can be rewritten:

$$t \cdot (\overrightarrow{r} \times \overrightarrow{s}) = \left(\overrightarrow{edge}_1 - \overrightarrow{ac}_1\right) \times \overrightarrow{s} \tag{4}$$

Now the equation can be solved for t:

$$t = \frac{\left(\overrightarrow{edge}_1 - \overrightarrow{ac}_1\right) \times \overrightarrow{s}}{(\overrightarrow{r} \times \overrightarrow{s})} \tag{5}$$

Similarly, by cross multiplying both sides of Equation 3 with r, the equation can be solved for u. The aircraft is about to cross a zone edge within the look-ahead time if $0 \leq u \leq 1$ and $0 \leq t \leq 1$. Based on whether the aircraft is flying in an arrival or departure zone, and whether it is flying closer to the left or the right edge, the aircraft is directed to a correctional waypoint in the appropriate direction.

The second mechanism prevents aircraft from entering the wrong zone. Conflict resolutions in the surrounding area can cause arriving aircraft to skip the waypoint at the zone edge and fly a direct route to their destination. In this case, arriving aircraft risk entering a departure zone. To avoid this, the intent of arriving aircraft that enter the circular area with a radius of 110% of the zone radius is evaluated. If an arriving aircraft in this area is flying towards a waypoint that is more than the zone radius away, it means that it has discarded the waypoint at the outer zone edge. If this is the case, it is evaluated whether the aircraft is about to enter a departure zone and if so, it is directed to the zone that belongs to the Point Merge sequencing leg that is programmed in its flight plan.

III. Experiment Design

Fast-time simulation experiments of high traffic densities were conducted. This experiment is performed using BlueSky, an open data and open source ATC simulator developed at the TU Delft [23]. The tool was extended with a plug-in to simulate the zone structure as described in the previous chapter. In this section the design of the experiment is described.

A. Simulation area

Since designing circular area edges requires many waypoints, polygonal shapes are used instead to design the zone structure (Figure 10).

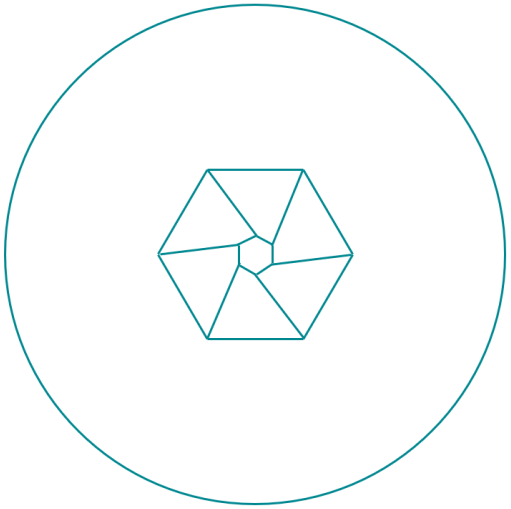

Fig. 10. The circular shapes of the zones are designed to be polygonal shapes.

The radius of the inner circle is derived from the descent angle of arriving aircraft. In congested areas, the Federal Aviation Administration (FAA) prescribes flying at a Minimum Safe Altitude (MSA) of 1,000 ft above the highest obstacle [24]. Taking into account the maximum building height of 1,000 ft in big cities, a MSA of 2,000 ft should be accounted for in this experiment. This can be directly translated into a minimum constraint on the radius of the inner circle, allowing aircraft to continuously descend to the runway. Most PAVs that are currently under development are Vertical Take-Off and Landing (VTOL) aircraft, or autogyros. Therefore, the descent angle of autogyros will be used to

derive the radius of the inner circle. Autogyros typically have a descent angle between 10 and 20 degrees, depending on different performance parameters of the vehicle [25]. For this research, a descent angle of 15 degrees in combination with the merge altitude of the autogyros is used to compute the required radius. The resulting inner radius that is used in all scenarios, is 4500 m.

In a preliminary investigation, the outer radius of the zones was varied to evaluate its effect on airspace performance. The motivation for the selected outer radius will be explained in detail in Section III-E. The simulation area is directly related to this outer radius, and is computed such that it introduces a maximum detour of 5% compared to a direct route from origin to destination in the airspace concept with 10 zones. To allow a fair comparison between the configurations with 6 and 10 zones, the simulation area is kept the same for all concepts.

Aircraft leaving the simulation area are deleted from the experiment. Inside the simulation area aircraft parameters are logged. To avoid spawning aircraft directly on top of departing aircraft at the edge of the simulation area, arriving aircraft are spawned slightly outside the area. In this way, head-on conflicts at the outer edge of the simulation area can still be solved instead of directly causing a (false) intrusion. Departing aircraft are spawned at the edge of the inner radius, where they leave the inner area.

B. Traffic scenarios

To test the ability of the different concepts to deal with traffic subjected to different performance limitations, a mix of different PAVs is used. Three different types are simulated: PAL-V, Terrafugia TF-X (TSTX) and Agusta Westland AW609 (A609). A combination of these three PAVs is chosen since the three types represent future substitutes for motorbikes, cars and minivans respectively. Both the TSTX and A609 are VTOL aircraft, and the PAL-V is an autogyro. In prior research on urban airspace design, an estimation for future traffic volumes per type was made. Based on the Metropolis project [26], a traffic distribution of 82% TSTX, 6% PAL-V and 12% A609 was adopted.

To simulate and predict the vehicle trajectories, adequate performance specifications are required. Unfortunately some PAVs are still in development, such that not all specifications are available yet. Therefore, a similar approach as in the Metropolis project [16] was taken to solve this. Parameters of existing aircraft performance models based on Eurocontrol's Base of Aircraft Data (BADA) were adapted to approximate the performance of the PAVs. From BADA release 3.12, the F-27, Piper Navajo, and Piper Cherokee BADA files were adapted to approach the A609, TSTX, and PAL-V performance respectively. Although this method is only a rough approximation of the performance of PAVs, it enables the comparison between different future airspace concepts with a mix of aircraft types.

The economic cruise speed for all three aircraft are provided by the manufacturer. Flying the highest possible altitude results in the highest engine efficiency [27], and therefore the aircraft performance models were used in simulations to evaluate the highest possible altitudes at which the aircraft were able to fly their economic speed. Table II summarizes the variables per aircraft type.

TABLE II
TRAFFIC VARIABLES PER AIRCRAFT TYPE

	TSTX	**PAL-V**	**A609**
Aircraft type	VTOL	Autogyro	VTOL
BADA model adapted	Piper Navajo	Piper Cherokee	F-27
Distribution [%]	82	6	12
Cruise speed [kts]	172	75	275
Cruise altitude [FL]	100	90	110

Naturally, the number of conflicts increases with increasing traffic densities. It is expected that the benefit of the zones is higher for scenarios with a high traffic flow. To verify this hypothesis, scenarios are developed with three different traffic flows.

Aircraft are spawned in a period of 3 hours. Three different traffic flows are tested, with an increasing number of aircraft per flow. Table III shows the total number of aircraft in the scenario and the fixed spawn interval per traffic flow. Departing and arriving aircraft are spawned in turns, meaning that in case of the medium traffic flow, an aircraft is entering the simulation area every 14 seconds.

TABLE III
TOTAL NUMBER OF AIRCRAFT IN THE SCENARIO AND SPAWN INTERVAL PER TRAFFIC FLOW

Traffic flow	**Total aircraft number**	**Spawn interval [s]**
Low	889	12.2
Medium	1539	7.0
High	2665	4.1

Finally, the demand pattern of the traffic (the ratio between departing and arriving aircraft) is kept constant (50-50) in this experiment. Although the possibility to absorb a changing demand pattern is relevant in evaluating the different concepts, the zones concept could be changed in the future to a dynamic zone definition. This capability is considered to be out of scope for this research, and therefore only the differences between the concepts at an equal distribution of departing and arriving traffic are evaluated.

C. Independent variables

The research question focuses on the question whether structuring traffic into lateral zones can be beneficial compared to an unstructured airspace. Multiple zone configurations are tested to evaluate the effect of changing the size of the zones. The first independent variable is therefore the number of zones. Concepts with 0 (unstructured), 6 and 10 zones are evaluated and compared. As explained in the previous section, traffic flow is increased over three levels. Table IV summarizes the variables that are taken up in the experiment matrix of phase II. To calculate the stability of the different concepts, the CD&R mode is toggled on and off. As a

result, $3 \times 3 = 9$ experimental conditions are tested, and each condition is evaluated for 100 repetitions. 50 repetitions are simulated with CD&R switched on, and the same 50 scenarios are repeated with CD&R switched off.

TABLE IV
EXPERIMENT MATRIX: TESTING DIFFERENT ZONE CONFIGURATIONS

Variable	Levels	Different values
Concept	3	0, 6 or 10 zones
Traffic flow	3	Low, medium or high

D. Dependent variables

The dependent variables are used as a metric to measure performance of the different airspace concepts. The research question aims to compare a structured airspace to an unstructured airspace in terms of safety, efficiency, and stability. The following sections address the dependent variables used to measure the performance in terms of these three categories.

1) Safety: It is hypothesized that fewer conflicts need to be solved in the structured airspace concept. Therefore, the first two variables that will be measured are the total number of conflict pairs, n_{conf}, and the total number of intrusion pairs, n_{intr}. Conflicts are defined as a predicted loss of separation (LOS) within the look-ahead time of the state propagation, whereas intrusions are defined to be an actual LOS. The Airborne Separation Assurance System (ASAS) implemented in BlueSky makes use of a nominal state propagation method. Aircraft only broadcast their own position and velocity by means of Automatic Dependent Surveillance-Broadcast (ADS-B), so intent information is not taken into account to estimate future aircraft positions. This results in situations as illustrated in Figure 11, where a conflict is detected between two arriving aircraft flying in a different zone. To avoid undesired conflict resolutions in these situations, resolutions are suppressed if both aircraft fly in the same direction but in different, non-adjacent zones (Figure 11), or if either one of the two aircraft in conflict is flying inside the inner radius. For safety reasons, conflicts within one zone or in adjacent zones are never suppressed, and neither are conflicts between aircraft that differ in flight direction. Although the suppressed conflicts were logged during the experiment, they were not taken into account for the conflict count (n_{conf}).

The intrusion count is not enough to evaluate safety, since one near-collision is still less desirable than four slight intrusions. Therefore, it is also important to compute the severity of the intrusions [17]:

$$LoS_{sev} = \max_{t_{0_{\text{int}}} - t_{1_{\text{int}}}} \left(\min \left(1 - \frac{d_h(t)}{R_h(t)}, 1 - \frac{d_v(t)}{R_v(t)} \right) \right) \quad (6)$$

Here, d_h and d_v are the horizontal and vertical distances between two aircraft, and R_h and R_v are the horizontal and vertical separation requirements respectively. $t_{0_{\text{int}}}$ and $t_{1_{\text{int}}}$ are the start and end times of the intrusion. The terms $1 - \frac{d}{R}$ are the horizontal and vertical intrusions that are normalized

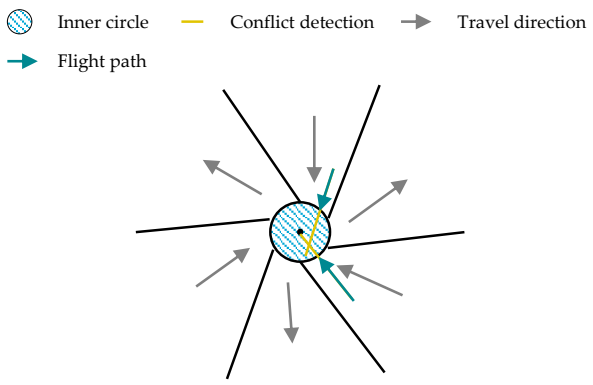

Fig. 11. At the center of the concept, a conflict between two arriving aircraft is detected. Since both aircraft will soon enter their Point Merge System, MVP method does not need to resolve this conflict.

to the separation requirements as visualized in Figure 12. In essence, the intrusion severity is a measure of how deeply the IPZ is intruded. By computing the maximum intrusion, the intrusion severity for the path in Figure 12 would be equal to the normalized horizontal intrusion at A. For all 50 repetitions of the experiment conditions, the maximum intrusion severity in the scenario is logged.

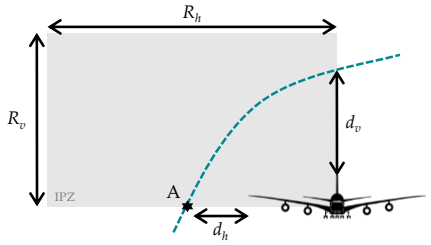

Fig. 12. Intrusion path through the IPZ (adapted from [16]).

The Intrusion Prevention Rate (IPR) will be computed to evaluate the ability to avoid conflicts from becoming intrusions. It is computed as follows:

$$IPR = \frac{n_{\text{conf}} - n_{\text{intr}}}{n_{\text{conf}}} \quad (7)$$

The last variable that is measured to evaluate safety is the number of sequencing issues ($n_{seqIssue}$). In the simulation, aircraft are programmed to fly the full Point Merge System sequencing leg to arrive to the runway, whereas in real operations they would have been directed to the merge point as soon as it was available. This results in the latest possible arrival time being logged for each aircraft. Post-processing this arrival data, realistic arrival times can be computed regressively.

A separate experiment was conducted to evaluate the absorption capabilities of the Point Merge sequencing legs for the different aircraft types. For the three types, two different scenarios were evaluated. In the first scenario, 500 aircraft flew the full sequencing leg to arrive to the runway. The second scenario considered equal flight plans and aircraft,

but now aircraft immediately received a "direct-to merge point" instruction when entering the sequencing leg. Based on the differences in arrival time between these two scenarios, the Point Merge System absorption time per aircraft was computed. Figure 13 shows that the absorption capability is smaller for the faster flying aircraft, as expected.

The latest possible arrival time followed directly from the simulation, and in combination with the absorption time the earliest possible arrival time can now be computed. From the preceding arrival time, the earliest safe arrival time can be determined using separation requirements. The spatial separation requirement is converted in a time based separation requirement, dependent on the aircraft type. When the earliest possible arrival time is later than the time separation requirement added to the arrival slot of the preceding aircraft, it can be concluded that the aircraft could have landed earlier. A sequencing problem is logged when there is no possibility to find an arrival slot that satisfies this condition. The total number of sequencing problems ($n_{seqIssue}$) per concept is compared.

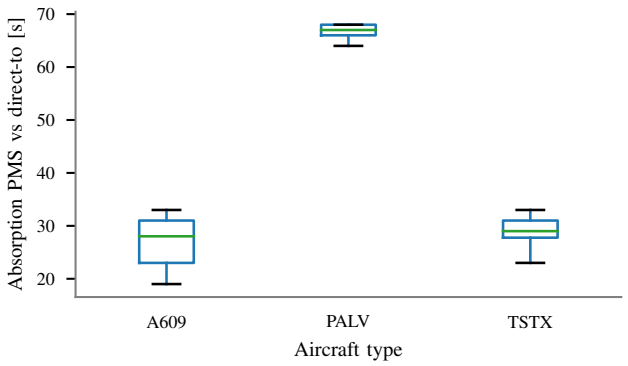

Fig. 13. Absorption capability of the sequencing leg of the Point Merge System (PMS) per aircraft type.

2) Efficiency: If the safety is improved at the cost of major deficiencies in flight paths, it can be concluded that the airspace organization is not successful. Therefore, it is important to quantify the differences in efficiency between the concepts. For the second category, two variables are measured. To compare the efficiency of the arrival sequence, the delay with respect to the earliest possible arrival slot in the Point Merge System is computed as follows:

$$t_{delay_i} = t_{arrival_i} - t_{earliest\_arrival_i}; i \in [1, n] \quad (8)$$

Here, n is the total amount of aircraft that are landing during the logging time, $t_{arrival}$ is the post-process computed arrival time of the aircraft, and $t_{earliest\_arrival}$ is the arrival time in case the aircraft would have gotten a "direct-to merge point" instruction directly upon entrance of the sequencing leg of the Point Merge System. The latter corresponds to the logged arrival time minus the absorption capability of the Point Merge System, as explained in the previous section. By computing all required delays based on the post-processed arrival slots, the average delay of the scenario can be computed. If the average delay is increased due to the airspace concept, it indicates less efficient aircraft arrivals.

Secondly, the extra distance flown due to the structure of the concept is computed by using the following formula:

$$d_{extra} = \frac{d_{flown} - d_{direct}}{d_{direct}} \cdot 100 \quad (9)$$

The distances are the three-dimensional distances flown by the aircraft.

3) Stability: One of the main concerns with decentralized traffic separation is that at high traffic densities, conflict chain reactions will occur. Therefore, airspace stability is included in the performance evaluation. Airspace stability is best described using the Domino Effect Parameter (DEP) [28]. Figure 14 shows a Venn diagram that can be used to visualize the DEP.

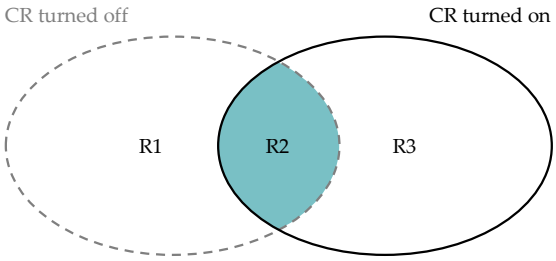

Fig. 14. Venn diagram visualizing the DEP (adapted from [16]).

R1 represents all aircraft that were in conflict when resolution was off, but did not have a conflict when CR was switched on. R2 are all aircraft that were in conflict in both situations, and R3 are all aircraft that did not have a conflict when resolution was off, but did have a conflict when it was on. DEP is defined as [29]:

$$DEP = \frac{R3 - R1}{R1} = \frac{R3}{R1} - 1 \quad (10)$$

High DEP values indicate airspace instability.

Table V summarizes all dependent variables in the experiment per category.

TABLE V
SUMMARY OF DEPENDENT VARIABLES

Category	Variable	Description
Safety	n_{conf} [-]	Number of conflict pairs
	n_{intr} [-]	Number of intrusion pairs
	LoS_{maxsev} [-]	Maximum severity of intrusions
	IPR [-]	Intrusion Prevention Rate
	$n_{seqIssue}$ [-]	Number of sequencing issues
Efficiency	t_{delay} [s]	Average arrival delay w.r.t. 'direct-to'
	d_{extra} [%]	Extra distance flown w.r.t direct flight
Stability	DEP [-]	Domino Effect Parameter

E. Zone radius selection

To evaluate the effect of varying the outer zone radius, a preliminary experiment was conducted. It was expected that

the zone radius had a strong effect on the safety metrics of the experiment. In case the zones are too small, aircraft could have difficulty to spread laterally at the outer zone edge. Since it was expected that the effect would be more apparent when the zone angles are smaller, the number of zones was fixed to 10 in this experiment. Table VI shows the experiment matrix for the zone radius experiment. Each experimental condition was repeated 24 times: 12 times with CD&R switched on, and 12 times with CD&R switched off.

TABLE VI
EXPERIMENT MATRIX: ZONE RADIUS SELECTION

Variable	Levels	Different values
Outer zone radius	3	Factor 5, 10 or 15 times the inner radius
Traffic flow	3	Low, medium, high

It was found that the effect of varying the zone radius was not significant. Figure 15 shows that the number of conflicts for the different zone radius factors is not drastically different, and Figure 16 shows that the number of intrusions is also not significantly different. A less constrained airspace is preferred over a more constrained airspace if no safety improvements are gained from the constraints. In addition, a bigger zone structure directly disturbs a larger area, which is disadvantageous for the traffic flying over the departure/arrival. Since no significant performance differences were found, the smallest zone radius was chosen and fixed for the main experiment.

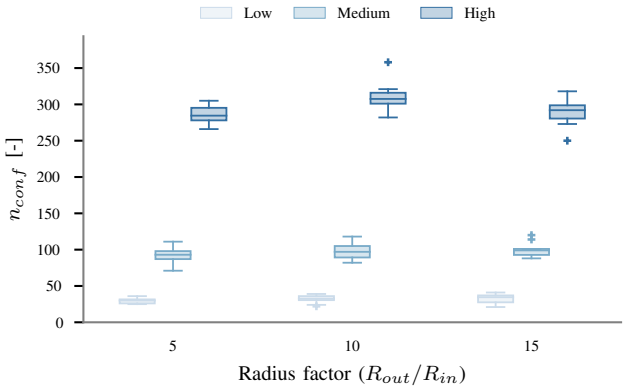

Fig. 15. Effect of traffic flow on number of conflicts for different zone radii.

IV. RESULTS

This section presents the results of the main experiment. Box-and-whisker plots are used to visualize the distribution of the dependent variables. The box represents the middle 50% of the dataset, with the median line drawn inside the box. The difference between the 25th and 75th percentiles is known as the interquartile range. The whiskers show the rest of the data points found in the distribution up to 1.5 times the interquartile range away from the middle 50% of the data set.

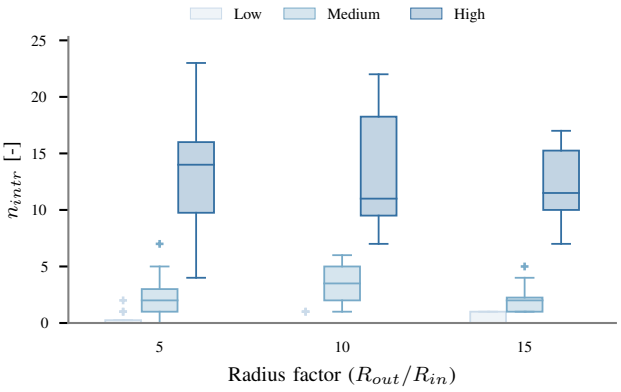

Fig. 16. Effect of traffic flow on number of intrusions for different zone radii.

Finally, data points that are more than a factor 1.5 times the interquartile range away from the box edges are considered to be outliers [30], and are plotted with a plus sign. Each experimental condition was repeated 50 times with CD&R on and 50 times with CD&R off, changing the randomized origins and destinations of the aircraft per repetition. As a result, 900 different scenarios are evaluated and compared in this section.

To verify significance of the effect of the airspace concept and the cross effect between airspace concept and traffic flow on the dependent variables, the Repeated Measures ANOVA is used with F-statistic [31] when appropriate. This statistical test is also used to test the significance of the interaction of the airspace concept and traffic flow. Although not all data passed the Kolmogorov-Smirnov and Shapiro-Wilk normality tests, it is assumed that the sample sizes are big enough to ensure that the means are approximately normally distributed even when the population is not normally distributed [32]. The ANOVA has been demonstrated not to be very sensitive to deviations from normality [32]. More important is the sphericity assumption, and data sets that do not pass Mauchly's test of sphericity need to be corrected [31]. In this research, a Greenhouse-Geisser adjustment is applied to adjust the degrees of freedom, since it is the most conservative correction in case the sphericity assumption is violated [31]. The Repeated Measures ANOVA can also be used to study the effect of the traffic flow on the dependent variables, but this research does not focus on whether traffic flow on its own has a significant effect on the performance. Instead, the effect of the interaction is reported, indicating whether a cross effect between airspace concept and traffic flow was found. A significant effect is demonstrated when the p-value is smaller than 0.05. The significance levels in this research should be taken with care. Due to the high number of repetitions per experimental condition, even small effects were found to be significant. Therefore, significant differences should not be interpreted to be large differences. In case of a significant effect, post-hoc pairwise comparisons were done to evaluate whether the differences between the airspace concepts were all significant. Since multiple comparisons were conducted on the same dependent variable, a Bonferroni correction was used

for these comparisons [33]. All post-hoc comparisons were found to be significant, and therefore they are not reported in this research. Again, this does not mean that all significant differences were large.

A. Safety

The total number of conflicts and intrusions are shown in Figure 17 and 18. The airspace concept has a significant effect on the number of conflicts ($F(2, 98) = 974, p < 0.01$) and on the number of intrusions ($F(2, 98) = 259, p < 0.01$). The cross effect of the airspace concept and the traffic flow is also found to be significant for both dependent variables ($F(2.68, 131) = 388, p < 0.01$ and $F(2.33, 114) = 87.0, p < 0.01$ respectively). This means that the effect of the zones is different for the different traffic flows.

It can be seen that the added value of zones becomes more apparent with 10 zones, and a configuration with 6 zones results in a smaller reduction of conflicts. This can be explained by the fact that in the scenarios with 6 zones, arriving aircraft are spawned at the same distance away from the center of the area as in the scenarios with 10 zones. This results in some arriving aircraft that closely cut in front of departure zones, directly affecting safety in these regions. The more zones, the better the arriving and departing aircraft can be channeled and therefore separated in the region around the zones.

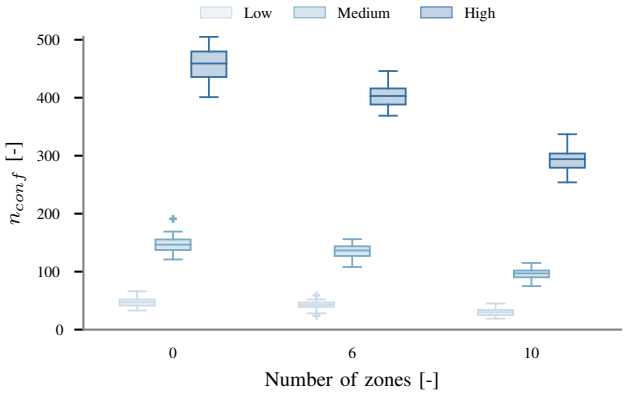

Fig. 17. Effect of traffic flow on number of conflicts for different airspace concepts.

Figure 19 shows the maximum intrusion severity that is measured in each repetition. Although the mean differences between the different data sets are small, both the effect of the airspace concept, as the interaction, were found to be significant ($F(2, 98) = 88, p < 0.01$ and $F(3.27, 160) = 16.9, p < 0.01$). It can be seen that severe intrusions occur in all airspace concepts, even at low traffic flow. This can be explained by the fact that currently, no conflict prevention algorithm is implemented in the ASAS of BlueSky. As a result, aircraft that make a turn at the outer edge of the zones, can directly turn into an intrusion with other aircraft. Similarly, aircraft that are climbing can directly turn into an intrusion when leveling off, since the state-based Conflict Detection

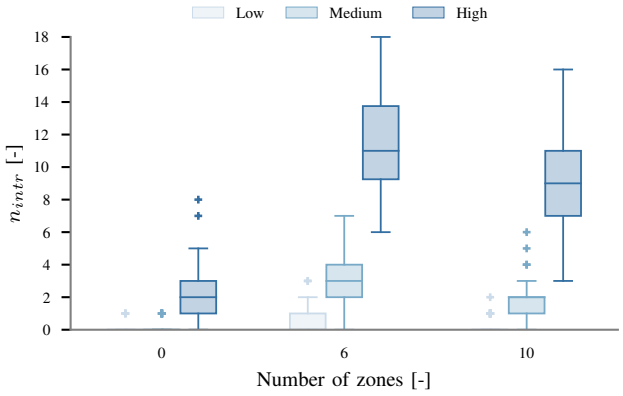

Fig. 18. Effect of traffic flow on number of intrusions for different airspace concepts.

(CD) method did not predict a conflict. This demonstrates that for all airspace concepts, it is necessary to implement a conflict prevention algorithm.

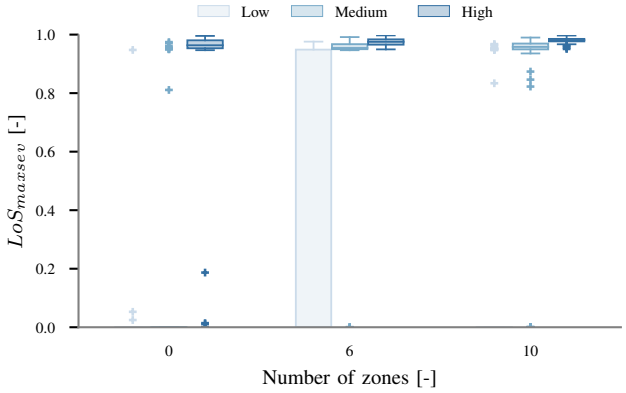

Fig. 19. Effect of traffic flow on maximum intrusion severity in the scenario for different airspace concepts.

When not only the maximum severity of all repetitions is plotted, but the severity of all measured intrusions is plotted (Figure 20), a large spread becomes visible for all densities. Since the total number of intrusions is different for the different experimental conditions, no significance tests could be performed. The number of intrusions is relatively small in all scenarios, causing high variability in the measured variable. It also indicates that improvements of the ASAS currently implemented in BlueSky are necessary. Although only a small amount of intrusions occurred, most were severe and resulted in actual collisions.

Figure 21 shows the Intrusion Prevention Rate (IPR). As expected, it displays that all airspace concepts are successful in preventing most conflicts from becoming intrusions. However, the unstructured concept is best in preventing intrusions from happening. The differences are small, but the effect of the airspace concept is found to be significant ($F(2, 98) = 160, p < 0.01$).

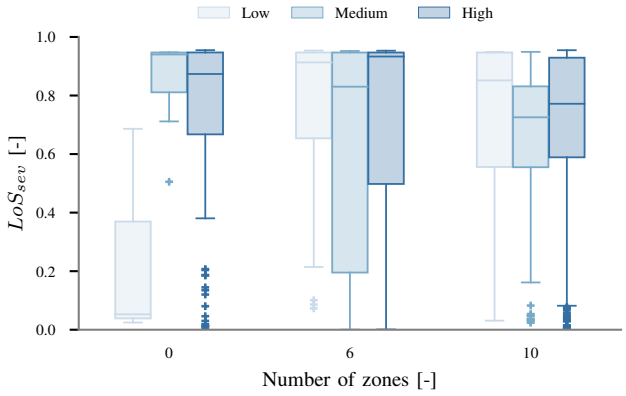

Fig. 20. Effect of traffic flow on the intrusion severity for all measured intrusions in the scenarios.

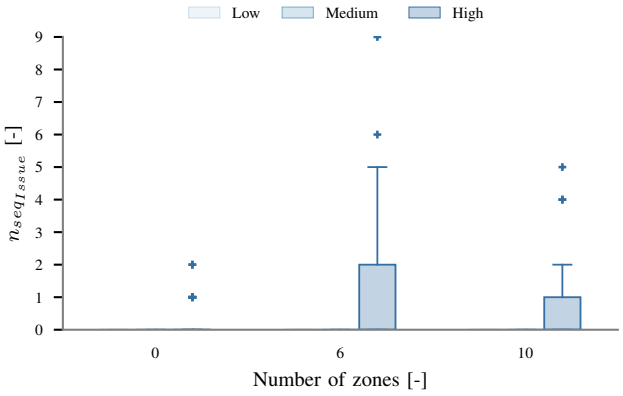

Fig. 22. Effect of traffic flow on the total number of sequencing problems per scenario for different airspace concepts.

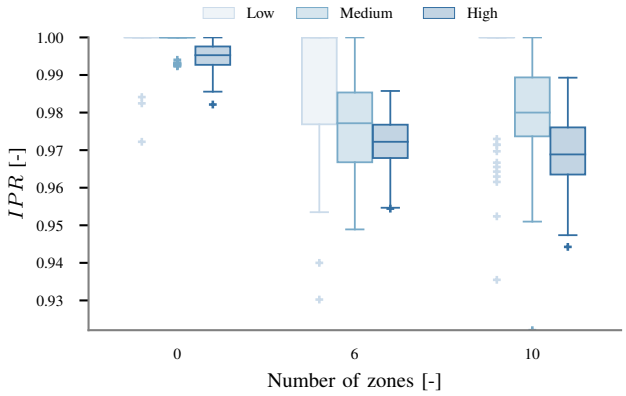

Fig. 21. Effect of traffic flow on the Intrusion Prevention Rate for different airspace concepts.

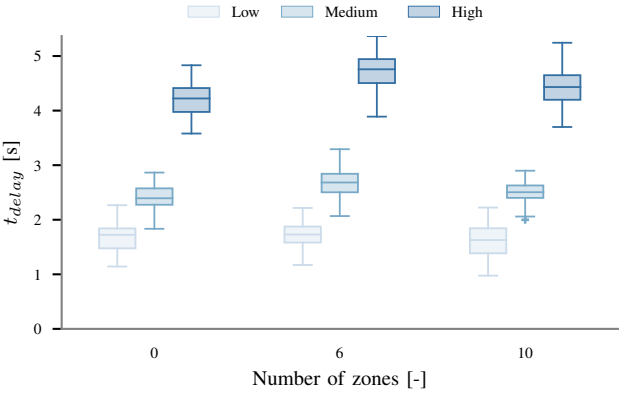

Fig. 23. Effect of traffic flow on the average delay with respect to the earliest possible arrival time for different airspace concepts.

Finally, the total number of sequencing problems is shown in Figure 22. It can be seen from the boxplots that the normality assumption is too heavily violated to do statistical tests, since in most scenarios the number of sequencing problems is zero. This means that in most scenarios, the different Point Merge Systems provide enough absorption capability to ensure a safe arrival slot for all aircraft. For higher traffic flows, sequencing issues arise. This indicates that a sequencing algorithm is required to ensure safe arrival for all aircraft.

B. *Efficiency*

The second category that is used to evaluate the performance is efficiency. Figure 23 shows the average delay with respect to the earliest time slot aircraft could have arrived. It can be seen that the delays are slightly higher once the zone structure is active. Although the effect of the airspace concept is significant ($F(1.7, 83.2) = 100, p < 0.01$), Figure 23 shows that the absolute differences are small.

Figure 24 shows the average inefficiency per flight with respect to a direct flight. As expected, the constraining structure of the zones results in less efficient flight paths than the unstructured concept. It is interesting that the variation of efficiency per concept is very small, so a limited number of repetitions is sufficient to accurately determine the efficiency. The airspace concept has a significant effect on the inefficiency metric ($F(1.15, 56.3) = 129 \cdot 10^3, p < 0.01$), but the cross effect between airspace concept and density is not significant ($F(2.13, 104.3) = 1.47, p = 0.23$). The extra distance flown in the unstructured concept is mainly caused by the Point Merge System at the end of the flight plan. Since aircraft were spawned at the same distance from the center, aircraft had to make larger deviations in the scenarios with only 6 zones compared to 10 zones.

C. *Stability*

Finally, the different concepts are evaluated in terms of airspace stability. Figure 25 displays the Domino Effect Parameter, and it becomes apparent that the values are small for all concepts. The effect of the airspace concept on the DEP was found to be significant ($F(2, 98) = 45.7, p < 0.01$). It is interesting to see that the increasing traffic flow has no significant effect on the DEP values ($F(2, 98) = 0.38, p = 0.68$).

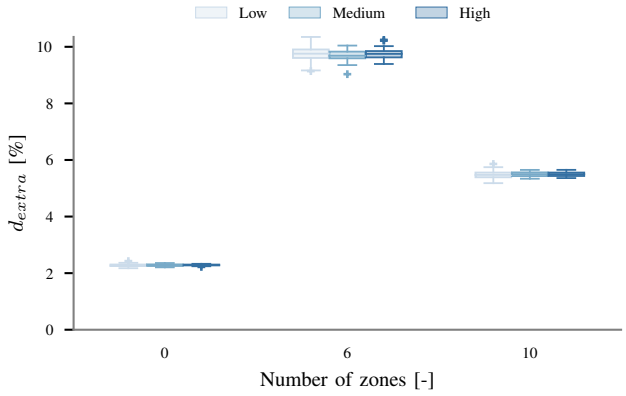

Fig. 24. Effect of traffic flow on the extra distance flown with respect to a direct flight for different airspace concepts.

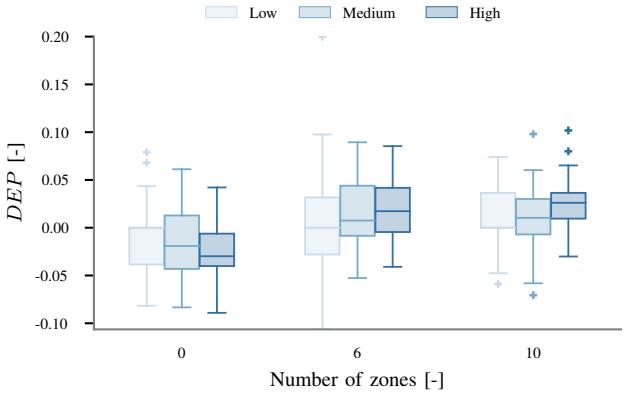

Fig. 25. Effect of traffic flow on the Domino Effect Parameter for different airspace concepts.

V. Discussion

This work has demonstrated that structuring airspace into lateral zones can act as a conflict prevention mechanism in a departure/arrival area, significantly reducing the number of conflicts. Especially in the scenarios with a high traffic flow, separating traffic into diverging and converging lateral zones resulted in a reduction of the total number of conflicts. The interaction between airspace concept and traffic flow was found to have a significant effect on the number of conflicts, and in the high traffic flow scenarios the zones performed significantly better than the unstructured concept. This confirms the hypothesis that the benefit of the zone structure is higher for more crowded traffic scenarios. The reduction in total number of conflicts can be explained by the fact that closer to the center of the departure/arrival area, the traffic has less maneuvering space since the airspace becomes more densely filled. The lateral zones force the traffic to leave the crowded center first, and from there continue the journey to their destination. This has a positive effect on the overall conflict count.

Figure 26 illustrates the total number of conflicts in the high traffic flow scenarios divided into different conflict categories. It can be seen that the number of conflicts between one arriving and one departing aircraft is significantly reduced if the zone structure is active. This confirms that the total reduction in conflicts when the aircraft are separated into diverging and converging lateral zones can mainly be attributed to the decrease in conflicts between aircraft flying in different directions in the center of the area. At the same time, the total number of conflicts between arriving pairs is slightly increased. Although this result was not expected, it can be explained by the fact that the zone structure forces aircraft into narrower arrival streams. As a result, chances of aircraft trying to enter the sequencing leg simultaneously increases. No sequencing algorithm was active that instructed aircraft to slow down or speed up towards the Point Merge System based on their assigned arrival slot. This demonstrates that in a departure/arrival area distributed control should always be accompanied by a centrally organized sequencing algorithm.

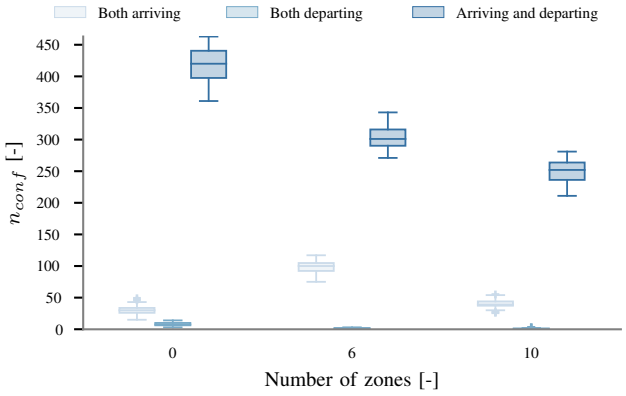

Fig. 26. Total number of conflicts in high traffic flow scenarios. The conflict is categorized to be between two arriving aircraft, two departing aircraft, or between one arriving and one departing aircraft.

In terms of safety, it was found that a higher number of lateral zones was beneficial. Figures 27 and 28 show the area where both departing and arriving aircraft fly in the concepts with 6 and 10 zones respectively. With more zones, the area of interference is smaller, positively affecting safety. This gives rise to the question whether a configuration with 14 or 18 zones would result in even better performance. If the number of zones becomes too big, aircraft do not have the possibility to maneuver inside the zones anymore. The narrower the zones get, the more the structure starts to resemble fixed arrival and departure routes. In this way it is no longer possible to use Point Merge Systems, thereby losing the absorption possibility at the inner radius. It is therefore expected that a configuration with too many zones results in a less safe and less efficient airspace, since the airspace becomes over-constrained and loses its flexibility. It should be further investigated what the optimal configuration is.

Although the zones were successful in reducing the number of conflicts in the scenario, the number of intrusions was significantly higher. This result was unexpected, but it can be explained by two phenomena. As explained before, more

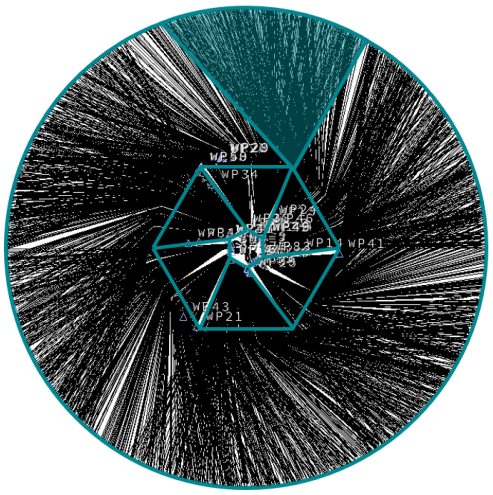

Fig. 27. Overlap between arriving and departing traffic in the concept with 6 zones.

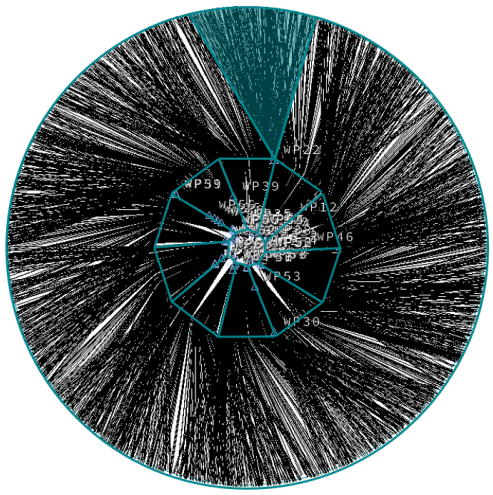

Fig. 28. Overlap between arriving and departing traffic in the concept with 10 zones.

conflicts arise between arriving aircraft when the zone structure is active. The zone structure forces aircraft into narrower arrival streams, therefore also causing more intrusions between arriving aircraft. By assigning a sequence prior to entering the Point Merge Systems, it is expected that most intrusions could have been prevented by using linear holding merging tactics for aircraft flying towards the sequencing leg. Secondly, no conflict prevention algorithm was active in the implemented ASAS, and this was a bigger problem for the structured concepts. When the zone structure was active, aircraft directly turned in and out of the zones, and these turns sometimes directly resulted in an intrusion.

Figures 29, 30, and 31 show the intrusion locations for the three different airspace concepts for the high traffic flow scenarios. It shows that for the unstructured concept (Figure 29), most intrusions occur at the center of the area where departing and arriving aircraft are mixed. The intrusions further away from the center were found to be intrusions between arriving aircraft and departing aircraft that were leveling off their climb. The CD method did not detect any conflict to resolve, since no intrusion would have occurred if the climb would have been continued. With a conflict prevention method available, aircraft would not turn into these intrusions. Figure 30 and 31 show that the concepts with zones resulted in an increase of intrusions in the arrival zones as explained in the previous section. Furthermore, the location of the intrusions suggests that the sharp edges of the turns are negatively influencing the safety of the airspace. It can be concluded that before implementation of the airspace concepts for departure/arrival areas, appropriate conflict prevention and sequencing algorithms should be investigated and developed. Furthermore, it is proposed to investigate the effect of smoothening out the sharp edges in the flight trajectory near the edges of the zone.

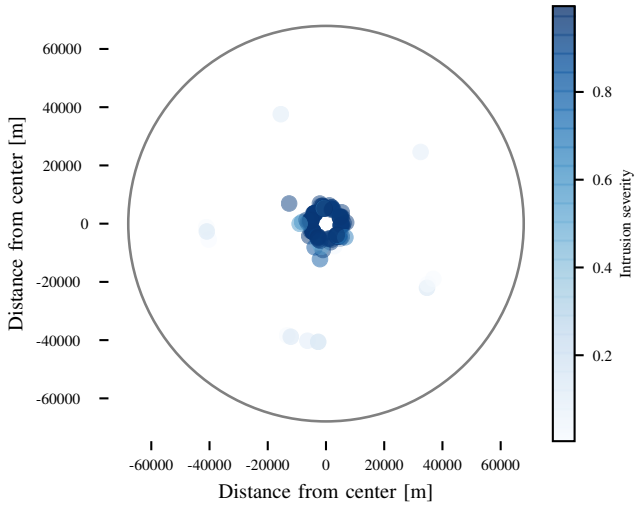

Fig. 29. Intrusion locations and severities at high traffic flow for the unstructured airspace concept.

As stated in the research question, the different concepts were not only compared in terms of safety. It was expected that constraining the airspace would result in a slight efficiency loss, and this was confirmed by the simulation results. In this research, only the traffic departing or arriving in the area was simulated. The effect on the efficiency of traffic flying over the departure/arrival area was not measured. Since the zone structure consumes airspace at the cost of other traffic flying in the area, it is expected that the flight distance of these aircraft also increases.

In this research it was shown that small zone radii are already capable of reducing the conflicts significantly. In reality, aircraft that originate further away from the zone concept could anticipate and adapt their flight plan accordingly to reduce the overall inefficiency and avoid sharp maneuvering

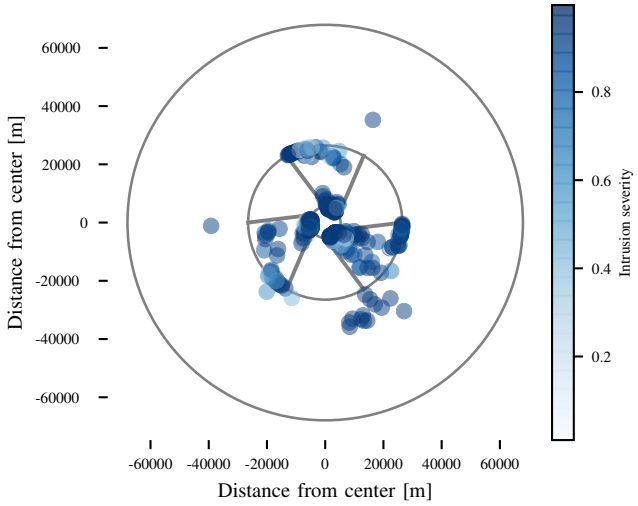

Fig. 30. Intrusion locations and severities at high traffic flow for the airspace concept with 6 zones.

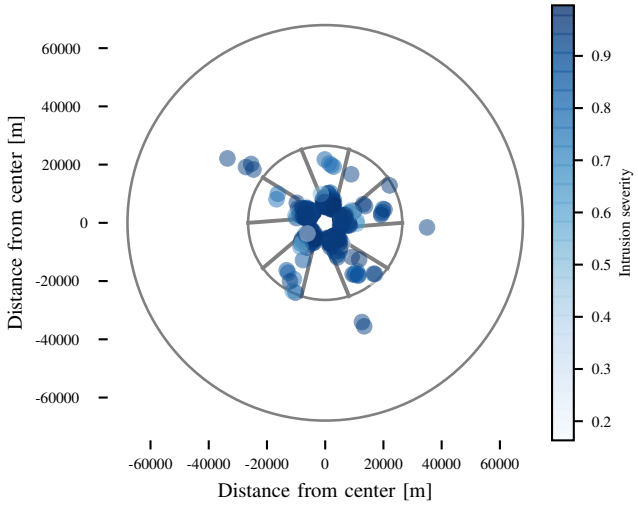

Fig. 31. Intrusion locations and severities at high traffic flow for the airspace concept with 10 zones.

at the edge of the zone structure. Therefore, the total efficiency penalty for the zones concept is expected to be overestimated in this research.

Finally, the concepts were evaluated in terms of stability. All different airspace concepts have shown to be relatively stable for the tested traffic flows. The negative DEP values were unexpected and imply that there is a net stabilizing effect in the airspace concepts. However, initial research in the relationship between airspace stability and capacity illustrated that negative DEP values can often be attributed to the scenario generation rather than to the self-structuring capabilities of the airspace or conflict resolution method [34]. In this research, a possible cause for the negative DEP values could be that the conflict resolution method acts as a pre-sequencing method for the arriving traffic. It should be further investigated whether in an arrival/departure area, conflict resolution can indeed have a stabilizing effect. For all simulations, the measured DEP was small and therefore it could be concluded that the concepts did not directly cause any instability problems. The fact that the traffic flow had no significant effect on the DEP values, suggests that airspace capacity limits were not yet reached.

Although the safety performance decreased with increasing traffic flow, no major inflation in conflict count was measured, again suggesting that the capacity limits were not yet reached. In peak hours, a big airport like Schiphol currently has 110 movements [35]. This corresponds to an average interval of 32.7 seconds between different movements, compared to an average interval of 4.1 seconds in scenarios with the highest traffic flow in this study. Although operations at Schiphol are not directly comparable to operations in a future departure/arrival area with PAVs, these values indicate that the simulated traffic demand was high compared to current airport levels.

VI. Conclusion and Recommendations

This research aimed to investigate the value of defining lateral zones in a departure/arrival traffic scenario with PAVs. The results demonstrate that lateral zones can lead to a significant reduction of conflicts, at the cost of a decrease in efficiency. The optimal airspace would perform best in terms of safety, efficiency, and stability. However, in this case, a trade-off needs to be made between safety and efficiency. Since the airspace is a safety critical system, a strong reduction in conflicts may outweigh the efficiency losses. Simulation results show that a bigger reduction of conflicts is possible at higher traffic flows, and that better performance is achieved with a higher number of zones. In the configuration with more zones, traffic is merged into narrower streams, causing less interference between arriving and departing traffic outside the lateral zones.

Although simulations provide a proof-of-concept in terms of conflict reduction, severe intrusions were measured in all airspace concepts. This demonstrates that implementation of conflict prevention and sequencing algorithms is necessary. With the conflict prevention and sequencing algorithms implemented, it is expected that most remaining intrusions can be prevented. Once such algorithms are implemented, it should be evaluated at what traffic flows the airspace concepts can guarantee collision-free flight. In this way, the capacity of the different concepts can be evaluated and compared. Furthermore, the dynamics of departing traffic inside the inner circle should be included in the simulation to fully test the airspace concept.

Based on the outcome of this research, it is recommended to further investigate different zone configurations. Configura-

tions with a smaller zone radius and a higher number of zones should be tested to evaluate what the optimum is. Additionally, different shapes could be explored, for example configurations with curved zone edges or different tilting angles. Possible refinements could be to include speed layers inside the zones, or to make the zone radius a function of altitude and speed of the aircraft. Furthermore, this research focused on traffic scenarios with a 50-50 distribution of arriving and departing traffic. However, the possibility of dynamically adapting the number of converging and diverging zones to the traffic demand should be further investigated for future implementation of the concept.

Finally, the effect of the surrounding airspace structure on the outcome of the results should be examined. Prior research has shown that in urban areas, distributed control with a limited structure of layers is successful [11]. Therefore, the joint composition of zones and layers should be tested to validate compatibility.

REFERENCES

[1] R. T. Force, "3: Free flight implementation," *Final Report, RTCA*, 1995.

[2] P. Kopardekar, K. Bilimoria, and B. Sridhar, "Initial concepts for dynamic airspace configuration," in *AIAA Aviation Technology Integration and Operations Conference*, Sep. 2007, pp. 18 – 20.

[3] A. Majumdar, W. Ochieng, and J. Polak, "Estimation of European Airspace Capacity from a model of controller workload," *Journal of Navigation*, vol. 55, pp. 381 – 403, 2002.

[4] N. Smith and K. Lee, "Current Airspace Configuration Practices and Their Implications for Future Airspace Concepts," *The 26th Congress of International Council of the Aeronautical Sciences (ICAS)*, pp. 1–13, Sep. 2008.

[5] K. M. Corker, B. F. Gore, K. Fleming, and J. Lane, "Free Flight and the Context of Control : Experiments and Modeling to Determine the Impact of Distributed Air-Ground Air Traffic Management on Safety and Procedures," *3rd USA/Europe Air Traffic Management R & D Seminar*, pp. 13–16, Jun. 2000.

[6] J. Hoekstra, R. Ruigrok, and R. Van Gent, "Free flight in a crowded airspace?" *Progress in Astronautics and Aeronautics*, vol. 193, pp. 533–546, Jun. 2001.

[7] T. Prevot, V. Battiste, E. Palmer, and S. Shelden, "Air Traffic Concept Utilizing 4D Trajectories and Airborne Separation Assistance," *AIAA Guidance, Navigation, and Control Conference and Exhibit*, pp. 1–11, Aug. 2003. [Online]. Available: http://arc.aiaa.org/doi/abs/10.2514/6.2003-5770

[8] J. Klooster, S. Torres, D. Earman, M. Castillo-Effen, R. Subbu, L. Kammer, D. Chan, and T. Tomlinson, "Trajectory synchronization and negotiation in Trajectory Based Operations," in *29th Digital Avionics Systems Conference*, 2010, pp. 1–11. [Online]. Available: http://ieeexplore.ieee.org/lpdocs/epic03/wrapper.htm?arnumber=5655536

[9] M. D. Moore, "NASA Personal Air Transportation Technologies," SAE Technical Paper, Tech. Rep., 2006. [Online]. Available: http://www.sae.org/technical/papers/2006-01-2413

[10] A. Sulleyman. (2017) World's first commercial flying car is now on sale. Online. Available online at http://www.independent.co.uk/ Accessed 23 March 2017.

[11] E. Sunil, J. Hoekstra, J. Ellerbroek, F. Bussink, D. Nieuwenhuisen, A. Vidosavljevic, and S. Kern, "Metropolis : Relating Airspace Structure and Capacity for Extreme Traffic Densities," *11th USA/Europe Air Traffic Management Research and Development Seminar*, vol. 341508, pp. 1–10, 2015.

[12] J. M. Hoekstra, J. Maas, M. Tra, and S. E., "How Do Layered Airspace Design Parameters Affect Airspace Capacity and Safety ?" in *7th International Conference on Research in Air Transportation (ICRAT)*, 2016.

[13] E. Sunil and J. Hoekstra, "The Influence of Traffic Structure on Airspace Capacity," *Proceedings of the 7th International Conference on Research in Air Transportation*, 2016. [Online]. Available: https://hal-enac.archives-ouvertes.fr/hal-01333624/

[14] M. S. Eby, "A Self-Organizational Approach for resolving Air Traffic Conflicts," *The Lincoln Laboratory Journal*, vol. 7, no. 2, pp. 239–253, 1994.

[15] J. M. Hoekstra, "Designing for Safety: the Free Flight Air Traffic Management Concept," Ph.D. dissertation, Delft University of Technology, 2001.

[16] E. Sunil, J. Ellerbroek, J. Hoekstra, A. Vidosavljevic, M. Arntzen, F. Bussink, and D. Nieuwenhuisen, "Analysis of Airspace Structure and Capacity for Decentralized Separation Using Fast-Time Simulations," *Journal of Guidance, Control, and Dynamics*, vol. 40, 2016.

[17] J. Maas, E. Sunil, J. Ellerbroek, and J. Hoekstra, "The Effect of Swarming on a Voltage Potential-Based Conflict Resolution Algorithm," *Proceedings of the 7th International Conference on Research in Air Transportation*, 2016.

[18] D. Ivanescu, C. Shaw, and C. Tamvaclis, "Models of Air Traffic Merging Techniques: Evaluating Performance of Point Merge," *9th AIAA Aviation Technology, Integration, and Operations Conference (ATIO)*, pp. 1–10, Sep. 2009.

[19] B. Favennec, E. Hoffman, A. Trzmiel, F. Vergne, and K. Zeghal, "The Point Merge Arrival Flow Integration Technique: Towards More Complex Environments and Advanced Continuous Descent," *9th AIAA Aviation Technology, Integration, and Operations Conference (ATIO)*, p. 6921, Sep. 2009.

[20] M. Liang, D. Delahaye, and P. Marechal, "A framework of point merge-based autonomous system for optimizing aircraft scheduling in busy tma to cite this version," in *5th SESAR Innovation Days*, Dec. 2015, pp. 1–8.

[21] M. Liang, D. Delahaye, M. Sbihi, and J. Ma, "Multi-layer point merge system for dynamically controlling arrivals on parallel runways," *AIAA/IEEE Digital Avionics Systems Conference - Proceedings*, Dec. 2016.

[22] R. Goldman, "Intersection of two lines in three-space," in *Graphics Gems*, A. S. Glassner, Ed. San Diego, CA, USA: Academic Press Professional, Inc., 1990, pp. 304–. [Online]. Available: http://dl.acm.org/citation.cfm?id=90767.90838

[23] J. M. Hoekstra and J. Ellerbroek, "BlueSky ATC Simulator Project: an open Data and Open Source Approach," in *Proceedings of the 7th International Conference on Research in Air Transportation*, 2016.

[24] (2010, Feb.) 14 cfr 91.119 - minimum safe altitudes: General. Legal Information Institute. Accessed on 14 November 2017. [Online]. Available: https://www.law.cornell.edu/cfr/text/14/91.119

[25] M. Pavel, "Expert opinion on typical performance of autogyros," contacted in September 2017.

[26] J. Hoekstra, S. Kern, O. Schneider, F. Knabe, and B. Lamiscarre, "Metropolis Scenario Definition Report (D1.2)," Delft University of Technology, Tech. Rep., 2015, available online at http://homepage.tudelft.nl/7p97s/Metropolis/ Accessed 3 April 2017.

[27] G. J. Ruijgrok, *Elements of airplane performance*. VSSD, 2009.

[28] M. R. Jardin, "Air Traffic Conflict Models," *4th Aviation Technology, Integration and Operations (ATIO) Forum*, pp. 1–13, Sep. 2004.

[29] J. Krozel and M. Peters, "Decentralized control techniques for distributed air/ground traffic separation," *Seagull Technology Inc., Los Gatos*, Aug. 2000.

[30] M. Waskom. (2017) Python seaborn documentation. Accessed on 28 December 2017. [Online]. Available: https://seaborn.pydata.org/generated/seaborn.boxplot.html

[31] A. Field, *Discovering Statistics Using SPSS*. SAGE Publications Ltd, 2009.

[32] G. V. Glass, P. D. Peckham, and J. R. Sanders, "Consequences of failure to meet assumptions underlying the fixed effects analyses of variance and covariance," *Review of educational research*, vol. 42, no. 3, pp. 237–288, 1972.

[33] R. A. Armstrong, "When to use the bonferroni correction," *Ophthalmic and Physiological Optics*, vol. 34, no. 5, pp. 502–508, 2014.

[34] E. Sunil, J. Maas, J. Ellerbroek, J. Hoekstra, and M. Tra, "The Relationship Between Traffic Stability and Capacity for Decentralized Airspace," *Proceedings of the 7th International Conference on Research in Air Transportation*, 2016.

[35] Schiphol. (2017) Amsterdam airport schiphol airport facts. Accessed on 17 December 2017. [Online]. Available: https://www.schiphol.nl/nl/route-development/pagina/amsterdam-airport-schiphol-airport-facts/

Part II
Appendices

A

Zone radius experiment

As discussed in Section III-E of the scientific paper, a preliminary experiment was conducted to evaluate the effect of varying the outer zone radius. In Table A.1 the experiment matrix for the zone radius experiment is repeated. Each experimental condition was tested for 24 repetitions, of which 12 were using CD&R, and the same 12 were repeated with CD&R off to calculate the Domino Effect Parameter.

Table A.1: Experiment matrix: Zone radius selection

Variable	**Levels**	**Different values**
Outer zone radius	3	Factor 5, 10 or 15 times the inner radius
Traffic flow	3	Low, medium, high

As discussed in Section II-A, a single-layer Point Merge System for multiple aircraft types was used in early stages of the zone radius experiment. Section A.1 presents the results in terms of safety, efficiency, and stability for the zone radius experiment with single-layer Point Merge Systems. For all aircraft types, the clockwise sequencing leg was designed at FL20 and the counterclockwise leg at FL30. It was found that the number of conflicts and intrusions could be reduced by redesigning the Point Merge Systems as discussed in Section II-A of the scientific paper. Section A.2 presents the results if a Point Merge System with layers for different aircraft types is used. By comparing Figure A.1 with A.10 and Figure A.2 with A.11, it can be concluded that the number of conflicts and the number of intrusions decreases by introducing the multi-layer Point Merge Systems.

A.1. Single-layer Point Merge System

This chapter contains all the box-and-whisker plots for the experiment with single-layer Point Merge Systems. The dependent variables were introduced in Section III-D of the scientific paper in Part I of this report. Visualization by means of the box-and-whisker plot was explained in Section IV of the same paper. The following subsections present the results in terms of safety, efficiency, and stability respectively.

A.1.1. Safety

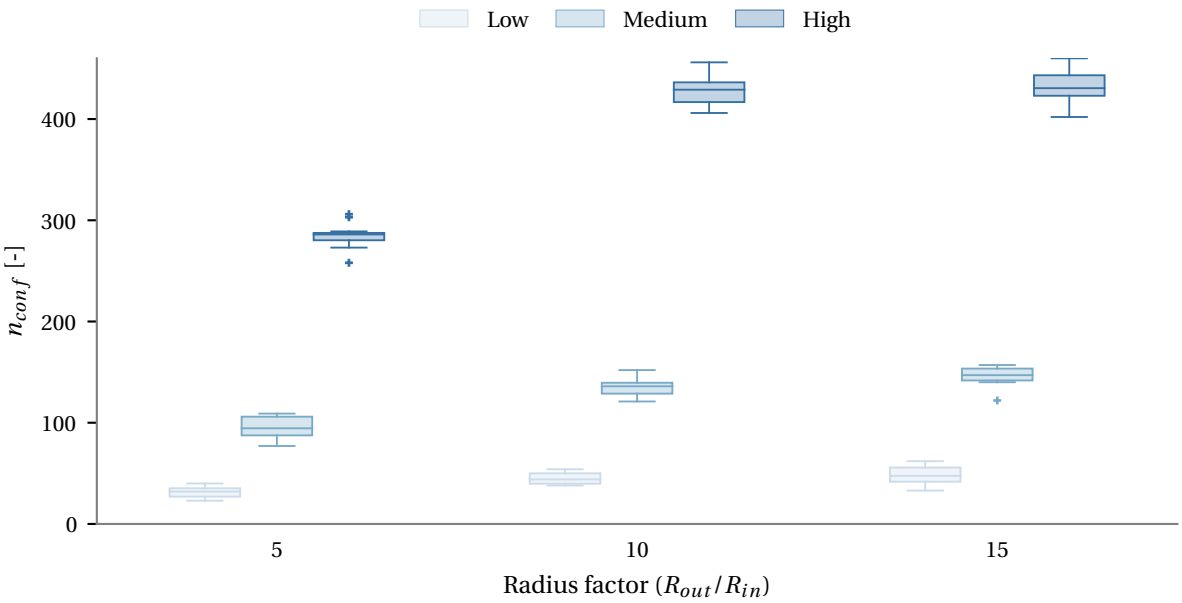

Figure A.1: Effect of traffic flow on number of conflicts for different zone radii with single-layer Point Merge Systems.

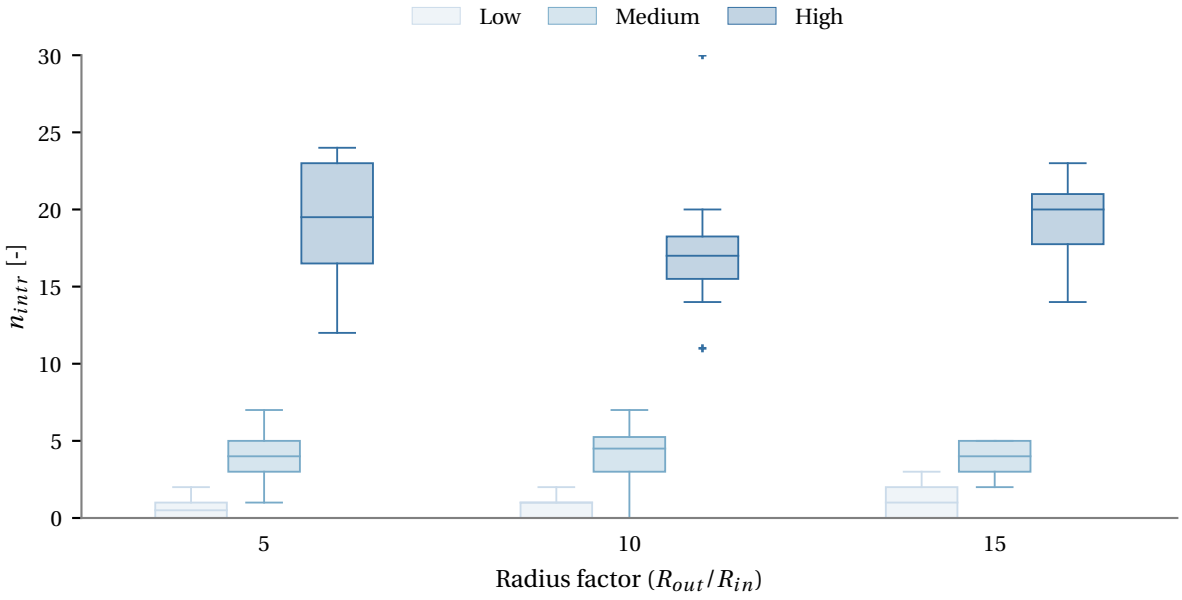

Figure A.2: Effect of traffic flow on number of intrusions for different zone radii with single-layer Point Merge Systems.

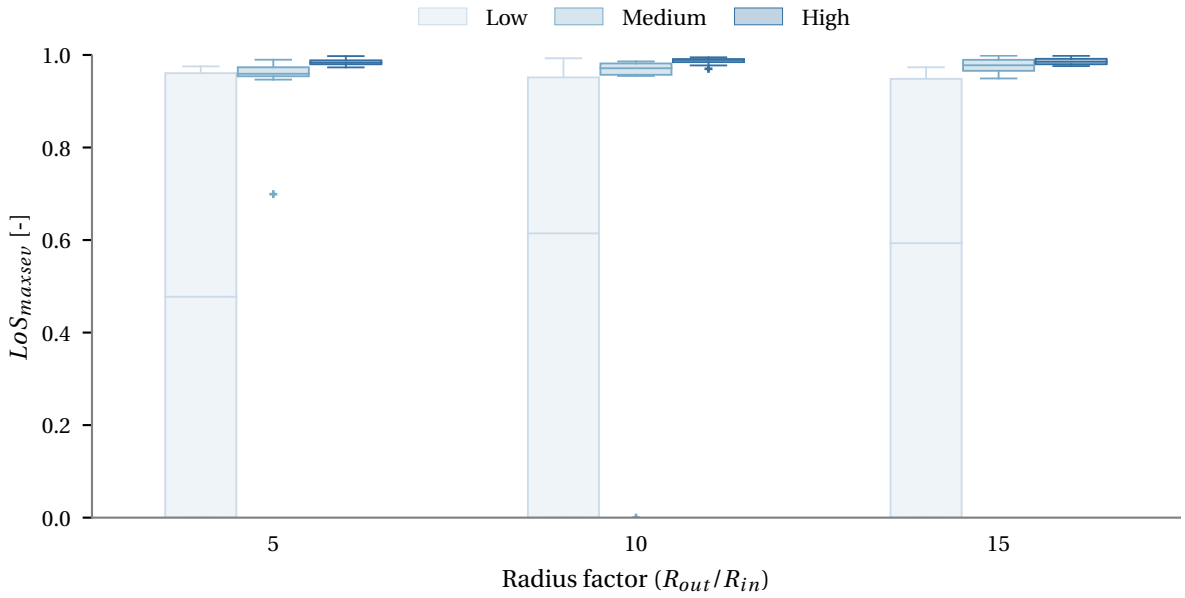

Figure A.3: Effect of traffic flow on maximum intrusion severity in the scenario for different zone radii with single-layer Point Merge Systems.

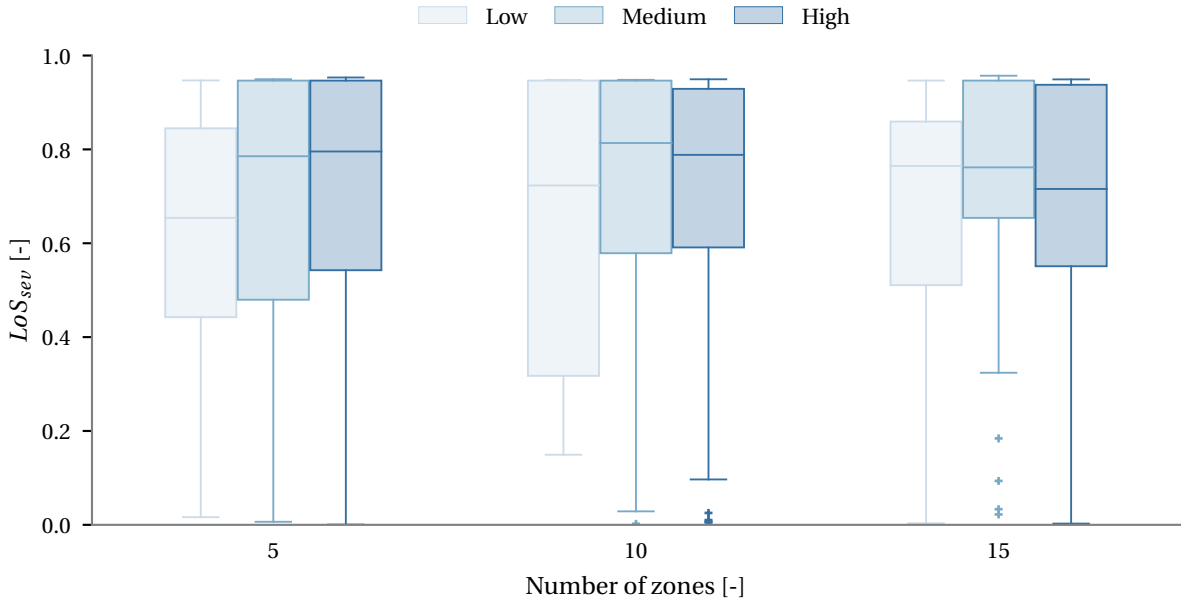

Figure A.4: Effect of traffic flow on the intrusion severity for different zone radii with single-layer Point Merge Systems.

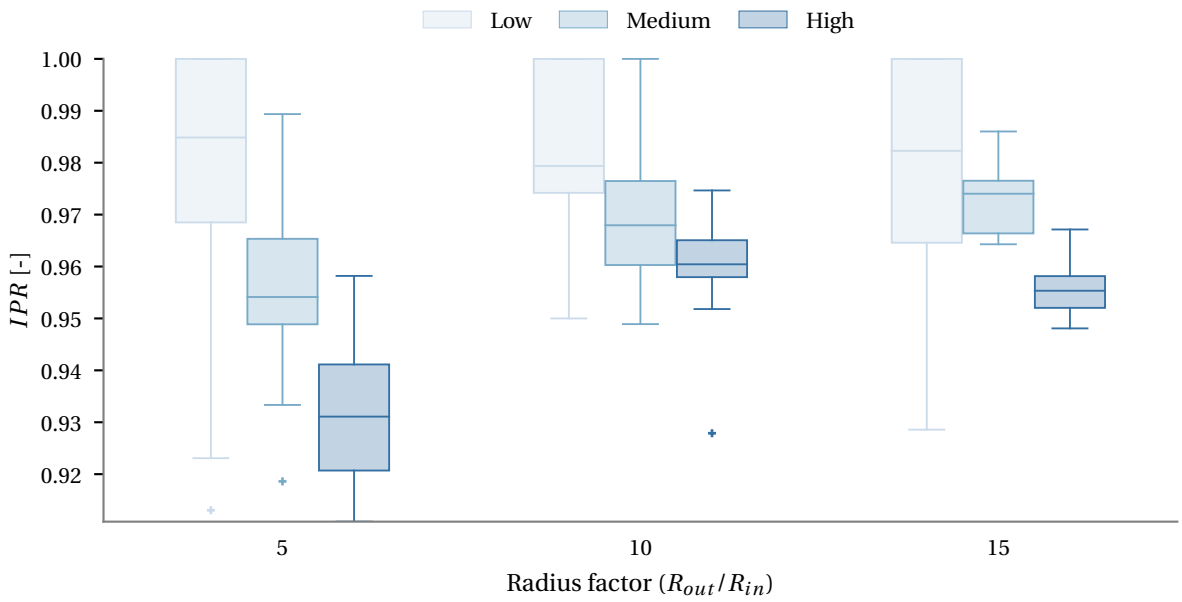

Figure A.5: Effect of traffic flow on the Intrusion Prevention Rate for different zone radii with single-layer Point Merge Systems.

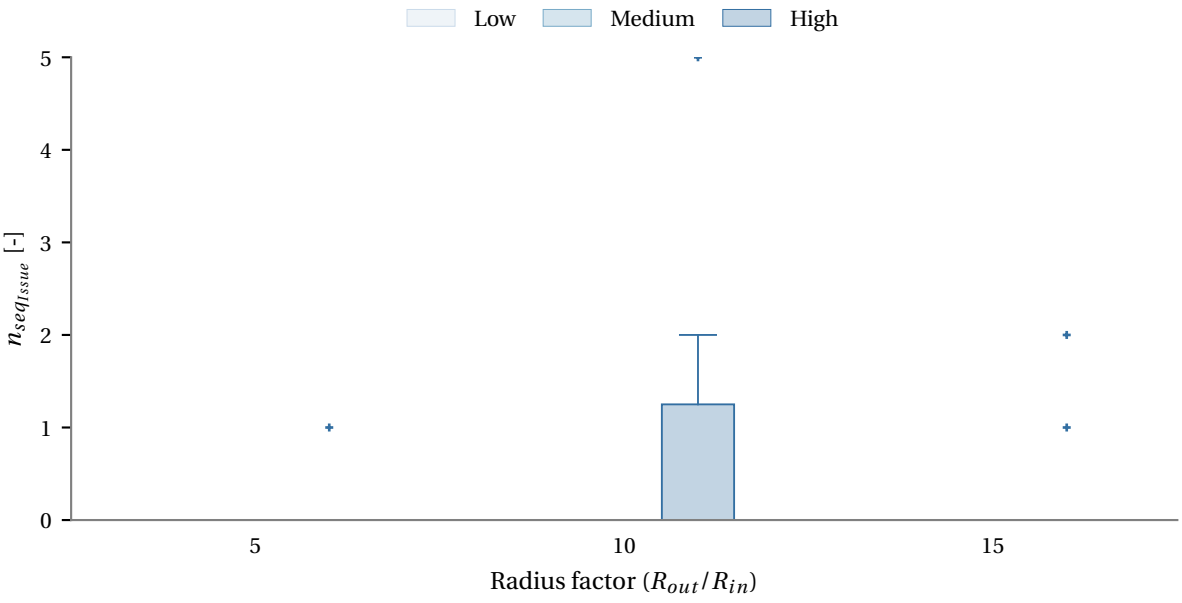

Figure A.6: Effect of traffic flow on the total number of sequencing problems per scenario for different zone radii with single-layer Point Merge Systems.

A.1.2. Efficiency

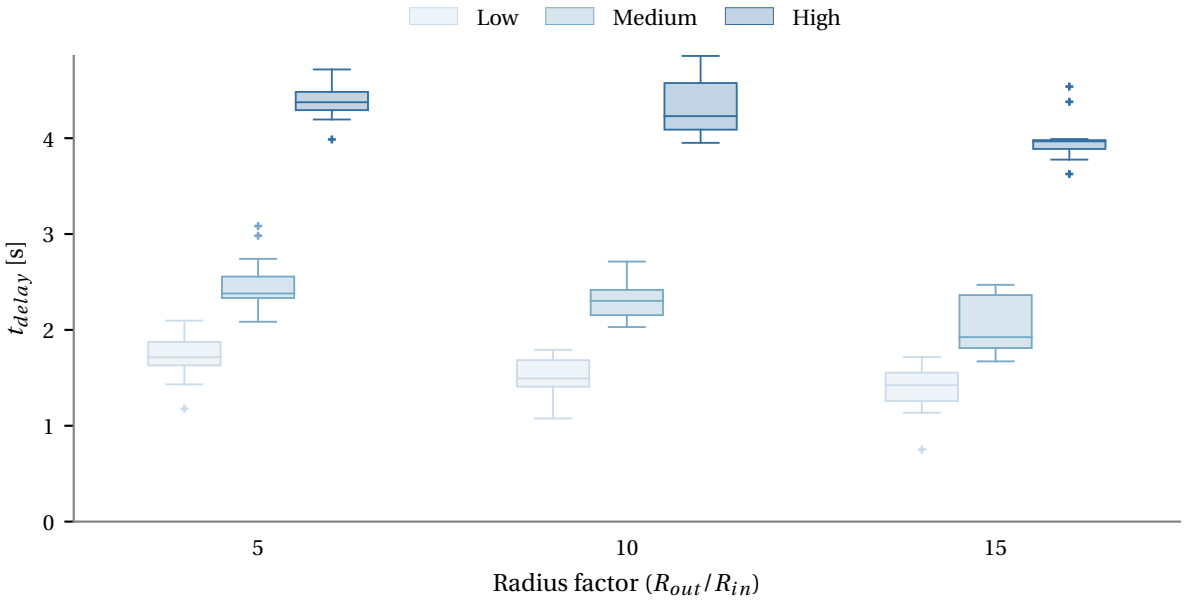

Figure A.7: Effect of traffic flow on the average delay w.r.t. earliest possible arrival time for different zone radii with single-layer Point Merge Systems.

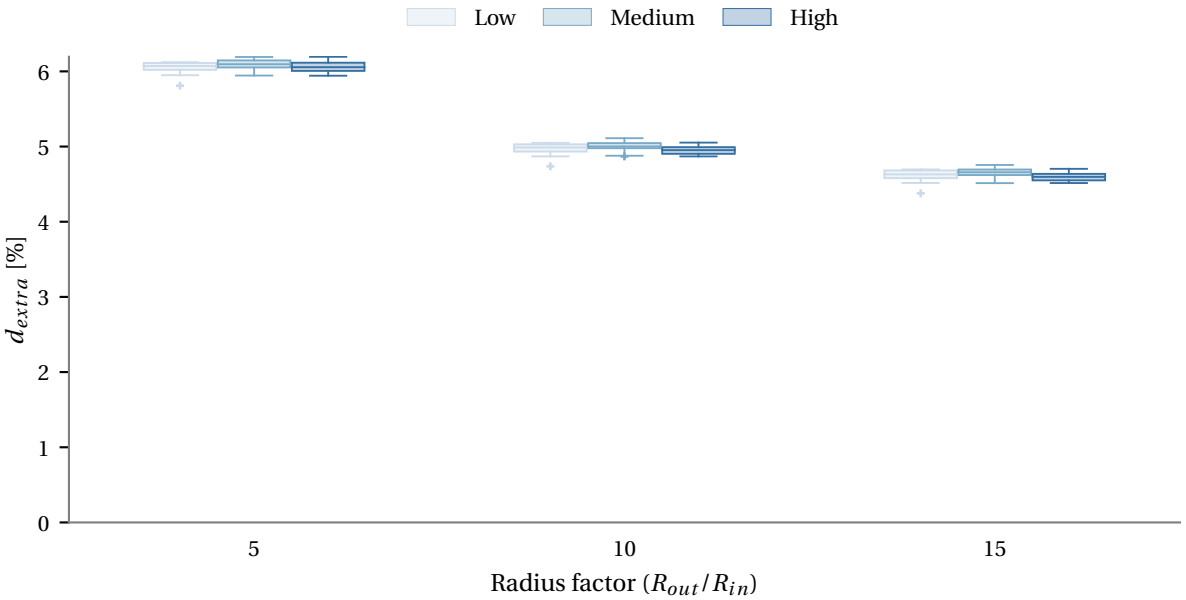

Figure A.8: Effect of traffic flow on the extra distance flown w.r.t. a direct flight for different zone radii with single-layer Point Merge Systems.

A.1.3. Stability

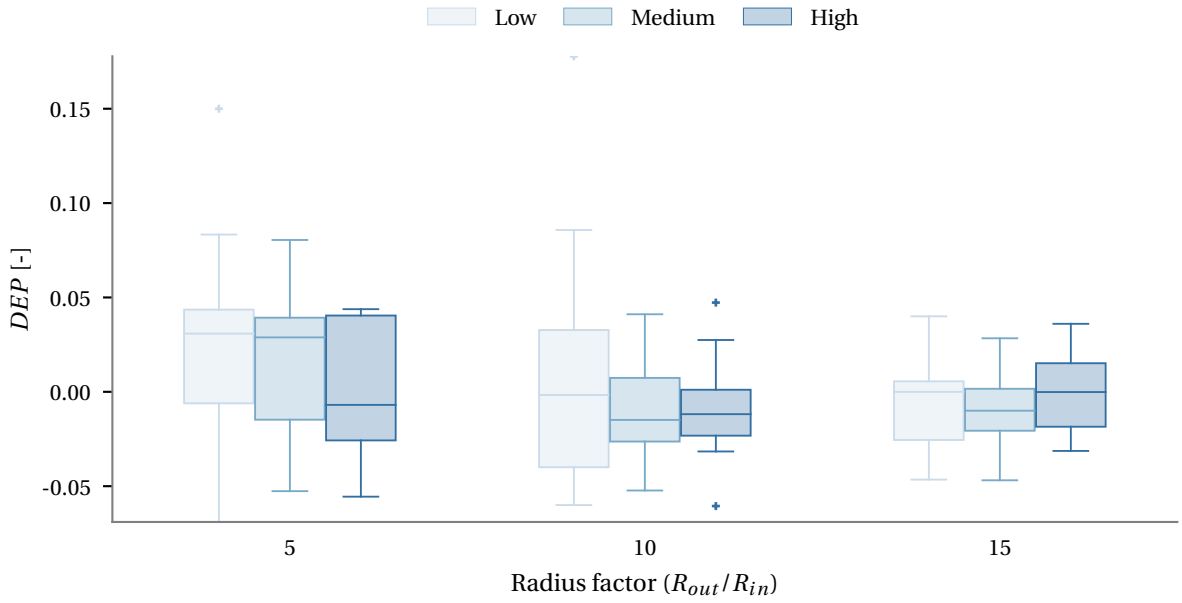

Figure A.9: Effect of traffic flow on the Domino Effect Parameter for different zone radii with single-layer Point Merge Systems.

A.2. Multi-layer Point Merge Systems

This chapter contains similar box-and-whisker plots for the experiment with multi-layer Point Merge Systems. Again, the results are categorized in safety, efficiency, and stability.

A.2.1. Safety

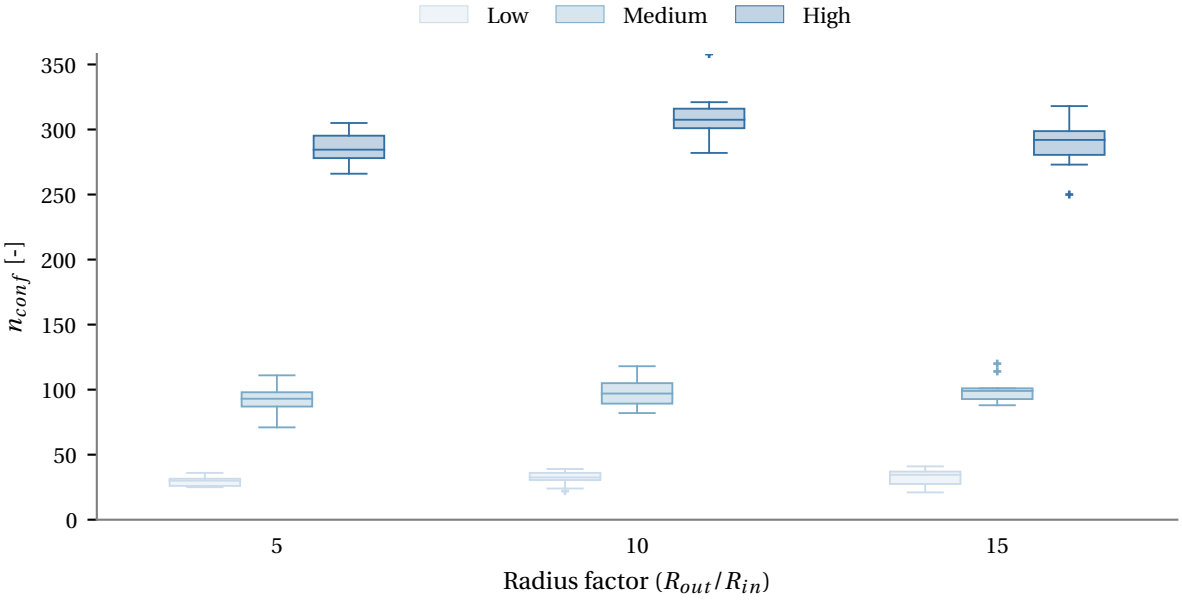

Figure A.10: Effect of traffic flow on number of conflicts for different zone radii with multi-layer Point Merge Systems.

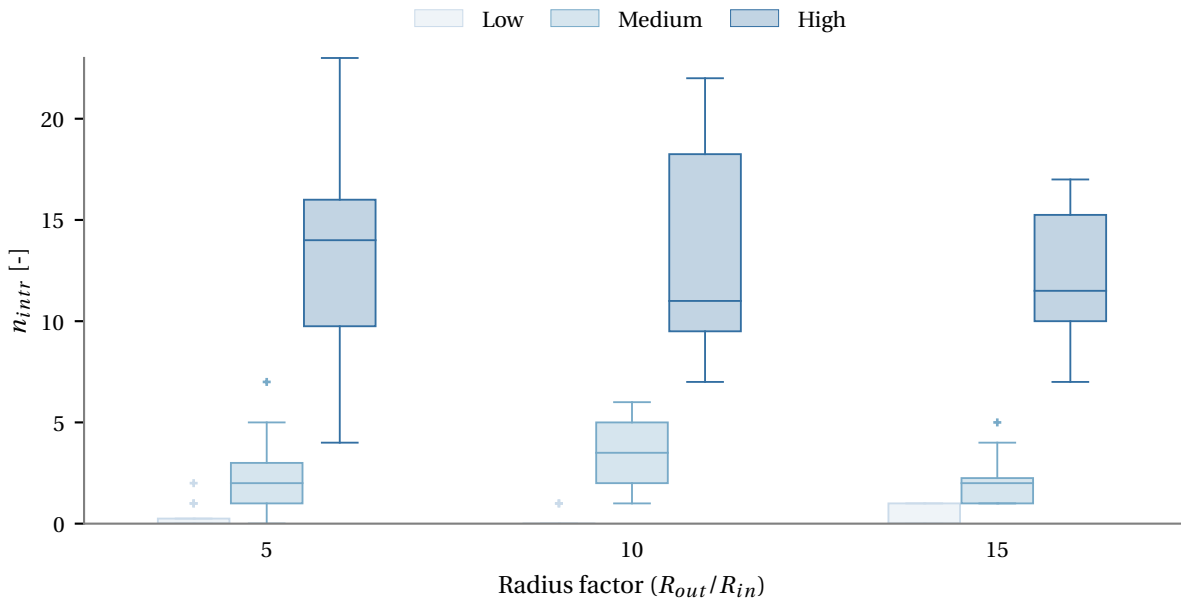

Figure A.11: Effect of traffic flow on number of intrusions for different zone radii with multi-layer Point Merge Systems.

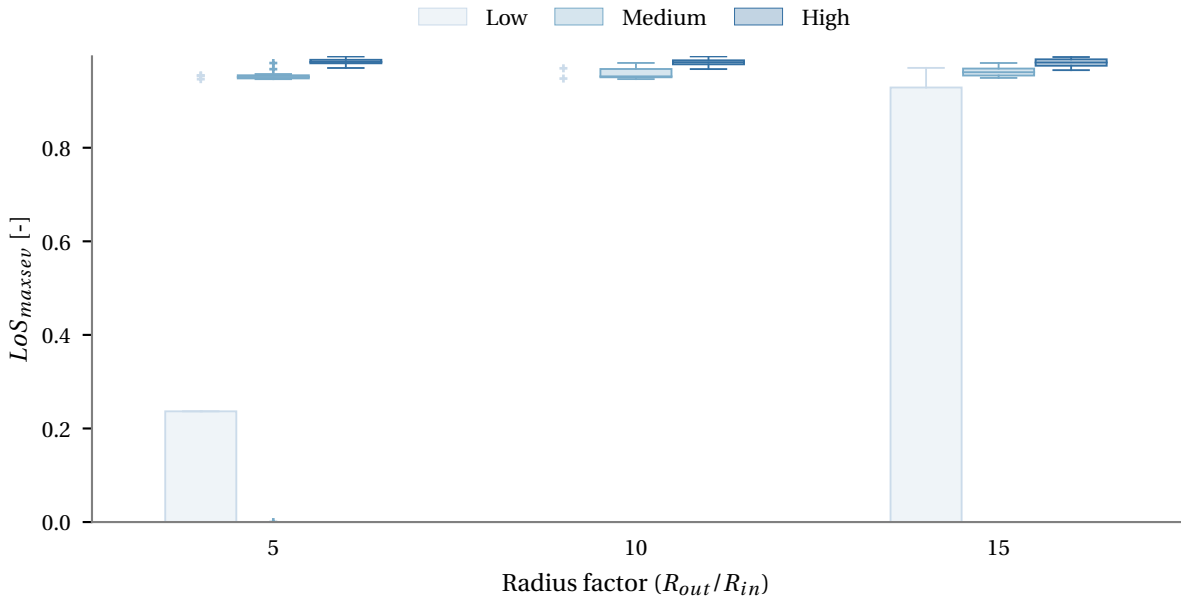

Figure A.12: Effect of traffic flow on maximum intrusion severity in the scenario for different zone radii with multi-layer Point Merge Systems.

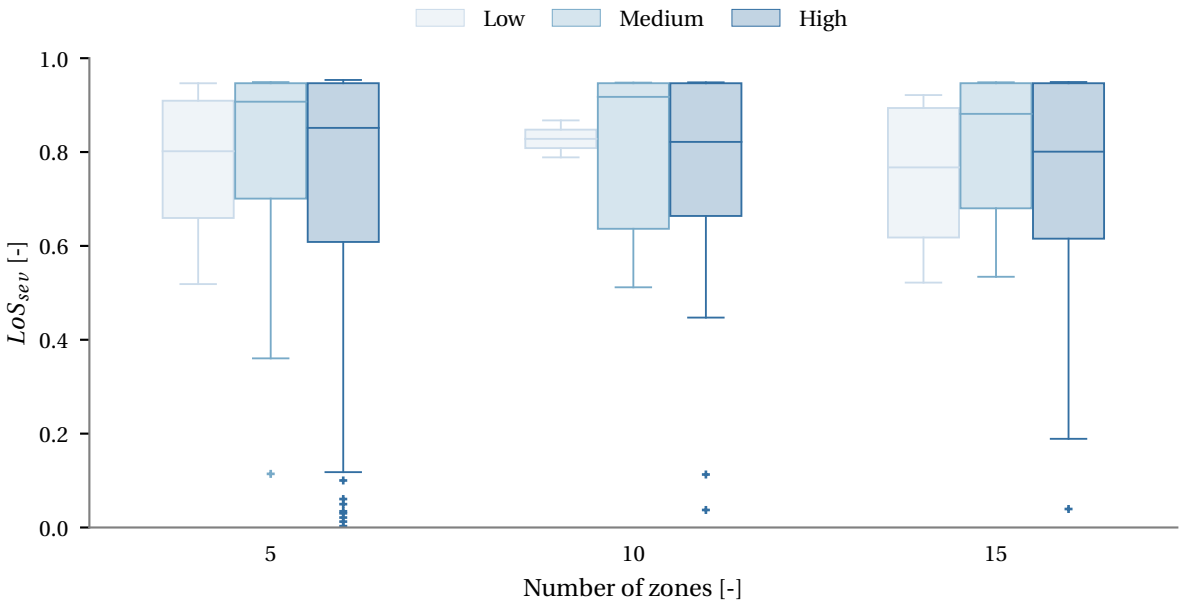

Figure A.13: Effect of traffic flow on the intrusion severity for different zone radii with multi-layer Point Merge Systems.

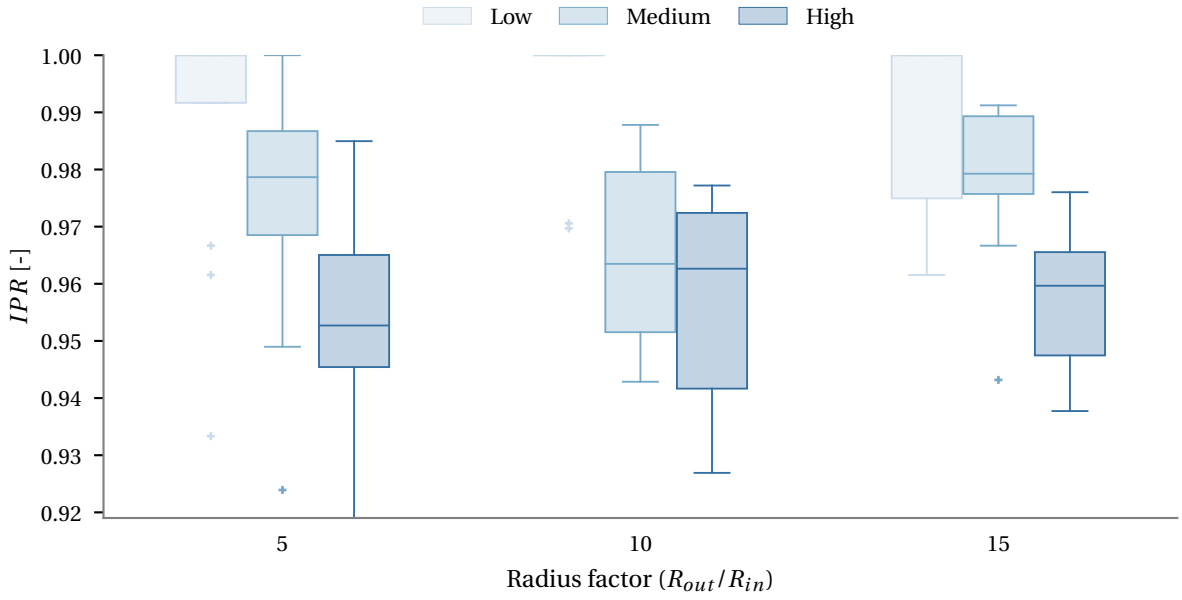

Figure A.14: Effect of traffic flow on the Intrusion Prevention Rate for different zone radii with multi-layer Point Merge Systems.

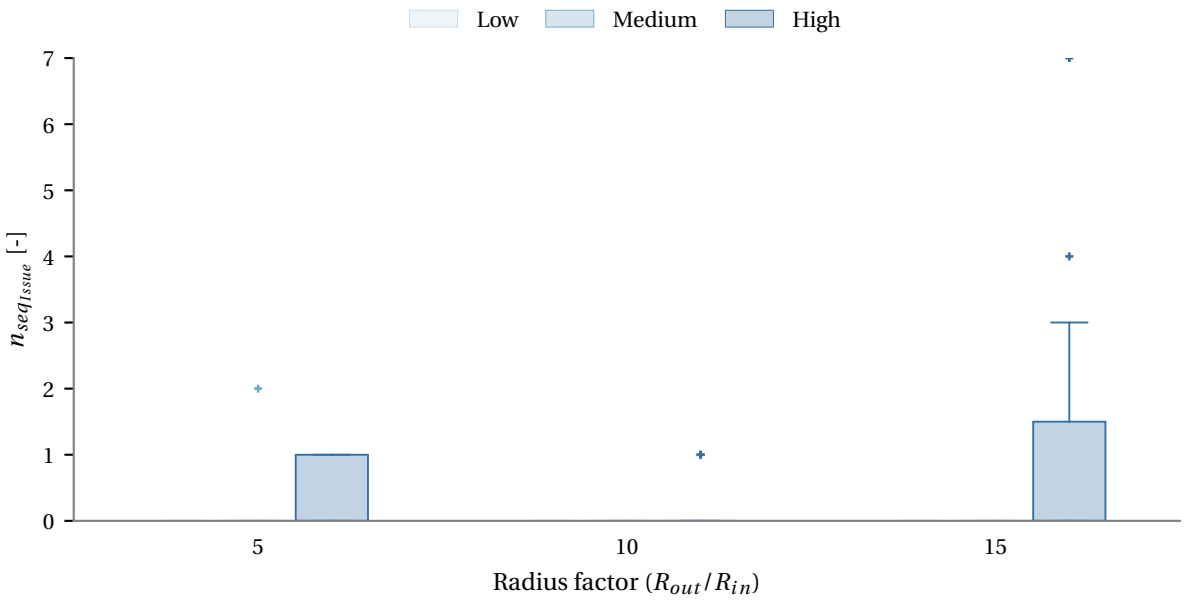

Figure A.15: Effect of traffic flow on the total number of sequencing problems per scenario for different zone radii with multi-layer Point Merge Systems.

A.2.2. Efficiency

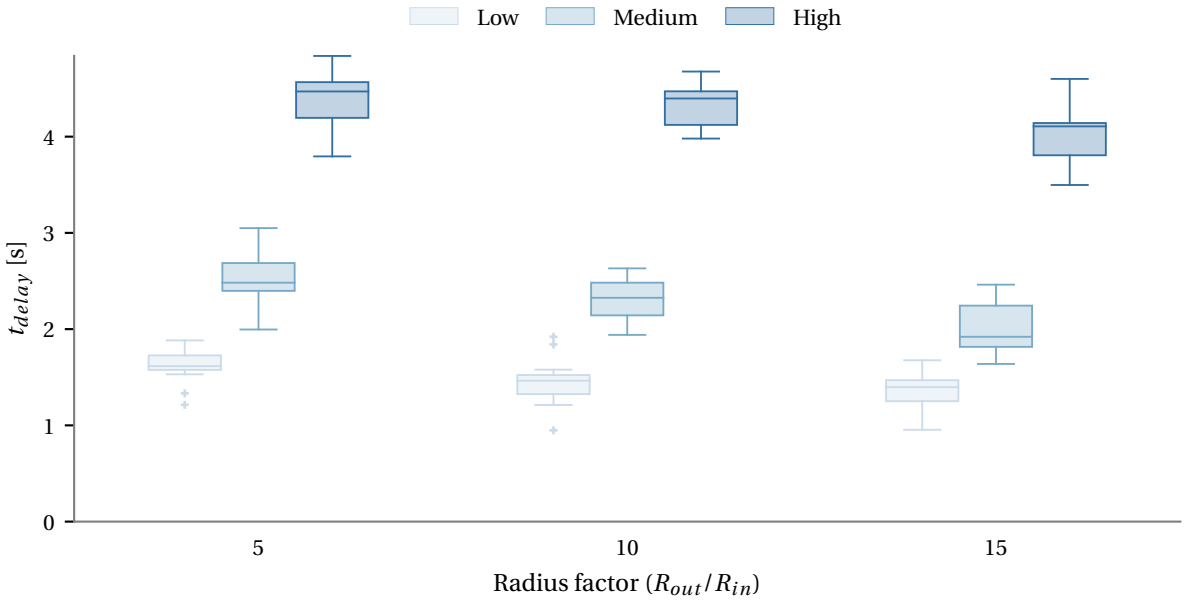

Figure A.16: Effect of traffic flow on the average delay w.r.t. the earliest possible arrival time for different zone radii with multi-layer Point Merge Systems.

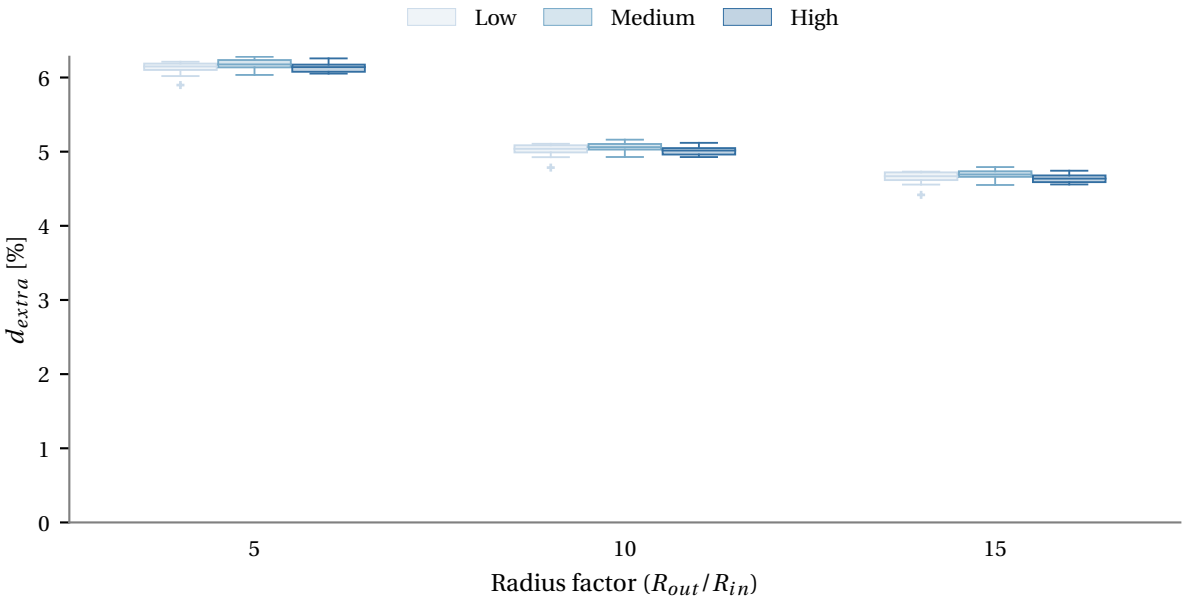

Figure A.17: Effect of traffic flow on the extra distance flown w.r.t. a direct flight for different zone radii with multi-layer Point Merge Systems.

A.2.3. Stability

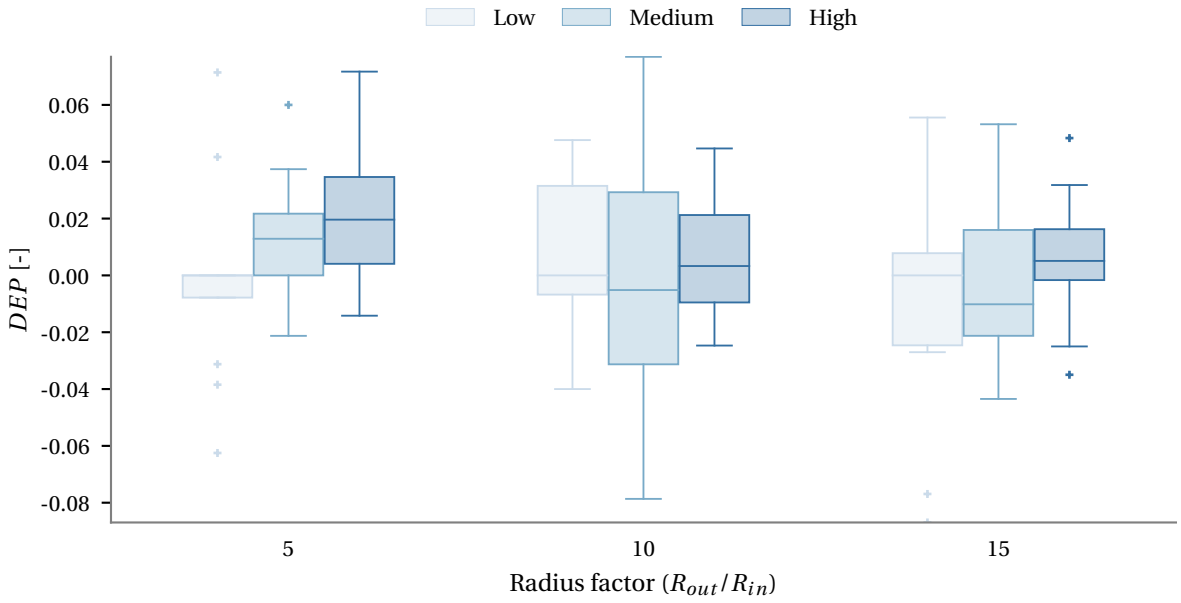

Figure A.18: Effect of traffic flow on the Domino Effect Parameter for different zone radii with multi-layer Point Merge Systems.

B

Absorption capability of the Point Merge Systems

Section III-D-1 of the scientific paper states that a separate experiment was conducted to evaluate the absorption capability of the Point Merge Systems. This chapter explains the experiment in more detail. Section B.1 explains the scenario generation of the experiment, and Section B.2 presents the results.

B.1. Scenario generation

During the zone radius experiment that was explained in Appendix A, it was found that a configuration of multi-layer Point Merge Systems was effective for this experiment. Table B.1 repeats the chosen altitudes for the Point Merge Systems per aircraft type used in this research (Table 1 in the scientific paper).

Table B.1: Altitude restrictions for the sequencing legs of the Point Merge Systems per aircraft type

Aircraft type	**Clockwise leg**	**Anticlockwise leg**
A609	FL70	FL60
TSTX	FL50	FL40
PAL-V	FL30	FL20

In the main experiment of this research, all aircraft are programmed to fly the entire Point Merge sequencing leg to the center of the circle. This means that the arrival time that is logged, resembles the arrival time if the whole sequencing leg of the Point Merge System would have been used. In this experiment, the absorption capabilities per aircraft type were evaluated to determine the earliest possible arrival time. Table B.2 shows the experiment matrix.

Table B.2: Experiment matrix: Point Merge System absorption

Variable	**Levels**	**Different values**
Aircraft type	3	A609, TSTX, PAL-V
Merging instruction	2	Full sequencing leg or direct-to-center at the start of the leg

In each scenario, 500 arriving aircraft were generated from the same aircraft type. In this experiment, a configuration with 10 zones was used. Figure B.1 and B.2 illustrate the differences between the two merging instructions. The aircraft in the *direct-to-center* scenario are spawned at exactly the same time and location

as in the *full sequencing leg* scenario, but this time they are directed to the center as soon as they enter the sequencing leg. Figure B.1 shows the pattern that the aircraft trails leave behind in case the full sequencing leg is flown, and Figure B.2 shows the straight lines that can be seen when aircraft directly leave the sequencing leg.

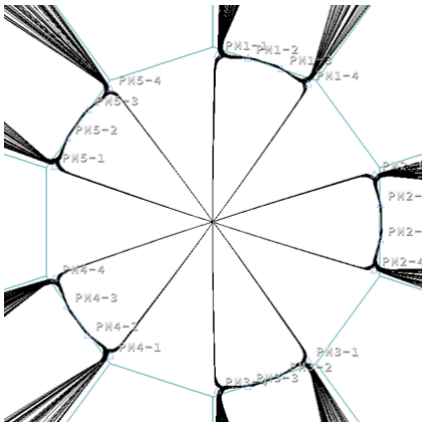

Figure B.1: PAL-V trails in the inner circle after flying the full sequencing leg of the Point Merge System.

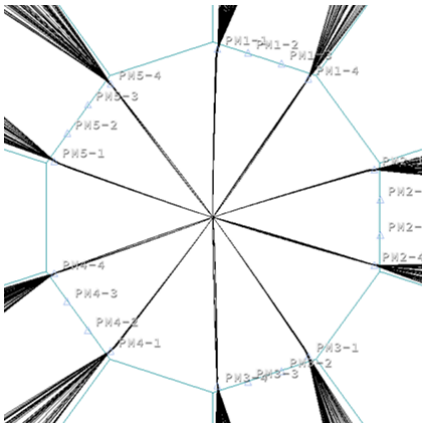

Figure B.2: PAL-V trails in the inner circle after a direct-to instruction upon entry of the sequencing leg of the Point Merge System.

The unstructured airspace concept is designed with the same 5 Point Merge Systems as the concept with 10 zones. The concept with 6 zones uses only 3 similar sized Point Merge Systems. This is illustrated by Figure B.3. Although the sequencing legs in the concept with 6 zones could have been designed to be bigger, similar configurations were chosen to enable the best comparison between the concepts. A separate study to optimize the Point Merge System would be required before actual implementation.

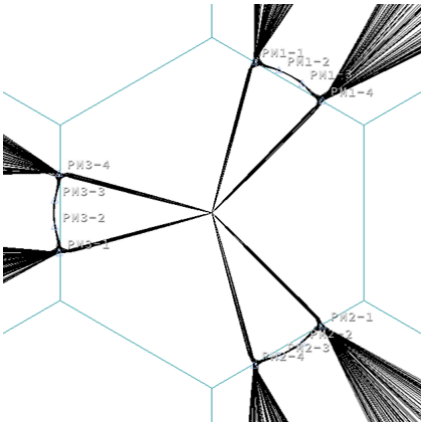

Figure B.3: The Point Merge Systems in the concept with 6 zones are designed to be similar in size to the ones in the concept with 10 zones.

B.2. Results

By comparing the arrival times in the two different scenarios, the difference between the earliest and latest arrival can be compared per aircraft. By evaluating the difference for all 500 aircraft, the absorption capability of the sequencing leg is determined. Figure B.4 shows the results of this experiment, and is a repetition of Figure 13 of the scientific paper.

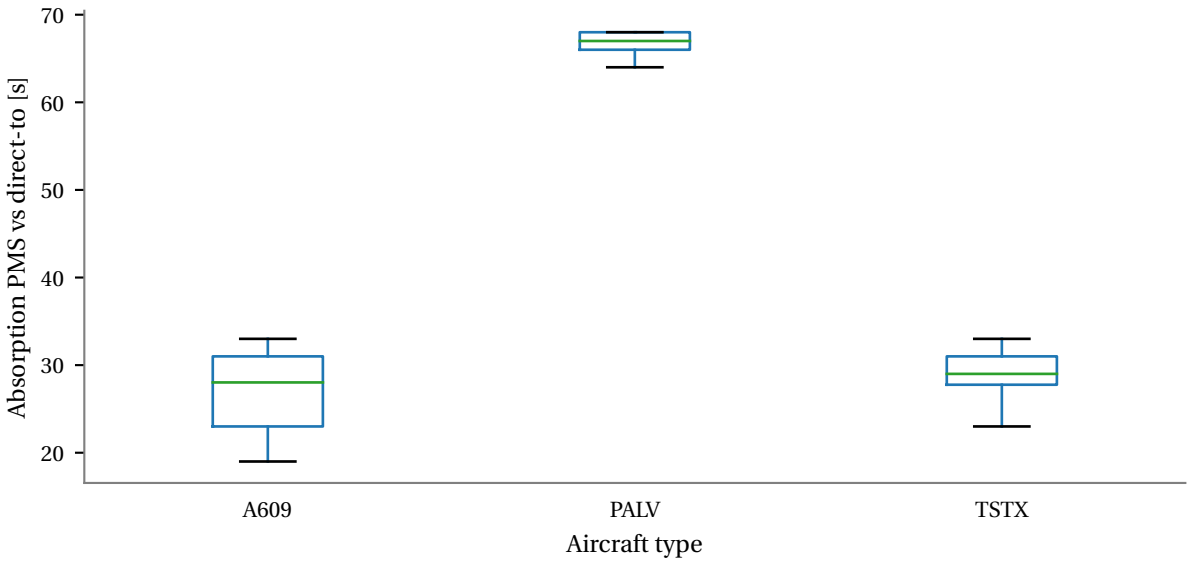

Figure B.4: Absorption capability of the sequencing leg of the Point Merge System (PMS) per aircraft type.

In the main experiment, the logged arrival time is the arrival time in case the full sequencing leg would have been flown. As explained in the scientific paper, the earliest possible arrival time can now be computed in combination with the absorption time. From the preceding arrival time, the earliest safe arrival time can be determined using separation requirements. The spatial separation requirement is converted in a time-based separation requirement, dependent on the aircraft type. When the earliest possible arrival time is later than the time separation requirement added to the arrival slot of the preceding aircraft, it can be concluded that the aircraft could have landed earlier. Figure B.5 illustrates the computation. A sequencing problem is logged when there is no possibility to find an arrival slot that satisfies this condition.

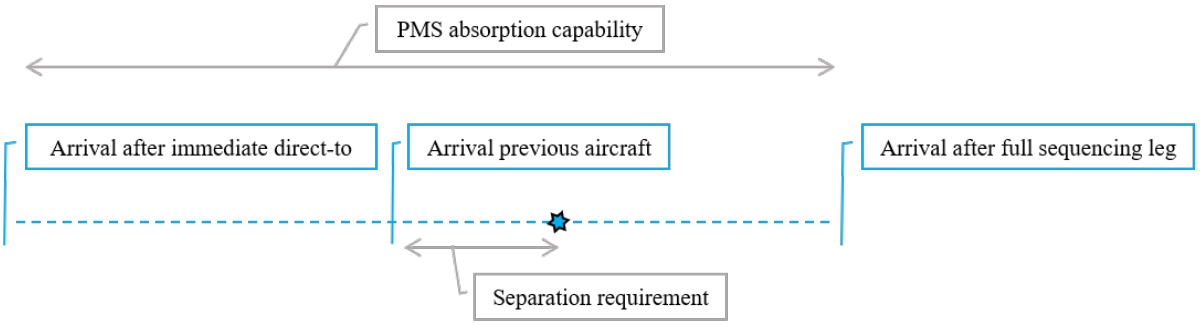

Figure B.5: The earliest safe arrival slot, indicated with a blue star, can be determined by combining the logged arrival time with the absorption capability, the arrival time of the preceding aircraft, and the time separation requirement.

C

Details conflicts and intrusions measured in the main experiment

This chapter provides a detailed overview of all the conflicts and intrusions measured in the main experiment of this research. It provides more information about the different travel directions and aircraft types present in the conflict and intrusion pairs. Furthermore, the conflict and intrusion are plotted in the simulation area to visualize their locations and severity.

C.1. Conflicts

C.1.1. Box plots categorized by traffic mix

This section presents three figures with different box-and-whisker plots, one for each traffic flow respectively. The conflicts are categorized to be between two arriving aircraft, between two departing aircraft, or between one arriving and one departing aircraft. As discussed in Section V of the scientific paper, it can be seen that the number of conflicts between departing and arriving aircraft is significantly reduced once the zone structure is active.

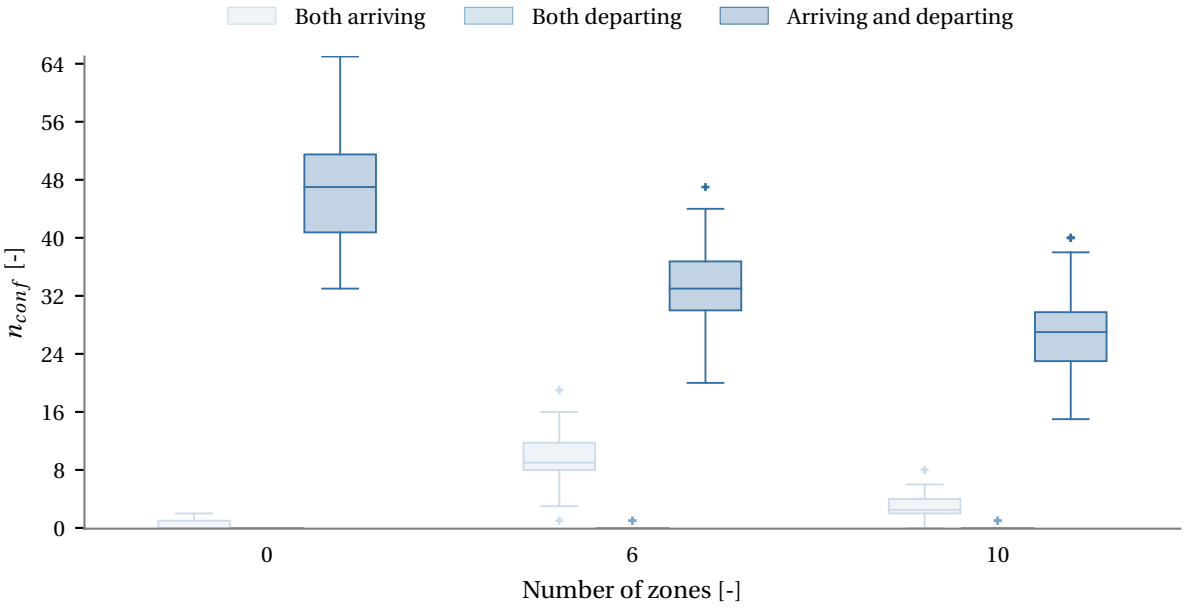

Figure C.1: Number of conflicts measured for low traffic flow, sorted by traffic mix for different airspace concepts.

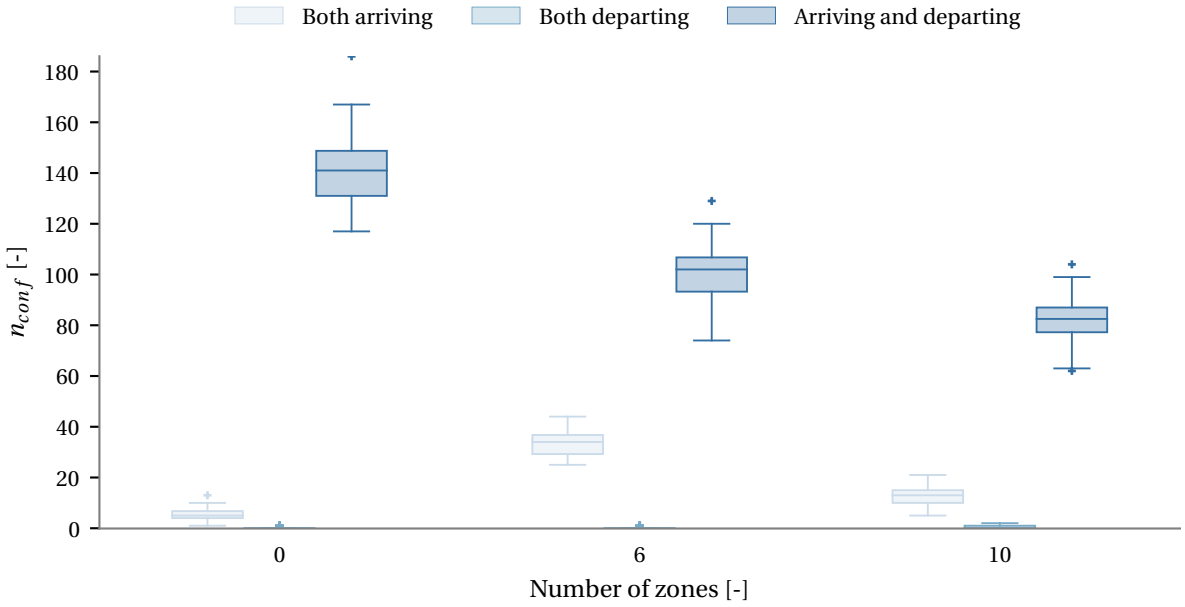

Figure C.2: Number of conflicts measured for medium traffic flow, sorted by traffic mix for different airspace concepts.

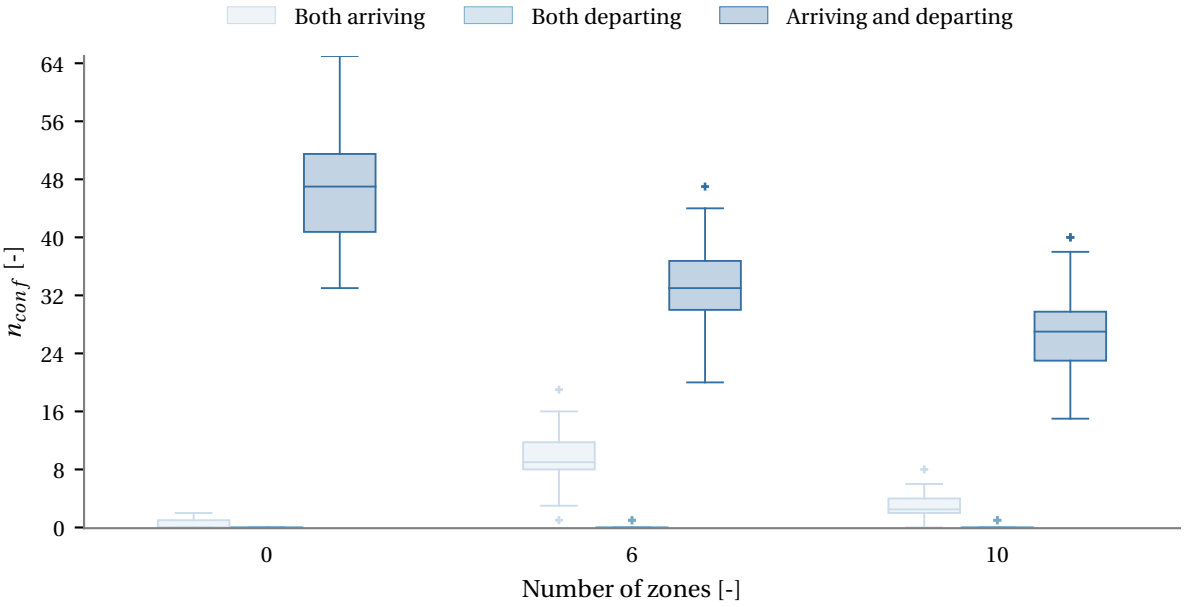

Figure C.3: Number of conflicts measured for high traffic flow, sorted by traffic mix for different airspace concepts.

C.1.2. Box plots categorized by aircraft type

This section again presents three figures with different box-and-whisker plots, one for each traffic flow respectively. This time, the conflicts are categorized based on their traffic type. It can be seen that most conflicts occur between two aircraft of the same type. The number of conflicts between two TSTX aircraft is highest, which can be explained by the fact that the majority of PAVs in the traffic scenarios was of this type. It is interesting to note that not a lot of conflicts occur between different aircraft types, which can be explained by the layered Point Merge Systems.

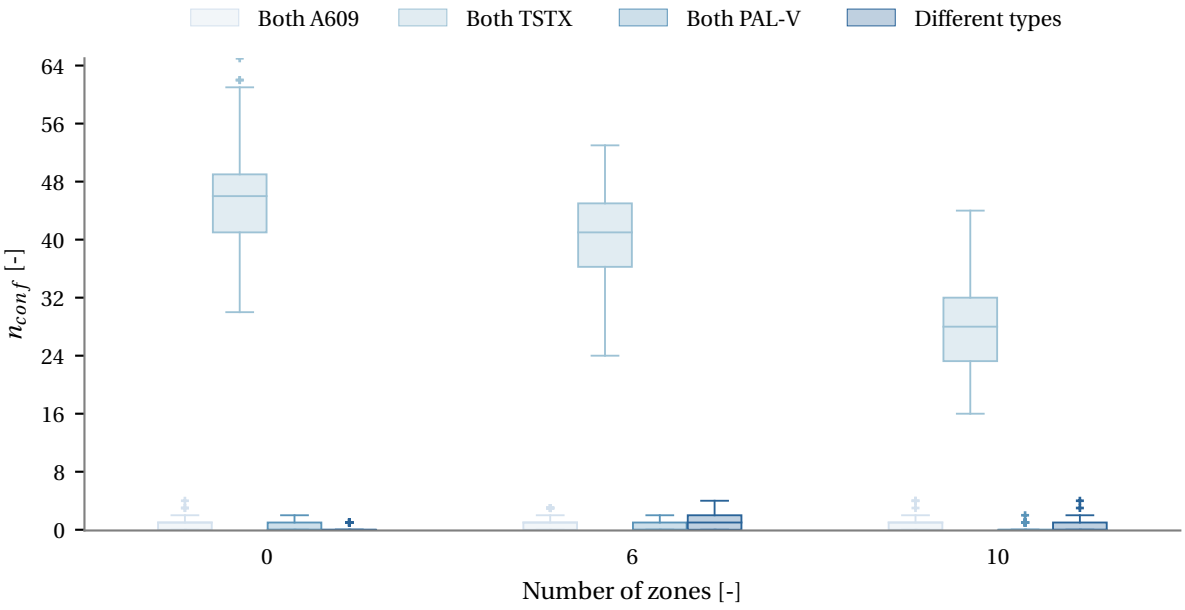

Figure C.4: Number of conflicts measured for low traffic flow, sorted by aircraft type for different airspace concepts.

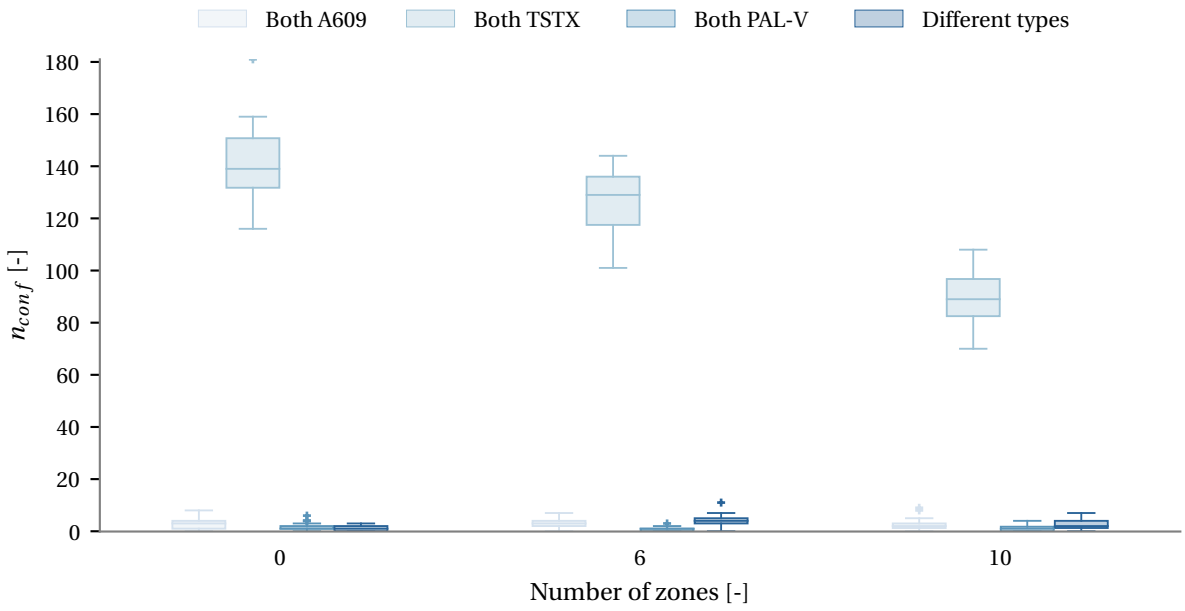

Figure C.5: Number of conflicts measured for medium traffic flow, sorted by aircraft type for different airspace concepts.

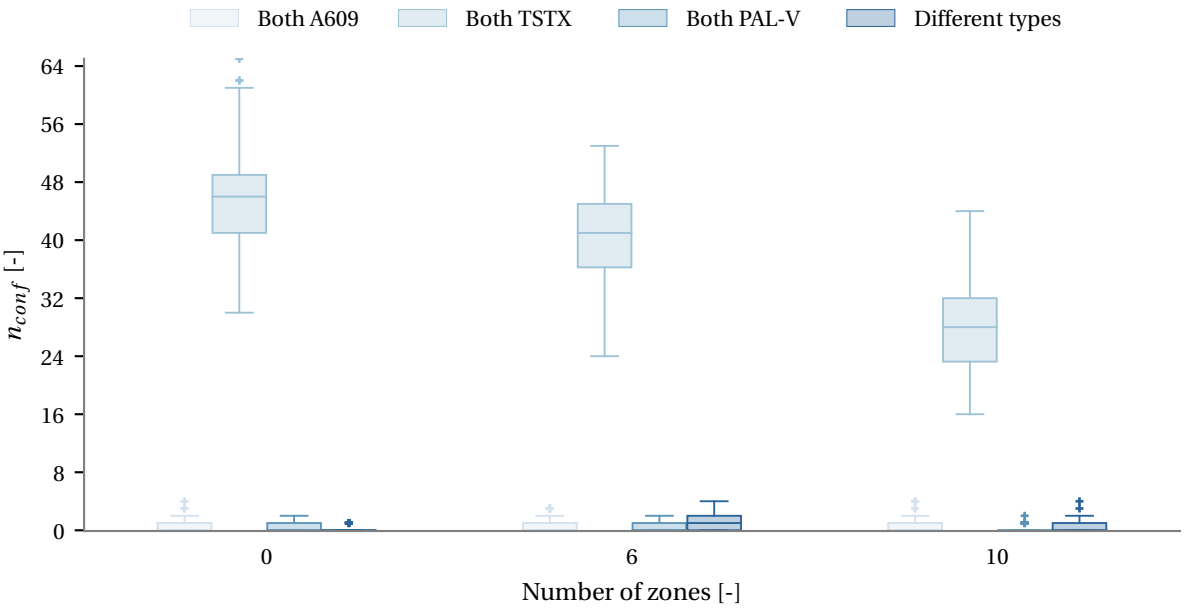

Figure C.6: Number of conflicts measured for high traffic flow, sorted by aircraft type for different airspace concepts.

C.1.3. Conflict locations categorized by traffic mix

In this section, the locations of the conflicts are plotted for the different airspace concept. The color of the conflict shows whether it was between two arriving, two departing, or a mix of travel directions. Again, all three traffic flows are plotted separately, resulting in 3 times 3 different plots.

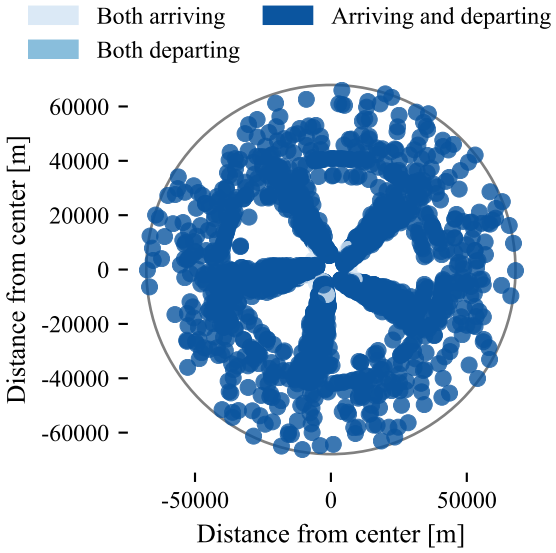

Figure C.7: Conflict locations at low traffic flow for the unstructured airspace concept, categorized by traffic mix.

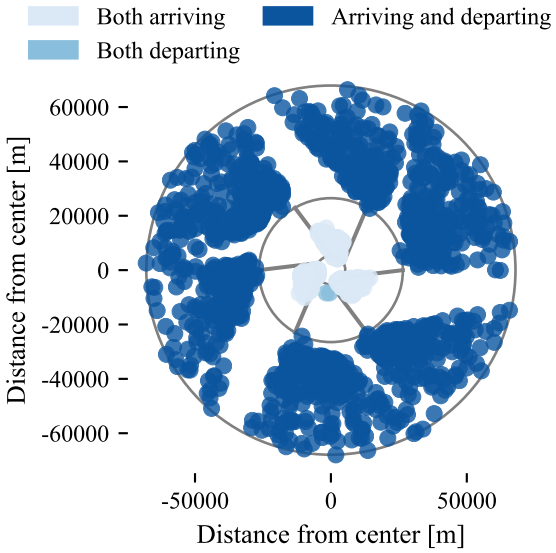

Figure C.8: Conflict locations at low traffic flow for the airspace concept with 6 zones, categorized by traffic mix.

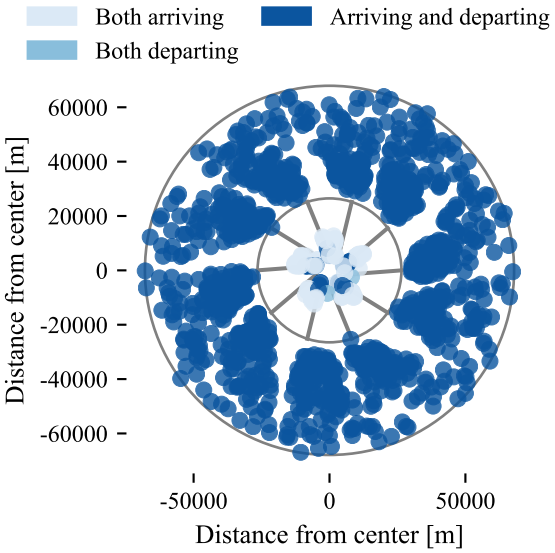

Figure C.9: Conflict locations at low traffic flow for the airspace concept with 10 zones, categorized by traffic mix.

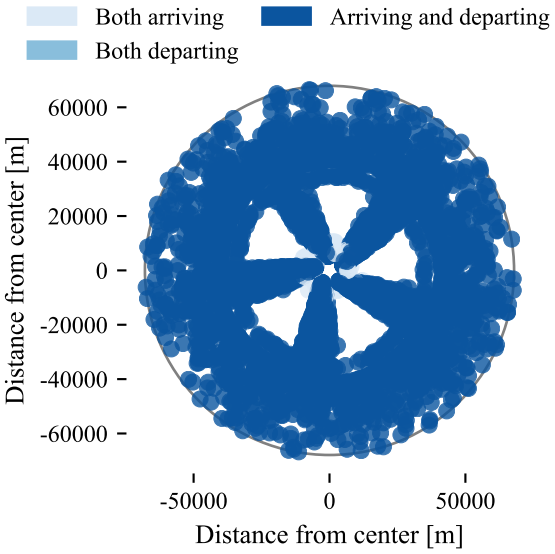

Figure C.10: Conflict locations at medium traffic flow for the unstructured airspace concept, categorized by traffic mix.

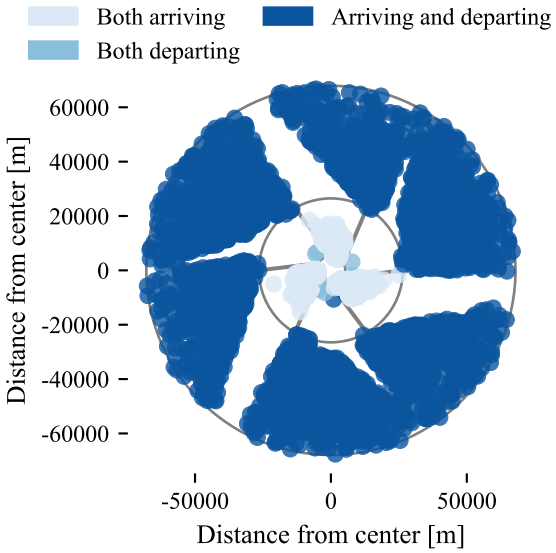

Figure C.11: Conflict locations at medium traffic flow for the airspace concept with 6 zones, categorized by traffic mix.

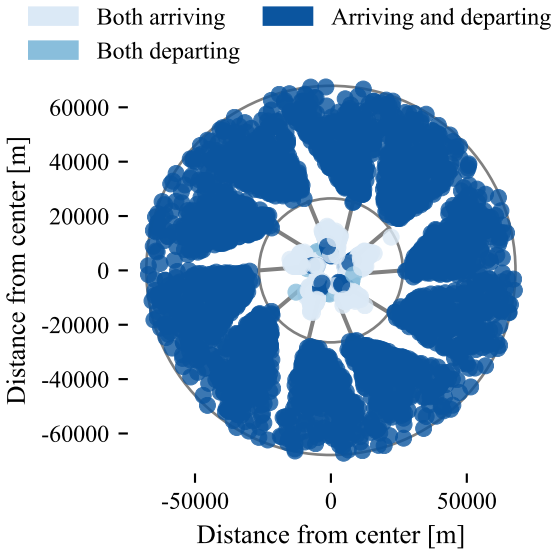

Figure C.12: Conflict locations at medium traffic flow for the airspace concept with 10 zones, categorized by traffic mix.

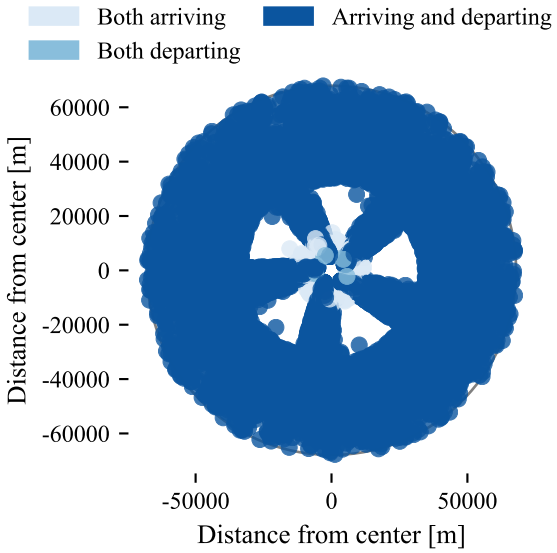

Figure C.13: Conflict locations at high traffic flow for the unstructured airspace concept, categorized by traffic mix.

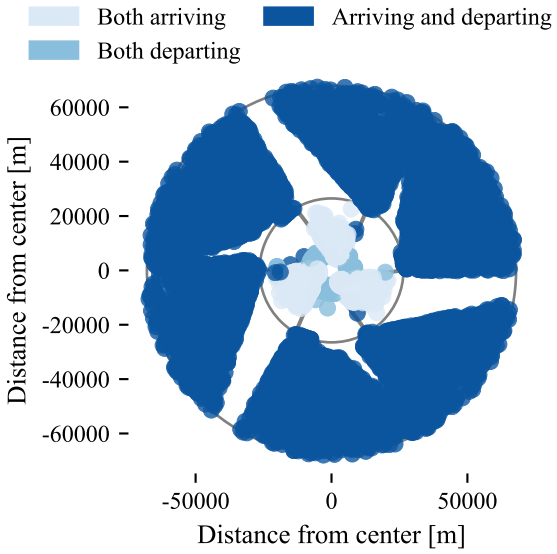

Figure C.14: Conflict locations at high traffic flow for the airspace concept with 6 zones, categorized by traffic mix.

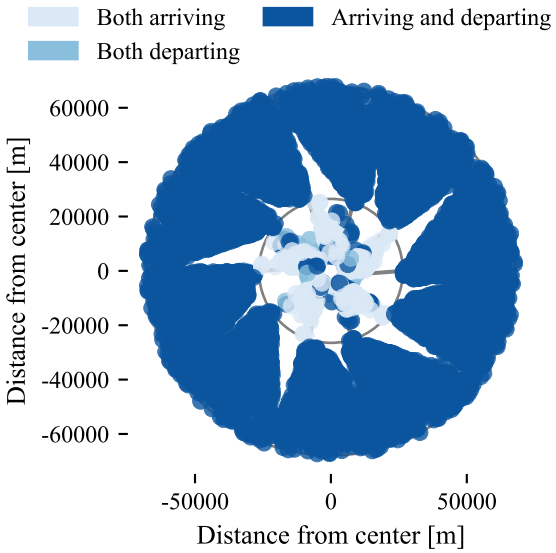

Figure C.15: Conflict locations at high traffic flow for the airspace concept with 10 zones, categorized by traffic mix.

C.1.4. Summarizing tables

Finally, this section provides the summarizing tables for all conflicts measured in the experiment. It also shows the amount of conflicts detected that were categorized to be false based on the structure of the concept (Figure 11 in the scientific paper).

Table C.1: Total number of conflicts for low traffic flow

Zones	Traffic mix	Same zone	Different zones	Outside zones	False detection	Inner radius	**Total**
0	Both arriving	11	7	0	41	6271	6330
0	Both departing	0	0	0	2	0	2
0	Arriving & departing	1285	281	801	0	19	2386
6	Both arriving	485	0	0	691	6311	7487
6	Both departing	2	0	0	72	0	74
6	Arriving & departing	0	17	1637	0	1	1655
10	Both arriving	140	0	0	344	7598	8082
10	Both departing	2	0	0	7	0	9
10	Arriving & departing	0	57	1286	0	2	1345

Table C.2: Total number of conflicts for medium traffic flow

Zones	Traffic mix	Same zone	Different zones	Outside zones	False detection	Inner radius	**Total**
0	Both arriving	201	64	0	968	21074	22307
0	Both departing	8	2	0	6	0	16
0	Arriving & departing	3910	731	2421	0	50	7112
6	Both arriving	1685	0	0	2602	19399	23686
6	Both departing	8	0	0	320	0	328
6	Arriving & departing	2	66	4966	0	1	5035
10	Both arriving	637	0	0	1714	23944	26295
10	Both departing	14	3	0	113	0	130
10	Arriving & departing	0	168	3950	0	9	4127

Table C.3: Total number of conflicts for high traffic flow

Zones	Traffic mix	Same zone	Different zones	Outside zones	False detection	Inner radius	**Total**
0	Both arriving	1250	243	0	4762	66942	73197
0	Both departing	371	31	0	11	0	413
0	Arriving & departing	11596	2093	7250	0	152	21091
6	Both arriving	4955	2	0	8114	57364	70435
6	Both departing	56	1	0	1191	0	1248
6	Arriving & departing	3	131	15054	0	1	15189
10	Both arriving	2031	2	0	6681	73492	82206
10	Both departing	42	2	0	499	0	543
10	Arriving & departing	6	511	11994	0	19	12530

C.2. Intrusions

This section provides a similar overview of the intrusion details. In addition to the plots provided in the conflict section, section C.2.3 is added to show the severity of the different intrusions.

C.2.1. Box plots categorized by traffic mix

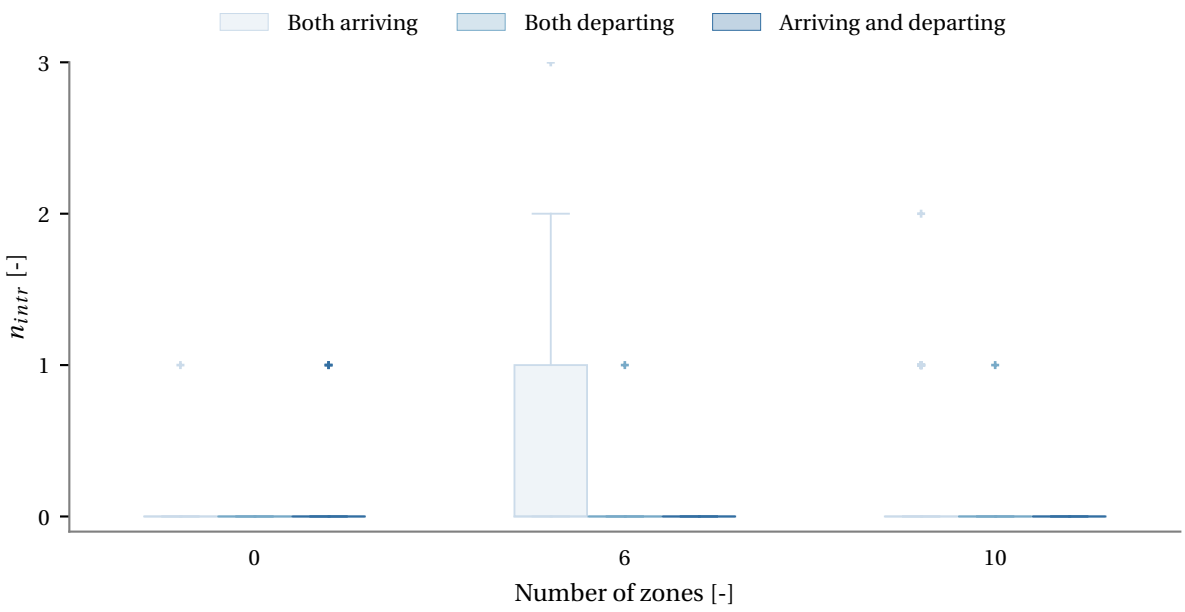

Figure C.16: Number of intrusions measured for low traffic flow, sorted by traffic mix for different airspace concepts.

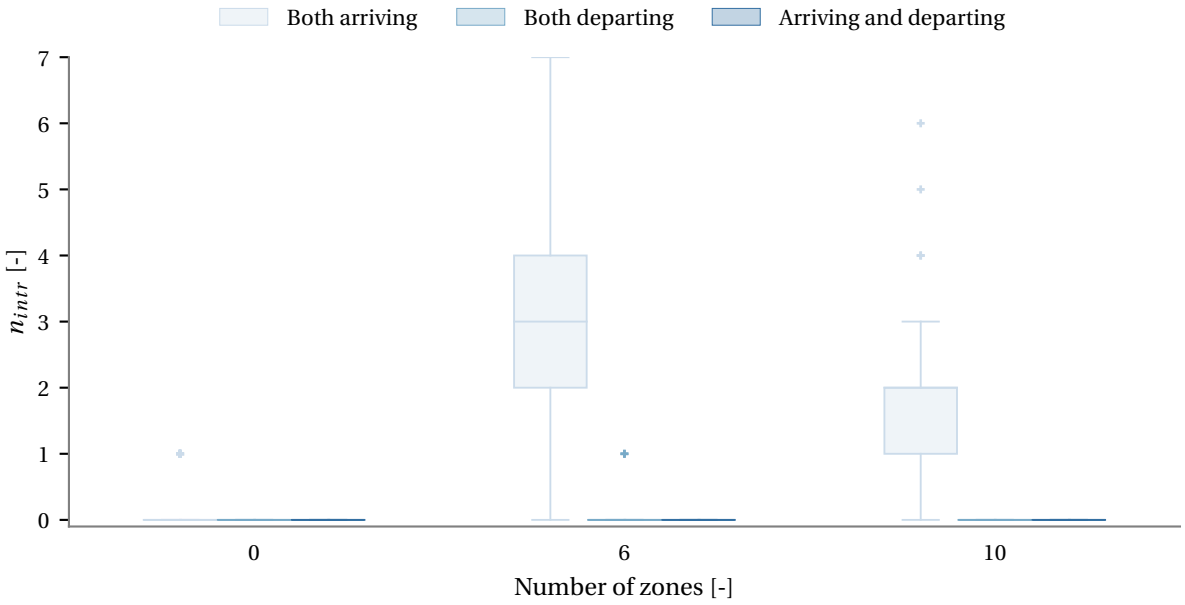

Figure C.17: Number of intrusions measured for medium traffic flow, sorted by traffic mix for different airspace concepts.

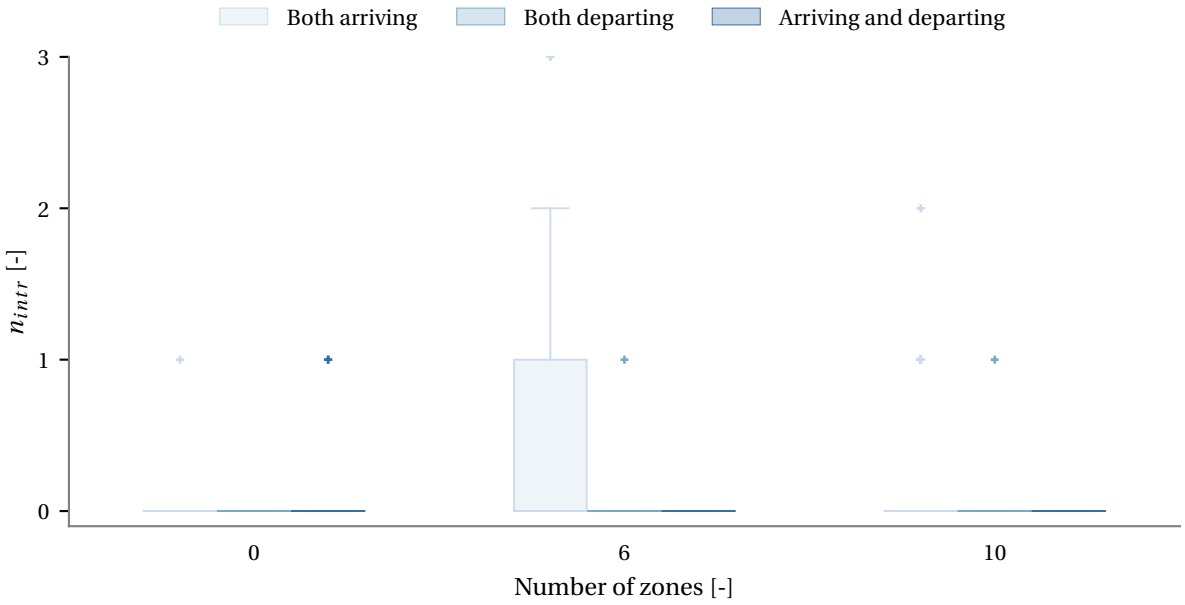

Figure C.18: Number of intrusions measured for high traffic flow, sorted by traffic mix for different airspace concepts.

C.2.2. Box plots categorized by aircraft type

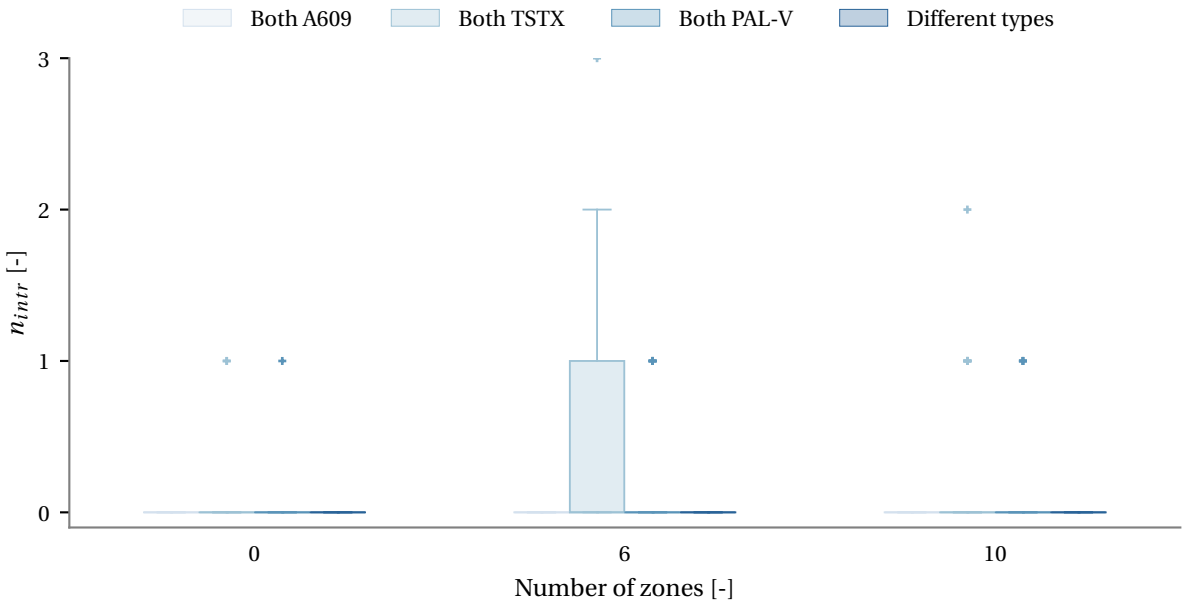

Figure C.19: Number of intrusions measured for low traffic flow, sorted by aircraft type for different airspace concepts.

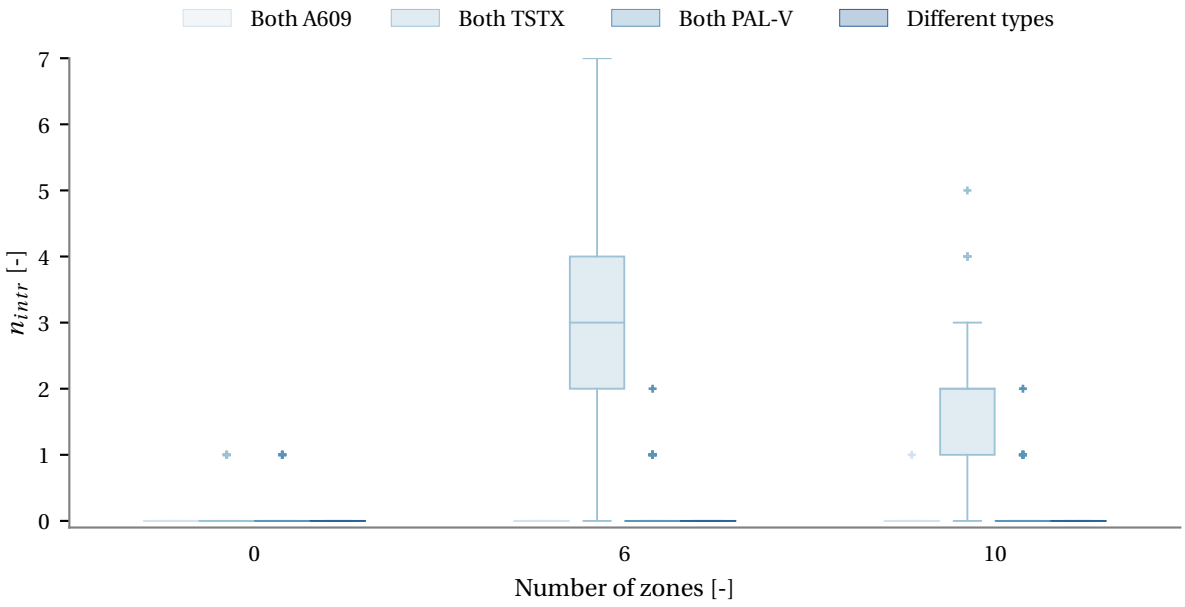

Figure C.20: Number of intrusions measured for medium traffic flow, sorted by aircraft type for different airspace concepts.

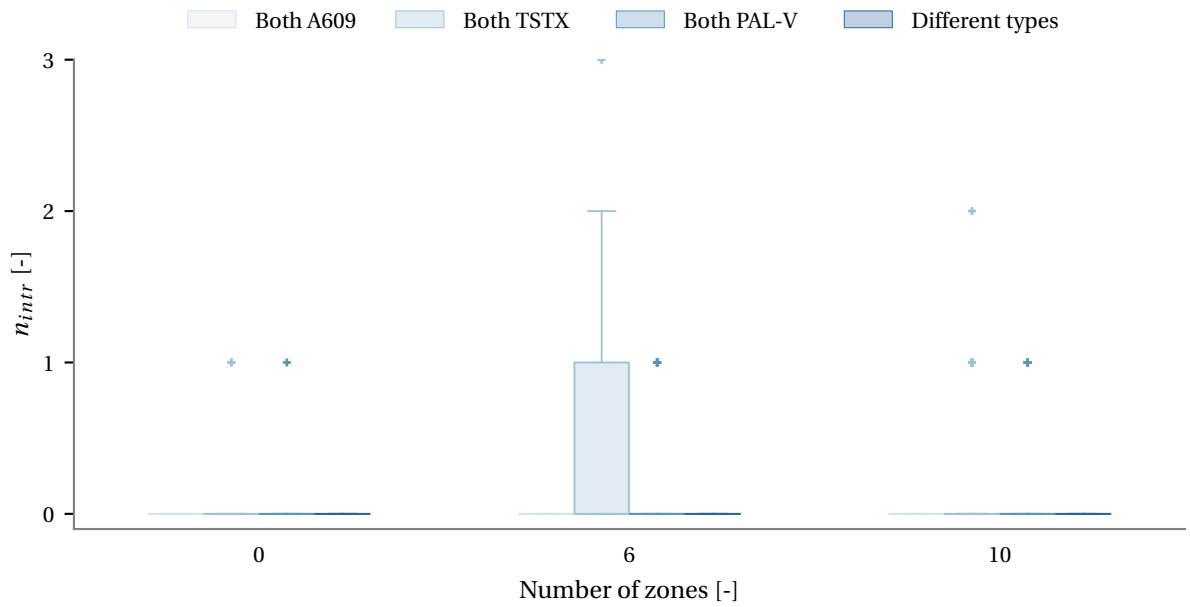

Figure C.21: Number of intrusions measured for high traffic flow, sorted by aircraft type for different airspace concepts.

C.2.3. Intrusion locations categorized by intrusion severity

This section shows the locations of the intrusions. The color indicates the severity of the measured intrusion.

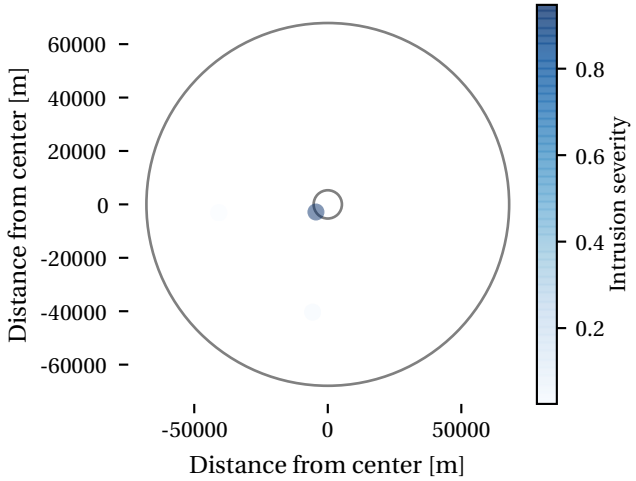

Figure C.22: Intrusion locations at low traffic flow for the unstructured airspace concept, categorized by intrusion severity.

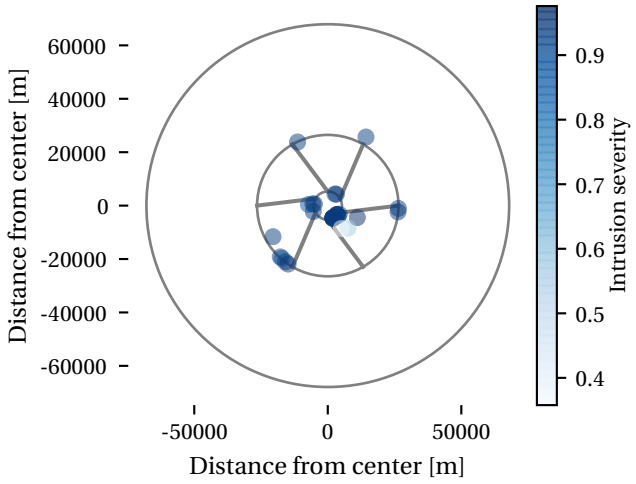

Figure C.23: Intrusion locations at low traffic flow for the airspace concept with 6 zones, categorized by intrusion severity.

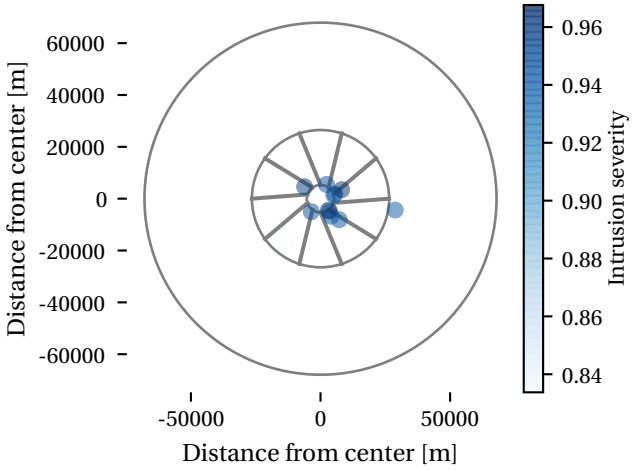

Figure C.24: Intrusion locations at low traffic flow for the airspace concept with 10 zones, categorized by intrusion severity.

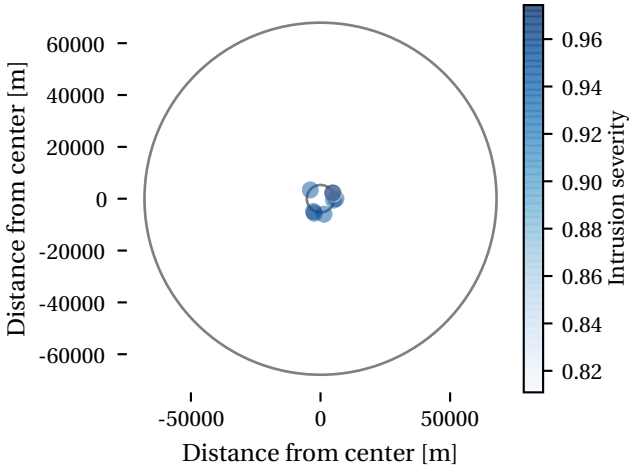

Figure C.25: Intrusion locations at medium traffic flow for the unstructured airspace concept, categorized by intrusion severity.

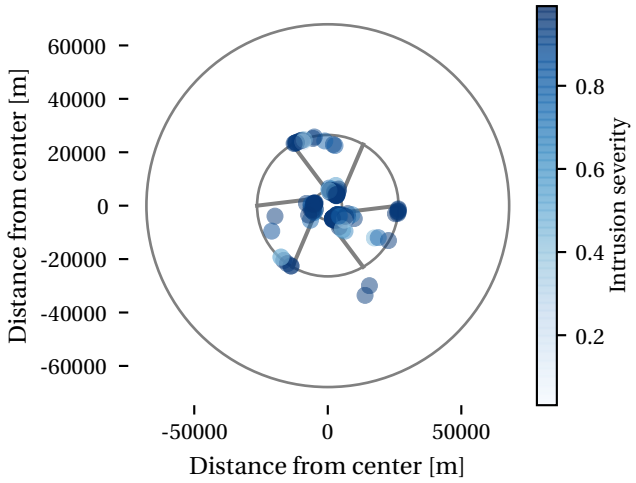

Figure C.26: Intrusion locations at medium traffic flow for the airspace concept with 6 zones, categorized by intrusion severity.

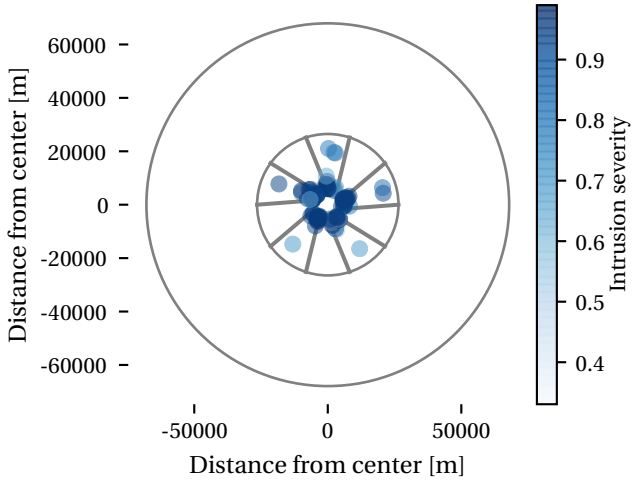

Figure C.27: Intrusion locations at medium traffic flow for the airspace concept with 10 zones, categorized by intrusion severity.

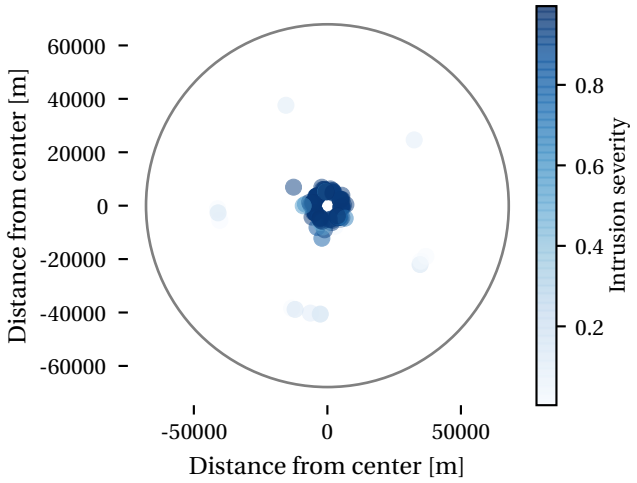

Figure C.28: Intrusion locations at high traffic flow for the unstructured airspace concept, categorized by intrusion severity.

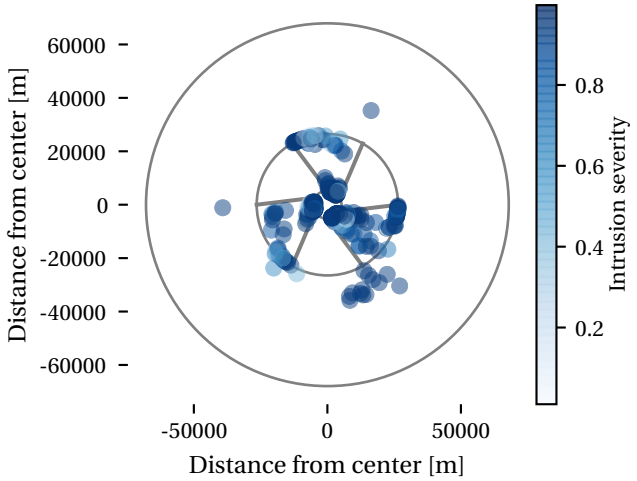

Figure C.29: Intrusion locations at high traffic flow for the airspace concept with 6 zones, categorized by intrusion severity.

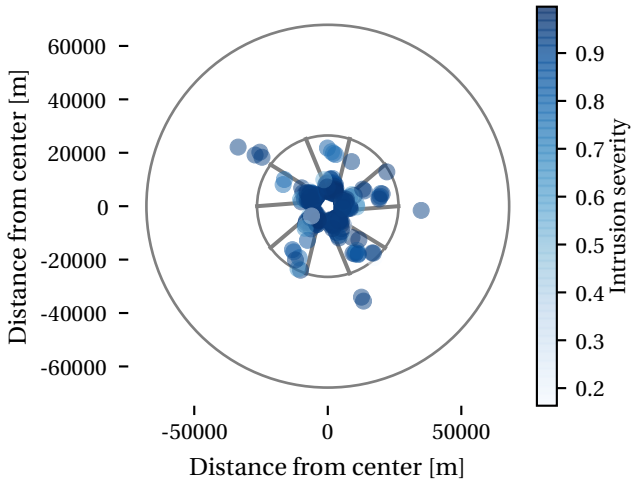

Figure C.30: Intrusion locations at high traffic flow for the airspace concept with 10 zones, categorized by intrusion severity.

C.2.4. Intrusion locations categorized by traffic mix

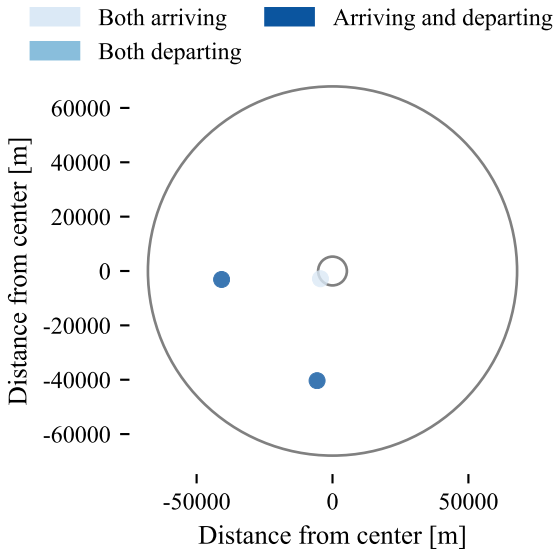

Figure C.31: Intrusion locations at low traffic flow for the unstructured airspace concept, categorized by traffic mix.

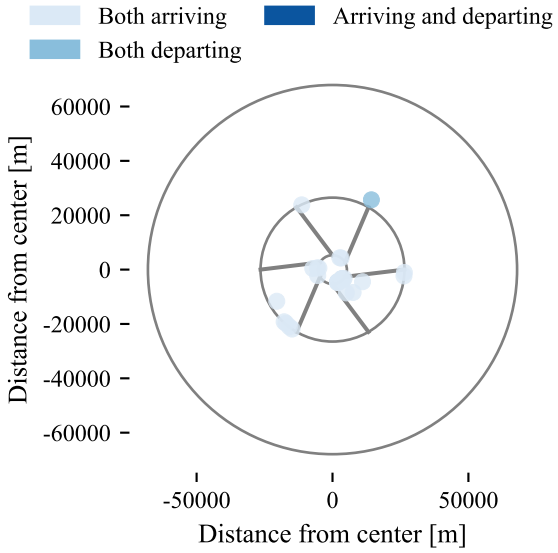

Figure C.32: Intrusion locations at low traffic flow for the airspace concept with 6 zones, categorized by traffic mix.

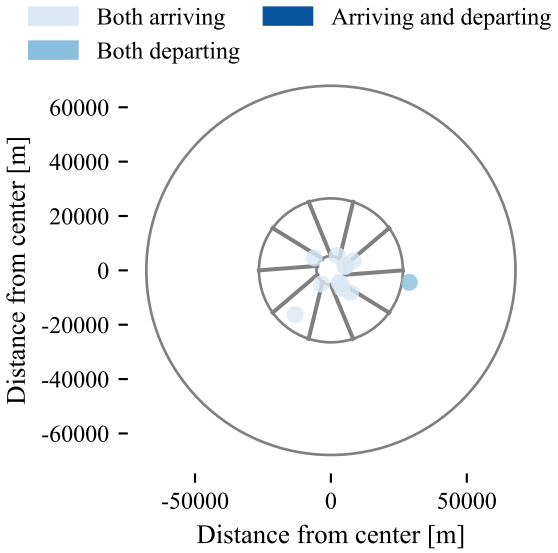

Figure C.33: Intrusion locations at low traffic flow for the airspace concept with 10 zones, categorized by traffic mix.

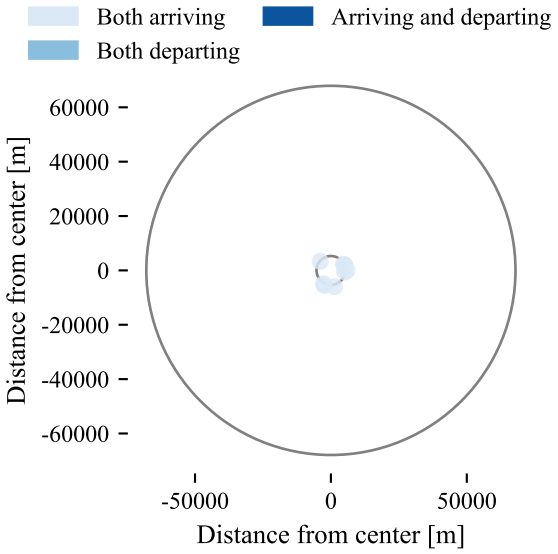

Figure C.34: Intrusion locations at medium traffic flow for the unstructured airspace concept, categorized by traffic mix.

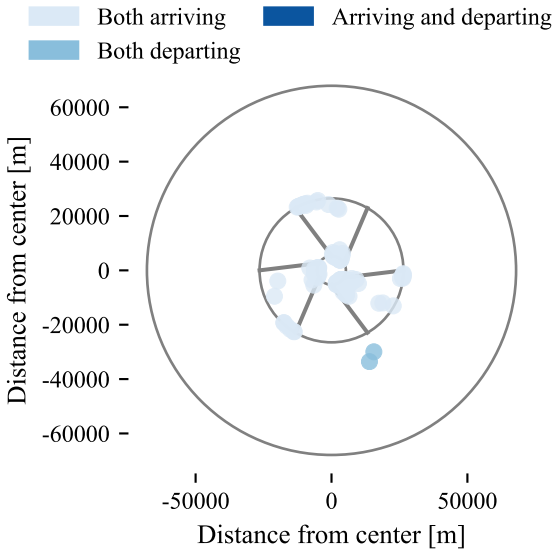

Figure C.35: Intrusion locations at medium traffic flow for the airspace concept with 6 zones, categorized by traffic mix.

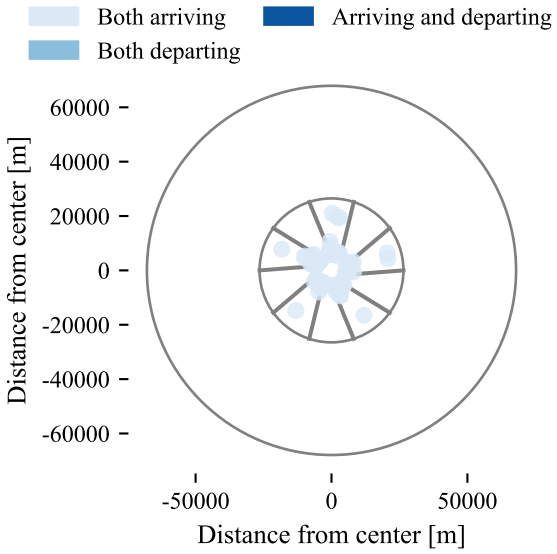

Figure C.36: Intrusion locations at medium traffic flow for the airspace concept with 10 zones, categorized by traffic mix.

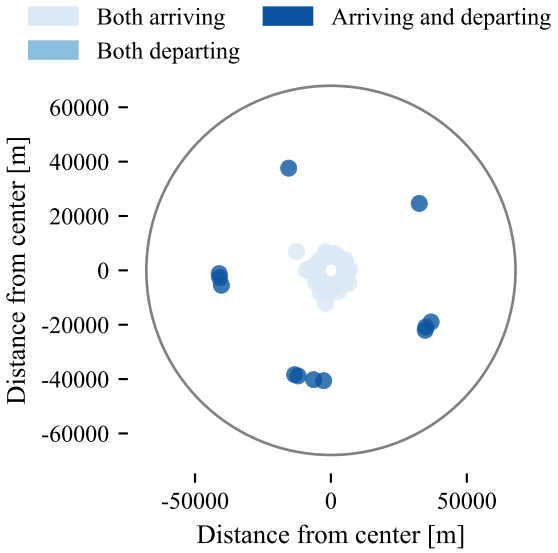

Figure C.37: Intrusion locations at high traffic flow for the unstructured airspace concept, categorized by traffic mix.

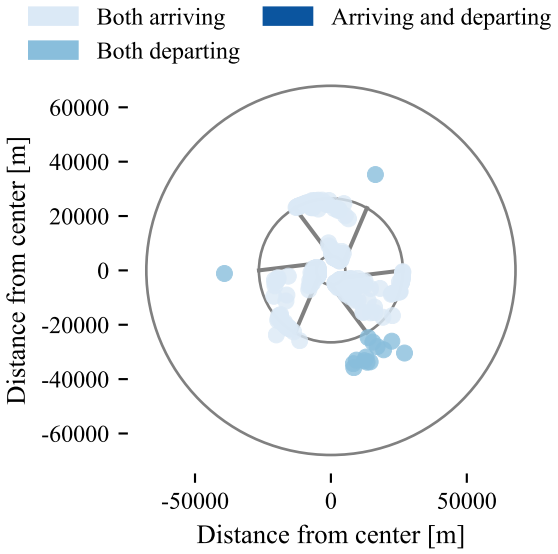

Figure C.38: Intrusion locations at high traffic flow for the airspace concept with 6 zones, categorized by traffic mix.

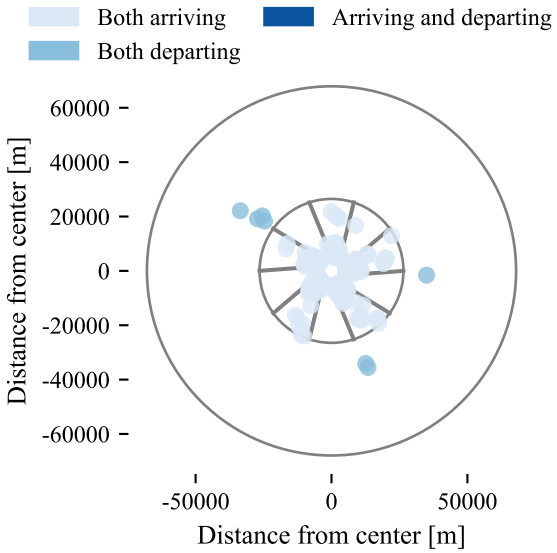

Figure C.39: Intrusion locations at high traffic flow for the airspace concept with 10 zones, categorized by traffic mix.

C.2.5. Summarizing tables

Finally, this section provides the summarizing tables for all intrusions measured in the experiment.

Table C.4: Total number of intrusions for low traffic flow

Zones	Traffic mix	Same zone	Different zones	Outside zones	Inner radius	**Total**
0	Both arriving	1	0	0	1931	1932
0	Both departing	0	0	0	0	0
0	Arriving & departing	93	4	14	19	130
6	Both arriving	21	0	8	2604	2633
6	Both departing	0	0	1	0	1
6	Arriving & departing	0	0	11	0	11
10	Both arriving	11	0	0	2228	2239
10	Both departing	0	0	1	0	1
10	Arriving & departing	0	17	7	2	26

Table C.5: Total number of intrusions for medium traffic flow

Zones	Traffic mix	Same zone	Different zones	Outside zones	Inner radius	**Total**
0	Both arriving	8	1	0	6415	6424
0	Both departing	3	0	0	0	3
0	Arriving & departing	351	17	18	49	435
6	Both arriving	132	1	28	8207	8368
6	Both departing	1	0	2	0	3
6	Arriving & departing	0	0	15	0	15
10	Both arriving	91	0	0	7251	7342
10	Both departing	0	0	0	0	0
10	Arriving & departing	0	45	19	7	71

Table C.6: Total number of intrusions for high traffic flow

Zones	Traffic mix	Same zone	Different zones	Outside zones	Inner radius	**Total**
0	Both arriving	112	5	0	21821	21938
0	Both departing	184	2	0	0	186
0	Arriving & departing	1051	47	68	152	1318
6	Both arriving	459	3	90	24308	24860
6	Both departing	20	0	15	0	35
6	Arriving & departing	0	0	58	0	58
10	Both arriving	434	2	3	22537	22976
10	Both departing	9	0	7	0	16
10	Arriving & departing	0	125	63	18	206

D

Significance tables

To verify significance of the effect of the airspace concept and traffic flow on the dependent variables, the Repeated Measures ANOVA was used with the F-statistic [12]. This statistical test assumes that the relationship between pairs of the experimental conditions is similar, also known as sphericity. To test sphericity, Mauchly's test was performed. Mauchly's test tests the hypothesis that the variances of the differences between conditions are equal. Therefore, if Mauchly's test statistic is significant ($p < 0.05$), the condition of sphericity is not met. In case the sphericity assumption is violated, the test loses power and this increases the chances of for example Type II errors [12]. As explained in Section IV of the scientific paper, in this case a conservative Greenhouse-Geisser adjustment was applied to adjust the degrees of freedom of the Repeated Measures ANOVA. Additionally, a pairwise comparison test was performed post-hoc to test whether all pairwise comparisons individually resulted in significant differences. In these analyses, a Bonferroni correction was used to correct for the fact that multiple comparisons were made on one dataset [2]. In this chapter, four tables are presented for each dependent variable:

1. Mauchly's test of sphericity
2. Tests of within-subjects effects
3. Pairwise comparison effect of the number of zones on the variable
4. Pairwise comparison effect of the traffic flow on the variable

In case of a Greenhouse-Geisser adjustment, the degrees of freedom in the second table are printed in italics.

D.1. Number of conflicts

Table D.1: Mauchly's test of sphericity for the number of conflicts

Variable	Degrees of freedom	χ^2	p
Number of zones	2	0.670	0.715
Traffic flow	2	18.878	0.000
Interaction	9	57.928	0.000

Table D.2: Tests of within-subjects effects for the number of conflicts

Variable	Degrees of freedom	F-statistic	p
Number of zones	2	973.642	0.000
Traffic flow	*1.509*	18691.610	0.000
Interaction	*2.675*	387.775	0.000

Table D.3: Pairwise comparison effect of the number of zones on the number of conflicts

Number of zones (I)	Number of zones (J)	Mean difference (I-J)	p
0	6	23.240	0.000
	10	78.073	0.000
6	0	-23.240	0.000
	10	54.833	0.000
10	0	-78.073	0.000
	6	-54.833	0.000

Table D.4: Pairwise comparison effect of the traffic flow on the number of conflicts

Traffic flow (I)	Traffic flow (J)	Mean difference (I-J)	p
Low	Medium	-85.500	0.000
	High	-344.087	0.000
Medium	Low	85.500	0.000
	High	-258.587	0.000
High	Low	344.087	0.000
	Medium	258.587	0.000

D.2. Number of intrusions

Table D.5: Mauchly's test of sphericity for the number of intrusions

Variable	Degrees of freedom	χ^2	p
Number of zones	2	4.595	0.101
Traffic flow	2	38.452	0.000
Interaction	9	94.886	0.000

Table D.6: Tests of within-subjects effects for the number of intrusions

Variable	Degrees of freedom	F-statistic	p
Number of zones	2	259.186	0.000
Traffic flow	*1.289*	705.981	0.000
Interaction	*2.334*	86.987	0.000

Table D.7: Pairwise comparison effect of the number of zones on the number of intrusions

Number of zones (I)	Number of zones (J)	Mean difference (I-J)	p
0	6	-4.120	0.000
	10	-2.720	0.000
6	0	4.120	0.000
	10	1.400	0.000
10	0	2.720	0.000
	6	1.400	0.000

Table D.8: Pairwise comparison effect of the traffic flow on the number of intrusions

Traffic flow (I)	Traffic flow (J)	Mean difference (I-J)	p
Low	Medium	-1.453	0.000
	High	-7.307	0.000
Medium	Low	1.453	0.000
	High	-5.853	0.000
High	Low	7.307	0.000
	Medium	5.853	0.000

D.3. Intrusion severity

Table D.9: Mauchly's test of sphericity for the intrusions severity

Variable	Degrees of freedom	χ^2	p
Number of zones	2	1.114	0.573
Traffic flow	2	1.046	0.593
Interaction	9	24.531	0.004

Table D.10: Tests of within-subjects effects for the intrusions severity

Variable	Degrees of freedom	F-statistic	p
Number of zones	2	88.025	0.000
Traffic flow	2	221.621	0.000
Interaction	*3.274*	16.921	0.000

Table D.11: Pairwise comparison effect of the number of zones on the intrusions severity

Number of zones (I)	Number of zones (J)	Mean difference (I-J)	p
0	6	-0.422	0.000
	10	-0.315	0.000
6	0	0.422	0.000
	10	0.107	0.007
10	0	0.315	0.000
	6	-0.107	0.007

Table D.12: Pairwise comparison effect of the traffic flow on the intrusions severity

Traffic flow (I)	Traffic flow (J)	Mean difference (I-J)	p
Low	Medium	-4.040	0.000
	High	-0.716	0.000
Medium	Low	0.404	0.000
	High	-0.312	0.000
High	Low	0.716	0.000
	Medium	0.312	0.000

D.4. Intrusion Prevention Rate

Table D.13: Mauchly's test of sphericity for the Intrusion Prevention Rate

Variable	Degrees of freedom	χ^2	p
Number of zones	2	1.891	0.388
Traffic flow	2	10.543	0.005
Interaction	9	67.380	0.000

Table D.14: Tests of within-subjects effects for the Intrusion Prevention Rate

Variable	Degrees of freedom	F-statistic	p
Number of zones	2	159.843	0.000
Traffic flow	*1.671*	59.730	0.000
Interaction	*2.594*	8.139	0.000

Table D.15: Pairwise comparison effect of the number of zones on the Intrusion Prevention Rate

Number of zones (I)	Number of zones (J)	Mean difference (I-J)	p
0	6	0.019	0.000
	10	0.017	0.000
6	0	-0.019	0.000
	10	-0.003	0.000
10	0	-0.017	0.000
	6	0.003	0.000

Table D.16: Pairwise comparison effect of the traffic flow on the Intrusion Prevention Rate

Traffic flow (I)	Traffic flow (J)	Mean difference (I-J)	p
Low	Medium	0.007	0.000
	High	0.014	0.000
Medium	Low	-0.007	0.000
	High	0.006	0.000
High	Low	-0.014	0.000
	Medium	-0.006	0.000

D.5. Number of sequencing errors

Table D.17: Mauchly's test of sphericity for the number of sequencing issues

Variable	Degrees of freedom	χ^2	p
Number of zones	2	21.895	0.000
Traffic flow	-	-	-
Interaction	-	-	-

Table D.18: Tests of within-subjects effects for the number of sequencing issues

Variable	Degrees of freedom	F-statistic	p
Number of zones	*1.464*	5.861	0.009
Traffic flow	*1*	41.818	0.000
Interaction	*1.464*	5.861	0.009

Table D.19: Pairwise comparison effect of the number of zones on the number of sequencing issues

Number of zones (I)	Number of zones (J)	Mean difference (I-J)	p
0	6	-0.293	-
	10	-0.153	0.000
6	0	0.293	-
	10	0.140	0.000
10	0	0.153	0.000
	6	-0.140	0.000

Table D.20: Pairwise comparison effect of the traffic flow on the number of sequencing issues

Traffic flow (I)	Traffic flow (J)	Mean difference (I-J)	p
Low	Medium	0.000	-
	High	-0.647	0.000
Medium	Low	0.000	-
	High	-0.647	0.000
High	Low	0.647	0.000
	Medium	0.647	0.000

D.6. Average delays

Table D.21: Mauchly's test of sphericity for the average arrival delay with respect to a direct-to at the entrance of the Point Merge System

Variable	Degrees of freedom	χ^2	p
Number of zones	2	9.398	0.009
Traffic flow	2	3.945	0.139
Interaction	9	14.460	0.107

Table D.22: Tests of within-subjects effects for the average arrival delay with respect to a direct-to at the entrance of the Point Merge System

Variable	Degrees of freedom	F-statistic	p
Number of zones	*1.698*	100.101	0.000
Traffic flow	2	1344.489	0.000
Interaction	4	28.297	0.000

Table D.23: Pairwise comparison effect of the number of zones on the average arrival delay with respect to a direct-to at the entrance of the Point Merge System

Number of zones (I)	Number of zones (J)	Mean difference (I-J)	p
0	6	-0.286	0.000
	10	-0.094	0.000
6	0	0.286	0.000
	10	0.192	0.000
10	0	0.094	0.000
	6	-0.192	0.000

Table D.24: Pairwise comparison effect of the traffic flow on the average arrival delay with respect to a direct-to at the entrance of the Point Merge System

Traffic flow (I)	Traffic flow (J)	Mean difference (I-J)	p
Low	Medium	-8.660	0.000
	High	-2.784	0.000
Medium	Low	0.866	0.000
	High	-1.919	0.000
High	Low	2.784	0.000
	Medium	1.191	0.000

D.7. Extra distance flown

Table D.25: Mauchly's test of sphericity for the extra distance flown with respect to a direct flight

Variable	Degrees of freedom	χ^2	p
Number of zones	2	64.542	0.000
Traffic flow	0.968	1.627	0.443
Interaction	9	147.271	0.000

Table D.26: Tests of within-subjects effects for the extra distance flown with respect to a direct flight

Variable	Degrees of freedom	F-statistic	p
Number of zones	*1.15*	129431.619	0.000
Traffic flow	2	0.881	0.418
Interaction	*2.129*	1.470	0.234

Table D.27: Pairwise comparison effect of the number of zones on the extra distance flown with respect to a direct flight

Number of zones (I)	Number of zones (J)	Mean difference (I-J)	p
0	6	-7.456	0.000
	10	-3.207	0.000
6	0	7.456	0.000
	10	4.249	0.000
10	0	3.207	0.000
	6	-4.249	0.000

Table D.28: Pairwise comparison effect of the traffic flow on the extra distance flown with respect to a direct flight

Traffic flow (I)	Traffic flow (J)	Mean difference (I-J)	p
Low	Medium	0.015	1.000
	High	-0.006	1.000
Medium	Low	-0.150	1.000
	High	-0.210	0.546
High	Low	0.006	1.000
	Medium	0.021	0.546

D.8. Domino Effect Parameter

Table D.29: Mauchly's test of sphericity for the Domino Effect Parameter

Variable	Degrees of freedom	χ^2	p
Number of zones	2	3.337	0.189
Traffic flow	2	2.118	0.347
Interaction	9	22.090	0.090

Table D.30: Tests of within-subjects effects for the Domino Effect Parameter

Variable	Degrees of freedom	F-statistic	p
Number of zones	2	45.700	0.000
Traffic flow	2	0.382	0.684
Interaction	*3.151*	2.915	0.034

Table D.31: Pairwise comparison effect of the number of zones on the Domino Effect Parameter

Number of zones (I)	Number of zones (J)	Mean difference (I-J)	p
0	6	-0.032	0.000
	10	-0.034	0.000
6	0	0.032	0.000
	10	-0.001	1.000
10	0	0.034	0.000
	6	0.001	1.000

Table D.32: Pairwise comparison effect of the traffic flow on the Domino Effect Parameter

Traffic flow (I)	Traffic flow (J)	Mean difference (I-J)	p
Low	Medium	0.001	1.000
	High	-0.002	1.000
Medium	Low	-0.001	1.000
	High	-0.003	1.000
High	Low	0.002	1.000
	Medium	0.003	1.000

E

Source code BlueSky plug-in

This chapter contains the Python source code of the plug-in that was developed to implement the zone structure in BlueSky, an open data and open source air traffic simulator developed at the TU Delft [16]. The gray arrows emphasizes a broken line. Additional tools and functions that were developed for this thesis are not included in this report, but they can be found online: `https://github.com/anoukscholtes/bluesky`.

```
"""
This module is used to implement the zone concept in BlueSky.

File name: zone_implementation.py
Author: Anouk Scholtes (4139011)
Date created: 26/06/2017
Date last modified: 03/12/2017
Python Version: 3.6
"""

# Import the global bluesky objects.
from bluesky import stack, traf, tools, zonetools, scr
import bluesky as bs
import numpy as np

# Set up a global class that contains all descriptive variables for the zone structure
class Zone:
    def __init__(self):
        self.center_lat = 0.0   # Latitude of the zone center [deg]
        self.center_lon = 0.0   # Longitude of the zone center [deg]
        self.R_in = 0.0         # Inner radius of the zone structure [m]
        self.R_out = 0.0        # Outer radius of the zone structure [m]
        self.number = 0         # Number of zones [-]
        self.dangle = 0.0       # Degrees subtended by a single zone [deg]
        self.skew = 0.0         # Skewness factor of outer radius w.r.t. inner radius [-]
        self.dhdg = 0.0         # Heading change in case correction steering is required [deg]
        self.startlat = []      # List of latitudes for the start of the zone edges [deg]
        self.startlon = []      # List of longitudes for the start of the zone edges [deg]
        self.endlat = []        # List of latitudes for the end of the zone edges [deg]
        self.endlon = []        # List of longitudes for the end of the zone edges [deg]
```

```
31          self.arrivalBool = []    # List with booleans to check which zones are
    ↪ arrival zones [-]
32          self.acIDrisk = []       # List with all aircraft IDs that risk edge
    ↪ surpassing [-]
33
34  # Globals
35  zonedef = None
36  wpidx   = 1
37  switch = False
38
39  ### Initialization function of the plugin.
40  def init_plugin():
41      # Initiate global variable zonedef as an object of class Zone
42      global zonedef
43      zonedef = Zone()
44      scr.swlabel=1
45
46      # Initiate way point id for corrections with 1
47      global wpidx
48      wpidx = 1
49
50      # Configuration parameters
51      config = {
52          # The name of this plugin
53          'plugin_name':      'ZONES',
54
55          # The type of this plugin: a simulation plugins.
56          'plugin_type':      'sim',
57
58          # Update interval in seconds.
59          'update_interval': 2.5,
60
61          # The update function is called after traffic is updated.
62          'update':        update,
63
64          # The preupdate function is called before traffic is updated.
65          'preupdate':           preupdate,
66
67          # The reset function is used to clear the state in between simulations.
68          'reset':          reset
69          }
70
71      stackfunctions = {
72          # The command name for calling the zone function from the stack
73          'DEFINEZONES': [
74              # A short usage string, printed when you type HELP DEFINEZONES in
    ↪ the BlueSky console
75              'DEFINEZONES switch,center,inner radius,outer radius,number of
    ↪ zones',
76
77              # A list of the argument types the function accepts.
78              'bool,latlon,float,float,int',
79
80              # The name of the function in this plugin
81              definezones,
82
83              # a longer help text for the function.
84              'Define and draw zone structure on the screen. ']
85      }
86
87      # init_plugin() should always return these two dicts.
```

```
88      return config, stackfunctions
89
90
91  ### Periodic update functions that are called by the simulation.
92  def update():
93      pass
94
95  def preupdate():
96      global switch
97
98      # Check if the zones are turned on
99      if switch:
100         # Check if there is traffic in the scenario
101         if traf.ntraf:
102             # Check if aircraft are about to leave their zone ...
103             checkEdgeSurpassing()
104             # .. or if arriving aircraft are about to enter a departure zone
105             checkWrongZoneEntry()
106
107 def reset():
108     global wpidx, zonedef
109     wpidx = 1
110     zonedef.acIDrisk = set()
111
112 ### Other functions of the plugin
113 def definezones(switchinput,center_lat,center_lon,R_in,R_out,number):
114     """ Sets up the definition of the zones and draws them on the screen
115     In:     switchinput [-]     (Zone actions switched on or off)
116             center_lat [deg]    (Center latitude),
117             center_lon [deg]    (Center longitude),
118             R_in [m]            (Inner radius of the zone structure),
119             R_out [m]           (Outer radius of the zone structure),
120             number [-]          (Number of zones)"""
121
122     # Turn the switch to ensure that the zone actions start when the zones are
    ↪ defined
123     global switch
124     switch = switchinput
125
126     # Fill the global variable zonedef based on the input from the stack
127     global zonedef
128     zonedef.center_lat = center_lat
129     zonedef.center_lon = center_lon
130     zonedef.R_in = R_in
131     zonedef.R_out = R_out
132     zonedef.number = number
133     zonedef.dangle = 360. / zonedef.number
134     zonedef.skew = 0.5 #Fixed for this experiment, could be added as an input
135     zonedef.dhdg = 0.25*zonedef.dangle #Also fixed for this experiment
136     zonedef.startlat = np.zeros(zonedef.number,dtype=float)
137     zonedef.startlon = np.zeros(zonedef.number,dtype=float)
138     zonedef.endlat =  np.zeros(zonedef.number,dtype=float)
139     zonedef.endlon =  np.zeros(zonedef.number,dtype=float)
140     zonedef.arrivalBool = np.zeros(zonedef.number,dtype=bool)
141
142     # Draw circle with outer zone radius on the screen
143     stack.stack("CIRCLE outer " + str(zonedef.center_lat) +" " + str(zonedef.
    ↪ center_lon) + " " + str(zonedef.R_out/tools.aero.nm))
144     # Define a margin circle to determine wrong entry threats in next function
145     stack.stack("CIRCLE MARGIN " + str(zonedef.center_lat) +" " + str(zonedef.
    ↪ center_lon) + " " + str((1.1*zonedef.R_out)/tools.aero.nm))
```

```
146
147     # Compute the start and endpoints of the zone edges by converting their
    ↪ polar coordinates to lat/lon locations
148     for i in range(0,zonedef.number):
149         zonedef.startlat[i],zonedef.startlon[i] = zonetools.conversions.
    ↪ polartolatlon_matrix((zonedef.dangle*i+360.)%360.,zonedef.R_in,zonedef.
    ↪ center_lat,zonedef.center_lon)
150         zonedef.endlat[i],zonedef.endlon[i] = zonetools.conversions.
    ↪ polartolatlon_matrix((zonedef.dangle*(i-zonedef.skew)+360.)%360.,zonedef
    ↪ .R_out,zonedef.center_lat,zonedef.center_lon)
151
152     # Draw the zone edges on the screen & define zones
153     for i in range(0,zonedef.number):
154         if i%2 == 0:
155             zonedef.arrivalBool[i] = True
156         else:
157             zonedef.arrivalBool[i] = False
158
159         j = i + 1
160         if j == zonedef.number:
161             j = 0
162
163         # The zone is drawn as a polygon with 4 corner points
164         stack.stack("POLY ZONE" + str(i+1) + " " + str(zonedef.startlat[i]) + "
    ↪  " + str(zonedef.startlon[i]) + " " + str(zonedef.endlat[i]) + " " + str
    ↪ (zonedef.endlon[i]) +  " " +  str(zonedef.endlat[j]) + " " + str(zonedef
    ↪ .endlon[j]) + " " + str(zonedef.startlat[j]) + " " + str(zonedef.
    ↪ startlon[j]))
165
166     # Print a message on the screen for the user
167     stack.stack("ECHO Zones have been succesfully defined")
168
169 def  checkEdgeSurpassing():
170     """ Checks whether aircraft are about to leave their zones,
171         and if so sends adequate commands to the stack"""
172
173     currentids = []      # List with aircraft IDs currently risking edge
    ↪ surpassing
174     zonenumbers = {}     # Dict used to store the zone number per aircraft ID
175     zoneedge = {}        # Dict used to store the edge number per aircraft ID
176     global wpidx
177
178     # Check what aircraft are flying inside each zone by looping over the zones
179     for zonenr in range(zonedef.number):
180         insideLst = tools.areafilter.checkInside('ZONE%d' % (zonenr + 1), traf.
    ↪ lat, traf.lon, traf.alt)
181         for idx, inside in enumerate(insideLst):
182             if inside:
183                 # Check if they are about to surpass one of the zone edges
184                 t1,t2,u1,u2 = zonetools.conversions.lineintersect(idx,zonedef,
    ↪ zonenr)
185                 if 0 < t1 < 0.3 and 0 < u1 < 1:
186                     # Aircraft is about to surpass the first zone edge
187                     currentids.append(traf.id[idx])
188                     zonenumbers[traf.id[idx]] = zonenr
189                     zoneedge[traf.id[idx]] = 1
190                 if 0< t2 < 0.3 and 0 < u2 < 1:
191                     # Aircraft is about to suprass the second zone edge
192                     currentids.append(traf.id[idx])
193                     zonenumbers[traf.id[idx]] = zonenr
194                     zoneedge[traf.id[idx]] = 2
```

```
195
196     # Check which aircraft are about to surpass an edge, but have not been
        ↪ corrected in the previous time step. Comparison needs to be made with
        ↪ IDs, not indexes because they could have been deleted in the previous
        ↪ time step.
197     newids = set(currentids) - set(zonedef.acIDrisk)
198
199     # The correction direction depends on whether the aircraft is about to
        ↪ surpass edge 1 or 2, and whether it is flying inside an arrival or
        ↪ departure zone
200     corrEdge1 = np.ones(zonedef.number,dtype=float) - 2*zonedef.arrivalBool
201     corrEdge2 = -1 * np.ones(zonedef.number,dtype=float) + 2*zonedef.
        ↪ arrivalBool
202
203     # Convert aircraft IDs to index numbers
204     idxnos = [traf.id2idx(newid) for newid in newids]
205     for idxno in idxnos:
206         # Find required correction direction based on location and intersection
        ↪  edge
207         currentzone = zonenumbers[traf.id[idxno]]
208         corrDir = corrEdge1[currentzone]
209         if zoneedge[traf.id[idxno]] == 2:
210             corrDir = corrEdge2[currentzone]
211         # Define a correction waypoint in the right direction
212         wplat,wplon = tools.geo.qdrpos(traf.lat[idxno],traf.lon[idxno],traf.hdg
        ↪ [idxno]+corrDir*zonedef.dhdg,(traf.tas[idxno]*5)/tools.aero.nm)
213         stack.stack("DEFWPT "+"WP"+str(wpidx)+" "+str(wplat)+" "+str(wplon))
214         # Add the waypoint to the flight plan, in front of the next waypoint
215         nextwp = bs.traf.ap.route[idxno].wpname[bs.traf.ap.route[idxno].iactwp]
216         stack.stack(str(traf.id[idxno]) + " ADDWPT FLYOVER")
217         stack.stack(str(traf.id[idxno]) + " BEFORE " + str(nextwp) + " ADDWPT
        ↪ WP"+str(wpidx))
218         stack.stack(str(traf.id[idxno]) + " DIRECT " + " WP"+str(wpidx))
219         wpidx +=  1
220
221     # Store aircraft IDs of this time step for the next step
222     zonedef.acIDrisk = currentids
223
224 def checkWrongZoneEntry():
225     """ If arriving aircraft are about to enter a departure zone,
226         immediately correct them"""
227
228     global wpidx
229
230     # Compute which aircraft are flying inside the margin and outer circle
231     insideMargin = tools.areafilter.checkInside('MARGIN', traf.lat, traf.lon,
        ↪ traf.alt)
232     insideOuter = tools.areafilter.checkInside('OUTER', traf.lat, traf.lon,
        ↪ traf.alt)
233     arrivalBool = np.array([int(ac[2:])%2 for ac in traf.id])
234     # Compute their angle and distance away from the zone center in polar
        ↪ coordinates
235     polarangle,polardist = np.squeeze(np.asarray(zonetools.conversions.
        ↪ latlontopolar_matrix(traf.lat,traf.lon,np.array(zonedef.center_lat),np.
        ↪ array(zonedef.center_lon))))
236
237     # Set up an array that contains the polar angles of the edges of the zone
        ↪ structure at the outer radius
238     zoneedge = np.arange(zonedef.dangle,361.,zonedef.dangle)
239     # If the skewness is not zero, the outer radius edge needs to be corrected
        ↪ with the skewness
```

```
240     if zonedef.skew != 0:
241         zoneedge = np.arange(zonedef.dangle*zonedef.skew,360.,zonedef.dangle)
242 
243     for idx, inside in enumerate(insideMargin):
244         # Check which arriving aircraft are flying in the margin strip.
245         if inside and not insideOuter[idx] and arrivalBool[idx] == 1:
246             # Compute the distance to the next waypoint in their flight plan
247             nextwplat = bs.traf.ap.route[idx].wplat[bs.traf.ap.route[idx].
    ↪ iactwp]
248             nextwplon = bs.traf.ap.route[idx].wplon[bs.traf.ap.route[idx].
    ↪ iactwp]
249             disttonextwp = tools.geo.kwikqdrdist(traf.lat[idx],traf.lon[idx],
    ↪ nextwplat,nextwplon)[1] #[m]
250             # If aircraft have skipped the waypoint at the zone edge after
    ↪ conflict resolution, check if they are still on track to enter an
    ↪ arrival zone instead of a departure zone.
251             if disttonextwp > 0.7*zonedef.R_out:
252                 # Check the different sectors defined in the zone structure
    ↪ based on the zone edge array.
253                 for i in np.arange(0,int(len(zoneedge)/2)):
254                     if zonetools.anglecalc.checkinbetween(polarangle[idx],
    ↪ zoneedge[i*2-2],zoneedge[i*2]):
255                         # By default, place a waypoint on the outer radius that
    ↪  is equal to current angle.
256                         wpang = polarangle[idx]
257                         # If the aircraft is approaching the departure zone of
    ↪ the sector, correct to arrival.
258                         if zonetools.anglecalc.checkinbetween(polarangle[idx],
    ↪ zoneedge[i*2-2],zoneedge[i*2-1]):
259                             wpang = (zoneedge[i*2-1] + 0.05*zonedef.dangle)%360
260                 wplat, wplon = zonetools.conversions.polartolatlon_matrix(wpang
    ↪ ,zonedef.R_out,zonedef.center_lat,zonedef.center_lon)
261                 # Add command to the stack to fly to the waypoint first.
262                 stack.stack("DEFWPT "+"WP"+str(wpidx)+" "+str(wplat)+" "+str(
    ↪ wplon))
263                 nextwp = bs.traf.ap.route[idx].wpname[bs.traf.ap.route[idx].
    ↪ iactwp]
264                 stack.stack(str(traf.id[idx]) + " ADDWPT FLYOVER")
265                 stack.stack(str(traf.id[idx]) + " BEFORE " + str(nextwp) + "
    ↪ ADDWPT WP"+str(wpidx))
266                 stack.stack(str(traf.id[idx]) + " DIRECT " + " WP"+str(wpidx))
267                 wpidx +=  1
```

Part III
Preliminary report (already graded)

1 Introduction

Conventional air traffic has traditionally been guided and separated by centralized control [53]. As a result, the current breakdown of the airspace is mainly based on controller workload limitations [31] [37]. In the meantime, air traffic demand is still increasing, and current architecture is reaching the limits of its ability to accommodate this increasing demand [45].

Much research in the field of air traffic control is dedicated to find the airspace organization that best suits the future needs. Some research focuses on upgrading the current centralized control by restructuring sectors or by changing the sectors more dynamically based on demand [31]. On the other hand, some research tries to prove that distributed control is the only way to achieve the needed capacity increase. A distributed control strategy seems to be inevitable to remove the controller workload limitations in the future, but research on how this distributed control should be organized has not yet reached consensus. Free flight researchers predict that higher traffic densities can be achieved when the traffic flow constraints are reduced [8] [22]. On the other hand, some research predicts that structuring of airspace is key in increasing the airspace capacity [43] [30]. This illustrates that the research community has not yet found the answer on what level of structuring is required to maximize capacity.

In addition to the growing demand of conventional air traffic, new forms of air transport such as drones and personal air vehicles are entering the market. The current airspace structure is not able to support these new types of airspace usage [39], and in the future the number of vehicles in the airspace will definitely exceed the capacity of the current concept. Although the first flying cars are now for sale [46], it is still unclear how the airspace and air traffic control need to be re-organized to facilitate them.

Little research has been done in the field of urban airspace design. Prior research by TU Delft has shown that in urban areas, distributed control with a limited structure of layers can result in a safer and more efficient use of the airspace than an unstructured airspace [48]. It was demonstrated that the conflict rate can be reduced by spreading the traffic over altitude layers and by sorting the traffic by heading [20]. However, when considering traffic scenarios that have primarily horizontal demand patterns, for example around a departure/arrival area, the layers concept is no longer adequate. In these scenarios, all aircraft are trying to leave or reach the same location on the ground, and spreading aircraft into altitude layers makes this impossible. In this research it will be investigated whether in these areas it is best to provide a different structure, or to switch to an unstructured airspace. It is expected that also in these scenarios, airspace organization can act as conflict prevention. By separating aircraft into diverging and converging lateral zones, it is hypothesized that less conflicts need to be solved.

The objective of this thesis is to investigate the value of defining lateral zones in a traffic scenario with a horizontal demand pattern, by running and comparing fast-time simulations of high density traffic in a structured and unstructured airspace. The thesis objective is linked to the following research question:
"How does a structured airspace with lateral zones compare to an unstructured airspace in terms of safety, efficiency and capacity in high density traffic scenarios with a horizontal demand pattern?"

A literature review has been performed to better understand the context and scope of the research, and to converge to possible scenarios in which the lateral zones could lead to a more efficient and safer airspace use. Chapter 2 describes the differences between centralized, decentralized, and distributed control. The Metropolis research conducted by the TU Delft serves as a basis for understanding how layers can result in a safer and more efficient use of the airspace, and is summarized in Chapter 3. Based on the results from Metropolis, theoretical relationships were derived between traffic structure and airspace capacity. These relationships will be discussed in Chapter 4. In decentralized control, conflict detection & resolution algorithms are an important tool to avoid conflicts. An overview of the different possibilities is given in Chapter 5. Based on interviews with the researchers of the Metropolis project, it became clear that the merging and sequencing of traffic flows is difficult in the zone concept. Therefore, Chapter 6 and 7 address merging and sequencing possibilities respectively. Finally, the information gathered in the literature review was combined to formulate an experiment proposal. Chapter 8 present the proposed approach to answer the research question.

2

Network organization

The current Air Traffic Management (ATM) is performed by centralized authorities, and controller workload limitations result in capacity limitations for the airspace [45]. Decentralization can help to remove these limitations, and at the same time provide collision avoidance solutions that take into account local conditions and knowledge [53]. This has motivated research in the field of optimal airspace network organization.

Control theory categorizes all networks into centralized (star), and distributed (mesh) networks [4]. A combination between these two networks is referred to as a decentralized network [4]. Each network consists of nodes and links. The nodes are the elements where the information is created, processed or redirected. Links are in place to connect the nodes, and represent how the information is transferred throughout the network. In a centralized network, a central node links to all other nodes, and the other nodes are not linked in between. A distributed network has no hierarchical structure [53]. The decentralized network is a combination of these two, and consists of multiple centralized networks that are connected. A visualization of the three types is presented in Figure 2.1.

The growing number of drones and personal air vehicles will enable more people to personalize air travel in the future. To allow for an airspace where everyone can travel where, when and how he or she wants, a highly distributed air transportation system seems inevitable [39]. To fully understand the need for this transition and to understand the meaning of a distributed network in this context, this chapter focuses on the differences between a centralized, decentralized and distributed network. Furthermore, it provides some examples of current practices that already apply these different network structures. Section 2.1, 2.2 and 2.3 describe a centralized, decentralized and distributed network respectively. Talking about ATM, these three different types do not strictly follow the definitions of control theory. To clarify the differences, Section 2.4 describes how these terms are used in the context of ATM.

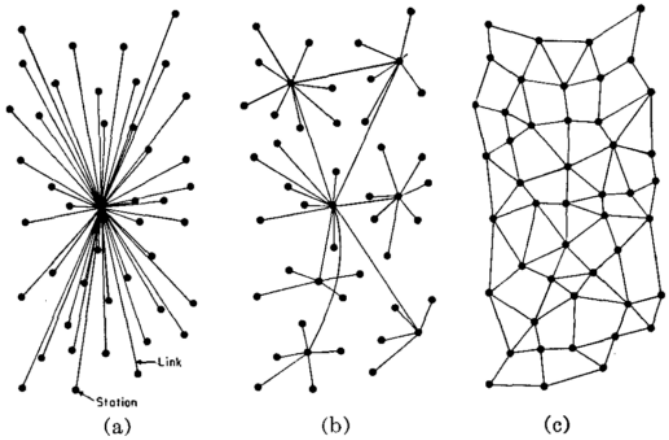

Figure 2.1: Different network structures: a) centralized b) decentralized c) distributed [4]

2.1. Centralized network

In a centralized network, the central node (e.g. the ATM authority) collects all the information from the other nodes in the network (e.g. aircraft states). At the central node, the decision-making takes place, and after all information has been collected, it can be processed and distributed to the other nodes in the network if needed. The advantage of this centralized approach is that it is possible to find the global optimum of the entire network, since one single node has all information available. Because the central node is able to communicate with all other nodes, it can easily communicate this with all the other nodes. However, a disadvantage of this is that the central node should have enough capacity and resources available to make decisions and distribute them. This results in limitations and constraints on the network based on the resources available at the central node [53].

2.2. Decentralized network

A decentralized network does not have a single authority that is responsible for the decision-making. Instead, this responsibility is distributed across different nodes. Each of these nodes has its own local network, and collects information about the nodes in its neighborhood. The result is that the responsibilities are with local entities, instead of with one central authority. It is expected to have a positive effect on network stability and performance, since it is more robust than the centralized network. Decentralization can help solve the limitations and constraints from capacity and resources that were discussed in the past section. In addition, knowledge about the local conditions can help to find a more efficient and suitable answer to the problem at that location. Although local entities can still share information between each other, local optimization is used to make decisions. A disadvantage of decentralized control is therefore that it is not guaranteed that a global optimum for the entire network will be used [53]. In addition, local solutions might appear to be safe, while in reality they initiate an unsafe situation in the global picture. An example is the so called domino effect, in which solving one conflict results in many new conflicts.

2.3. Distributed network

A distributed network takes decentralization one step further. In a distributed network all nodes are connected to adjacent nodes, rather than being connected to a (local) central node [4]. The ground control that is currently in place, would be taken out of the loop, completely moving the separation responsibilities from the ground to the air. Unmanned Aerial Vehicles (UAVs) are an example of distributed systems. These systems process and collect information autonomously, and take actions decentrally. The introduction of these vehicles in the airspace asks for a distributed airspace concept, like the free flight concept. Intuitively one would say that in cases of high traffic density, a centralized control should be applied, since the centralized authority is able to solve for the global optimum. However, previous studies on the free flight concept have proven that these high density scenarios require the power of a distributed system [22].

2.4. Network organization in the context of ATM

It is said that the current air transport network is a centralized network [53]. The main nodes are Air Traffic Control (ATC), Traffic Flow Management (TFM) and the Airline Operation Control Center (AOCC), and they all act as one centralized authority [3]. Strictly following the definitions of control theory however, it can be argued that this centralized air transport network should be called a decentralized system. Many different ATC organizations cooperate and share information, and not a single ATC organization computes the global solutions. It can therefore be concluded that the difference between a centralized and decentralized air traffic network is not strictly following the categorization from control theory that was discussed in the previous sections.

In addition, the terms decentralized and distributed are used interchangeably when talking about airspace organization. In literature, an example of decentralization in the air transport network is mentioned to be the introduction of the Traffic Alert and Collision Avoidance System (TCAS) [53]. The TCAS identifies potential conflicts between aircraft and solves potential collisions with a predefined logic [56]. The TCAS system uses local knowledge to solve the potential conflict, and acts independent of the ground control. Strictly following the definitions of control theory, it can be argued that this is a move towards a distributed network, rather than to a decentralized network. The free flight concept developed by the Nederlands Lucht- en Ruimtevaart-

centrum (NLR) and National Aeronautics and Space Administration (NASA) is mentioned to be an example of a distributed network [22]. Although it takes decentralization even further than TCAS, completely taking ground control out of the loop, it can be argued that there is not a big difference in the network organization following control theory definitions.

Based on the literature review, it can be concluded that talking about airspace organization, the definitions of centralized, decentralized, and distributed, do not strictly follow the definitions from control theory as visualized in Figure 2.1). Instead, decentralization in ATM can be understood as the move towards taking ground control out of the loop. In the following sections, airspace organization is therefore only categorized in centralized and decentralized airspace, following the definitions as described in this section.

3

Metropolis: urban airspace design

Although the first flying cars are now for sale [46], it is still unclear how the airspace and air traffic control need to be organized. Not a lot of research has been done on urban airspace design, most research focusses on separation assurance between Unmanned Aerial Vehicles (UAVs) rather than on separating Personal Aerial Vehicles (PAVs) or a combination of these vehicles. The research on UAV airspace varies from a completely unstructured (free flight) concept [7], to a very structured concept with highways in the sky [38]. In literature no comparison is made, and it remains unclear whether structuring the airspace can maximize capacity. From this it can be concluded that the relationship between structure and capacity was still unclear. To overcome these two shortcomings of prior research on airspace structuring, the Metropolis project was initiated. The goal was to investigate airspace design options for an urban environment, an environment where PAV and UAV operations have to be integrated [25]. However, the focus of the Metropolis project was on addressing the relationship between airspace structure and capacity for decentralized separation, rather than providing a specific conclusion about the future design of an urban airspace [49].

Figure 3.1 shows the work plan of Metropolis. Based on the societal demand, traffic scenarios were developed that suited future demand patterns in urban areas. Afterwards, different airspace concepts where developed that were tested on the different scenarios. Different dependent variables were selected and used as metrics to compare the outcome of a lot of simulations. Finally, the results of these simulations were compared to find out which concept resulted in the highest capacity, while maintaining safe separation between the vehicles.

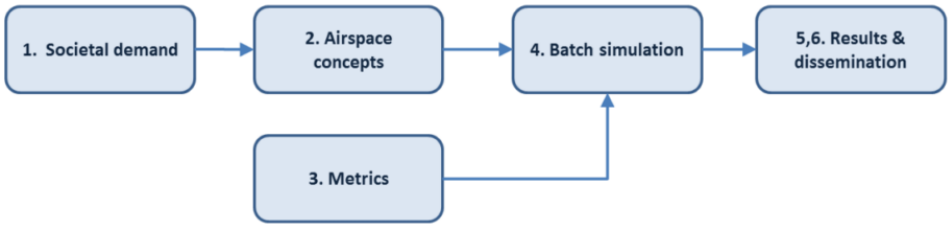

Figure 3.1: Work plan of the Metropolis project [25]

This chapter focuses on the outcome of the Metropolis project, and addresses the lessons learned that are relevant for this assignment in particular. Since the idea of this assignment is to develop a structure of lateral zones, specific emphasis is put on the outcome of the zones in the Metropolis project. Section 3.1 gives an introduction to the traffic scenario that was considered during the project. Section 3.2 outlines the different concepts that were tested, after which Section 3.3 presents the results. The conclusions from the project are formulated in 3.4. Finally, Section 3.5 gives an overview of the lessons learned from Metropolis that are relevant for this thesis assignment.

3.1. Traffic scenarios

In future urban airspace scenarios, PAVs and UAVs will be widely available. To test which airspace is best suitable to integrate these two types of vehicles in a safe and efficient manner, it is important to predict the expected travel volumes. The Metropolis project predicted travel volumes by extrapolating the relationship between (past and current) road traffic and population size in Paris.
This section focuses on the prediction of the traffic volumes and on understanding the city layout. It should be noted that the intention is not to completely understand all the details of the traffic scenarios in Metropolis, but to understand the context of the results and conclusions. Furthermore, it is used to get a feeling for the different aspects that are important when designing traffic scenarios. Section 3.1.1 explains how the future population size was predicted. This growth was linked to traffic volumes, as explained in Section 3.1.2. Finally, decisions were made regarding the simulation area, which will be explained in Section 3.1.3.

3.1.1. Population size

The city Paris forms the baseline for the scenarios that were developed for Metropolis. Based on the population numbers of Paris from 1991 to 2012, a prediction was made for the population size in 2050. This estimation resulted in a population size of 14 million, and in addition three additional scenarios were defined with population sizes of 18, 22 and 26 million inhabitants.
Inhabitants are normally not uniformly spread through the city, and to account for that Paris served as an example again. Paris was split into 3 zones: city center, inner and outer ring, and the population size and area of each zone were determined. From this, the population densities in the different zones could be computed. In all the scenarios that were tested in Metropolis, the population size was divided over three zones with the same ratio as the computed ratio in Paris. Population growth has always been accompanied with an increase in city area, therefore the considered areas in the center, inner and outer rings were increased with 10, 15 and 20% compared to the baseline. This is based on the assumption that the city center gets saturated at some point, and as a result the outer rings grow faster [26].

The result of the computations were 4 future scenarios that could be used as a starting point for computing traffic densities and volumes. The scenario with 14 million inhabitants and an increased city area was not meant to be a realistic prediction of the city layout and inhabitants of Paris in 2050, but served as a basis to evaluate the different airspace concepts. The area in the other 3 scenarios was not increased, while the population size was increase. This resulted in population sizes and densities that were not typical for European cities. However, the extreme conditions in terms of population density are needed to test the capacity limits of the concepts [26].

3.1.2. Traffic volumes

Based on the population sizes of the 4 scenarios, estimations for the traffic volumes per hour were derived. The relationship between population size and road traffic in Paris was investigated and extrapolated. Market research was done to predict the market penetration of PAVs, and from this it was computed that 16.7% of all traffic would be replaced by the aerial vehicles by 2050. The current ratio of cars, motorbikes and vans was used to compute the ratio of different PAVs. Each PAV was compared to a road transportation method (e.g. PAL-V resembles a motorbike more than a car), and it was decided what type of PAV had to substitute the road transportation method. To determine the amount of UAVs in the different scenarios, the average amount of packages that are ordered online was used as a baseline. Based on several assumptions (e.g. only packages under 2.3 kg are delivered using UAVs), the demand for UAV delivered packages was computed. Combining the population size and the traffic ratios, the average traffic volume per hour could be computed per vehicle. In total, Metropolis used 4 different vehicles: 3 PAVs and 1 UAV.

On top of just computing the average traffic volumes, Metropolis considered the differences between the volumes at different times of the day. Although it is not important to understand the details of these different distributions, it is important to get a feeling for the differences. The traffic distribution by time of the day was found for Great Britain, and the average hourly traffic was corrected for these percentages. In addition, the traffic was divided into four different types: residential-residential, residential-commercial, commercial-residential, and commercial-commercial. Based on the location within the city (city center, inner and outer ring), the distribution of the traffic types was categorized. The morning scenarios have a higher percentage of residential-commercial traffic, since people are traveling to work. In the lunch scenario, the focus is in

the other direction, since most traffic will be commercial-residential. The lunch scenario had a more equal distribution of the different types of traffic. Although the exact percentages of the distribution are not important at this stage, it is important to understand that the differences between the morning, evening, and lunch distributions.

3.1.3. Simulation area

The predicted travel volumes need to be simulated in a realistic urban environment. In addition to the size of the city that was determined in Section 3.1.1, other characteristics (e.g. the distinction between commercial and residential areas, or the street and building layout) have to be addressed. These characteristics are designed very detailed, but at this stage only the shape and size of the simulation area are regarded to be relevant to understand the context of the results.
To estimate the minimum physical area that was necessary for the simulations, horizontal conflicts with different conflict angles were simulated. The distance that is traveled to avoid a conflict is considered as the minimum length of the simulation area. By simulating the conflicts for different ground speeds, the minimum simulation area is computed to be 11.3% of the total city area [26]. This 11.3% is cut out from the city as a pie slice, as illustrated in Figure 3.2. The experiment area is surrounded by a background area to spawn aircraft for the simulation.

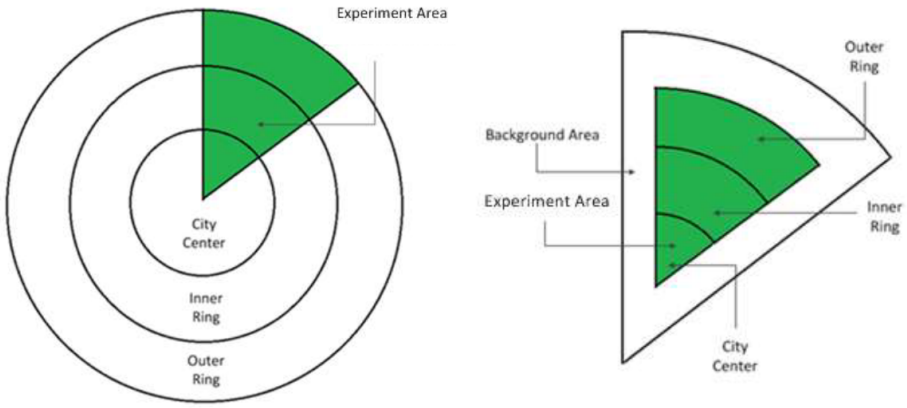

Figure 3.2: The experiment area is a pie slice of the entire city, with a background area around it [26]

The pointy edge of the city center area makes it difficult to study the traffic in the angular point. To solve this problem, the final simulation area was made trapezoidal instead. Figure 3.3 presents the final geometry of the simulation area. The city street and building layout has been carefully selected, but at this point it is sufficient to understand that the height of the buildings is different per zone of the area.

The initial articles that were published about Metropolis considered the triangular shape [47]. However, it was found that aircraft steering away from the conflict disappeared from the simulation area, and where therefore not logged. In later publications, a squared area was used, changing some specific results (e.g. the number of conflicts with Conflict Detection & Resolution on/off) [51]. Fortunately, the overall trends that were visible remained the same.

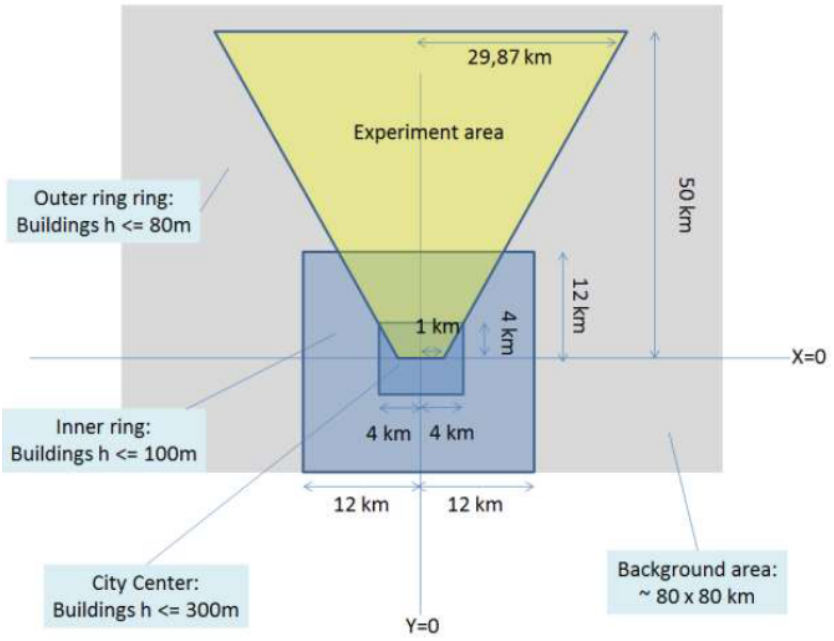

Figure 3.3: Final simulation area geometry: trapezoidal experiment area surrounded by a squared background area [26]

3.2. Concepts

Airspace structure is used to separate and organize en route air traffic in advance. Structure always results in constraints on one or more of the degrees of freedom of the aircraft [49]. In the Metropolis project, four different concepts were defined for which the level of structure was increased by incrementally increasing the number of applied constraints. Figure 3.4 shows the constraints of the four different concepts used in Metropolis. In this section, an introduction to the four concepts is given. Section 3.2.1 describes the common elements between the different concepts. Section 3.2.2 to Section 3.2.5 describe the four different concepts in more detail.

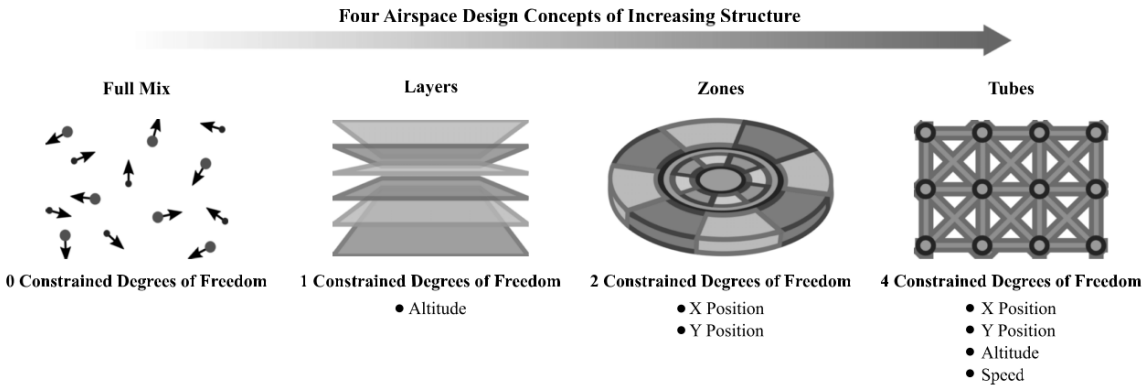

Figure 3.4: Four Metropolis concepts: number of constraints is incrementally increased [49]

3.2.1. Common elements

The four concepts in Figure 3.4 are very different, each requiring a very different implementation. However, some concept elements are common to all airspace concepts, as discussed in this section. In all concepts, it is assumed that the on-board avionics have the structure implemented, and all other constraints (e.g. terrain or uplinked weather information) are known in the cockpit [23].

The Metropolis project considers PAV and UAV operations. The lower airspace seems to be most suitable

for the use of these aircraft, separating them from the faster commercial aircraft flying higher. All concepts therefore incorporated airspace limits in terms of minimum and maximum altitude, as well as no-fly zones near arrival and departure sectors of existing airports [23]. As a result, no drastic restructuring of the current airspace is required, the Metropolis concept focuses on airspace that is currently not regularly used.

It is assumed that in the future all PAVs will be equipped with the latest positioning avionics and an Automatic Dependent Surveillance-Broadcast (ADS-B) system. This ADS-B system will enable pilots to know their exact location and also enables them to send this information to the neighboring aircraft. In combination with an on-board conflict detection and resolution system, the aircraft are able to extrapolate flight paths of the neigboring aircraft and detect possible conflicts [23]. In all concepts, the Modified Voltage Potential (MVP) algorithm is used for conflict detection and resolution. The MVP algorithm has proven to be successful for high densities and for multi-aircraft conflicts, without the need for explicit coordination [22]. Explicit coordination requires hand-shaking and sending messages to agree on the resolution move. In multi-aircraft conflicts, making use of implicit coordination that is based on the geometry is beneficial for safety [17]. In all concepts, cruising aircraft have priority over climbing and descending aircraft.

The separation requirements that were adopted in the Metropolis project depend on the vehicle type, phase of flight and on the concept. In general the PAVs and UAVs fly much slower than commercial aircraft, making wake-vortex separation unnecessary. The general minimum that is handled in Metropolis is a one second spacing between PAVs or UAVs, calculated with respect to the fastest flying vehicle. On top of this one second spacing, 10% safety margin is added [23].

In all concepts, the PAVs have to fly between buildings during climb and descent. Therefore, the takeoff and landing procedures are similar in all concepts. In all concepts, the climb and descent angle, as well as the heading angle, will be kept constant during take-off and descent. The spawn rate is adopted to the demand of the scenarios, and in combination with the constant departure routes, no conflicts occur during takeoff. However, during landing some difficulties in simulation occur, since flights need to be delayed in case the runway is occupied. To solve this issue with the simulations, aircraft are deleted once they reach the minimum safe altitude for landing. The problem with this simplification is that the capability to absorb delays is not measured. If a conflict occurs after the removal of the aircraft, it will not be logged. Therefore, a new metric was developed to test and evaluate the differences in delay absorption between the concepts [23].

Finally, weather and abnormal situations are kept constant throughout the different concepts. It is assumed that the UAVs and PAVs are highly automated, meaning that visual conditions have no impact on the operation of the vehicles. During vehicle certification, wind minima are established. In all simulations, the starting position of the weather conditions were identical. In addition, dynamic no-go areas were introduced in the airspace, embodying areas with safety issues (e.g. thunderstorms) [23]. For validation reasons, the dynamic no-go areas also had to comply to the same initial situation.

3.2.2. Full mix

The full mix airspace concept can be described as an unstructured airspace. Figure 3.4 shows that the aircraft are not subjected to constraints, the only constraints on the aircraft will be physical constraints like weather. The full mix concept uses the free flight principles as presented in [15] and [22]. This will be addressed in more detail in Chapter 5. Since the aircraft are not constrained in their flight path, they can use direct routing, reducing fuel burn. Free flight is a perfect example of distributed control, where the entire Collision Detection and Resolution (CD&R) responsibility is moved from the ground to the cockpit. Since the centralized ATC is no longer responsible for separation of aircraft, no flight plans have to be send in advance [23]. The only time aircraft are constrained to a location is during take-off and landing, when they follow prescribed paths as described in Section 3.2.1.

3.2.3. Layers

The layers concept resembles the current hemispheric rule, used to separate east and westbound traffic in different flight levels [44]. In the layers concept, the airspace is also segmented vertically, with traffic in each layer being limited to an allowed heading range. The heading range is different than for the hemispheric rule, as can be seen in Figure 3.5. By implementing two different sets of PAV layers (see first and second set in Figure 3.5), fast flying PAVs can be separated from slower flying vehicles [23].

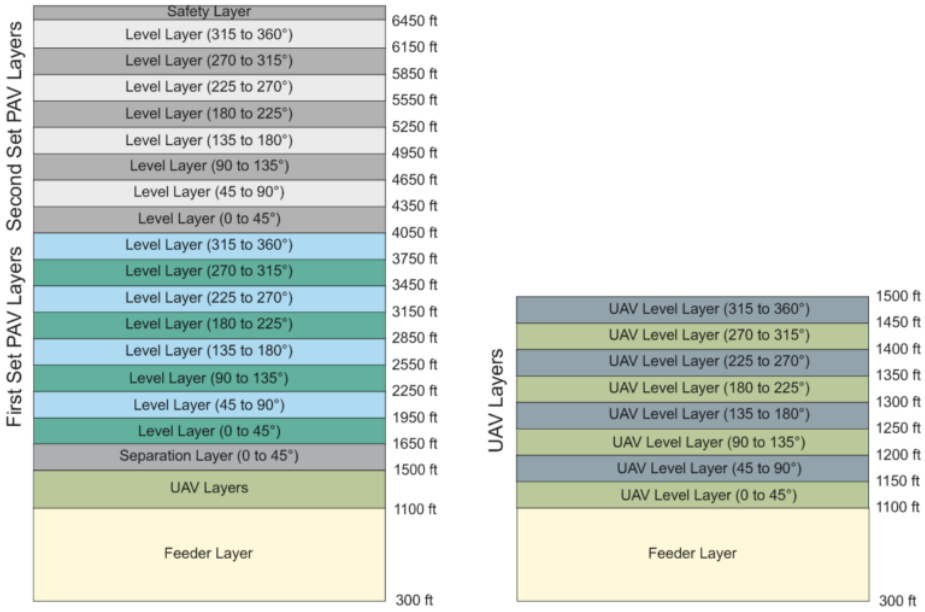

Figure 3.5: Layer concept for PAVs and UAVs [23]

3.2.4. Zones

The third concept has two constrained degrees of freedom: the x and y position of the aircraft. The traffic in different zones is organised in such a way that it follows the same direction and speed. The UAV and PAV topology is defined separately, to ensure strict separation between the fast and slower flying vehicles. The UAV topology has a grid-like structure as presented in Figure 3.6. The area is split up into smaller zones, each covering one distribution area. The intersections between the airways are designed as an octagonal structure that resembles a roundabout pattern.

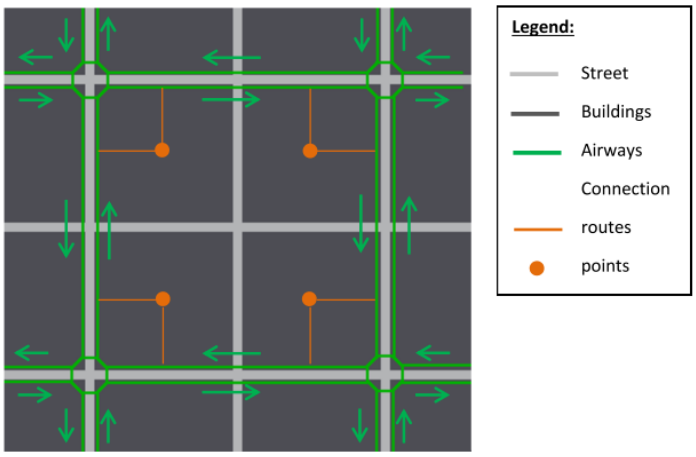

Figure 6.3: UAV Topology – Horizontal View

Figure 3.6: Top view on grid-like topology for UAVs [23]

The first layer of UAV topology is located at the Minimum Safe Altitude (MSA) for UAVs, and several layers are stacked until the MSA for PAVs is reached (see Figure 3.7). Unlike the UAV topology, the PAV topology spans the entire city area. The zones concept was developed with the idea that mixing converging and diverging traffic of all flight phases would result in a lower airspace capacity. The zones are designed in such a way, that the PAVs follow nearly the same heading and speed in each zone.
The city area is split into pie-shaped collector/distributor areas, alternately assigned to inbound and outbound traffic. Some aircraft in the Metropolis scenarios have both their origin as their destination outside of

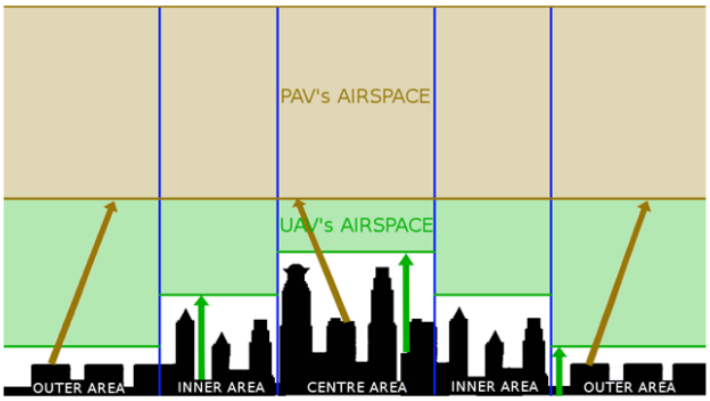

Figure 3.7: Side view of zone concept [23]

the city center. To prevent these aircraft from having to fly all the way to the city center to change zone and fly back through a different zone, intermediate traffic rings are designed. As shown in Figure 3.8, the rings alternately allow clockwise and counterclockwise traffic. It can be seen that the inner center, as well as the rings, are designed to be a polygonal shape structure, since designing flight routes for circular paths requires a lot of additional waypoints [23].

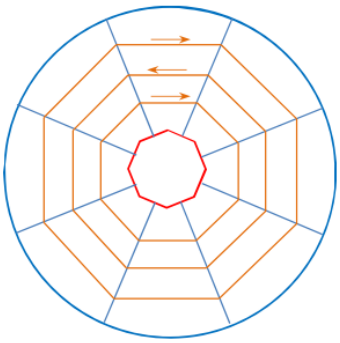

Figure 3.8: Zone topology with distributor/collector areas and rings [23]

To ensure safe separation and merging of the traffic, major flow areas are designed in every collector/distributor area (see Figure 3.9). This means inbound and outbound traffic are separated horizontally, and they operate in the same horizontal plane. The traffic flow direction in the rings varies between successive layers. All these different measures ensure that shorter and more efficient routes are possible, since it will not be necessary to fly a full circle before reaching the desired destination.

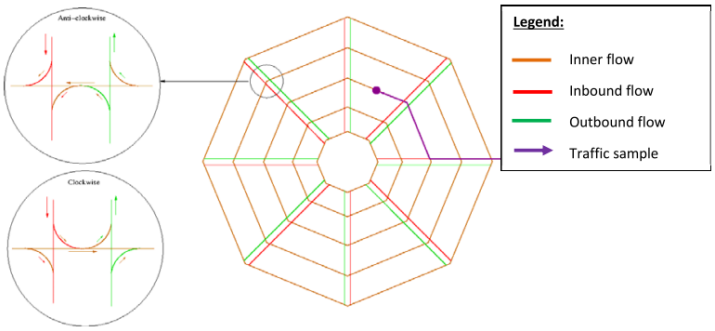

Figure 3.9: Major flow areas in the zone concept enables safe merging of the flows [23]

The zone topology is mostly defined in the horizontal plane, with a repetitive pattern of major flow areas and ring traffic in the successive layers. To allow traffic to move in the third dimension, the traffic exchange areas

were designed. To avoid that climbing/descending traffic is mixed with the cruising traffic in the major flow areas, this traffic exchange area is horizontally separated from it. Figure 3.10 shows how left and right slope exchange tracks are used to smoothly manage horizontal separation.

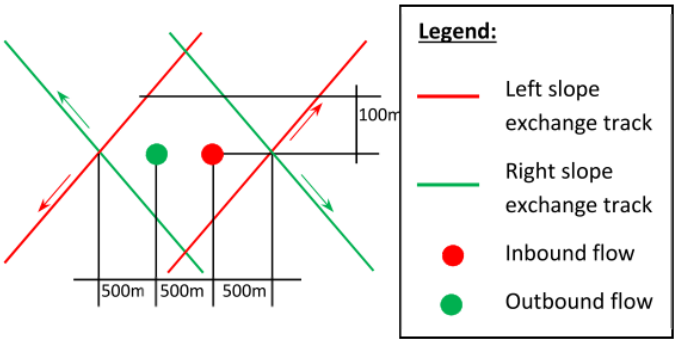

Figure 3.10: Side view of traffic exchange area [23]

Finally, the take-off and landing areas were carefully designed for the zones concept. Pre-defined landing and take-off routes were defined from the MSA to the ground. Since the PAV approach/departure area uses the UAV airspace, the pre-defined routes were designed to minimize interaction. For the structure of the landing strips, the infrastructure of the city was used. The PAV landing strips are all situated at the crossing of streets, to allow for take-off and landing in four directions depending on the wind direction.

3.2.5. Tubes

The tube concept is the most structured concept used in the Metropolis project. In this concept, 4 degrees of freedom are constrained: x position, y position, attitude and speed. Three-dimensional tubes force a fixed route structure on the traffic in the airspace. All aircraft in the tubes have to travel at the same speed in order to guarantee safe separation, therefore different layers of tubes were designed. The lower layers of the tube topology are based on a diagonal grid with a high granularity. This facilitates the possibility to travel to a lot of destinations in many directions, since the tubes are always placed in bi-directional pairs. Different diagonal grids are placed on top of each other, gradually decreasing granularity. Figure 3.11 shows an example topology for the tube concept, illustrating the difference between the layers. The topology makes use of connecting tubes (black arrows in Figure 3.11), transitional tubes (red and green arrows), and horizontal tubes (the bi-directional arrows in the layers).

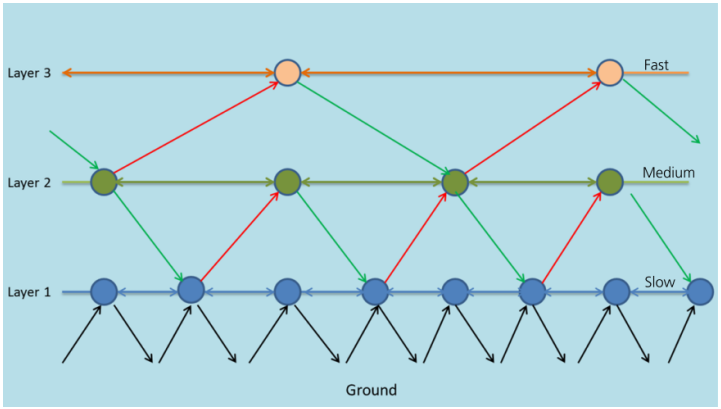

Figure 3.11: Example topology for the tube concept, illustrating the difference between the layers [23]

Different than in the other concepts, separation is ensured based on time. Whenever an aircraft passes a node, the nodes becomes unavailable for other aircraft for a short interval in time. By ensuring that it is impossible that two aircraft exit a node at the same time, it is ensured that no conflicts occur within the tubes.

3.3. Results

In the Metropolis project, two experiments were performed: a nominal and a non-nominal experiment. The nominal experiment focused on evaluating the impact of adding structure on the airspace capacity. The main independent variable in this experiment was therefore the airspace concept as described in the previous section. In addition, different traffic densities and demand scenarios (morning, lunch, evening) were tested. The last independent variable in the experiment matrix was the conflict resolution, turned on or off to test stability of the concept. The non-nominal experiment focused on evaluating the robustness of the different concepts, testing whether the concepts were able to cope with rogue aircraft abandoning the rules.

In this chapter, the focus is on the results of the nominal experiment. The traffic volumes and densities that were realized are presented in Section 3.3.1. These numbers serve as a basis for the interpretation and evaluation of the variables. Although ultimately the question whether adding structure helps maximizing capacity needs to be answered, it is also important to evaluate other aspects of the concepts. Section 3.3.2 up to 3.3.6 describe the difference in complexity, safety, efficiency, stability and capacity between the different concepts. In the Metropolis project, other dependent variables (e.g. noise generation) were also evaluated, but these variables are considered to be less important at this stage of the assignment.

3.3.1. Traffic volume and density

The four airspace concepts were tested with four different traffic volumes, as explained in Section 3.3.1. Although the traffic volumes were the same in all four concepts, the realized volumes and densities differed between the concepts. Figure 3.12 shows that the traffic volumes for the full mix, layers and zones are the same. However, the tubes concept has a significantly lower number of flights per run. This shows that the tubes concept did not successfully meet the traffic demand. The difference with the other concepts is that the tube concept uses a pre-departure delay, preventing some aircraft from flying.

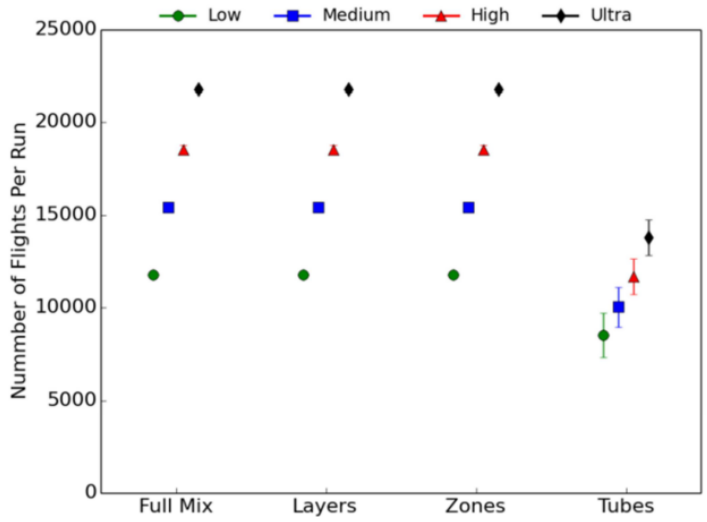

Figure 3.12: Number of simulated flights per run for four different traffic volumes [25]

The differences in realized traffic volume are important to consider when interpreting the differences in the other dependent variables. In Figure 3.13, the density in the simulation and experiment area is shown. The traffic densities in the simulation area of the full mix, layers and zones concepts closely resembles the densities of the desired scenarios described in Section 3.1. Interesting to see is that the tube concept results in the highest density, whilst Figure 3.12 showed that tubes had the lowest number of flights per run. Most probably this is caused by the fact that the tubes concept forced aircraft to take longer routes through the airspace, resulting in longer trip time and distance. It should be noted that the same is seen for zones in the experiment area, also caused by the increased trip time in this concept compared to the full mix and layers.

3.3.2. Complexity

In earlier research, complexity has been addressed in many different ways. The different approaches can be categorized into two options: measurement of the workload for the air traffic control officer (ATCo), or mea-

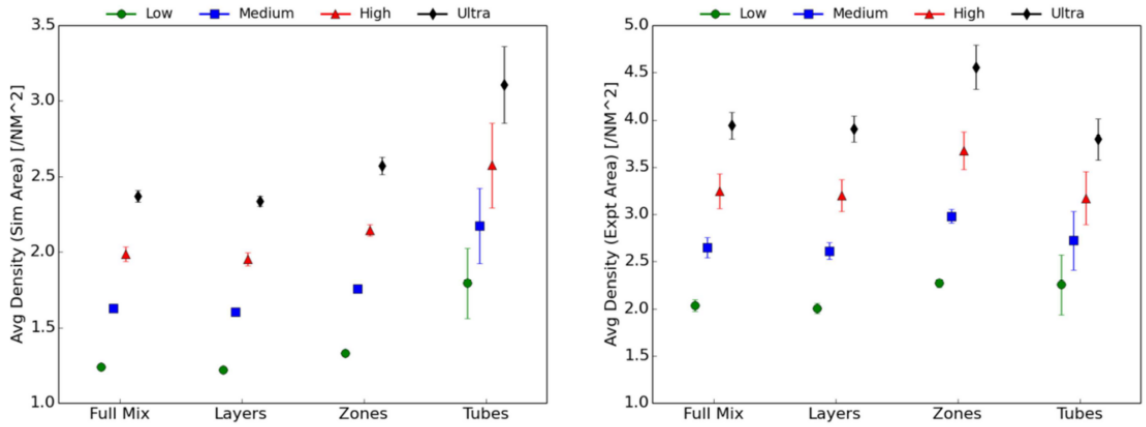

Figure 3.13: Traffic density in simulation area (left) and experiment area (right) [25]

surement by means of automatic conflict resolution algorithms. The last approach models the complexity by measuring the number of required trajectory changes in a given situation. However, the complexity is then highly dependent of the used algorithms. Since the level of structure and airspace management changes between the different concepts, the above approaches were not suitable to measure complexity in the Metropolis project. Therefore, a geometrical approach was chosen, that calculated proximity and convergence of aircraft.
Proximity is a measure of geographical distribution of aircraft in a given volume of airspace [24]. A high proximity value in the sector means that the aircraft are mostly clustered, and are not homogeneously distributed throughout the sector. The problem with the indication of proximity is that it is unable to distinguish between situations were aircraft fly towards or away from each other. The method does not make use of the speed vectors, but that is were convergence comes in. Convergence is used to evaluate the structure of the speed vectors, making it possible to distinguish between diverging and converging traffic. Complexity at a given moment in time is calculated as the sum of the convergence of the vehicles in that zone, corrected for relative distance between the vehicles and stochastic effects [24].

Figure 3.14 shows the complexity function in time, and the proximity-convergence graphs for the different periods in time. These graphs are evaluated for the ultra-high level of traffic density and with conflict resolution switched on. It can be seen that the order of complexity is: tubes, layers, full mix, zones. However, the fact that tubes comes out best is a direct result of the structure of the tubes. By using time separation and delays between aircraft, the concept decreases convergence and proximity of the aircraft, and therefore reduces complexity. Interesting to see is the effect of layers compared to full mix. By vertically separating aircraft, both proximity and convergence are reduced for the layers concept, being beneficial for the total complexity of the concept.
In general it can be seen that the zones concept performs worse than the other concepts. A possible reason could be that all radials converge to the city center, causing a high concentration there. In addition, the zones concept is mostly structured in the horizontal dimension and not in the third dimension, creating high convergence areas around the ring and radial intersections. Another interesting thing to see is the increase in complexity at the evening period, which is only seen for the zones concept. A possible reason mentioned in the result report of Metropolis is that traffic structure in the evening mainly involves traffic from the commercial areas. The result is a very high concentration in the city center right after flight departure, but this does not explain the situation entirely. Another possible cause for the artifact are the altitude bounds implemented in Metropolis. The departure phase is simulated, but arriving aircraft are removed at a certain height. This could be one of the possible causes of the sudden increase in complexity, but it is more plausible that it is caused by the merging problem for the zones concept. In an interview with one of the researchers it was addressed that the city center in the zones concept was designed as a full mix area. This means that all aircraft needed to line up for the zones in the city center, causing merging problems to enter the zones. Also, merging between the radials and rings causes high proximity and convergence problems, further increasing complexity.

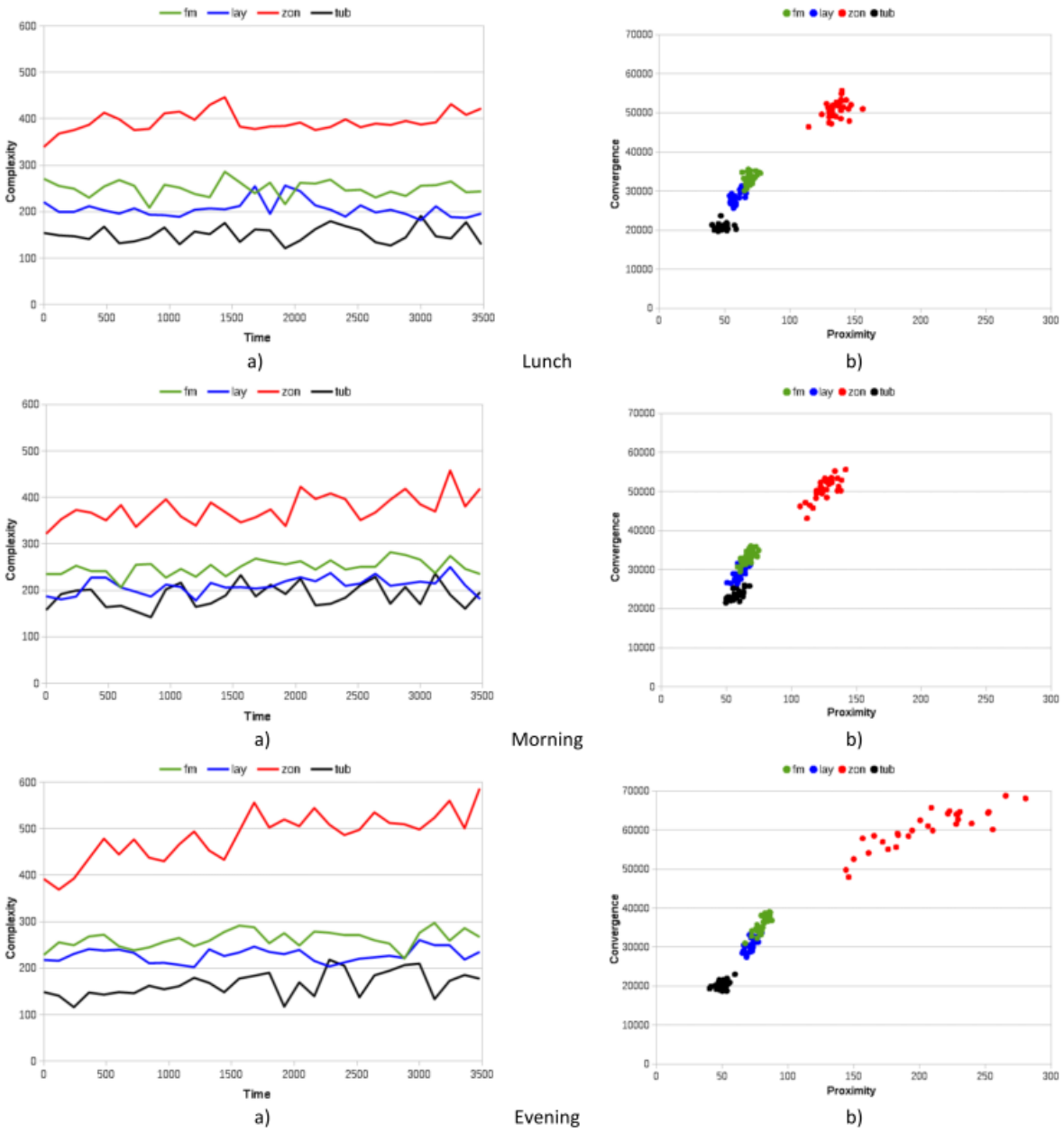

Figure 3.14: Complexity function and proximity-convergence graph for different periods of the day [25]

Figure 3.15 shows the average complexity value for different traffic densities. It can be clearly seen that complexity increases with traffic density for all concepts, but for the zones concept the increase is much steeper.

The complexity results need to be taken into account in evaluating the other dependent variables, since it directly effects other parameters. It should be noted that an increase in complexity in basis is not a bad thing, introduction of higher structure in general results in higher traffic complexity [25].

3.3.3. Safety

The airspace will always be a safety critical system, and although Metropolis is trying to address whether adding structure maximizes capacity, safety should always be taken into account. Separation performance was measured in terms of number of intrusions and conflicts. Intrusions are defined as situations where the separation distance between two aircraft is below the minimum required distance. A conflict is defined as a predicted intrusion [34]. Intrusions can differ in severity, ranging from a situation in which the aircraft just

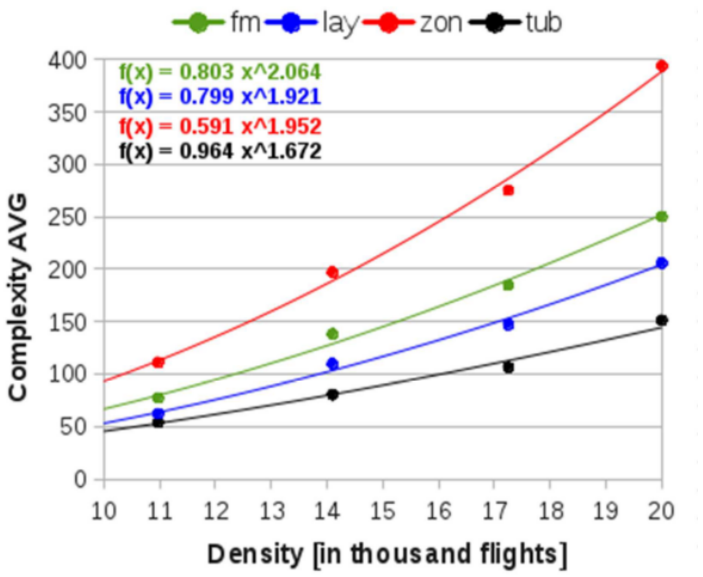

Figure 3.15: Average complexity value for different traffic densities [25]

slightly enters the protected zone of another aircraft, to (near) collisions. Therefore, the intrusion severity is calculated based on the path of the aircraft through the protected zone of the other aircraft. The last metric that is used to compute safety is the intrusion prevention rate (IPR). The IPR measures the number of conflicts that were successfully avoided before becoming an intrusion.

Looking at the number of conflicts and intrusion in Figure 3.16 and 3.17, it can be seen that both numbers increase with increasing traffic demand. The left plots clearly show that the more structured concepts (zones, tubes) result in higher numbers. Looking at the right plots, it is interesting to note that the number of conflicts increased with conflict resolution (CR) turned on increases for the full mix and zones. This effect can be explained by the fact that the maneuvers to resolve conflicts increase the flight distances of aircraft, therefore increasing probability of encountering other aircraft. Figure 3.17 shows that the number of intrusions is significantly lower when CR is turned on, especially for the zones concept. This can be explained by the fact that in the zones concept all aircraft are forced in the same radials away and towards the center. Without CR on, this results in a significant amount of intrusions.

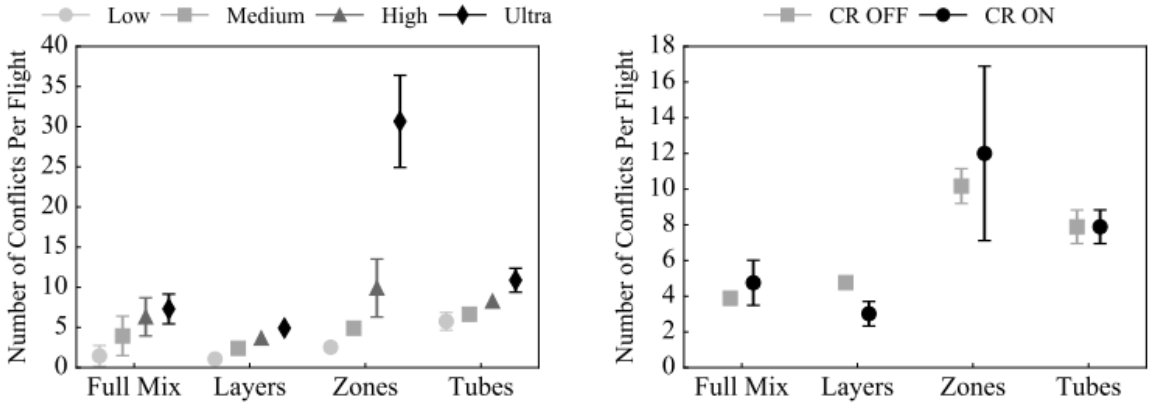

Figure 3.16: Means and 95% confidence intervals of the number of conflicts per flight [49]

When looking at the intrusion severity (Figure 3.18), it can be seen that the zones concept results in the lowest severity. The differences in severity between the different concepts are much smaller than for the other variables, suggesting that the severity is more dependent on the CR method chosen, than on the structure of

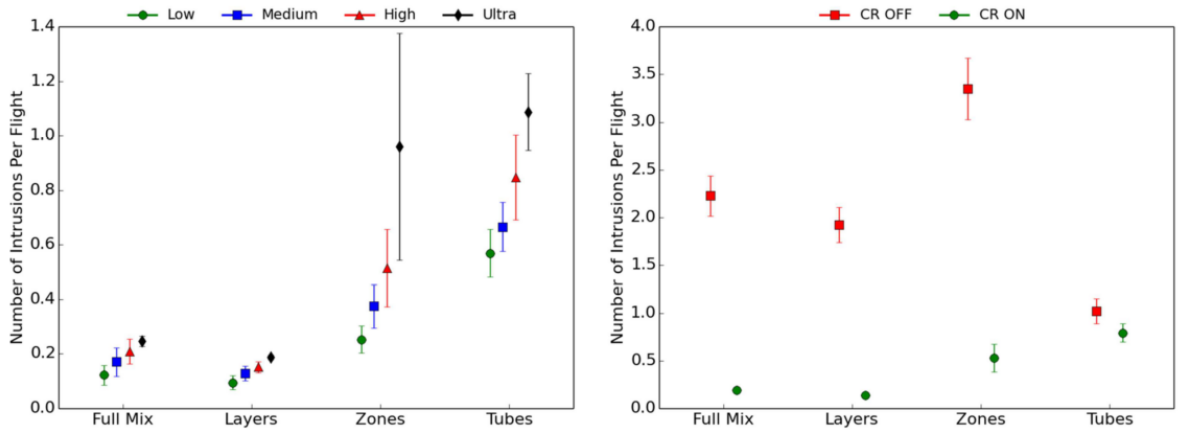

Figure 3.17: Means and 95% confidence intervals of the number of intrusions per flight [25]

the airspace. The severity in all the concepts is around 40% or higher, meaning that the algorithm that the MVP algorithm might need to be optimized for the vehicles used in the Metropolis project.

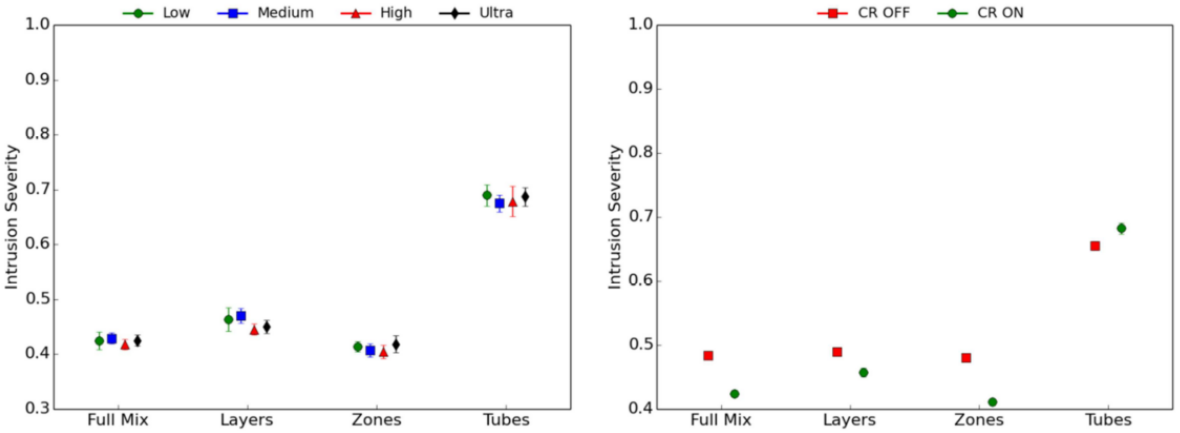

Figure 3.18: Means and 95% confidence intervals of the intrusion severity [25]

Finally, the IPR was computed for the different concepts. Figure 3.19 shows that the IPR is nonzero for all concepts, even when CR is turned off. This is caused by the fact that the conflict detection (CD) method is state-based, and linearly extrapolates aircraft trajectories to predict future conflicts. As a result, some predicted conflicts turn out to pass by without being a conflict. Looking at the IPR when CR is turned off, it looks like the more structured concepts are able to avoid more intrusions, even though the total number of intrusions was higher. However, when CR was turned on, the relative performance of the different concepts is equal, indicating that the performance of the MVP algorithm is constant.

3.3.4. Route efficiency

To evaluate the efficiency of the different concepts, the work done was evaluated. The work done is computed by taking integrating the thrust vector with respect to the displacement vector, therefore it takes into account the vertical and horizontal path of the aircraft. The work done is strongly related to the fuel and energy consumption and a lower value for the work done therefore corresponds to a higher efficiency.

Figure 3.20 shows the work done for the different concepts. It can clearly be seen that an increase in structure results in a higher work done. The difference between full mix and layers can be addressed by the fact that aircraft are not able to fly at their optimal altitude in the latter, leading to a higher work done. The tube concept results in the most extreme value for work done. From these results in can be concluded that efficiency clearly decreases with increasing airspace structure, increasing traffic density, and when CR is turned on.

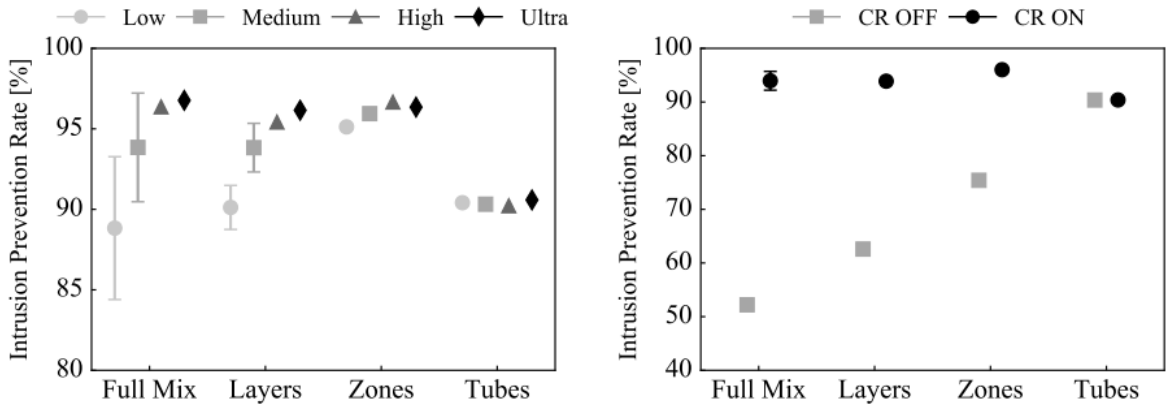

Figure 3.19: Means and 95% confidence intervals of the IPR [49]

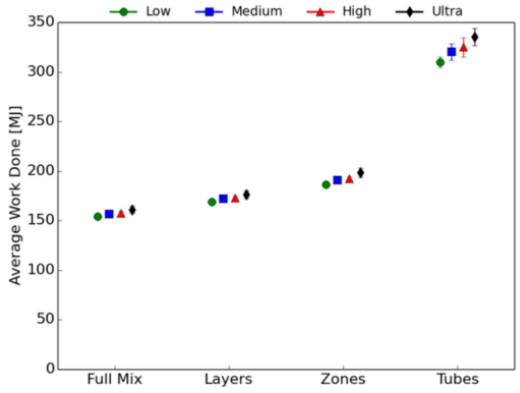

Figure 3.20: Means and 95% confidence intervals of the work done [25]

3.3.5. Stability

The above results have demonstrated that CD&R methods increase the total distance traveled. As discussed in Section 3.3.3, this can cause additional conflicts to emerge. Especially at high traffic volumes, the effect might be that conflicts propagate to such an extent that little maneuvering room remains. To measure the stability of the airspace, the Domino Effect Parameter (DEP) is used. Figure 3.21 shows a Venn diagram that visualizes the DEP.

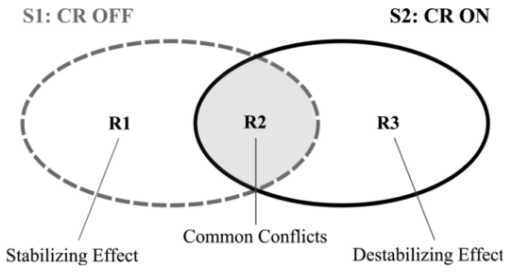

Figure 3.21: Venn diagram visualizing the DEP [49]

R1 represents all aircraft that were on conflict when resolution was off, but did not have a conflict when CR was switched on. R2 are all aircraft that were in conflict in both situations, and R3 are all aircraft that did not have a conflict when resolution was off, but did have a conflict when it was on. DEP is defined as:

$$DEP = \frac{R3 - R1}{R1} = \frac{R3}{R1} - 1 \tag{3.1}$$

A high value of DEP indicates instability, since a lot of additional conflicts are caused. Figure 3.22 shows the

DEP values for the different concepts. The value for DEP is constantly 0 for the tubes concept, since it does not use tactical conflict resolution. It can be seen that for low traffic densities, the DEP is negative and similar for the 3 other concepts. However, increasing the traffic density results in higher values for DEP. For full mix and zones, this value even increases to positive value, indicating that the airspace is becoming unstable for these densities. Possibly this is caused by the fact that there is less or no more maneuvering room available at these densities, making it more difficult to avoid aircraft without triggering new conflicts.

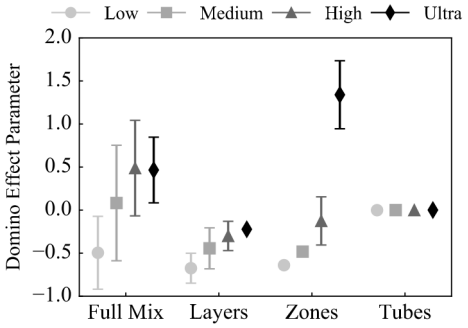

Figure 3.22: Means and 95% confidence intervals of DEP [49]

3.3.6. Capacity

The main research goal of Metropolis was to investigate the relationship between airspace structure and capacity. Capacity is however difficult to explicitly define, and is therefore evaluated by studying the variation of safety and efficiency with respect to the traffic demand. In Figure 3.23 it can be seen that the tubes and zones concept experience a rapid increase in number of conflicts between the high and ultra scenario, indicating that a capacity limit has been reached in between these levels. The layers concept has the smallest slope, suggesting that it will have the highest capacity of all concepts. The relationship between efficiency and traffic demand is less explicit and showed almost no variation (not shown here).

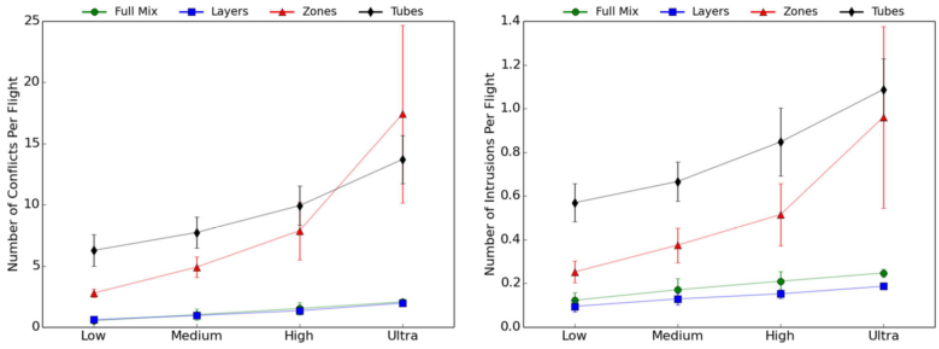

Figure 3.23: Variation of safety with traffic demand [25]

3.4. Conclusions

In the Metropolis project, four different airspace structures were put to the test to find out which would be the most suitable structure for future urban airspace scenarios. The goal of the project was not to design an airspace that was completely ready to be operational, but instead the focus was on the effect of airspace structure on capacity. Overall, the layers concept seems to be the best trade-off between structure and full flexibility. The concept dispersed the traffic and grouped traffic that was flying in the same direction. The layers concept was slightly outperformed by the full mix in terms of efficiency, but this is compensated by the fact that it was clearly the most stable concept of all. In a stable concept, resolving existing conflicts does not trigger many new conflicts, meaning that the capacity limit is not yet reached. The following conclusions were drawn at the end of the Metropolis project [49]:

1. It is beneficial for capacity when the horizontal path is not overconstrained.

2. It is beneficial for capacity when traffic is vertically constrained to separate traffic in different directions.
3. Convergence of traffic in the intersections of the structural elements of the zones and tubes concepts resulted in a decrease in performance.
4. The best method of structuring was found to be independent of density.
5. Robustness to uncertainties is significantly reduced when decentralized separation is combined with a fixed 3D route structure.

3.5. Lessons learned

To be able to revise the zones concept of Metropolis, it was important to dive into the details of the project. The research has provided a lot of insights into the zone specific results, as well as some general things to keep into mind when setting up an experiment. This section addresses the lessons learned that are relevant for this assignment. Section 3.5.1 explains the general lessons learned, after which Section 3.5.2 summarizes the zone specific conclusions.

3.5.1. Setting up an experiment

By carefully going through all the different work packages of the Metropolis project, it became clear how detailed the project has been. Developing the traffic scenarios and simulation area is a research on its own, which is not addressed in the articles and papers that followed from Metropolis. This approach enabled the author to be aware of the different aspects of designing an experiment, instead of only understanding the results and conclusions. In addition, it gave some insights on how to decide for the independent variables of an experiment, and what possible dependent variables there are to consider.

3.5.2. Zone specific results

The zones concept in the Metropolis project resulted in a poor overall performance. It is hypothezised that this is caused by the fact that traffic does not show a predominant pattern in the horizontal plane. As a result, designing a strict structure in the horizontal dimension possibly causes a mismatch with the demand pattern [49]. It is very important to take this into account in the scenario definition.

The poor performance can partly be allocated to the mismatch in demand, but it can also partly be allocated to the definition and implementation of the zone concept. The zones were intended to give aircraft the freedom to move through the zones freely. However, implementation of major flow zones to facilitate merging resulted in a concept with crowded traffic ways that closely resembled the tubes concept. This, in combination with the merging problems in the center and at the intersections of radials and rings of the concept, results in under-performance of the zones in the Metropolis project. It is expected that the benefit of zones is found in traffic scenarios with a more horizontal demand pattern (e.g. hub-and-spoke, weather cell avoidance). In addition, the merging problem that was encountered in the Metropolis project should be well addressed when the zones are revised if any benefit is to be expected. Finally, the fact that the CD&R method was not successfully tuned to the vehicles in the Metropolis project also needs to be taken into account in this thesis. Possibilities to optimize the MVP algorithm to PAVs and UAVs should be investigated.

4

Influence of traffic structure on airspace capacity

In the past, a lot of research has been conducted in the field of airspace capacity maximization. This research can coarsely be subdivided into research focusing on optimizing and adapting the current centralized network, and research focusing on developing new, decentralized or even distributed control networks. As shown in Figure 4.1, research focusing on decentralized control can again be categorized into structured and unstructured airspace options. In both divisions of research, successful options are documented, proving that literature has not yet reached consensus on the level of structure that is required to maximize capacity.

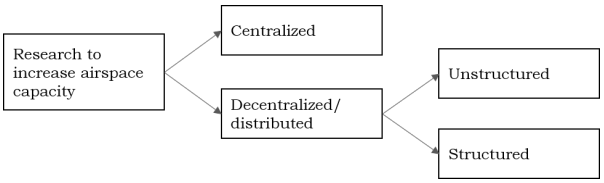

Figure 4.1: Research to increase airspace capacity can be subdivided into different categories

The Metropolis project described in Chapter 3 was the first to compare different levels of structuring in the same research. At extreme traffic densities, a layered airspace with vertically stacked bands used for a different span of headings performed best in terms of safety. Compared to the full mix concept in which every aircraft flies its desired path, the layers only resulted in a small decrease in efficiency. Although the experimental simulations prove the relation between airspace structure and the conflict rate, a theoretical relationship was still missing.

This chapter summarizes the research that was done to express the conflict rate in terms of the design parameters of an airspace. Section 4.1 describes the theoretical relationships for the global conflict rate. In the layered airspace concept of Metropolis, two phenomena were found to contribute to the positive effect on the conflict rate. The effects of spreading and reduction of relative velocity are discussed in Section 4.2 and 4.3, respectively. Finally, these two effect were combined with the global conflict rate to formulate a theoretical relationship between airspace structure and the conflict rate. This final relationship is discussed in Section 4.4. Based on this relationship, a new research proposal was formulated, which will be discussed in Section 4.5.

4.1. Global conflict rate

When the probability p_2 of two aircraft being in a conflict is assumed to be known, the global conflict probability can be calculated as a function of the number of aircraft in a sector (N). When the number of possible combinations of two aircraft is multiplied with the probability of a conflict, the global conflict rate in the airspace can be computed [22]:

$$CR_{global} = \left(\begin{array}{c} N \\ 2 \end{array} \right) p_2 = \frac{1}{2} N (N-1) p_2 \tag{4.1}$$

The effect of decentralizing the task can be evaluated using this relationship. In this case, there is a change of p_2 of meeting $N-1$ other aircraft, resulting in a local conflict rate of [22]:

$$CR_{local} = (N-1)\, p_2 \tag{4.2}$$

The difference between this global (centralized) and local (decentralized) conflict rates can be seen in Figure 4.2.

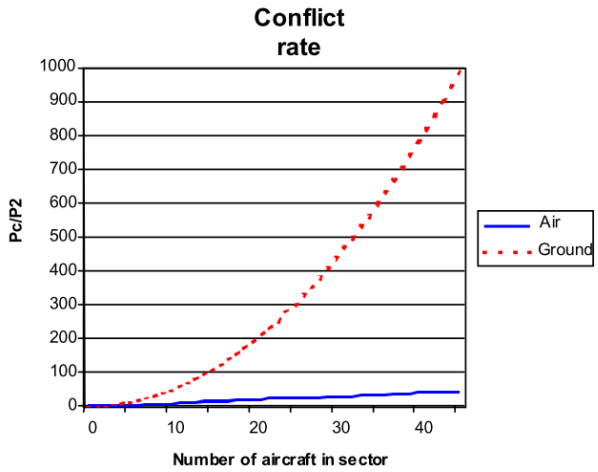

Figure 4.2: Relationship between the number of aircraft in the airspace and the global ('ground') and local ('air') conflict rate [22]

The local conflict rate in Equation 4.2 was used as a basis for Jardin to study the effect of fixed or free routing on the conflict rate. Jardin found that the conflict rate is proportional to [28] [29]:

$$CR_{global} \sim \frac{\overline{V} \cdot R \cdot T_{FL}}{A \cdot T_{tot}} \tag{4.3}$$

Here, $\overline{V}$ is the average ground speed, R is the minimum lateral separation, T_{FL} is the average time the aircraft spends in the airspace, A is the total airspace area and T_{tot} the total observation time.

In addition, the conflict rate is proportional to the relative velocity of the aircraft. If all aircraft fly twice as fast, they start to approach other aircraft twice as fast. This shows that the ground speed affects the conflict rate via the relative velocity of the aircraft. When average velocities are used, the following relationships also hold on a global level [20]:

$$CR_{global} \sim \overline{V}_{rel} \tag{4.4}$$

$$p_2 = c \cdot \overline{V}_{rel} \tag{4.5}$$

Here, $\overline{V}_{rel}$ is the average relative velocity of all the aircraft pairs in the airspace, and c is a constant for a given number of aircraft and airspace. The relationship in Equation 4.5 forms the basis for the derivation in the rest of this chapter.

4.2. Spreading effect

In the layered airspace concept of Metropolis, two phenomena were found to contribute to the positive effect on the conflict rate. The first effect is the spreading effect. As can be seen in Equation 4.1, the number of possible combinations has a direct effect on the conflict rate. Separating aircraft into different layers reduces the amount of possible combinations in each layer. For each layer, the conflict rate can now be written as [20]:

$$CR_{layer} = \frac{1}{2} N_{layer} \left(N_{layer} - 1\right) p_{layer} \tag{4.6}$$

The total expected conflict rate is the summation of Equation 4.6:

$$CR_{global} = \sum_{layer=1}^{L} \frac{1}{2} N_{layer} \left(N_{layer} - 1\right) p_{layer} \tag{4.7}$$

Here, L is the amount of layers that the airspace is divided into. When the heading ranges in the different layers are chosen carefully, the traffic will be evenly spread over the layers. Assuming the aircraft are indeed spread homogeneously, and assuming p_{layer} is equal in each layer, the global conflict rate can now be written as:

$$CR_{global} = \frac{1}{2} N \left(\frac{N}{L} - 1\right) p_2 \tag{4.8}$$

4.3. Reduction of relative velocity effect

The second phenomena that was found to contribute to the positive effect on the conflict rate, was the reduction of the relative velocity in the different layers. Each vertically stacked band of the layers concept was assigned to aircraft with headings within a certain heading range. To understand what the effect of heading difference is on the average relative ground speed, the geometric relationship in Figure 4.3 needs to be understood.

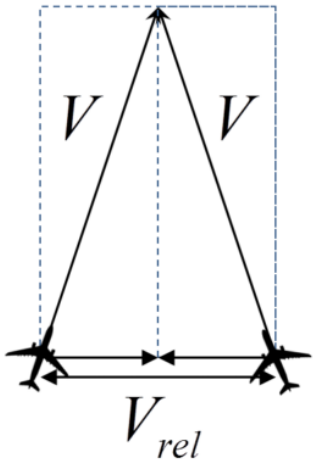

Figure 4.3: Relative velocity of two aircraft flying with the same ground speed [20]

By assuming that the velocity of the two aircraft is equal (V), the resulting geometry will always be an isosceles triangle. The angle between the two velocity vectors is therefore the absolute value of the heading difference between the two ground speed vectors. Although the ground speed of the different aircraft will not be equal in practice, the global effect of heading difference can be written as [20]:

$$V_{rel}\left(\left|\Delta hdg\right|\right) = 2V \sin\left(\frac{\left|\Delta hdg\right|}{2}\right) \tag{4.9}$$

The speeds in this equation are scalars, and $\left|\Delta hdg\right|$ is the absolute value of the heading difference. In Figure 4.3, the aircraft are assumed to fly with equal speed and towards the same point in time. In reality, this will not always be the case. However, aircraft that miss each other at a much larger distance will not be relevant for the conflict rate.

Equation 4.9 shows that the average relative velocity in a layer can be computed from the distribution of headings in that layer. Assuming the heading span of a layer is set to be a value α. Making the assumption that the headings in one layer are then uniformly distributed, the probability function of heading becomes a uniform distribution. The absolute value of the difference of two headings ($\left|\Delta hdg\right|$) comes down to subtracting two uniform distributions. The result is a triangular distribution as illustrated in Figure 4.4 [20].

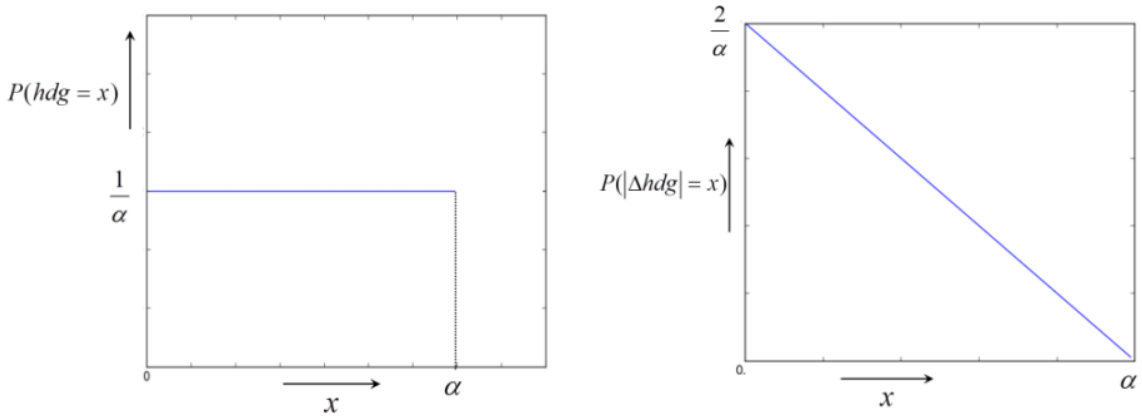

Figure 4.4: The probability density function of the absolute difference between two uniform distributions becomes triangular [20]

From the triangular probability density function in Figure 4.4, it follows that the probability density function of the absolute heading difference is:

$$P\left(\left|\Delta hdg\right| = x\right) = \frac{2}{\alpha}\left(1 - \frac{x}{\alpha}\right) = \frac{2}{\alpha^2}\left(\alpha - x\right) \tag{4.10}$$

By combining Equation 4.5, 4.9 and 4.10, the following function can be derived:

$$p_{layer} = c \cdot \overline{V}_{rel} = \int_0^{\alpha} c \cdot P\left(\left|\Delta hdg\right| = x\right) \cdot V_{rel}\left(\left|\Delta hdg\right| = x\right) dx \tag{4.11}$$

By integrating the terms, p_{layer} can be derived to be:

$$p_{layer} = 4c\overline{V} \cdot \frac{1}{\alpha}\left(1 - \frac{2}{\alpha}\sin\left(\frac{\alpha}{2}\right)\right) \tag{4.12}$$

However, at this point of the derivation, the goal is to analyze the effect of the heading span α in the layer. Therefore, all other terms are moved to a constant k. The effect of the relative velocity on the conflict rate can therefore be brought back to:

$$p_{layer} = k \cdot \frac{1}{\alpha}\left(1 - \frac{2}{\alpha}\sin\left(\frac{\alpha}{2}\right)\right) \tag{4.13}$$

4.4. Conflict rate in terms of airspace design parameters

When combining the two effects of Section 4.2 and 4.3, the effect on the global conflict rate can be formulated. By combining Equation 4.13 and Equation 4.8, the following relationship can be formulated:

$$CR_{global} = \frac{1}{2}N\left(\frac{N}{L} - 1\right) \cdot \frac{1}{\alpha}\left(1 - \frac{2}{\alpha}\sin\left(\frac{\alpha}{2}\right)\right) \cdot k \tag{4.14}$$

This equation can be compared to the situation where no layers are used ($L = 1$ and $\alpha = 2\pi$). In this way, the relation between the global conflict rate with and without can be determined [20]:

$$\left[CR_{global}\right]_L = \left[CR_{global}\right]_{L=1} \cdot \frac{N - L}{L(N-1)} \cdot \frac{2\pi}{\alpha}\left(1 - \frac{2}{\alpha}\sin\left(\frac{\alpha}{2}\right)\right) \tag{4.15}$$

From this relationship it can be seen that the conflict rate of an airspace without layers can be reduced by either increasing the amount of layers (L), or by decreasing the heading span (α).

Finally, Equation 4.14 can be combined with the function of Jarin (Equation 4.3) to consider all relevant airspace design parameters that effect the global conflict rate. This results in the final relationship [20]:

$$CR_{global} = k \cdot \frac{\overline{V}RT_{FL}}{AT_{tot}} \cdot \frac{1}{2}N\left(\frac{N}{L} - 1\right) \cdot \frac{1}{\alpha}\left(1 - \frac{2}{\alpha}\sin\left(\frac{\alpha}{2}\right)\right) \tag{4.16}$$

To validate the theoretical relationships derived in this chapter, experiments were conducted. It was found that the theoretical prediction of the conflict count closely matched the experimental results [20].

4.5. Onion research proposal

The relationships in this chapter have provided some insights in how airspace structure can help in reducing the conflict rate. The principles of spreading and relative velocity reduction have proven to have a positive effect on capacity, and a better understanding of the general mechanisms is required. A new project is proposed to further exploit the combination of these two principles: Onion. The name Onion is chosen because "A good airspace is like an onion: it has layers" [21]. The key difference with Metropolis is that Onion will use a more general definition to increase capacity and that it should be applicable to a wider variety of missions. This thesis contributes to the research objectives of Onion.

5

Conflict detection & resolution algorithms

In the early days of instrument-based navigation, pilots made use of radio beacons and airway systems to navigate through the airspace. This meant they had to fly directly over navigation aids on the ground (e.g. NDB (Non-Directional Beacon), VOR (Very high frequency Omni Directional Range)) [40]. Nowadays, aircraft are no longer limited to this, and four-dimensional (space and time) navigation capabilities have enabled the use of area navigation (RNAV). As a result, flight trajectories can be planned using direct routes. Although there are various advantages of these direct routes (e.g. fuel efficiency, increased airspace capacity), most aircraft still follow airways these days. The reason for this is not that technology of the aircraft didn't advance, or that pilots prefer to use the airways, but it is mostly due to the fact that air traffic controllers rely on airways for separation. By limiting the trajectories that aircraft can fly, air traffic controllers simplify the separation problem. The three-dimensions-plus-time conflict resolution problem now becomes a series of one-dimension-plus-time problems. Since a breakthrough technique that helps humans solve the difficult three-dimensions-plus-time problem does not yet exist, it is assumed that automation and decentralization will be developed to solve the conflict resolution in the future [10].

The cockpit is already equipped with automated systems for separation assurance (e.g. traffic alert and collision avoidance system (TCAS)), providing the pilot with decision support systems to predict and solve conflicts. In the past years, a lot of advanced automation tools have been developed to detect and resolve traffic conflicts. Many tools make use of the on-board avionics function that automatically transmits aircraft position data, the Automatic Dependent Surveillance Broadcast (ADS-B). This data can be used to detect conflicts, and to compute possible resolutions. The Conflict Detection & Resolution (CD&R) process is illustrated in Figure 5.1. In literature, many different CD&R methods are discussed. In this chapter, the different options will be introduced, after which the selected method will be covered in more detail. Section 5.1 describes the different possibilities for state estimation. Section 5.2 and 5.3 explain the different conflict detection and resolution possibilities. Finally, the selected method is explained in more detail in Section 5.4. Some final modifications are proposed in Section 5.5 to optimize the algorithm for small vehicles.

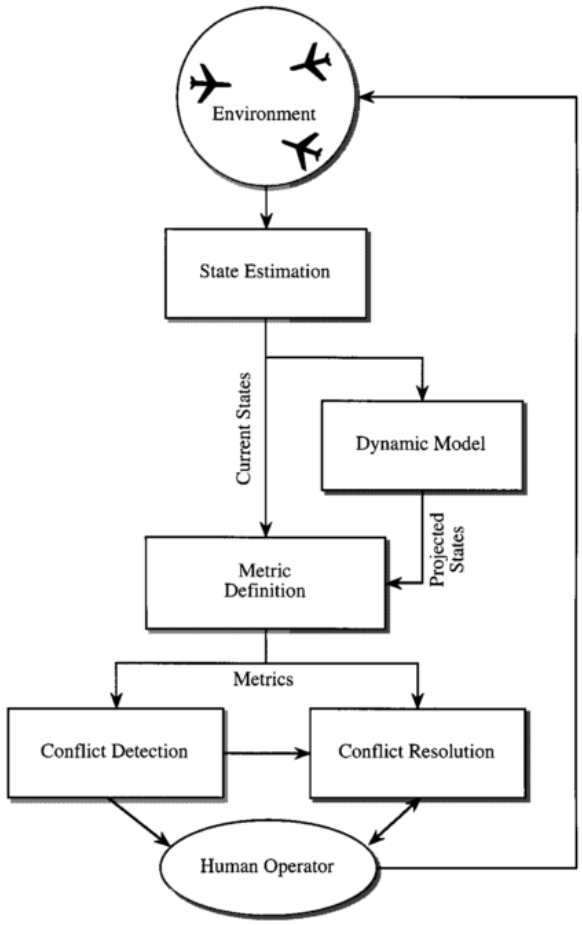

Figure 5.1: Conflict Detection & Resolution process [33]

5.1. State estimation and projection

An important (first) step in the CD&R process is the state estimation and projection. It is important that a reliable prediction of the future aircraft state is available to be able to detect conflicts and intrusions. To estimate the future aircraft states, the current states are propagated and projected in the future. To extrapolate the current state, three different methods are available: nominal, worst case and probabilistic (Figure 5.2).

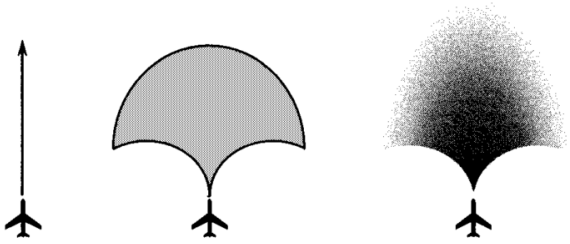

Figure 5.2: Different state propogation methods: nominal, worst case, probabilistic [33]

The nominal method (left in Figure 5.2) uses the current state and directly projects it in the future. An example is the case where the current velocity vector is used to predict the future position, without taking any uncertainties into account. When the look-ahead time of the algorithm is small, the nominal method is accurate enough in predicting the new state. However, no alerts or maneuvering instructions should be given for conflicts that are predicted to happen in the far future [33].
The worst case projection (middle in Figure 5.2) models all possible trajectories an aircraft will be able to follow. Within the limits of the aircraft's performance, the method takes into account all possible maneuvering

actions. If one of the potential trajectories could cause a conflict, a conflict is predicted. The worst case projection is very conservative, and often it results in a high false alarm rate. As a result, the airspace capacity can be significantly reduced [33].
Finally, the probabilistic method is a balance between the nominal and worst case method. This method incorporates uncertainties, either by adding a position error to the nominal method, or by weighting the different options in the worst case method with their probability of occurrence. Although the probabilistic method is probably the most general option, it might be difficult to model the probabilities of the future trajectories [33].

In addition to the state propagation methods, the state dimensions that are estimated also differ between CD&R methods. Some models purely involve the horizontal or vertical plane, whereas others already combines both. Preferably, the CD&R method uses a full four-dimensional prediction of the future trajectories to detect and resolve conflicts [33].

5.2. Conflict detection

An important step in the CD&R process is the actual conflict detection. A conflict is defined as a predicted Loss Of Separation (LOS) [34]. A LOS occurs when an aircraft enters the protected zone of another aircraft, and therefore the horizontal and vertical dimensions of the protected zone need to be taken into account.
Setting appropriate detection thresholds is important to distinguish between conflicts and nonconflicts. CD&R methods found in literature can be categorized into methods that explicitly defines when a conflict alert was issued, and methods that don't. The last category of methods might still provide valuable information about what possible actions can be taken, but do not explictly draw a line between a situation with or without a conflict [33].

5.3. Conflict resolution

Whenever a conflict is detected, the CD&R method should be able to provide ways to resolve it. In literature, many different resolution algorithms are addressed, which can roughly be divided into four categories: prescribed, optimized, force field or manual.

Prescribed conflict resolution makes use of a fixed set of procedures that are predefined. Instead of computing an optimal escape from the conflict, it always solves conflicts with the same maneuver (e.g. pull up). The benefit of this resolution method is that operators can be trained to reflexively perform the maneuvers, significantly decreasing the response time when an alert is issued. However, it is impossible to adapt the maneuver to its environment and all conflicts will be corrected in the same way while some might only require a less aggressive resolution maneuver [33].
The approaches with optimization make use of a cost metric that needs to be minimized. Typically, the cost functions in the metric include predicted separation distance, fuel, time, cost or workload. By properly setting the weights of these cost functions, the resolution maneuver can be optimized to the conflict, instead of using the same solution for any conflict. This method is mostly used for strategic conflict resolution, so before quick and tactical maneuvering is actually required [33].
Whereas the resolution methods in the optimization methods are often genetic algorithms, the force field method makes use of geometrical algorithms. In this method, the predicted positions at the closest point of approach are treated as charged particles. Similar to two charged particles that repel each other, the aircraft are modeled to repel each other [15]. As a result, relatively simple equations can be used to continuously steer away from (future) conflicts. Whereas most resolution maneuvers in other methods involve simple heading changes, the complexity of the maneuvers in the force field method can be extended (e.g. changing speed) [33].
Last, in the manual method, the pilot enters a potential solution himself, after which the CD&R method provides feedback whether this is an acceptable solution. An advantage of this method is that the human can include and integrate information from different systems (e.g. weather) and based on this provide an intuitive solution. The automated methods might not always take all relevant information into account, sometimes causing nuisance solution [33].

In literature, many different methods are found that can all be brought back to the four categories described above. In addition, the dimensions of the resolution maneuvers can also differ. Possible dimensions are:

turns, vertical maneuvers, speed changes. Some methods are able to combine two or more of these maneuvers simultaneously, whereas others use only one type of maneuver. In general, providing more freedom in maneuvering results in a more efficient solution to the conflict [33].

Finally, to operate in a realistic traffic environment, a CD&R method should be able to handle encounters that involve more than two aircraft at the same time. A good solution can be achieved by pairwise solving of each problem, or by finding a global solution from the start. Finding a global solution in these situations results in a more complex algorithm, but it might result in a more robust solution. If CD&R methods do not use a global solution to solve conflicts, they should be tested in situations with multiple aircraft to test their robustness to these scenarios [33].

5.4. Modified voltage potential algorithm

In a free flight study performed by the Nederlands Lucht- en Ruimtevaartcentrum (NLR) and National Aeronautics and Space Administration (NASA), several different conflict resolution algorithms were tested [22]. The resolution method that was developed by Eby [10] prove to be most effective for decentralized control, also in high traffic density scenarios [22]. The algorithm of Eby makes use of the nominal state propagation method, and considers the horizontal and vertical dimensions. The resolution algorithm is a geometrical algorithm, making use of the force field method described in the previous section.

An analogy for the method that forms the basis of Eby's algorithm is the voltage potential. This method compares aircraft and their destinations to electrically charged particles. All aircraft are regarded as negative particles, and their destinations as positive particles. As a result, repulsive forces between the aircraft exist, and attractive forces between the aircraft and their destinations. By summing all the repulsive and attractive forces of the traffic, a vector can be determined that ensures separation with other aircraft is maintained, but that brings the aircraft to their destination in an efficient way. This resolution method on its own however does not guarantee a minimum separation, and it is impractical to sum all forces of all aircraft in practice. Therefore, Eby developed an algorithm that uses the feature of voltage potential, but is slightly modified to provide a more pragmatic approach to solving conflicts [15].

This Modified Voltage Potential (MVP) algorithm uses three steps to resolve conflicts, illustrated in Figure 5.3. The charged particles repel each other away from their Closest Point of Approach (CPA), such that an intrusion, or Loss of Separation (LOS), is no longer predicted [36]. A predicted intrusion or LOS is also called a conflict.

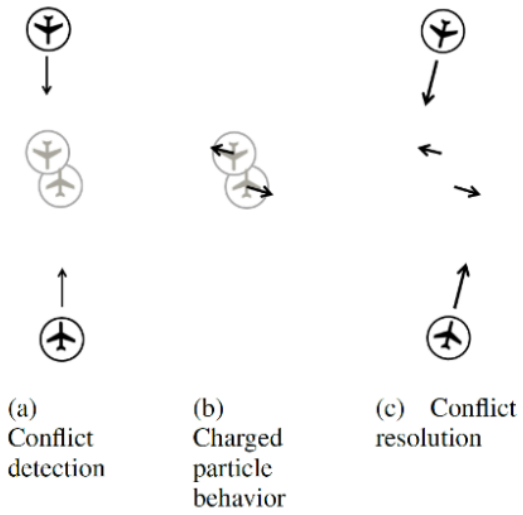

Figure 5.3: Three steps of the Modified Voltage Potential algorithm [36]

The geometry of a conflict situation should be evaluated more thoroughly to understand how the displacement vector is computed. Figure 5.4 shows two aircraft, A and B, and the relative velocity of aircraft B with

respect to aircraft A is pointing through the Intruder Protected Zone (IPZ) of A. The CPA of A and B is point C, and the goal is to move point C outside of the IPZ. Point O is the closest distance out of the IPZ, however the straight line from B to O still crosses the IPZ of A. Therefore, line CO needs to be multiplied with a slight factor, computed by [15]:

$$\frac{|CO|}{|CO'|} = \left|\cos\left(\arcsin\left(\frac{R}{AB}\right) - \arcsin\left(\frac{AC}{AB}\right)\right)\right| \tag{5.1}$$

Here, R is the radius of the IPZ as can be seen in Figure 5.4. Once CO' is computed, the displacement vector can be computed based on the time at which the CPA is predicted (t_C):

$$v_{MVP} = \frac{CO'}{t_C} + v_{\text{current}} \tag{5.2}$$

To compute t_C, the relative velocity and position (v_{rel} and x_{rel}) can be used. AC can be calculated:

$$AC = t_C v_{rel} - x_{rel} \tag{5.3}$$

Since AC is perpendicular to the relative speed (v_{rel}), the dot product of these two vectors is 0, and from this t_C can be computed [18]:

$$(t_C v_{rel} - x_{rel}) \cdot v_{rel} = 0 \tag{5.4}$$

$$t_C = \frac{x_{rel} \cdot v_{rel}}{v_{rel} \cdot v_{rel}} \tag{5.5}$$

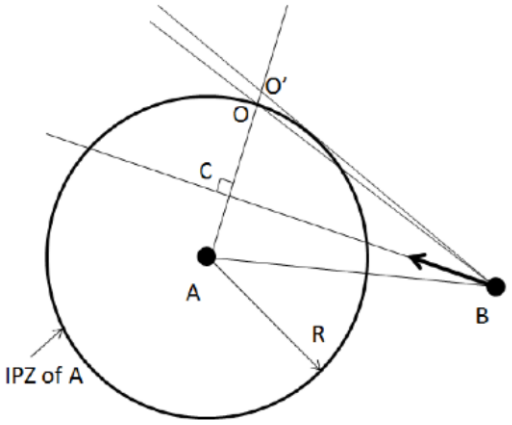

Figure 5.4: Computation of the MVP displacement vector [36]

Conflict resolution by the MVP algorithm is coordinated implicitly and cooperatively, meaning that both aircraft in conflict take measures to avoid each other. Since the displacement vector is based on a repelling force, both aircraft always take opposite measures. When an aircraft encounters multiple conflicts at the same time, the resolution vectors of all different conflict resolutions are summed together, to compute a general steering action [36].

5.5. Modifications for small vehicles

In the Metropolis project, the MVP algorithm was also used. Based on initial test runs, separation margins of 0.135 nm horizontally and 150 ft vertically were used, in combination with a look-ahead time of 60s. The average severity of the intrusions in Metropolis however was around 40% [49]. From this it can be concluded that the MVP algorithm needs to be optimized to account for the high maneuverability and small size of the PAVs and UAVs.

Research has been done to optimize a geometrical CD&R method to ensure separation between UAVs and commercial aircaft [1]. In this research, Alignol addresses some of the major differences between the resolution maneuvers of commercial aircraft and UAVs. An important consideration is to constrain the maneuvers

only to heading changes at constant speed, since in general UAVs have poor speed up performance. Alignol evaluated the optimal strategy and target separation distances to improve the efficiency of the maneuvers. In this research, the interaction between UAVs and commercial aircraft was studied, therefore these optimized parameters are not directly applicable in a UAV of PAV scenario. In addition, the algorithm was tuned to such extent that instead of both aircraft in conflict maneuvering away from each other, the UAV was only maneuvering away from the commercial aircraft. The article of Alignol only considers conflicts in the horizontal plane, and therefore only serves as a source of inspiration on how to tune the CD&R method to the UAVs.

6

Merging

As discussed in Chapter 3, in the development of the zone concept of the Metropolis project merging of traffic in the center of the area prove to be a difficult task. A literature review is performed to evaluate current merging and spacing techniques to come up with a suitable solution. The merging of arrival flows can be represented as a black block, as illustrated in Figure 6.1. A number of N inbound flows are all converging along the vertical and lateral dimensions and need to be integrated into one single output flow. With high traffic densities, meeting the separation and sequencing order is already a challenging task on its own, but in addition the merging is subjected to local constraints [11].

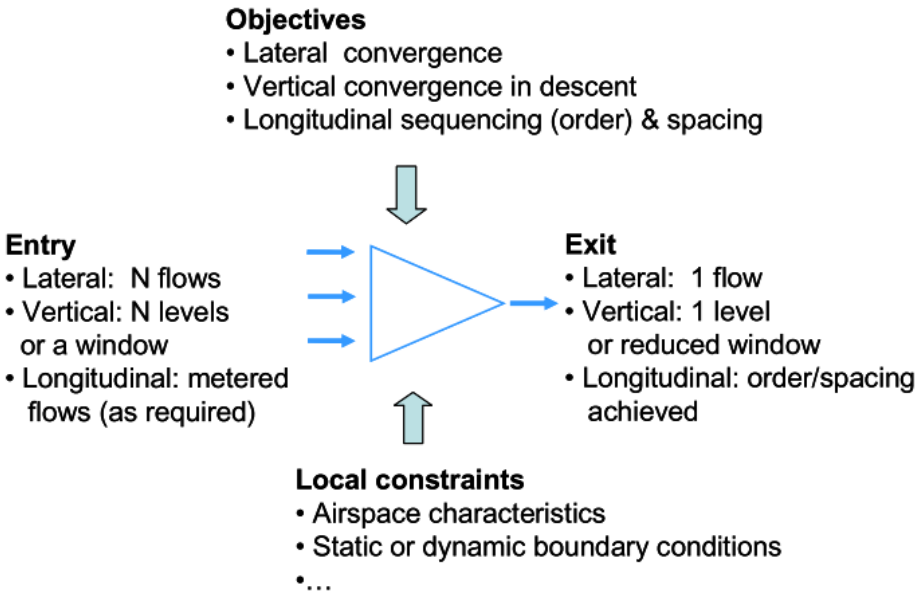

Figure 6.1: The merging of arrival flows can be represented as a black box [11]

Main drivers of research in the approach phase are the capacity limit, and environmental constraints [19]. As a result of uncertainties, many aircraft are delayed in their trajectories, and the merging techniques should also be designed to absorb this. Today's practice for merging and spacing is illustrated in Figure 6.2.

As can be seen in Figure 6.2, the merging of arrival flows mostly relies on the use of heading and speed instructions. This is efficient and flexible, but it reduces predictability [6]. In addition to this complication, the zone concept in this assignment asks for a merging technique that fits the circular geometry. The local airspace characteristics are an important input (local constraint) to the merging process, and therefore a merging technique that better fits the geometry is investigated. Initially, the circular runway concept that is being developed by Hesselink [14] was considered. The foreseen application of this concept is a small airport

Figure 6.2: Different merging and spacing techniques[19]

that is dedicated to autonomous aircraft [9], and therefore it was investigated whether a circular runway could be used in the inner circle. Implementation of the concept was found to require drastic changes of currently used methods. Since the goal of this assignment is not to investigate the effectiveness of a new concept, a more established method was preferred at this point.

In this chapter, the Point Merge technique that was developed by Eurocontrol is evaluated. Section 6.1 describes the theory of a single PMS. It has been investigated how multiple Point Merge Systems can be combined, this will be discussed in Section 6.2.

6.1. Theory of point merge technique

Eurocontrol designed a technique for merging aircraft in the terminal areas (TMA) without the need for heading changes and vectoring. The so called Point Merge technique makes use of a merge point and pre-defined sequencing legs that can be used to stretch or shorten the aircraft path [27]. The sequencing legs are designed to always have the same distance away from the merge point, and are separated vertically. An example geometry of a PMS with two entry points and sequencing legs is shown in Figure 6.3.

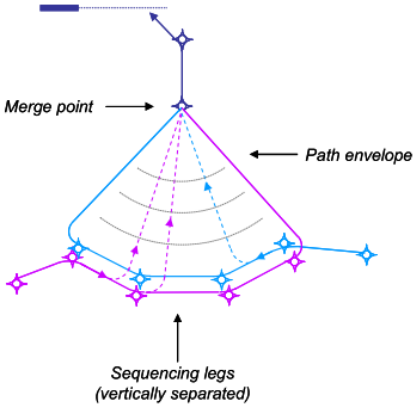

Figure 6.3: Example geometry of a Point Merge System [11]

The entire sequencing leg is programmed in the FMS and therefore no controller intervention is required to perform path stretching. Spacing is monitored by giving aircraft a "direct-to merge point" instruction at the appropriate time. After leaving the sequencing legs, spacing is maintained by speed control [11].

Eurocontrol did an initial assessment in 2006 and Point Merge was found to be safe and accurate, even under high traffic load. Although the method is less flexible than the use of heading instructions, the spacing between aircraft at final was as accurate as with conventional methods [6].
In a research by Ivanescu ([27]), the performance of Point Merge was evaluated with respect to the vectoring. The results showed that Point Merge can result in a significant improvement in performance. Figure 6.4 shows the mean and standard deviation of the flight level at a given time from landing. Two trends can be seen: the flight levels for Point Merge are higher, and standard deviations are smaller. Since aircraft fly higher on average, they fly higher average ground speeds, therefore reducing the distance and time inside the TMA. Also, descent profiles in the PMS are more homogeneous. From the altitude profiles, the fuel consumed per aircraft was comped, showing that the fuel consumption for Point Merge was in the range of $25 \pm 2\%$ less than for vectoring [27].

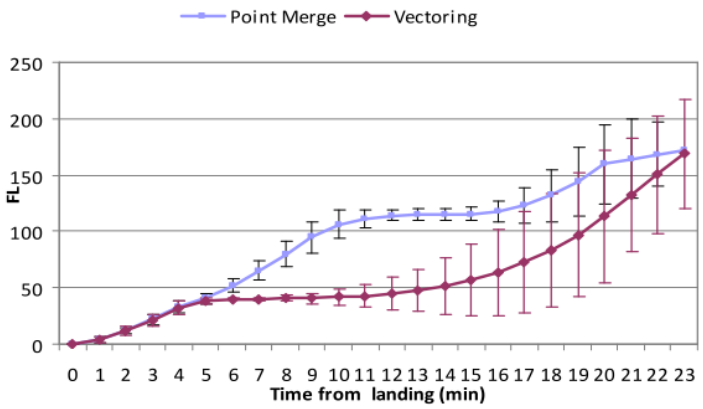

Figure 6.4: Means and standard diviation of the flight level inside the TMA [27]

6.2. Different configurations of the Point Merge method

In the research conducted by Boursier and Ivanescu, the simulated TMA was simplified to only one runway, without departures. The research only covered configurations with two or three entry points. All entry points had their own sequencing leg, and all lead to the same merge point. Favennec investigated different configurations to test Point Merge in more complex environments.

Figure 6.5 shows three examples of the configurations that were tested. The left image shows a PMS with 4 entry points and sequencing legs, with 4 traffic flows being merged into 1 point. The four sequencing legs were separated vertically. The disadvantages of this configuration is that the traveling distance for the two traffic flows coming from the left of the image is increased, since they have to fly beyond the runway. In this configuration, the Point Merge method was also found to be accurate and safe, but since there were no spare legs in between the four legs, the aircraft were bound to very strict vertical constraints.
The second configuration investigated the option to split one PMS into two subsystems. The middle option in Figure 6.5 shows two subsystems that are located opposite to each other, optimizing the distance flown to reach the entry points. This configuration has two potential issues: head-on situations can easily occur, and at the merge point the aircraft have to make very large turns, resulting in a potential loss of spacing accuracy. The third concept provides a solution for these two issues by separating the two merge points. The right option in Figure 6.5 uses a common point in the middle of the merge points in which the traffic from the two merge points is merged at a different altitude [11].

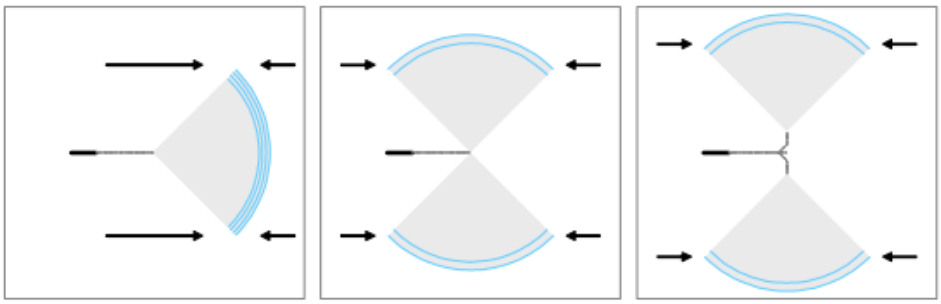

Figure 6.5: Different PMS configurations [11]

The use of two subsystems was found to be feasible and similar benefits were found as with the single PMS. All configurations were tested with a TMA of 50 to 60 nautical mile (nm). Reducing the size of the PMS results in a smaller leg and a smaller distance between the leg and the merge point. As a result, the distance to absorb delay is smaller and the "direct-to merge point" instruction needs to be more accurate since there will be less time to adjust spacing with speed control from the leg to the point. When the total dimensions of the TMA were halved, the PMS with two subsystems was still found to be feasible [11].

7

Sequencing

In order to maintain a safe, orderly and efficient flow of traffic in the air and on the ground, tactical queue management is important [41]. In the Point Merge method discussed in Chapter 6, multiple subsystems were integrated to merge traffic from different merge points. Whenever two merge points are merged into one, the sequence and ordering becomes very important. Although Point Merge can be an important building block in the queue management, Figure 7.1 shows that pre-sequencing (also called metering) is needed to also meet capacity and safety constraints when the different flows come together in a single node [11].

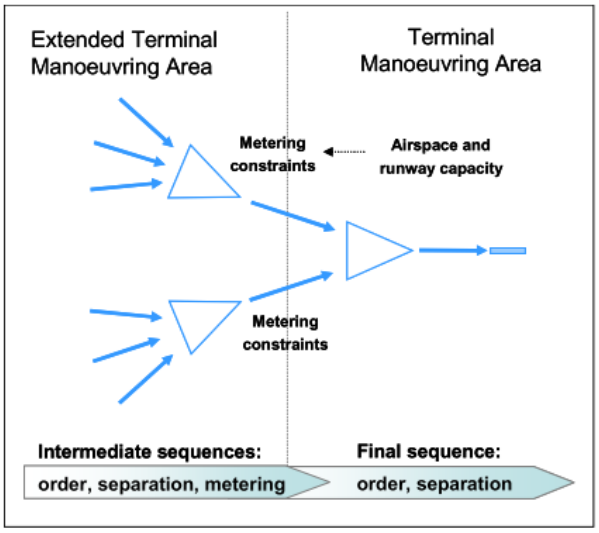

Figure 7.1: Pre-sequencing is needed to meet downstream capacity constraints [11]

Since the goal of this research is not to investigate or design new merging and sequencing methods, this chapter aims at investigating the current Arrival Manager (AMAN) tools that are used. Section 7.1 gives an introduction to the different modules that are required and is needed to get a basic understanding of the theory behind AMAN. Section 7.2 gives some insight in how a sequencing method could be used in combination with the point merge method described in Chapter 6.

7.1. Arrival Manager tool

Eurocontrol defines arrival management as "the process of safely and effectively arranging arrivals into a smooth efficient flow for landing at a destination airport" [13]. AMAN software is used to assist in metering and sequencing of the arrivals, and aims to optimize the capacity of the runway [13].

Although there is no standardized AMAN tool in Europe, the basic working principles of the different tools are the same. Figure 7.2 shows the different modules that form the basis for most systems [55].

The flight data source, aircraft performance and weather data modules serve as an input to the prediction module. The flight data module includes all information about the current aircraft state, as well as the intent of the aircraft. The performance module is used to compute the Expected Time of Arrival (ETA) at the runway, and often uses a point-mass or kinematic model. Since wind has a significant effect on the trajectory prediction, weather data is also integrated. However, at this stage it is assumed that wind can be neglected since its average effect on the system is zero. Sometimes it has a positive effect, sometimes a negative effect, meaning that it can be neglected when looking at the average performance at this stage [55].

The trajectory prediction module integrates the information from the different modules to predict the ETA at the runway and the Expected Time Over (ETO) at the Initial Approach Fix (IAF) for all aircraft. The trajectory prediction algorithms can again differ between different tools, as explained in Section 5.1. Since the TMA and runway have limited capacity, not all aircraft can arrive at their ETA [55].
The sequencer uses the unconstrained ETAs to allocate a runway to all aircraft. Based on this list, each aircraft is assigned a Scheduled Time of Arrival (STA), taking into account the required interval between landing aircraft [55]. The difference between ETA and STA needs to be absorbed by path lengthening (or shortening) instructions by the air traffic controllers.
The last three modules consider the human-machine interaction. The controller working position involves the user interface, and normally involves a timeline with a schedule list. Based on the information in this list, air traffic controllers should give instructions (e.g. heading changes) to absorb the required delay or to shorten the path. The system supported coordination (SYSCO) module is used to exchange AMAN information between controllers. Finally, an advisory module is sometimes linked to the system, directly providing speed and route advisories to the air traffic controllers [55].

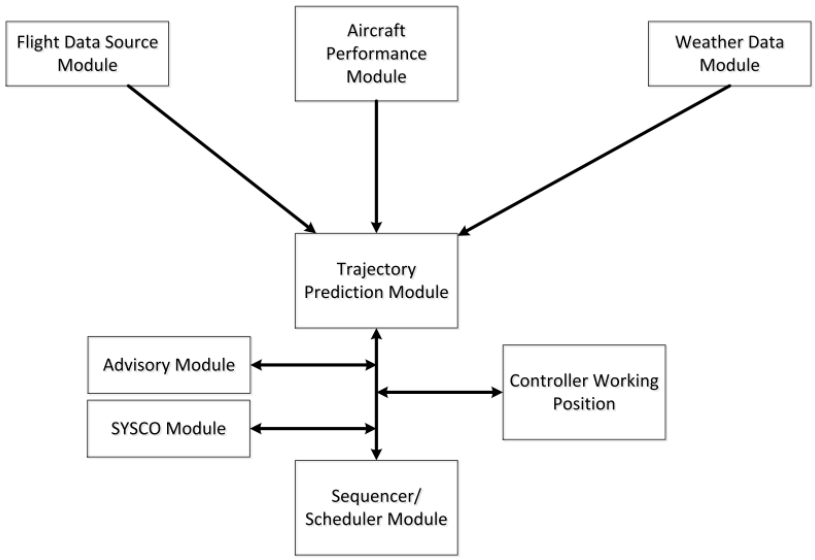

Figure 7.2: Different modules of the AMAN tool [55]

The horizon of the AMAN tool is an important variable in the system. There are three different horizon definitions that need to be considered when talking about an AMAN system: the Eligibility Horizon (EH), Freeze Horizon (FH) and the Active Advisory Horizon (AAH) [55]. Once an aircraft enters the EH, it is picked up by the AMAN tool and from then it can be taken into account for the scheduling. At that stage, an STA is not yet assigned to the aircraft. Once it enters the FH, the STA will be frozen and advisories to achieve the STA can be generated. Only in case new aircraft pop-up in the horizon, the STA will still be changed. Once the aircraft enters the last horizon (AAH), the advisories can actively be used by the traffic controllers, and the STA should not be changed anymore.

7.2. Combining sequencing tools with point merge

Previous research has already investigated how an AMAN system could be used in combination with an Airborne Separation Assurance System (ASAS) using point merge principles [5]. The objective of the research was to test the feasibility of using both systems together. In the experiment developed by Boursier, the AMAN

system indicated "time to lose" (delays) or "time to gain" upstream of the TMA, in the extended TMA (E-TMA) [5]. The AMAN system was used to sequence aircraft coming from different Initial Approach Fixes (IAF), which will also be relevant in this thesis assignment.

Two conditions were simulated and evaluated: one on which controllers only used the conventional merging instructions (e.g. heading, speed changes) as discussed in Chapter 6, and one in which ASAS was used. In both conditions, AMAN was used, and therefore the conditions can be described as AMAN and AMAN+ASAS respectively. The Freeze Horizon was set at 40 minutes before touchdown, and the STA were really fixed 20 minutes before touchdown.

The trajectories that were flown in this human-in-the loop experiment are shown in Figure 7.3. It can be clearly seen that after the merge point in the TMA, the trajectories in the AMAN+ASAS configuration remain straight and show little dispersion.

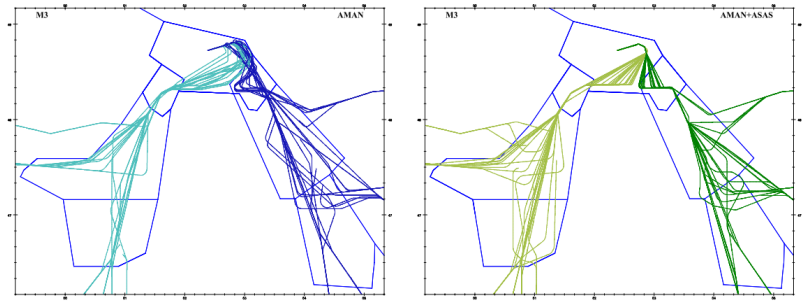

Figure 7.3: Flown trajectories with AMAN (left) and AMAN+ASAS (right) [5]

Also in terms of throughput, the AMAN+ASAS configuration shows benefit over only using AMAN. At the same time, the safety is of the system was found not to be effected negatively, since the time between the aircraft was still adhering the required landing interval [5].

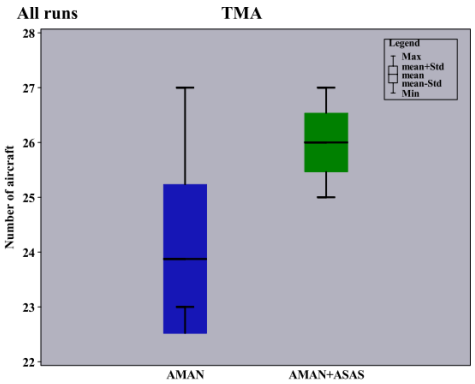

Figure 7.4: Throughput with AMAN (left) and AMAN+ASAS (right) [5]

From the research of Boursier, the positive effect of point merge is again confirmed. However, it also shows that an AMAN and ASAS system with different time scales can still be compatible in practice.

8

Experiment proposal

The objective of this thesis is to investigate the value of defining lateral zones in a traffic scenario with a horizontal demand pattern, by running and comparing fast-time simulations of high density traffic in a structured and unstructured airspace.

The thesis objective is linked to the following research question:
"How does a structured airspace with lateral zones compare to an unstructured airspace in terms of safety, efficiency and capacity in high density traffic scenarios with a horizontal demand pattern?"

The research question is split into four sub-questions that all contribute to answering the main question:

1. In what scenarios are altitude layers no longer adequate, and could lateral zones make the difference?
2. What is the safest airspace concept in terms of number of conflicts, number of intrusions, intrusion severity, and intrusion prevention rate?
3. What is the most efficient airspace concept in terms of work done, and average interval between successive arrivals?
4. What airspace concept results in the highest capacity?

In this chapter, the experiment proposal is presented. Section 8.1 explains the scenario choice. The independent and dependent variables in the experiment will be discussed in Section 8.2 and 8.3 respectively. The selected vehicle types are presented in Section 8.4, and the selected CD&R method in Section 8.5. Since separating arriving and departing traffic in the inner circle is a complex challenge, the structure of the inner circle will be addressed in Section 8.6. The simulation area will be introduced in Section 8.7. Finally, the proposed project planning will be presented in Section 8.8.

8.1. Scenario selection

At the start of this thesis, the aim was to revise the zone concept and to investigate whether an airspace with a lateral structure can be beneficial in certain scenarios, if defined properly. Initially, three different scenario options were considered:

- Full city area (similar to Metropolis, but with the zones defined differently)
- Departure/arrival area with high density converging and diverging traffic
- En-route airspace with a funnel generated by two (or more) weather cells

Based on thorough literature review of the Metropolis publications ([23–26, 48, 49]), it was found that the definition of the zones in the Metropolis concept was almost tube-like, with all traffic being forced into traffic flows on the edges of the zones. Although it is expected that the results from Metropolis could be improved by redefining the structure and organization of the zones concept, it is still not expected that this will outperform the layers concept. The reason for this is that the traffic demand in an urban area does not follow a horizontal pattern, and forcing aircraft to merge into radials and rings around the city center results in an airspace that

does not fully exploit the three dimensions. The benefit of a horizontal structure is expected to be highest in a departure/arrival area, where all aircraft converge and diverge from the same point. It is expected that the weather cell scenario can also benefit from a zone topology, but the scenario will be more difficult to simulate realistically. Therefore, it is chosen to investigate the lateral zone concept in the departure/arrival scenario, and to later expand the possible applications to different scenarios (e.g. the weather cell scenario).

The departure/arrival area has evolved over the different stages of the literature review. Figure 8.1 shows what changes the area went through. Starting with an area with 8 zones, alternating diverging and converging traffic (left in Figure 8.1), it was found that the traffic in the converging zones would be flying directly towards each other. This results in potential head-on conflicts, having a direct effect on safety. To ensure that opposing zones do not have opposing vectors, the following relationship should hold:

$$\frac{N}{2}\%2 == 1 \wedge N\%2 == 0 \tag{8.1}$$

The middle area in Figure 8.1 shows an example with 6 zones, mitigating the risk of head-on conflicts.
The inner (light blue) circle in the areas in Figure 8.1 needs to facilitate the merging of arriving traffic, and at the same time facilitates departure. The proposed traffic flow in the inner circle will be discussed in more detail in Section 8.6, but to facilitate efficient departure, an additional refinement was added. The right area shows that the zone boundaries are no longer perpendicular to the inner circle, making it easier for departing and arriving traffic to leave and enter the inner circle.

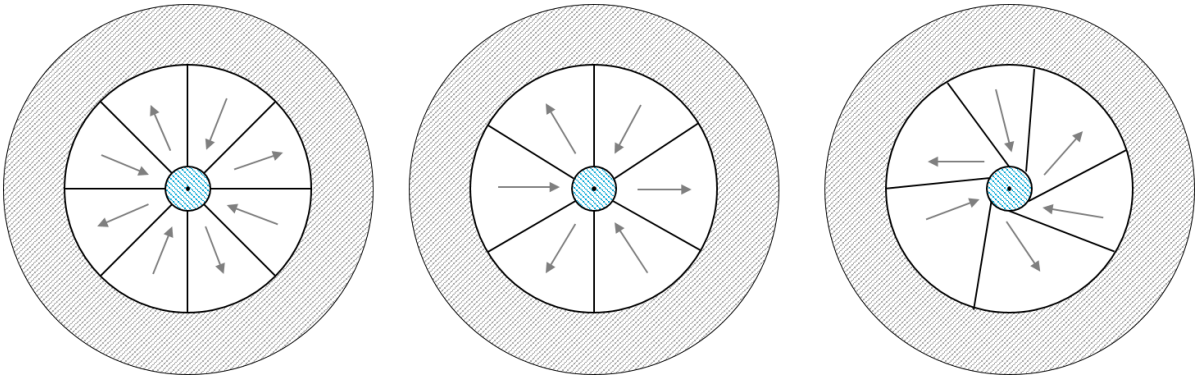

Figure 8.1: Different departure/arrival areas that were considered

8.2. Selecting independent variables

The independent variables are the variables that are changed in the experiment to test the effect on the performance. If all possible independent variables would be included in the experiment matrix, it would be impossible to identify the relationship between the variables and the measured performance. Therefore, it is important to carefully select the variables that are needed to answer the research question. Figure 8.2 shows the configuration of the zone concept that was selected. The following variables can be varied in this configuration:

- Number of zones
- Surrounding structure (e.g. unstructured or layers)
- Radius zones (R_{zones} in Figure 8.2)
- Radius inner circle (R_{inner} in Figure 8.2)
- Structure of the zones (e.g. speed layers inside the zones or R_{zones} as a function of altitude)

Regarding the traffic in the experiment, the following variables can be varied in addition:

- Traffic density (e.g. low, medium, ultra, high)
- Ratio between departing and arriving traffig (e.g. 30/70, 50/50)
- Conflict Resolution & Detection method (e.g. MVP or no CD&R)

- Method used to separate departing and arriving traffic in the inner circle (e.g. Point Merge, spiraling)
- Vehicle types (e.g. UAVs or PAVs)

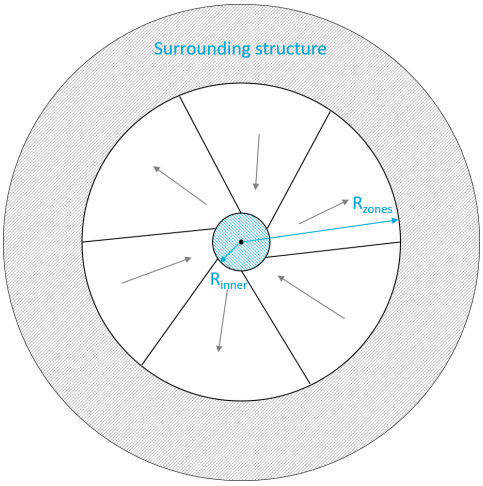

Figure 8.2: Selected concept configuration

The experiment matrix would be too big if all variables were to be taken up in it. Therefore, it was decided to split the experiment into three phases, carefully selecting the independent variables per phase:

1. Phase I: Compute fixed values for some of the configuration variables
2. Phase II: Evaluate experiment matrix and answer research question
3. Phase III: Additional refinement where possible

Which variables will be fixed after phase I, and which will be taken up in the experiment matrix will be discussed in the following sections. Section 8.2.1, 8.2.2 and 8.2.3 provide a more detailed description of phase I, II and III subsequently.

8.2.1. Experiment phase I

During the first phase of the experiment, the zone concept will be implemented and the effect of varying some of the configuration variables will be evaluated to make sure that the final experiment matrix is manageable in size. At the end of phase I, fixed values for the variables in Table 8.1 will be selected for the subsequent experiment phase.

Table 8.1: Variables to be computed in experiment phase I

Variable	Description
R_{zones}	Radius of the zones
R_{inner}	Radius of the inner circle
Inner circle structure	Method used to separate departing and arriving traffic in the inner circle
Settings of CD&R method	Look-ahead time, separation requirements

The radius of the zones and the inner circle are expected to have a strong effect on the outcome of the experiment. When the zones are too big, the aircraft have to deviate from the direct route to their destination significantly, resulting in a degraded performance in terms of efficiency. However, when the zones are too small, aircraft will have difficulty to spread laterally at the transition between the zones and the surrounding structure. Especially when the surrounding structure is divided into layers, this could possibly result in safety issues. The radius of the zones is dependent on the altitude and descent rate of the arriving aircraft. A theoretical value will be computed, and simulations in BlueSky will be used to test the sensitivity of changing the radii.

Another important variable to consider and test in advance is the structure in the inner circle. Not only the radius of the inner circle has a direct effect on the outcome of the experiment, also the structure and method used to separate arriving and departing traffic has a direct influence on the safety and efficiency metrics. Merging and sequencing of the arriving traffic should be done safely, whilst not degrading efficiency too much. Section 8.6 proposes a structure for the inner circle. In phase I the capacity and safety of the proposed method has to be evaluated and tweaked to find the final configuration for the full experiment (e.g. amount of Point Merge legs, sequence horizon).
Finally, the settings of the CD&R method will be varied to find an adequate look-ahead time and separation requirements.

It should be noted that the goal is not to compute the optimal value of the variables, but to evaluate the effect of changing the variables and to find an adequate value for the next experiment phases.

8.2.2. Experiment phase II

Once the effect of varying the variables in Table 8.1 is found, and adequate values are selected, the main research question will be answered in phase II. Since the research question focuses on the question whether structuring traffic into lateral zones can be beneficial compared to an unstructured airspace, the number of zones is the most evident independent variable to take up in the experiment matrix. It is expected that the benefit of the zones is higher for traffic scenarios with a high density, and therefore traffic density is selected as a second variable. Finally, to test the stability of the different concepts, the CD&R mode is also toggled on and off. Table 8.2 summarizes the variables that are taken up in the experiment matrix of phase II. As a result, $3 \times 3 \times 2 = 18$ experimental conditions will be tested, and multiple runs will be done for each condition.

Table 8.2: Experiment matrix of phase II

Variable	#	Different values
Concept	3	0, 6 or 10 zones
Traffic density	3	Medium, high or ultra
CD&R	2	On or off

The demand pattern of the traffic (the ratio between departing and arriving aircraft) will be kept constant (50/50) in phase II, since varying it does not help in answering the research question at this stage. Although the possibility to absorb a changing demand pattern is relevant in evaluating the different concepts, the zones concept could be changed in the future to a dynamic zone definition. This capability is considered to be out of scope for this stage of the research, and therefore, only the differences between the concepts at an equal distribution of departing and arriving traffic is evaluated.

Finally, it should be noted that all traffic inside the experiment will be of the same type (e.g. only PAVs or only UAVs), since it is most likely that the departure/arrival areas will be different for the two types. The method to separate arriving and departing traffic is different for UAVs than for PAVs, since most UAVs have better hovering capabilities. Using PAVs that require a landing and take-off distance is more complex, and therefore it is proposed to put the focus on PAVs in the first two phases.

8.2.3. Experiment phase III

Based on the outcome of phase II, additional refinements will be required to optimize the zone structure. At this point, several possible refinements are already addressed:

- Including speed layers inside the zones
- Making the zone size (R_{zones}) a function of altitude
- Dynamically adapting the number of converging and diverging zones to traffic demand

As many refinements as possible will be implemented in the remaining time, and others will be included in the recommendations and discussion of the research.

Since further research derived from Metropolis has shown that the layers concept is successful in the urban areas, it is valuable to test the joint composition of zones and layers. Once the final configuration for the zones is selected, a comparison is made between a layered and an unstructured surrounding.

Experiment phase I and II focus on scenarios with only PAVs. However, scalability of the problem to UAVs will be addressed in this phase. In Section 8.4 a hypothesis on the differences will be formulated. In addition, the sensitivity of the concept to changing the demand pattern or adding wind can be evaluated to test the robustness of the different concepts.

8.3. Dependent variables

Dependent or responding variables are variables that are not directly controlled in the simulations. They can be used as a metric to measure performance of the different airspace concepts. Eurcontrol uses safety, cost-efficiency, capacity and environment as the Key Performance Areas (KPAs) for evaluating the airspace performance [54]. This, in combination with other ATM research, served as a source of inspiration to select dependent variables for the experiment. The proposed dependent variables are categorized into safety, efficiency, stability and structural complexity. The following sections address these categories subsequently.

8.3.1. Safety

The airspace is a safety critical system, and therefore the most important metric will always be safety. Safety will be evaluated by means of the following variables:

- Number of conflicts
- Number of intrusions
- Severity of intrusions
- Intrusion prevention rate

Conflicts are defined as a predicted loss of separation within the look-ahead time of the state propagation, whereas intrusions are defined to be actual losses of separation. Counting the number of conflicts and intrusions for the different airspace concept, enables the identification of safety issues.

When only looking at the number of intrusions, a situation with 4 mild intrusions can be assessed to be less safe than a situation with 1 intrusion. However, one near-collision is less desirable than 4 slight intrusions. Therefore, it is also important to compute the severity of the intrusions, by means of the following formula [36]:

$$\text{int}_{severity} = \max_{t_{0_{\text{int}}} - t_{1_{\text{int}}}} \left(\min \left(1 - \frac{d_h(t)}{R_h(t)}, 1 - \frac{d_v(t)}{R_v(t)} \right) \right) \tag{8.2}$$

Here, d_h and d_v are the horizontal and vertical distance between two aircraft, and R_h and R_v are the horizontal and vertical separation requirements respectively. $t_{0_{\text{int}}}$ and $t_{1_{\text{int}}}$ are the start and end times of the intrusion. The terms $1 - \frac{d}{R}$ are the horizontal and vertical intrusions that are normalized to the separation requirements. In Figure 8.3, this is visualized by I_h and I_v. By computing the maximum intrusion, the intrusion severity for the path in Figure 8.3 would be equal to the normalized horizontal intrusion at A.
Additionally, the Intrusion Prevention Rate (IPR) will be computed to evaluate the ability to avoid conflicts from becoming intrusions. The IPR is computed as follows:

$$IPR = \frac{n_{\text{conflicts}} - n_{\text{intrusions}}}{n_{\text{conflicts}}} \tag{8.3}$$

Important to take into account when evaluating safety, is the difference between the variables inside and outside the zone area (R_{zones}). By measuring the conflicts and intrusions inside and outside this area separately, it can be evaluated whether the problem maybe moves to a different region.

8.3.2. Efficiency

The second metric that is relevant to evaluate, is efficiency. It will be evaluated by means of the following variables:

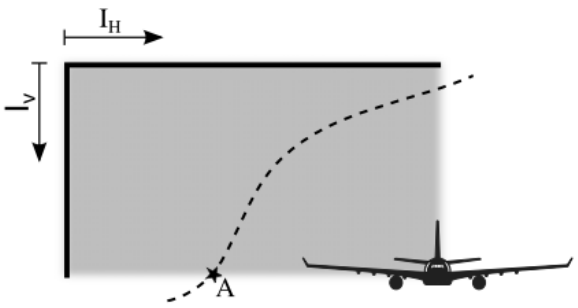

Figure 8.3: Intrusion path through the protected zone (gray area) of an aircraft [49]

- Work done
- Interval between successive arrivals

The work done variable is chosen over the normal route efficiency metric in the horizontal plane since it takes into account the vertical and horizontal path of an aircraft. Work done is analogous to fuel consumption and therefore gives a good indication about efficiency. It is computed as follows [49]:

$$W = \int_{path} T \cdot ds \tag{8.4}$$

Here, T is the thrust vector, and s is the displacement vector.

To compare the efficiency of the arrival sequence, the interval between successive arrivals will be computed as follows [24]:

$$t_{\text{int}_i} = t_{arrival_i} - t_{arrival_{i-1}}; i \in [2, n] \tag{8.5}$$

Here, n is the total amount of aircraft that are landing during the logging time. By computing all intervals in the logging time, the average and minimum intervals can be computed. From this, it can be concluded whether the concept results in unnecessary long, and therefore less efficient intervals between the arrivals. At the same time, this metric can also be used to address the safety, since it provides information on whether or not the interval requirement was met.

8.3.3. Stability

Previous research by Sunil has demonstrated that capacity measurements of decentralized airspace concepts need to consider safety, efficiency, and stability effects [50]. One of the main concerns with decentralized traffic separation is that at high traffic densities, conflict chain reactions will occur. In literature, airspace stability is best described using the Domino Effect Parameter (DEP). Figure 8.4 shows a Venn diagram that can be used to visualize the DEP.

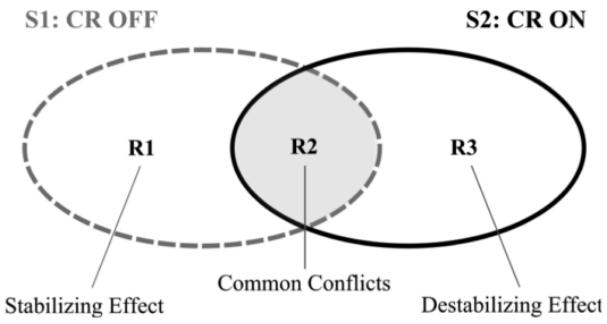

Figure 8.4: Venn diagram visualizing the DEP [49]

R1 represents all aircraft that were in conflict when resolution was off, but did not have a conflict when CR was switched on. R2 are all aircraft that were in conflict in both situations, and R3 are all aircraft that did not have a conflict when resolution was off, but did have a conflict when it was on. DEP is defined as [32]:

$$DEP = \frac{R3 - R1}{R1} = \frac{R3}{R1} - 1 \tag{8.6}$$

High DEP values indicate airspace instability. In previous research, it was found that at high traffic densities, CR maneuvers triggered additional conflicts since less maneuvering space was left [32, 49]. Preliminary research provided initial insight about the relationship between stability and capacity, but the model should be further developed in the future [50]. In this thesis, the differences between the stability of the concepts will be used to evaluate whether capacity limits have been reached.

8.3.4. Structural complexity

In Metropolis, it was seen that the zones concept performed bad in terms of structural complexity [25], and this has a direct effect on the other metrics. Therefore, structural complexity will also be addressed in this research. In literature, traffic complexity is mostly evaluated by traffic control workload or the number of trajectory modifications that are required. However, since this research involves different airspace concepts and structures, a geometrical approach is chosen [24]. Complexity will be evaluated by computation of:

- Proximity
- Convergence

Proximity will be used to evaluate whether aircraft are clustering, or homogeneously spreading over the available airspace. To calculate the proximity of a reference vehicle i, an expontential is used to increase the weight of closer aircraft. The proximity factor for one aircraft can be computed using [24]:

$$P(i) = \sum_{j=1}^{N} e^{-\alpha {d_{ij}}^2} \tag{8.7}$$

Here, N is the number of vehicles in consideration, α is a weighting factor that should be selected by the user, and d_{ij} is the normalized distance between aircraft i and j.
Since the horizontal and vertical separation distances are different, the Euclidian distance is not suitable in this case. Therefore, it should be computed using [24]:

$$d_{ij} = \sqrt{\frac{(x_i - x_j)^2 + (y_i - y_j)^2}{R_h} + \frac{(z_i - z_j)^2}{R_v}} \tag{8.8}$$

Here, R_h and R_v are again the horizontal and vertical separation requirements. The total proximity of the airspace can now be calculated by summing all the proximity factors of the vehicles in the airspace.

By only taking into account proximity, no distinction can be made between the different situations in Figure 8.5. Therefore, convergence has to be computed in addition.

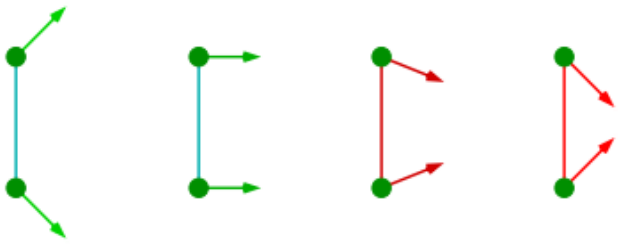

Figure 8.5: Converging and diverging aircraft [24]

The level of variation of the relative distance between two moving aircraft i and j can be computed as follows [24]:

$$r_{ij} = \frac{\partial}{\partial t}\left(d_{ij}\right) = \frac{\bar{p}_{ij} \cdot \bar{v}_{ij}}{d_{ij}} \tag{8.9}$$

Here, p_{ij} and v_{ij} are the normalized relative position vector and velocity vector respectively. The vectors are normalized to the separation requirements R_h and R_v in the appropriate dimensions.

Since the risk of high convergence between two aircraft is also dependent on the relative distance between them, an exponential function is used to put a higher weight to more risky situations. Therefore, the convergence factor for one aircraft is computed as follows:

$$C(i) = \lambda \sum_{j/r_{ij} \leq 0} -r_{ij} \cdot e^{-\alpha {d_{ij}}^2} \tag{8.10}$$

Here, λ and α are weighting coefficients. Similar to proximity, the convergence factor should be summed for all aircraft in the airspace to compute the convergence value.

When comparing the convergence and proximity of two different scenarios, the convergence over time should be considered. Instead of only looking at the average values, the maximum values should also be accounted for to differentiate between scenarios in Figure 8.6. Therefore, it is proposed to visualize complexity by plotting convergence versus time, since proximity is also accounted for in the convergence Equation 8.10.

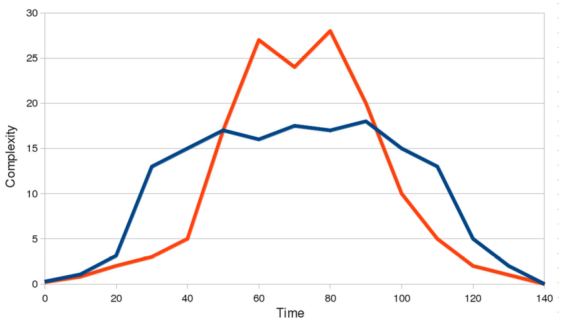

Figure 8.6: Similar average complexity can be a result of different complexity functions [24]

8.4. Vehicle types

As explained in Section 8.2, the first two phases of the experiment will mainly focus on PAVs. However, in phase III some conclusions can be made on the scalability of the concept to UAVs. In this section, the PAVs and UAVs that will be used will be introduced in Section 8.4.1 and 8.4.2. Finally, a hypothesis on the scalability of the zone concept is formulated in Section 8.4.3.

8.4.1. PAVs

To test the ability of the concept to deal with traffic subjected to different performance limitations, a mix of PAVs will be used. Similar to the Metropolis project, three different types will be simulated: PAL-V, Terrafugia TF-X and Agusta Westland AW609. A combination of these three PAVs is chosen since the three types can be seen as substitutes for motorbikes, cars and minivans respectively. To simulate and predict the vehicle trajectories, certain performance specifications are required. Unfortunately, not all performance specifications are yet available since some are still in development. Therefore, parameters of existing aircraft performance models based on Eurocontrol's Base of Aircraft Data (BADA), will be adapted to match the performance of the PAVs. Table 8.3, 8.4, and 8.5 present the specifications provided by the manufacturers. For the TF-X, some specifications are based on the similar Terrafugia Transition PAV [26].
It can be seen that significantly less data is available for the TF-X. In the implementation phase (experiment phase I), it should be evaluated whether enough data is available to simulate the TF-X and the AW609. If not, additional PAVs will be looked up, such that there will be 2 or more different PAV types in the scenario.

8.4.2. UAVs

Since a departure/arrival area for drones will most likely be a distribution center for packages, a drone with high payload capability is preferred. The Microones MD4-3000 quad-copter UAV from the Metropolis project

Table 8.3: Performance specifications PAL-V Europe [42]

Variable	Value
Type	Gyrocopter
Capacity	2 persons
Empty mass	664 kg
Maximum Take-Off Weight (MTOW)	910 kg
Dimensions Flight-mode	6.1 m L x 2 m W x 3.2m H
Rotor diameter	10.75 m
Economic cruise speed	140 km/h
Maximum speed	180 km/h
Minimum speed for level flight	50 km/h
Engine power	200 hp
Maximum operating altitude	3500 m
Take-off distance (at mean sea level, MTOW)	315 m
Landing roll distance	30 m
Mileage	26 l/h
Maximum range (MTOW)	400 km
Maximum endurance (MTOW)	4.3 h

Table 8.4: Performance specifications Terrafugia TF-X [52] [24]

Variable	Value
Type	Fixed wing, vertical take-off and landing vehicle
Capacity	4 persons
Payload	277 kg
Dimensions Flight-mode	fit in standard parking
Economic cruise speed	320 km/h
Engine power	1 MW
Take-off distance (MTOW)	30 m
Landing roll distance	30 m
Mileage	8.5 km/l
Max range	800 km

Table 8.5: Performance specifications AW609 [35]

Variable	Value
Type	Tilt-rotor
Capacity	2 crew, 9 passengers
Maximum Take-Off Weight (MTOW)	7620 (for VTOL, else 8164)
Economic cruise speed	510 km/h
Maximum speed	615 km/h
Engine power	1249 kW
Maximum operating altitude	7620 m
Maximum range (MTOW)	1389 km

will therefore also be used in this assignment. The performance specifications for this drone are provided in Table 8.6.

8.4.3. Scalability of the zone concept

Based on the relationship between the conflict rate and airspace parameters derived by Hoekstra et al., the changes between the PAV and UAV scenario can be addressed. In the literature review (Chapter 4) the following equation was addressed [20]:

$$CR_{global} = k \cdot \frac{\overline{V} R T_{FL}}{A T_{tot}} \cdot \frac{1}{2} N \left(\frac{N}{L} - 1 \right) \cdot \frac{1}{\alpha} \left(1 - \frac{2}{\alpha} \sin\left(\frac{\alpha}{2} \right) \right) \tag{8.11}$$

Table 8.6: Performance specifications MD4-3000 [24]

Variable	Value
Type	quadcopter UAV
MTOW	15 kg
Payload	3 kg
Cruise speed	31 kts
Endurance	0.75 hr
Range	23 NM
Service ceiling	13100 ft

Here, k is an airspace constant, N is the number of aircraft in the airspace, L is the number of layers, and α is the heading range. When comparing a zone configuration with PAVs to exactly the same configuration with UAVs flying in it, these variables can be assumed to be constant. Therefore, when deriving a situation where $CR_{PAV} = CR_{UAV}$, the following equation holds:

$$\left(\frac{\bar{V}RT_{FL}}{AT_{tot}}\right)_{PAV} = \left(\frac{\bar{V}RT_{FL}}{AT_{tot}}\right)_{UAV} \tag{8.12}$$

Here, $\bar{V}$ is the average ground speed, R is the minimum lateral separation, T_{FL} is the average time an aircraft spends in the airspace, A is the total airspace area and finally, T_{tot} is the total observation time. It is assumed that the time spend in the airspace over the total time ($\frac{T_{FL}}{T_{total}}$) is equal, therefore further reducing the problem to:

$$\left(\frac{\bar{V}R}{A}\right)_{PAV} = \left(\frac{\bar{V}R}{A}\right)_{UAV} \tag{8.13}$$

$$\bar{V}_{PAV}R_{PAV}A_{UAV} = \bar{V}_{UAV}R_{UAV}A_{PAV} \tag{8.14}$$

Therefore, the total area for the UAV scenario with similar configuration and conflict rate should be computed by scaling the PAV area as follows:

$$A_{UAV} = \frac{\bar{V}_{UAV}R_{UAV}}{\bar{V}_{PAV}R_{PAV}}A_{PAV} \tag{8.15}$$

Comparing the average cruise speed of the three PAVs to that of the UAV, it can be computed that the average ground speed for the considered PAVs will be a factor 6 times higher than for the UAVs (assuming the 3 types of PAVs occur equally often in the airspace). When assuming that the horizontal separation requirement for PAVs is around 250 m, and for the UAVs around 25 m, Equation 8.15 can be substituted:

$$A_{UAV} = \frac{1}{60}A_{PAV} \tag{8.16}$$

It should be noted that this scale factor is only computed to get an indication about the scale differences. In practice, the dynamics in the inner circle will be completely different for the UAV scenario, and this will directly effect the conclusion. However, it is hypothesized that the theoretical relationship (Equation 8.15) gives a good indication of the changes that need to be made to the zone concept.

8.5. Conflict detection & resolution

In the past years, a lot of advanced automation tools have been developed to detect and resolve traffic conflicts. Based on literature review (Chapter 5), the MVP method was selected for this assignment, since its success in a decentralized airspace is already demonstrated multiple times.

When using the MVP method, aircraft behavior can be compared to charged particle behavior. Conflict resolution by the MVP algorithm is coordinated implicitly and cooperatively, meaning that both aircraft in conflict take measures to avoid each other. Since the displacement vector is based on a repelling force, both aircraft always take opposite measures. Figure 8.7 shows the geometry that is used to calculate the displacement vector. The figure shows two aircraft, A and B, and the relative velocity of aircraft B with respect to aircraft A is pointing through the Intruder Protected Zone (IPZ) of A. The Closest Point of Approach (CPA) of A and B

is point C, and the goal is to move point C outside of the IPZ. Point O is the closest distance out of the IPZ, however the straight line from B to O still crosses the IPZ of A. Therefore, line CO needs to be multiplied with a small factor, computed by [15]:

$$\frac{|CO|}{|CO'|} = \left|\cos\left(\arcsin\left(\frac{R}{AB}\right) - \arcsin\left(\frac{AC}{AB}\right)\right)\right| \tag{8.17}$$

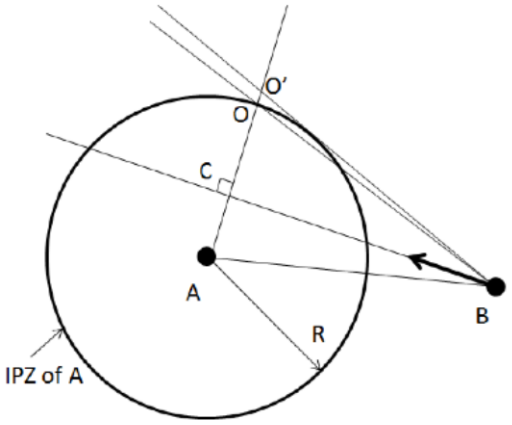

Figure 8.7: Computation of the MVP displacement vector [36]

Here, R is the radius of the IPZ as can be seen in Figure 5.4. Once CO' is computed, the displacement vector can be computed based on the time at which the CPA is predicted (t_C):

$$v_{MVP} = \frac{CO'}{t_C} + v_{current} \tag{8.18}$$

In Metropolis, the average severity of intrusions was around 40% [49]. A literature review was done to address possibilities to optimize the algorithm for drones. Most research that was reviewed focuses on different algorithms, and only takes into account horizontal conflict resolutions. Since these optimizations are not a proven concept, it is proposed to use the MVP algorithm as it is currently implemented in BlueSky. In experiment phase I, the settings of the CD&R method will be varied to find an adequate look-ahead time and separation requirements.

8.6. Traffic separation in the inner circle

The method that is used to separate departing and arriving traffic in the inner circle is a crucial element of the zone concept. At this stage, a proposal is formulated that has to be tested and optimized in experiment phase I. In the two subsequent subsections, the proposed methods for arriving and departing traffic are discussed.

8.6.1. Arriving traffic

The merging and sequencing of the arriving traffic is the biggest challenge in the inner circle. Since it is not part of the research objective to develop and evaluate a new merging concept, a literature review was performed on existing methods. The Point Merge method was chosen based on the literature review described in Chapter 6, since it fully relies on existing technology and it has been proven to be a safe and efficient method [27].

The so called Point Merge technique makes use of a merge point and pre-defined sequencing legs that can be used to stretch or shorten the aircraft path [27]. The sequencing legs are designed to always have the same distance away from the merge point, and are separated vertically. An example geometry of a Point Merge System (PMS) with two entry points and sequencing legs is shown in Figure 8.8.

The entire sequencing leg is programmed in the FMS and therefore no controller intervention is required to perform path stretching. Spacing is monitored by giving aircraft a "direct-to merge point" instruction at the appropriate time. After leaving the sequencing legs, spacing is maintained by speed control [11].

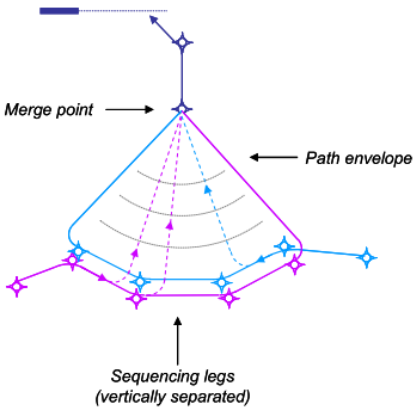

Figure 8.8: Example geometry of a Point Merge System [11]

Figure 8.9 shows the proposed structure for the arriving traffic. Since each converging zone will require its own Point Merge systems, the flow coming from multiple merge points needs to be safely integrated into one flow. Therefore, it is not sufficient to only sequence aircraft in one Point Merge System without considering the output flow of the other systems. An Arrival Manager (AMAN) tool is required to compute the sequence of all aircraft at the same time.

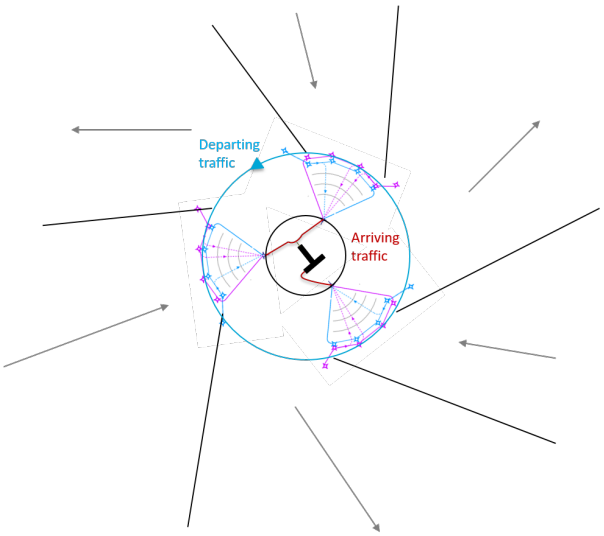

Figure 8.9: Arriving traffic flows from the zones will be merged by using multiple Point Merge Systems

For previous research, Vanwelsenaere implemented an AMAN Research Simulator (ARSIM) in BlueSky [55]. It is expected that ARSIM can serve as a basis for the scheduler used in this assignment. From the thesis report of Alexander Vanwelsenaere it was found that the Scheduled Time of Arrival (STA) that will be computed is always larger or equal to the Expected Time of Arrival (ETA), since it is computed by:

$$STA = \max(ETA, LAS + LIV) \tag{8.19}$$

Here, LAS is the Last Assigned Slot, and LIV is the required Landing Interval. This means STA is the maximum of the ETA and the first available landing slot. As discussed before, when using Point Merge, the entire sequencing leg is programmed in the FMS. Therefore, STA is preferably lower than ETA, and if possible, aircraft should be instructed to leave the sequencing leg earlier. At this point, it is expected that the scheduler from ARSIM can be adapted and used for sequencing arrivals using the Point Merge method. By evaluating the code, this should be further investigated in phase I of the experiment. Implementation inside the current ARSIM functionality is preferable for the long-term development of BlueSky. However, if after thorough evaluation of the code the required changes are assessed to be too drastic, a separate scheduler will be developed.

8.6.2. Departing traffic

The possible flight paths for leaving the inner circle are shown in Figure 8.10. Aircraft will fly towards the edge of the inner circle and from there fly a circular path. As soon as possible, they leave the circle at the location that suits their flight plan best.

When the zone concept is implemented, aircraft can only leave through a diverging zone, and therefore some of the possible paths in Figure 8.10 will not be applicable anymore. As discussed in Section 8.1, the zone boundaries are not perpendicular to the inner circle, still making it possible to leave the inner circle in the same way. It should be noted that the direction of the circular flow in the inner circle should match the zone configuration. From Figure 8.1 it can be seen that the zones are slightly tilted anti-clockwise, therefore anti-clockwise circling is required for the proposed zone configuration.

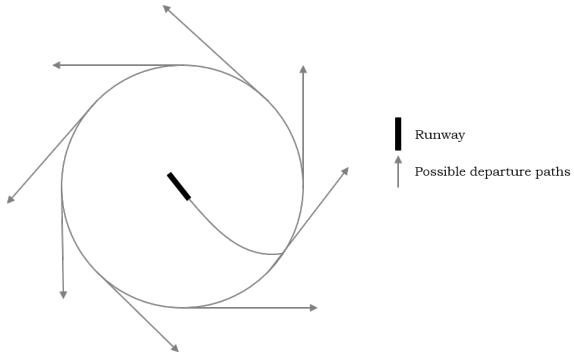

Figure 8.10: Departing traffic leaves the inner circle perpendicular to the radius

8.7. Simulation area

This thesis research will be performed using BlueSky, an open data and open source ATC simulator devloped at the TU Delft [16]. The tool will be extended with the feature to simulate the zone structure and adequate merging and sequencing algorithms.
Since designing circular flight paths requires a lot of additional waypoints, the circular shapes of the zones will be designed to be polygonal shapes instead as shown in Figure 8.11.

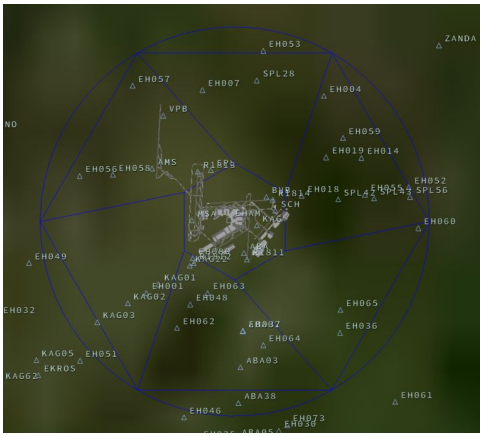

Figure 8.11: The circular shapes of the zones are designed to be polygonal shapes

In the Metropolis project, a triangular shape was initially used to define the simulation area. However, it was found that this led to boundary problems. When aircraft were steering away from the conflict, they disappeared from the simulation area, and newly generated conflicts were therefore not logged [51]. To avoid this artifact, it is proposed to only choose an experiment area with the desired density distribution after running the experiment.

8.8. Project planning

To be able to perform the proposed experiment successfully and efficiently, proper project planning is key. As already introduced in Section 8.2, the work was divided into manageable phases. Figure 8.12 shows the proposed work breakdown structure. This preliminary thesis report concludes the thesis preparation phase. Phase I is expected to take more time than phase II since it includes most of the implementation in BlueSky.

The project is planned to cover 38 full-time working weeks, split between the work packages as shown in Figure 8.12. In the Gannt chart in Figure 8.13 it can be seen that between the kick-off meeting and the thesis defense there are 46 weeks. The additional 8 weeks account for 6 weeks of holiday, other moments of planned absence, and unforeseen events. It should be noted that the Gantt chart is simplified for visualization purpose, the implementation and validation loops are in reality iterative processes.

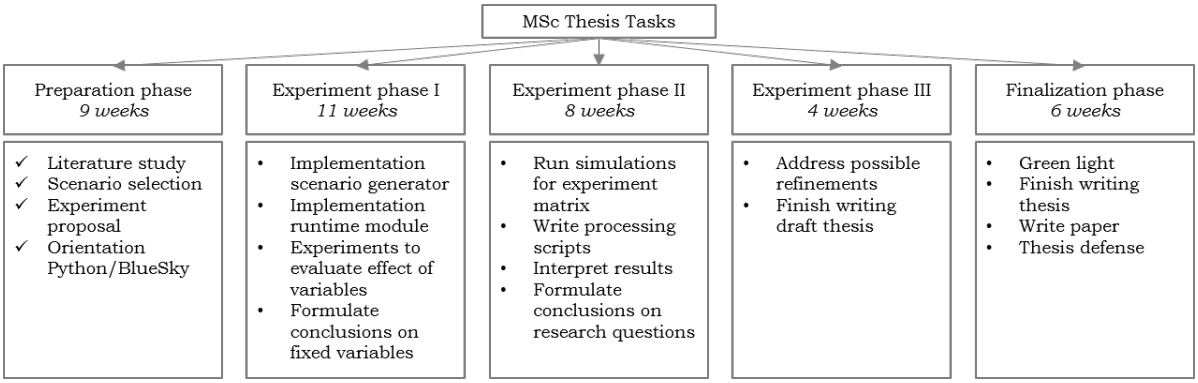

Figure 8.12: Proposed work breakdown structure

The proposed project milestones that are required to finish the thesis in time are presented in Table 8.7. The first three milestones have been successfully completed in time at the time of handing in this preliminary report.

Table 8.7: Proposed project milestones

Date	Milestone
06-03-2017	Kick-off meeting
19-05-2017	Draft preliminary report
11-08-2017	Preliminary report
14-08-2017	Preliminary presentation
13-10-2017	Mid term
01-12-2017	Draft thesis report
15-12-2017	Green light
05-01-2018	Thesis report
19-01-2018	Defense

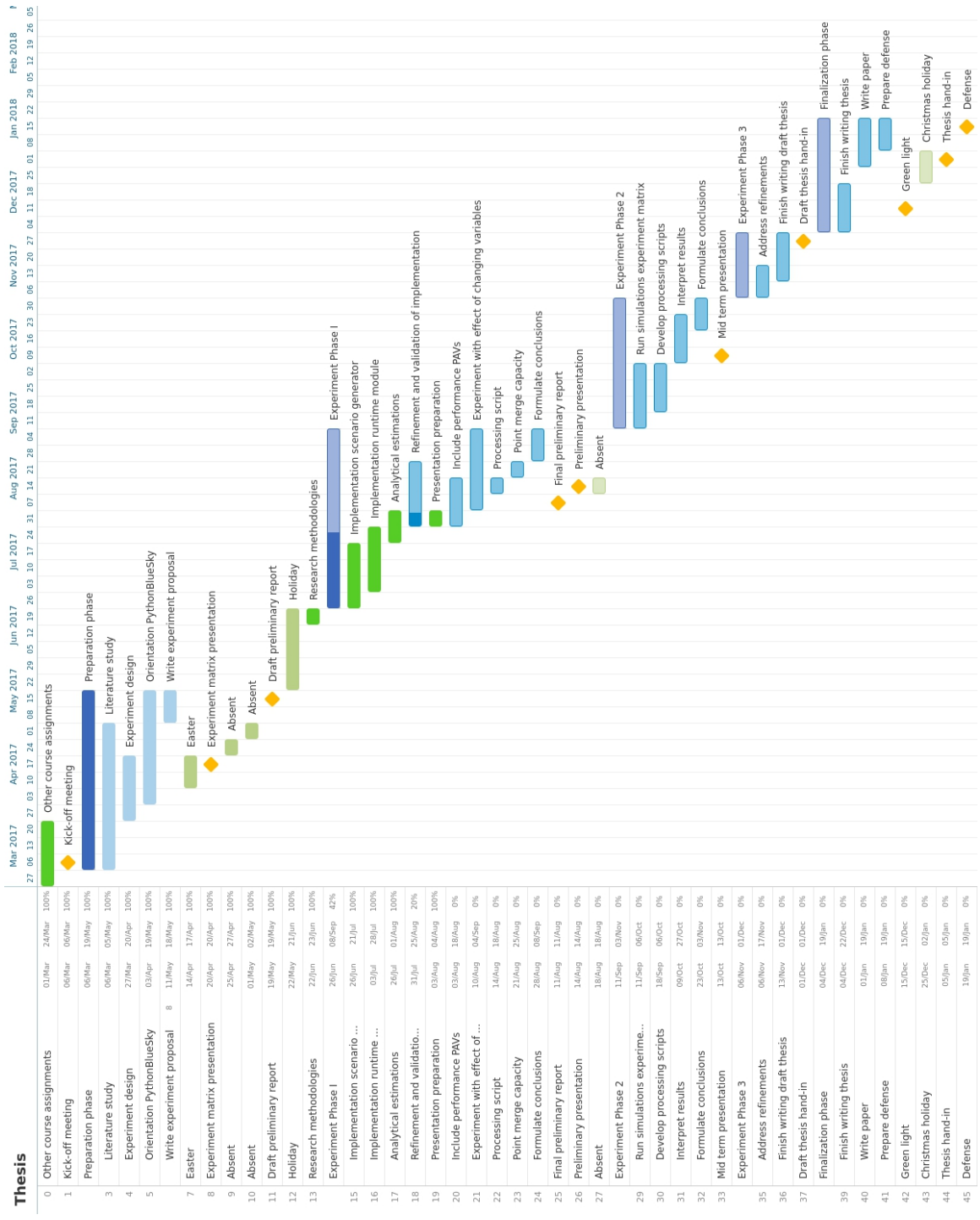

Figure 8.13: Gantt chart with work packages and milestones

Bibliography

[1] Cyril Allignol, Nicolas Barnier, and Nicolas Durand. Detect & Avoid , UAV Integration in the Lower Airspace Traffic. In *7th International Conference on Research in Air Transportation (ICRAT)*, 2016.

[2] Richard A Armstrong. When to use the bonferroni correction. *Ophthalmic and Physiological Optics*, 34 (5):502–508, 2014.

[3] Michael O Ball, Robert Hoffman, Chien-Yu Chen, and Thomas Vossen. Collaborative Decision Making in Air Traffic Management: Current and Future Research Directions. *Fifth International Workshop on Air Traffic Management*, 3(96):17–30, 2001. doi: 10.1007/978-3-662-04632-6.

[4] Paul Baran. On Distributed Communications Networks. *IEEE Transactions on Communications*, 12:1–9, 1964. ISSN 0096-2244. doi: 10.1109/TCOM.1964.1088883.

[5] Ludovic Boursier, Bruno Favennec, Eric Hoffman, Laurence Rognin, Francois Vergne, and Karim Zeghal. Combining sequencing tool and spacing instructions to enhance the management of arrival flows of aircraft. *AIAA 5th Aviation, Technology, Integration, and Operations Conference*, pages 1–14, September 2005. doi: 10.2514/6.2005-7302.

[6] Ludovic Boursier, Bruno Favennec, Eric Hoffman, Aymeric Trzmiel, François Vergne, and Karim Zeghal. Merging Arrival Flows Without Heading Instructions. *USA/Europe Air Traffic Management Research and Development Seminar*, pages 1–8, July 2007.

[7] Vishwanath Bulusu, Raja Sengupta, and Zhilong Liu. Unmanned Aviation : To Be Free or Not To Be Free ? In *7th International Conference on Research in Air Transportation (ICRAT)*, 2016.

[8] Kevin M Corker, Brian F Gore, Kenneth Fleming, and John Lane. Free Flight and the Context of Control : Experiments and Modeling to Determine the Impact of Distributed Air-Ground Air Traffic Management on Safety and Procedures. *3rd USA/Europe Air Traffic Management R & D Seminar*, pages 13–16, June 2000.

[9] M Dupeyrat, S Aubry, H Hesselink, S Loth, A Remiro, P Schmollgruber, R Verbeek, and C Welman. Evaluation of operations on an airport with a circular runway. In *29th Congress of the International Council of the Aeronautical Sciences (ICAS)*, 2014.

[10] Martin S Eby. A Self-Organizational Approach for resolving Air Traffic Conflicts. *The Lincoln Laboratory Journal*, 7(2):239–253, 1994. ISSN 0896-4130.

[11] Bruno Favennec, Eric Hoffman, Aymeric Trzmiel, François Vergne, and Karim Zeghal. The Point Merge Arrival Flow Integration Technique: Towards More Complex Environments and Advanced Continuous Descent. *9th AIAA Aviation Technology, Integration, and Operations Conference (ATIO)*, page 6921, September 2009. doi: 10.2514/6.2009-6921.

[12] Andy Field. *Discovering Statistics Using SPSS*. SAGE Publications Ltd, 2009.

[13] Nathalie Hasevoets and Paul Conroy. Arrival Manager: Implementation Guidelines and Lessons Learned. Technical report, EUROCONTROL, December 2010.

[14] H Hesselink and P Schmollgruber. Innovative Airport and ATM Concept (Operating an Endless Runway). In *4th CEAS Air&Space Conference*, 2013.

[15] J M Hoekstra. *Designing for Safety: the Free Flight Air Traffic Management Concept*. PhD thesis, Delft University of Technology, 2001.

[16] J M Hoekstra and J Ellerbroek. BlueSky ATC Simulator Project: an open Data and Open Source Approach. In *Proceedings of the 7th International Conference on Research in Air Transportation*, 2016.

[17] Jacco Hoekstra and Joost Ellerbroek. AE4321 Air Traffic Management Lecture Slides - Free Flight. Accessed on Blackboard AE4321 2015-2016 Q2, 2016.

[18] Jacco Hoekstra and Joost Ellerbroek. AE4321 Air Traffic Management Lecture Slides - Conflict Detection. Accessed on Blackboard AE4321 2015-2016 Q2, 2016.

[19] Jacco Hoekstra and Joost Ellerbroek. AE4321 Air Traffic Management Lecture Slides - Approach. Accessed on Blackboard AE4321 2015-2016 Q2, 2016.

[20] Jacco M. Hoekstra, J. Maas, M. Tra, and Sunil E. How Do Layered Airspace Design Parameters Affect Airspace Capacity and Safety ? In *7th International Conference on Research in Air Transportation (ICRAT)*, 2016.

[21] J.M. Hoekstra. Research Proposal Onion - Layered Airspaces and Geovectors. Proposal nr. SEP-20141642, July 2017.

[22] J.M. Hoekstra, R.C.J. Ruigrok, and R.N.H.W. Van Gent. Free flight in a crowded airspace? *Progress in Astronautics and Aeronautics*, 193:533–546, June 2001.

[23] J.M. Hoekstra, Stefan Kern, Olivier Schneider, Franz Knabe, and Bruno Lamiscarre. Metropolis Conceptual Definition Report (D2.2). Technical report, Delft University of Technology, 2015. Available online at `http://homepage.tudelft.nl/7p97s/Metropolis/` Accessed 4 April 2017.

[24] J.M. Hoekstra, Stefan Kern, Olivier Schneider, Franz Knabe, and Bruno Lamiscarre. Metropolis Development & Metrics Definition Report (D3.2). Technical report, Delft University of Technology, 2015. Available online at `http://homepage.tudelft.nl/7p97s/Metropolis/` Accessed 10 April 2017.

[25] J.M. Hoekstra, Stefan Kern, Olivier Schneider, Franz Knabe, and Bruno Lamiscarre. Metropolis Simulation Results and Analysis Report (D5.2). Technical report, Delft University of Technology, 2015. Available online at `http://homepage.tudelft.nl/7p97s/Metropolis/` Accessed 17 April 2017.

[26] J.M. Hoekstra, Stefan Kern, Olivier Schneider, Franz Knabe, and Bruno Lamiscarre. Metropolis Scenario Definition Report (D1.2). Technical report, Delft University of Technology, 2015. Available online at `http://homepage.tudelft.nl/7p97s/Metropolis/` Accessed 3 April 2017.

[27] Dan Ivanescu, Chris Shaw, and Constantine Tamvaclis. Models of Air Traffic Merging Techniques: Evaluating Performance of Point Merge. *9th AIAA Aviation Technology, Integration, and Operations Conference (ATIO)*, pages 1–10, September 2009.

[28] Matt R Jardin. Air Traffic Conflict Models. *4th Aviation Technology, Integration and Operations (ATIO) Forum*, pages 1–13, September 2004. doi: 10.2514/6.2004-6393.

[29] Matt R Jardin. Analytical Relationships Between Conflict Counts and Air-Traffic Density. *Journal of Guidance, Control, and Dynamics*, 28(6), 2005. ISSN 0731-5090. doi: 10.2514/1.12758.

[30] Joel Klooster, Sergio Torres, Daniel Earman, Mauricio Castillo-Effen, Raj Subbu, Leonardo Kammer, David Chan, and Tom Tomlinson. Trajectory synchronization and negotiation in Trajectory Based Operations. In *29th Digital Avionics Systems Conference*, pages 1–11, 2010. ISBN 978-1-4244-6616-0. doi: 10.1109/DASC.2010.5655536. URL `http://ieeexplore.ieee.org/lpdocs/epic03/wrapper.htm?arnumber=5655536`.

[31] Parimal Kopardekar, Karl Bilimoria, and Banavar Sridhar. Initial concepts for dynamic airspace configuration. In *AIAA Aviation Technology Integration and Operations Conference*, pages 18 – 20, September 2007. ISBN 978-1-62410-014-7. doi: 10.2514/6.2007-7763.

[32] J Krozel and M Peters. Decentralized control techniques for distributed air/ground traffic separation. *Seagull Technology Inc., Los Gatos*, August 2000. doi: 10.2514/6.2000-4062.

[33] J K Kuchar and L C Yang. A review of conflict detection and resolution modeling methods. *IEEE Transactions on Intelligent Transportation Systems*, 1(4):179–189, 2000. ISSN 15249050. doi: 10.1109/6979.898217.

[34] Thom Langejan, Emmanuel Sunil, Joost Ellerbroek, and Jacco Hoekstra. Effect of ADS-B Characteristics on Airborne Conflict Detection and Resolution. In *6th SESAR Innovation Days (SID)*, November 2016.

[35] Leonardo Company. *AugustaWestland AW609 Brochure*, 2017. Available on `https://aerospaceblog.files.wordpress.com/2012/04/m-11-0320-aw609-brochure-online.pdf` Accessed 12 May 2017.

[36] J Maas, E Sunil, J Ellerbroek, and J Hoekstra. The Effect of Swarming on a Voltage Potential-Based Conflict Resolution Algorithm. *Proceedings of the 7th International Conference on Research in Air Transportation*, 2016.

[37] Arnab Majumdar, Washington Ochieng, and John Polak. Estimation of European Airspace Capacity from a model of controller workload. *Journal of Navigation*, 55:381 – 403, 2002. ISSN 0373-4633. doi: 10.1017/S037346330200190X.

[38] Mohamed Faisal B. Mohamed Salleh and Kin Huat Low. Concept of Operations (ConOps) for Traffic Management of Unmanned Aircraft Systems (TM-UAS) in Urban Environment. *AIAA Information Systems Conference*, pages 1–13, January 2017. doi: 10.2514/6.2017-0223.

[39] Mark D. Moore. NASA Personal Air Transportation Technologies. Technical report, SAE Technical Paper, 2006. URL `http://www.sae.org/technical/papers/2006-01-2413`.

[40] M.S. Nolan. *Fundamentals of Air Traffic Control*. Delmar Cengage Learning, second edition, 1994.

[41] Dlugi Olaf, Astheimer Thorsten, Baldoni Cristiano, and Jean-Marc Bara et.al. The ATM target concept. Technical report, SESAR, September 2007.

[42] PAL-V. Pal-v specifications, 2017. URL `https://www.pal-v.com/`. Accessed May 2017.

[43] Thomas Prevot, Vernol Battiste, Everett Palmer, and Stephen Shelden. Air Traffic Concept Utilizing 4D Trajectories and Airborne Separation Assistance. *AIAA Guidance, Navigation, and Control Conference and Exhibit*, pages 1–11, August 2003. doi: 10.2514/6.2003-5770. URL `http://arc.aiaa.org/doi/abs/10.2514/6.2003-5770`.

[44] S Ratcliffe and R L Ford. Conflicts between Random Flights in a Given Area. *The Journal of Navigation*, 35(1):47–74, 1982.

[45] Nancy Smith and Katharine Lee. Current Airspace Configuration Practices and Their Implications for Future Airspace Concepts. *The 26th Congress of International Council of the Aeronautical Sciences (ICAS)*, pages 1–13, September 2008. doi: 10.2514/6.2008-8936.

[46] A. Sulleyman. World's first commercial flying car is now on sale. Online, 2017. Available online at `http://www.independent.co.uk/` Accessed 23 March 2017.

[47] E Sunil and J Hoekstra. The Influence of Traffic Structure on Airspace Capacity. *Proceedings of the 7th International Conference on Research in Air Transportation*, 2016. URL `https://hal-enac.archives-ouvertes.fr/hal-01333624/`.

[48] Emmanuel Sunil, Jacco Hoekstra, Joost Ellerbroek, Frank Bussink, Dennis Nieuwenhuisen, Andrija Vidosavljevic, and Stefan Kern. Metropolis : Relating Airspace Structure and Capacity for Extreme Traffic Densities. *11th USA/Europe Air Traffic Management Research and Development Seminar*, 341508:1–10, 2015.

[49] Emmanuel Sunil, Joost Ellerbroek, Jacco Hoekstra, Andrija Vidosavljevic, Michael Arntzen, Frank Bussink, and Dennis Nieuwenhuisen. Analysis of Airspace Structure and Capacity for Decentralized Separation Using Fast-Time Simulations. *Journal of Guidance, Control, and Dynamics*, 40, 2016. ISSN 0731-5090. doi: 10.2514/1.G000528.

[50] Emmanuel Sunil, Jerom Maas, Joost Ellerbroek, Jacco Hoekstra, and Martijn Tra. The Relationship Between Traffic Stability and Capacity for Decentralized Airspace. *Proceedings of the 7th International Conference on Research in Air Transportation*, 2016.

[51] Emmanuel Sunil, Joost Ellerbroek, Jacco Hoekstra, and Jerom Maas. Modeling Airspace Stability and Capacity for Decentralized Separation. *Twelfth USA/Europe Air Traffic Management Research and Development Seminar*, 2017.

[52] Terrafugia. Terrafugia tf-x specifications, 2017. URL `https://www.terrafugia.com/tf-x/`. Accessed May 2017.

[53] Heiko Udluft and Richard Curran. Decentralization in Air Traffic Management. In *Proceedings 5th Air Transport Operations Symposium*, pages 1–6, 2015.

[54] Performance Review Unit. Performance Review Report: An Assessment of Air Traffic Management in Europe during the Calender Year 2015. Technical Report June, EUROCONTROL, 2016.

[55] Alexander Vanwelsenaere. Effect of Pop-Up Flights on Extended Arrival Manager. Master's thesis, Delft University of Technology, 2016.

[56] Thomas Williamson and Ned A. Spencer. Development and Operation of the Traffic Alert and Collision Avoidance System (TCAS). *Proceedings of the IEEE*, 77(11):1735–1744, 1989. ISSN 15582256. doi: 10.1109/5.47735.